Department of Aeronautics and Astronautics
Stanford University
Stanford, California

THE CONTROL AND USE OF LIBRATION-POINT SATELLITES

by
Robert W. Farquhar

SUDAAR NO. 350
July 1968

Prepared for the National Aeronautics and Space Administration
Under Grant NsG 133-61

ABSTRACT

This study is primarily concerned with satellite station-keeping in the vicinity of the unstable collinear libration points, L_1 and L_2. Station-keeping problems at other libration points, including an "isosceles-triangle point," are also treated, but to a lesser degree.

A detailed analysis of the translation-control problem for a satellite in the vicinity of a collinear point is presented. Simple linear feedback control laws are formulated, and stability conditions are determined for both constant and periodic coefficient systems. It was found that stability could be achieved with a single-axis control that used only range and range-rate measurements. The station-keeping cost with this control is given as a function of the measurement noise. If Earth-based measurements are available, this cost is very low. Other translation-control analyses of this study include (1) solar-sail control at the Earth-Moon collinear points, (2) a limit-cycle analysis for an on-off control system, and (3) a method for stabilizing the position of the mass center of a cable-connected satellite at a collinear point by simply changing the length of the cable with an internal device.

For certain applications, a satellite is required to follow a small quasi-periodic orbit around a collinear libration point. Analytical estimates for the corrections to this orbit due to the effects of nonlinearity, eccentricity, and perturbations are derived.

Several possible libration-point missions are proposed. It is suggested that libration points could be utilized for (1) lunar far-side communications, (2) lunar and interplanetary transportation systems, (3) deep-space optical communications, (4) monitoring solar-induced phenomena in and beyond the Earth's magnetosphere, and (5) low-frequency radio astronomy.

ACKNOWLEDGMENTS

The author wishes to express his gratitude to his advisor, Prof. John V. Breakwell, for his inspirational guidance and continual availability throughout the course of this research. He also wishes to thank Ahmed Kamel for checking some of the mathematics.

The conscientious efforts of Marge Holmgren and Bill Terluin during the preparation of this report are appreciated.

The support of the Electronics Research Center of NASA in this research is gratefully acknowledged.

This work is dedicated to Bonnie, Pamela, Robin, and Patricia.

CONTENTS

CONTENTS (Cont)

CONTENTS (Cont)

CONTENTS (Cont)

NOTATION AND UNITS

Notation

A brief list of symbols is given here. Unlisted symbols are defined in the chapter where they appear.

A_x, A_y, A_z	oscillation amplitude along coordinate axis
B_L	defined by Eq. (1-44)
C_L	defined by Eq. (1-45)
D_L	defined by Eq. (1-46)
$\vec{F}_c$, (F_{cx}, F_{cy}, F_{cz})	control acceleration
K	acceleration magnitude
$\vec{P}(t)$, (P_x, P_y, P_z)	perturbing acceleration
e	orbital eccentricity
m	(1) mass (2) in Section C-1 of Chapter II, it is the ratio of the mean motions of the Earth and the Moon (m = 0.07480133) (3) in Chapter V, it is the fraction of the total time that the control is on--see page 127
s	Laplace transform variable
t	time
γ_L	distance ratio--see Fig. 1-3 and page 14
μ	normalized mass parameter--see top of page 7
ν	see Eq. (1-34) (1) for eccentricity contribution--see Eq. (1-6) (2) for Sun's effect in the Earth-Moon system--see Eq. (2-32)
ρ	see Eq. (1-33) (1) for eccentricity contribution--see Eq. (1-5) (2) for Sun's effect in the Earth-Moon system--see Eq. (2-31)

ω	frequency
$\odot$	Sun
$\oplus$	Earth
$\mathfrak{D}$	Moon

Note: A numerical subscript is added to the symbols B_L, C_L, D_L, and γ_L, for a particular libration point; e.g., B_{L1} refers to L_1.

Units

Unless other units are specified, the normalized units of the restricted three-body problem will prevail. These normalized units are defined at the top of page 7. Conversion factors for the normalized units are given in Tables 1-4 and 1-5 (see explanation at the bottom of page 35).

Accelerations are frequently expressed in Earth gravity units ($g \equiv 9.81$ m/sec^2). Note that 1 fps/yr $\cong 1 \times 10^{-9}$ g.

INTRODUCTION

A. Problem Statement

The five equilibrium solutions of the restricted three-body problem have intrigued mathematicians for many years, and more recently they have aroused the interest of engineers as well. The locations of these "libration points" relative to a rotating two-body system are essentially constant; three of them are located along the line joining the two primary bodies, while the other two form equilateral triangles with the two bodies. A satellite placed at one of these points with the proper velocity will be in equilibrium, since the gravitational and centripetal accelerations acting on the satellite will cancel. However, the three collinear points are unstable, and the equilateral-triangle points are only quasi-stable. Therefore, some form of translation control will usually be required to maintain the satellite's position in the vicinity of a libration point. This "station-keeping" problem is complicated by perturbative accelerations and additional control functions which are dictated by mission constraints. The primary objective of this research is to develop general analytical relationships for these control requirements.

A secondary objective is to examine critically, and in some cases to modify, existing proposals for libration-point satellite missions. This aim will be supplemented by new suggestions for possible applications of libration-point satellites. These mission analyses are needed to define various control problems as well as to provide motivation for the present research.

The following topics are beyond the scope of this study and are only discussed in a cursory manner.

(1) attitude control,

(2) analysis of transfer trajectories,

(3) propulsion systems, and

(4) measurement techniques.

B. Previous Contributions

Since their discovery by Lagrange in 1772, the libration points of the restricted three-body problem have been a favorite topic for researchers in celestial mechanics. Although this subject has been treated extensively, with significant contributions by Hill, Darwin, Brown, Moulton, Strömgren, etc., new papers are being published at an increasing rate. With the exception of a few perturbation studies, most of this work has little direct bearing on the main problems of the present study. However, some useful results can be gleaned from the theoretical literature, and one must be aware of what has been done in any case. An exhaustive list of references can be found in the recent treatise by Szebehely.[1] A less extensive list, but one that is primarily concerned with libration points, is included in the survey paper of Steg and DeVries.[2]

In sharp contrast to the vast literature concerning the classical problem, only six references that treat the problem of control of a libration-point satellite could be found. For an unstable collinear libration point of the Earth-Moon system, a pioneering paper by Colombo[3] has shown that:

(1) To first order, this point is an exact solution of a restricted four-body problem (Sun, Earth, Moon, satellite).

(2) It is possible to use a simple linear feedback control for position stabilization of a satellite.

(3) It is possible to obtain the acceleration needed for position and attitude stabilization of a satellite by simply varying the magnitude and direction of a solar-sail.

It should be noted that the analysis and the design of the feedback control mentioned in item (2) are not considered in Colombo's paper.

An interesting paper by Dusek[4] has shown that artificial libration points can be generated by constant low-thrust forces. Dusek also proved that, by varying these forces as a function of the satellite's position, the motion in the vicinity of a point is bounded. A special class of these artificial libration points, the "isosceles-triangle points," will be considered in the present study.

Dual-axis feedback controls have been treated by Fleming[5] and by Paul and Shapiro.[6] Fleming used an original method to design linear and

nonlinear controls for a satellite in the vicinity of an equilateral-triangle point. Paul and Shapiro determined general Routh stability conditions for all five of the classical libration points. However, the analysis of Paul and Shapiro was limited to three rather restricted controls.

For a satellite in the vicinity of a collinear libration point, the present author[7] has shown that a single-axis linear control, using only range and range-rate measurements, will guarantee asymptotic stability. The station-keeping cost for this control was given as a function of the measurement noise. Some special controls that are needed for an application were also presented.

In a recent paper, Kononenko[8] used Pontryagin's maximum principle to determine the optimal trajectory between a libration point and some initial point (in the vicinity of the libration point). It was assumed that the satellite was equipped with an engine of limited power.

Applications for libration-point satellites have been suggested in a number of papers.[7,9-18] A discussion of some of these proposals will be presented in Chapter VII.

C. Contributions of This Research

This study is a basic introduction to the libration-point satellite control problem. Most results are presented in a general analytical form, and can readily be adapted to a particular application. Since the most interesting libration-point satellite applications make use of the collinear points, the major portion of this research deals with these points. Some preliminary results of this study have already been published by the present author,[7,16] but more details are given here.

The following are the principal contributions of this research:

Chapter I

(1) General equations of motion in the vicinity of a libration point (classical and artificial) are formulated.

(2) To facilitate the application of general results to specific cases, numerical data for many of the collinear libration points of the Solar System are presented.

Chapter II

(1) The concept of nominal path control is developed.

(2) Analytical estimates for corrections to a small quasi-periodic orbit around a collinear point are given. Effects of nonlinearity, eccentricity, and perturbations are considered.

(3) Examples of gravitational perturbations, including a new "equilibrium solution" of the restricted four-body problem (Sun, Earth, Moon, satellite), are presented.

Chapter III

Simple linear feedback controls for collinear and equilateral-triangle points are analyzed. Floquet stability investigations for certain cases are also presented.

Chapter IV

(1) Analytical estimates of station-keeping costs at collinear points are presented. Costs are given as functions of the measurement noise.

(2) A solar-sail control technique at the Earth-Moon collinear points is discussed.

Chapter V

A limit-cycle analysis for an on-off control system at a collinear point is presented. A closed-form solution is obtained for an important special case, and the stability of the limit cycle is also examined. An approximate design technique for the general case is presented as well.

Chapter VI

A method is presented for stabilizing the position of the mass center of a cable-connected satellite at an unstable collinear libration point by simply changing the length of the cable with an internal device.

Chapter VII

(1) A novel method for maintaining a continuous communication link between the Earth and the far side of the Moon is presented.

(2) New applications for libration-point satellites are proposed.

Chapter I

PRELIMINARY DEVELOPMENTS

In this chapter, the equations of motion in the vicinity of libration points are formulated. The libration point concept is traced to its origin in the restricted three-body problem, and various assumptions, approximations, and modifications are discussed. Relevant numerical data for many of the collinear points are listed in the final section.

A. The Restricted Three-Body Problem

1. Equations of Motion

Consider the motion of an infinitesimal body in the gravitational field of two finite bodies (e.g., Earth and Moon) revolving around their common barycenter in elliptical orbits. It is assumed that the infinitesimal body does not influence the motion of the two larger bodies, hence the terminology, restricted three-body problem. The geometry for this problem is shown in Fig. 1-1. Here, the two finite bodies are located at P_1 and P_2, while the infinitesimal body is at P_3. An inertial reference system (ξ_o, η_o, ζ_o) is shown with its origin at the barycenter of the two finite bodies, and its ζ_o-axis normal to their orbital plane. A rotating coordinate system (ξ, η, ζ), with its ξ-axis passing through P_1 and P_2, is also introduced. From the figure, it is obvious that

$$\begin{aligned} \xi_o &= \xi \cos\theta - \eta \sin\theta \\ \eta_o &= \xi \sin\theta + \eta \cos\theta \\ \zeta_o &= \zeta \end{aligned} \tag{1-1}$$

Differentiation of Eq. (1-1) with respect to time gives

$$\begin{aligned} \dot{\xi}_o &= (\dot{\xi} - \dot{\theta}\eta)\cos\theta - (\dot{\eta} + \dot{\theta}\xi)\sin\theta \\ \dot{\eta}_o &= (\dot{\xi} - \dot{\theta}\eta)\sin\theta + (\dot{\eta} + \dot{\theta}\xi)\cos\theta \\ \dot{\zeta}_o &= \dot{\zeta} \end{aligned} \tag{1-2}$$

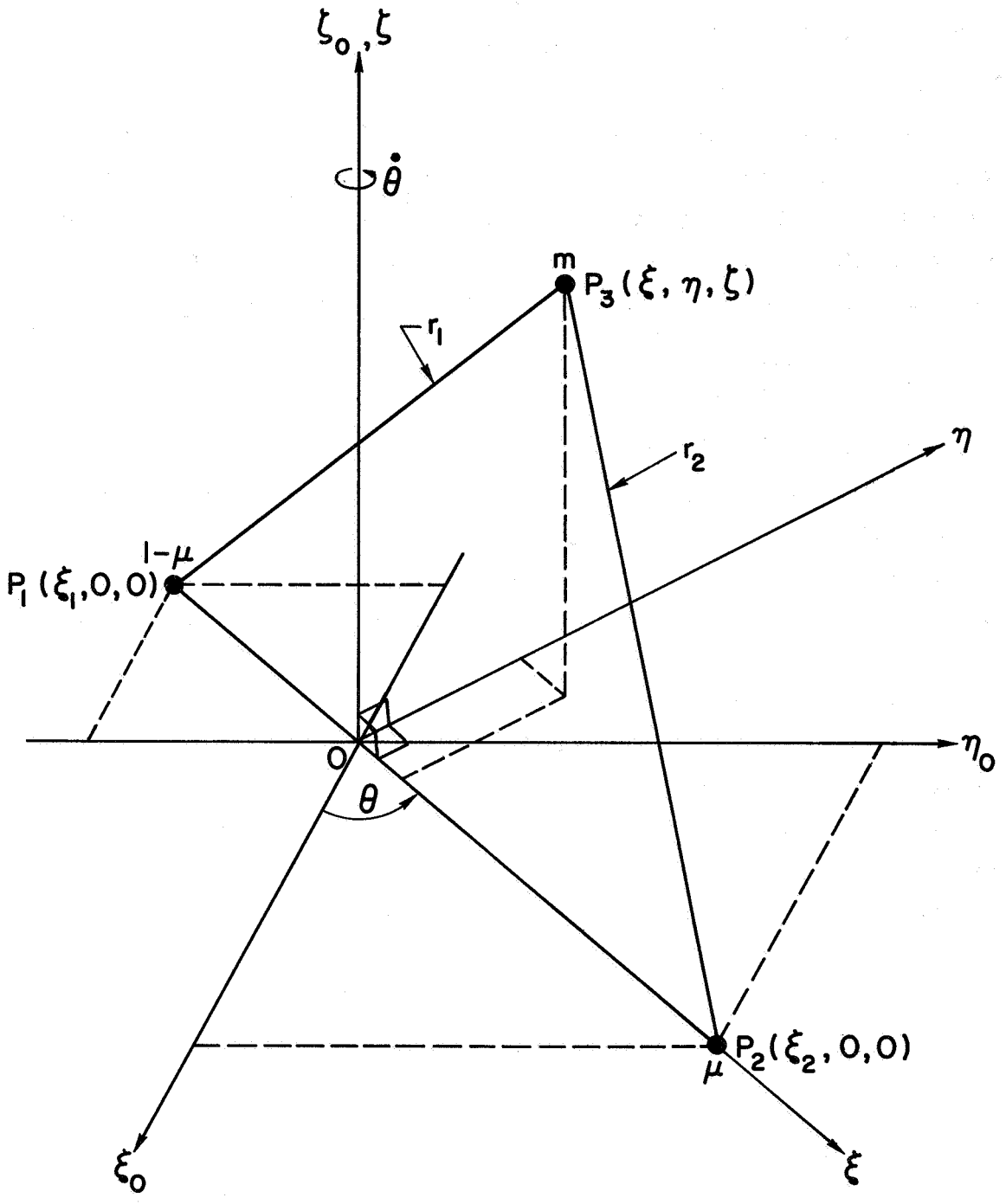

FIG. 1-1. GEOMETRY FOR THE RESTRICTED THREE-BODY PROBLEM.

To facilitate analytical manipulations, the following quantities are taken as unity:

(1) mean distance between P_1 and P_2,

(2) mean angular rate of the finite bodies about the barycenter,

(3) sum of the masses of the two finite bodies. The larger mass at P_1 is taken as $1 - \mu$, while the smaller mass at P_2 is μ. Therefore $\mu = 1/(1 + M_R)$, since the mass ratio is $M_R = (1 - \mu)/\mu$.

Unless other units are specified, this normalization will be used throughout this research.

Since the motion of the two finite bodies can be obtained from the solution of the two-body problem, it is possible to write the distance $|\overrightarrow{P_1P_2}|$ and the angular rate $\dot{\theta}$ as power series in the eccentricity. These series are[19]

$$|\overrightarrow{P_1P_2}| = (\xi_2 - \xi_1) \equiv R = 1 + \rho \tag{1-3}$$

$$\dot{\theta} = 1 + \nu \tag{1-4}$$

where

$$\rho = -e \cos (t + \varphi) + \frac{e^2}{2}\left[1 - \cos 2(t + \varphi)\right] + O(e^3) \tag{1-5}$$

$$\nu = 2e \cos (t + \varphi) + \frac{5}{2} e^2 \cos 2(t + \varphi) + O(e^3) \tag{1-6}$$

The phase angle φ is just the true anomaly at $t = 0$. It should be noted that these series converge rapidly when e is small, but are divergent when $e > 0.6627...$

Using Eq. (1-2), the kinetic energy of the infinitesmal body can be written as

$$\begin{aligned} T &= \frac{m}{2}\left[\dot{\xi}_o^2 + \dot{\eta}_o^2 + \dot{\zeta}_o^2\right] \\ &= \frac{m}{2}\left[(\dot{\xi} - \dot{\theta}\eta)^2 + (\dot{\eta} + \dot{\theta}\xi)^2 + \dot{\zeta}^2\right] \end{aligned} \tag{1-7}$$

The potential energy is

$$U = - m \left[\frac{(1 - \mu)}{r_1} + \frac{\mu}{r_2} \right] \tag{1-8}$$

where

$$r_1^2 = (\xi - \xi_1)^2 + \eta^2 + \zeta^2 \tag{1-9}$$

$$r_2^2 = (\xi - \xi_2)^2 + \eta^2 + \zeta^2 \tag{1-10}$$

Forming the Lagrangian $L = T - U$, the equations of motion are obtained from Lagrange's method. This gives

$$\ddot{\xi} - 2\dot{\theta}\dot{\eta} = \ddot{\theta}\eta + \dot{\theta}^2\xi - \frac{(1 - \mu)}{r_1^3} (\xi - \xi_1) - \frac{\mu}{r_2^3} (\xi - \xi_2)$$

$$\ddot{\eta} + 2\dot{\theta}\dot{\xi} = -\ddot{\theta}\xi + \dot{\theta}^2\eta - \left[\frac{(1 - \mu)}{r_1^3} + \frac{\mu}{r_2^3} \right] \eta \tag{1-11}$$

$$\ddot{\zeta} = - \left[\frac{(1 - \mu)}{r_1^3} + \frac{\mu}{r_2^3} \right] \zeta$$

For circular orbits $(e = 0)$ of the two finite bodies, Eq. (1-11) becomes

$$\ddot{\xi} - 2\dot{\eta} = \xi - \frac{(1 - \mu)}{r_1^3} (\xi - \xi_1) - \frac{\mu}{r_2^3} (\xi - \xi_2)$$

$$\ddot{\eta} + 2\dot{\xi} = \eta - \left[\frac{(1 - \mu)}{r_1^3} + \frac{\mu}{r_2^3} \right] \eta \tag{1-12}$$

$$\ddot{\zeta} = - \left[\frac{(1 - \mu)}{r_1^3} + \frac{\mu}{r_2^3} \right] \zeta$$

2. Jacobian Constant and the Surfaces of Zero Relative Velocity

It is the purpose of this section to elucidate an important conservation principle of the restricted three-body problem. Denoting generalized coordinates and velocities by q's and $\dot{q}$'s, respectively, the kinetic energy of a system can be written as

$$T = T(q, \dot{q}, t) = T_2 + T_1 + T_o \tag{1-13}$$

where

$$T_2 \equiv \sum_{i,j=1}^{n} \alpha_{ij}(q,t)\, \dot{q}_i \dot{q}_j \tag{1-14}$$

$$T_1 \equiv \sum_{i=1}^{n} \beta_i(q,t)\, \dot{q}_i \tag{1-15}$$

$$T_o \equiv T_o(q,t) \tag{1-16}$$

Taking the potential energy as

$$U = U(q,t) \tag{1-17}$$

and using the definitions

$$L \equiv T - U \quad \text{(Lagrangian)} \tag{1-18}$$

$$E \equiv T + U \quad \text{(total energy)} \tag{1-19}$$

$$H \equiv \sum_{i=1}^{n} \dot{q}_i \frac{\partial L}{\partial \dot{q}_i} - L \quad \text{(Hamiltonian)} \tag{1-20}$$

it follows that

$$H = T_2 - T_o + U = E - T_1 - 2T_o \tag{1-21}$$

It is important to note that, in general, the Hamiltonian is not equal to the total energy. Although this result is classical, it is often forgotten since "conventional" dynamical systems usually have a kinetic energy of the form $T = T_2$.

For the restricted three-body problem, it can be seen from Eq. (1-7) that the kinetic energy in the inertial coordinates is $T = T_2(\dot{q})$, and therefore $H = E$. If instead, the rotating coordinates are employed, the kinetic energy for a unit mass is $T = T_2 + T_1 + T_o$ where

$$T_2 = \frac{1}{2}(\dot{\xi}^2 + \dot{\eta}^2 + \dot{\zeta}^2) \tag{1-22}$$

$$T_1 = \dot{\theta}(\xi\dot{\eta} - \eta\dot{\xi}) \tag{1-23}$$

$$T_o = \frac{1}{2}\dot{\theta}^2(\xi^2 + \eta^2) \tag{1-24}$$

Therefore, in the rotating coordinate system, $H \neq E$.

If the two finite bodies are in circular orbits, $\dot{\theta} = 1$, and an interesting relation can be found. For this special case, the potential energy in the rotating coordinates is $U = U(q)$ and $\dot{H} = 0$. Although the Hamiltonian is a constant of the motion, total energy is not conserved* since $H \neq E$. This Hamiltonian is related to the "Jacobian constant" C ($H = -\frac{1}{2}C$), which is usually found in the form

$$V^2 = 2W - C \tag{1-25}$$

where $V^2 = \dot{\xi}^2 + \dot{\eta}^2 + \dot{\zeta}^2$ and

*This can also be seen by using inertial coordinates, where $U = U(q, t)$. It then follows that $\dot{H} \neq 0$, and since $H = E$, total energy is not conserved.

$$W \equiv T_o - U$$

$$= \frac{1}{2}(\xi^2 + \eta^2) + \frac{(1-\mu)}{r_1} + \frac{\mu}{r_2} \qquad (1\text{-}26)$$

By determining the Jacobian constant from the initial conditions of the infinitesimal body, bounds can be placed on the region of its subsequent motion. Since V^2 is always positive, Eq. (1-25) shows that motion is possible only so long as $2W > C$. Taking $V = 0$ (zero relative velocity) and making use of Eqs. (1-25) and (1-26), surfaces of zero relative velocity corresponding to different values of C can be constructed in the configuration space.*

The curves of zero relative velocity formed by the intersection of these surfaces with the orbital plane of the two finite bodies are depicted in Fig. 1-2 for the Earth-Moon system ($\mu = 0.0121507$). Here the Jacobi constants are $C_0 = 3.2880$, $C_1 = 3.1883$, $C_2 = 3.1724$, $C_3 = 3.0121$, $C_4 = 2.9980$, and $C_5 = 2.9880$. As noted earlier, the possible regions of motion for an infinitesimal body with given initial conditions can be determined from its Jacobi constant. For example, if the body is initially located near the surface of the Earth and its Jacobi constant is greater than C_0, then it can never leave the region bounded by the C_0 curve around the Earth. On the other hand, if its Jacobi constant is C_4, then motion can take place everywhere except for the region enclosed by the C_4 curve. Figure 1-2 is really just a contour map of the modified potential field of the Earth and Moon in the rotating coordinates. The regions surrounding the Earth and Moon in this modified potential field can be viewed as valleys, while the point at L_4 is a mountain peak. Notice that saddle-surfaces exist at L_1, L_2, and L_3.

---

*Details of this construction as well as many fine examples for various values of μ can be found in Ref. 1.

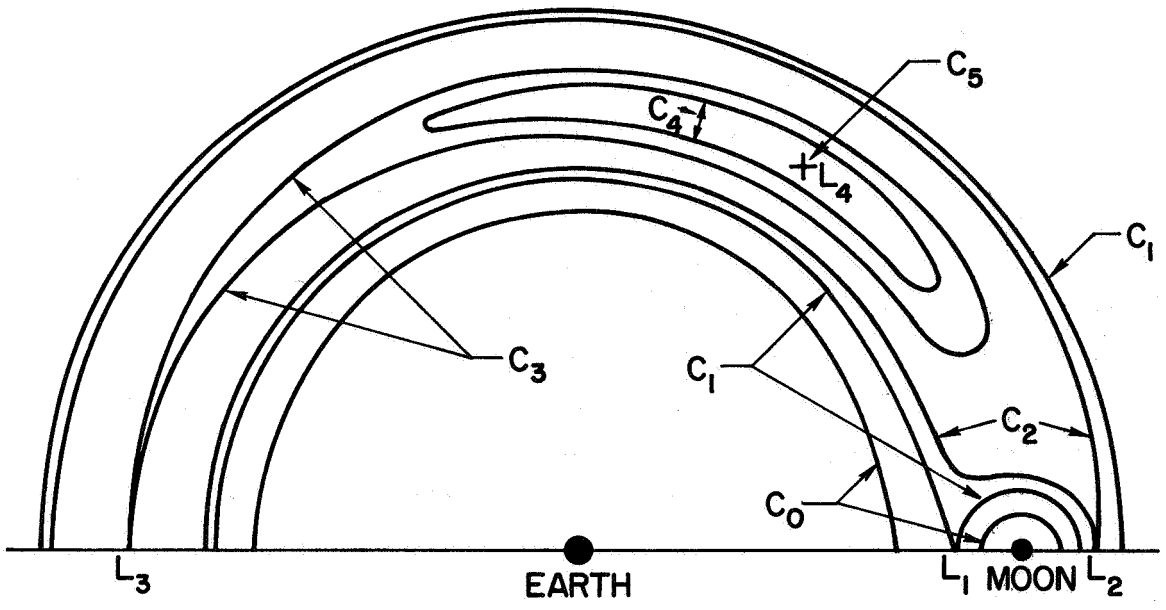

FIG. 1-2. CURVES OF ZERO RELATIVE VELOCITY FOR THE EARTH-MOON SYSTEM.

Returning to the more realistic case where the two finite bodies are in elliptical orbits, it can be seen at once that even for rotating coordinates, $U = U(q, t)$ and $\dot{H} \neq 0$. This means that the Jacobi constant does not exist in the elliptical case, and the usefulness of Fig. 1-2 may be severely limited. However, it is the opinion of the present author that Fig. 1-2 is still useful for intuitive reasoning when the eccentricity is small and time intervals are relatively short. For a discussion of this problem, see Refs. 20-22.

3. Libration Points

It is well known that there are five equilibrium solutions of Eq. (1-11). These equilibrium points are located in the orbital plane of the two finite bodies, and their general configuration is shown in Fig. 1-3. Two of the points (L_4 and L_5) form an equilateral triangle with the finite bodies, while the remaining three (L_1, L_2, and L_3) are collinear. A common name for these points, and one which will be used here, is "libration points."

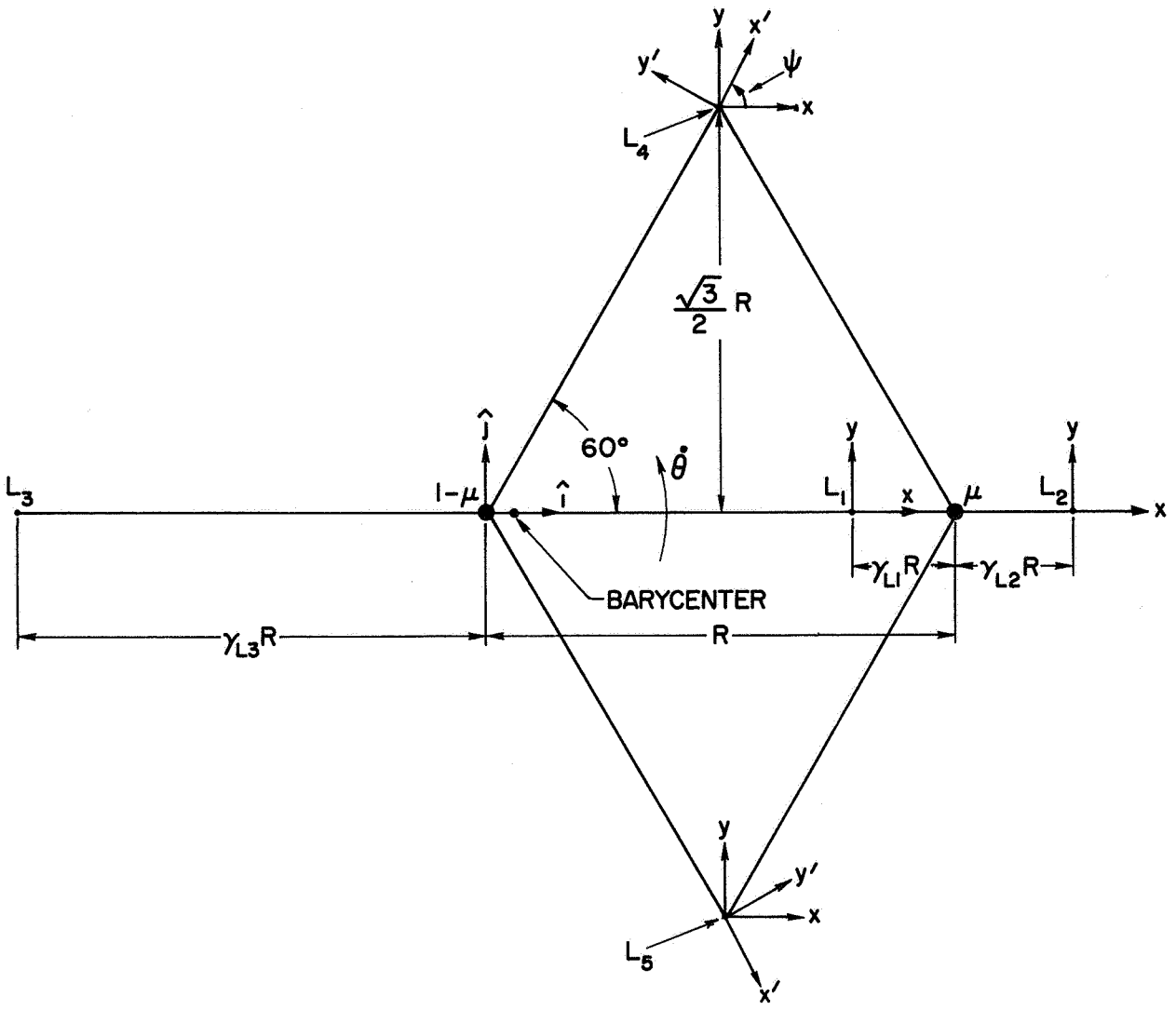

FIG. 1-3. LIBRATION POINT GEOMETRY.

The existence of these libration points is reasonable from a purely physical standpoint, since they are just points where the gravitational and centripetal accelerations are balanced in the rotating coordinate system. In the circular restricted three-body problem, these points will always be stationary. However, in the elliptical case, the distances from the finite bodies will vary periodically while the equilateral triangle and collinear configurations are maintained. A thorough discussion of the equilibrium solutions for both the circular and elliptical cases can be found in Ref. 1.

From Fig. 1-3, it can be seen that the collinear libration points are located at distances $\gamma_L R$ from the finite bodies.* The constant γ_L is obtained by finding the real root of a certain quintic equation. The quintic equations for the three collinear points are[1]

$$\gamma_{L1}^5 - (3 - \mu)\gamma_{L1}^4 + (3 - 2\mu)\gamma_{L1}^3 - \mu\gamma_{L1}^2 + 2\mu\gamma_{L1} - \mu = 0 \qquad (1\text{-}27)$$

$$\gamma_{L2}^5 + (3 - \mu)\gamma_{L2}^4 + (3 - 2\mu)\gamma_{L2}^3 - \mu\gamma_{L2}^2 - 2\mu\gamma_{L2} - \mu = 0 \qquad (1\text{-}28)$$

$$\gamma_{L3}^5 + (2 + \mu)\gamma_{L3}^4 + (1 + 2\mu)\gamma_{L3}^3 - (1 - \mu)\gamma_{L3}^2 - 2(1 - \mu)\gamma_{L3} - (1 - \mu) = 0 \qquad (1\text{-}29)$$

Series solutions for γ_L are also available, but are not recommended for numerical computations at L_1 and L_2 where the convergence is poor. However, abbreviated versions of the series at L_1 and L_2 are sometimes useful for analytic approximations. The series for L_1 and L_2 are[1]

$$\gamma_{L1} = \left(\frac{\mu}{3}\right)^{1/3}\left[1 - \frac{1}{3}\left(\frac{\mu}{3}\right)^{1/3} - \frac{1}{9}\left(\frac{\mu}{3}\right)^{2/3} + \ldots\right] \qquad (1\text{-}30)$$

$$\gamma_{L2} = \left(\frac{\mu}{3}\right)^{1/3}\left[1 + \frac{1}{3}\left(\frac{\mu}{3}\right)^{1/3} - \frac{1}{9}\left(\frac{\mu}{3}\right)^{2/3} + \ldots\right] \qquad (1\text{-}31)$$

*An additional subscript is added for a particular point; e.g., γ_{L1} refers to L_1.

The series solution for L_3 converges very rapidly, and since the real root of Eq. (1-29) is near +1, it is preferred for numerical computations. This series is given by[1]

$$\gamma_{L3} = 1 + \epsilon\left(1 + \frac{23}{84}\,\epsilon^2 + \frac{23}{84}\,\epsilon^3 + \frac{761}{2352}\,\epsilon^4 + \frac{3163}{7056}\,\epsilon^5 + \frac{30703}{49392}\,\epsilon^6\right) + O(\epsilon^8) \tag{1-32}$$

where $\epsilon \equiv 7\mu/12$.

B. Equations of Motion in the Vicinity of Libration Points

In this section, the equations of motion in the vicinity of libration points are obtained in a general form which is readily adaptable to the perturbation analyses of Chapter II. Although the derivation could proceed directly from Eq. (1-11), a more basic approach is followed here. All of the classical libration points with the exception of L_3, which is not too interesting from the standpoint of possible applications, are treated. In addition, an artificial libration point which forms an isosceles triangle with the two finite bodies is examined.

1. Collinear Points

In Fig. 1-3, the distance R and the angular rate $\dot{\theta}$ are defined as

$$R = 1 + \rho(t) \tag{1-33}$$

$$\dot{\theta} = 1 + \nu(t) \tag{1-34}$$

where the quantities $\rho(t)$ and $\nu(t)$ are functions of time which arise from the orbital eccentricity of the finite bodies and perturbations from bodies external to the primary two-body system. The unit vectors $\hat{i}$ and $\hat{j}$ are fixed in the rotating reference frame, which means that

$$\begin{aligned} \dot{\hat{i}} &= (1 + \nu)\hat{j} \\ \dot{\hat{j}} &= -(1 + \nu)\hat{i} \end{aligned} \tag{1-35}$$

A right-handed triad is formed by taking the cross product $\hat{k} = \hat{i} \times \hat{j}$.

From Fig. 1-3, it is evident that, for a satellite (infinitesimal mass) in the vicinity of either L_1 or L_2, the position vector relative to the larger body $(1 - \mu)$ is*

$$\vec{r} = \left[(1 \pm \gamma_L)(1 + \rho) + x\right] \hat{i} + y\hat{j} + z\hat{k} \tag{1-36}$$

(The position vector relative to the libration point is $\vec{r}_L = x\hat{i} + y\hat{j} + z\hat{k}$.) Differentiation of Eq. (1-36) yields the velocity vector (relative to the larger mass)

$$\dot{\vec{r}} = \left[(1 \pm \gamma_L)\dot{\rho} + \dot{x} - (1 + \nu)y\right] \hat{i} + \left\{(1 + \nu)\left[(1 \pm \gamma_L)(1 + \rho) + x\right] + \dot{y}\right\} \hat{j} + \dot{z}\hat{k} \tag{1-37}$$

The position vector for the smaller finite body is

$$\vec{R} = (1 + \rho)\ \hat{i} \tag{1-38}$$

For a satellite of unit mass, the kinetic energy is $T = \frac{1}{2}\, \dot{\vec{r}} \cdot \dot{\vec{r}}$, and the effective potential energy (for motion relative to the larger mass) is given by

$$\begin{aligned} U &= -\frac{(1 - \mu)}{|\vec{r}|} - \mu\left[\frac{1}{|\vec{r} - \vec{R}|} - \frac{\vec{R} \cdot \vec{r}}{|\vec{R}|^3}\right] \\ &= -\frac{(1 - \mu)}{r_1} - \mu\left\{\frac{1}{r_2} - \frac{\left[(1 \pm \gamma_L)(1 + \rho) + x\right]}{(1 + \rho)^2}\right\} \end{aligned} \tag{1-39}$$

---

*Whenever double signs appear in this section, the upper sign will hold at L_2, and the lower sign at L_1.

$$r_1^2 = \left[(1 \pm \gamma_L)(1 + \rho) + x\right]^2 + y^2 + z^2 \tag{1-40}$$

$$r_2^2 = \left[\gamma_L(1 + \rho) \pm x\right]^2 + y^2 + z^2 \tag{1-41}$$

Forming the Lagrangian $L = T - U$, standard manipulations lead to the equations of motion

$$\begin{aligned}
&\ddot{x} - 2(1 + \nu)\dot{y} + (1 \pm \gamma_L)\ddot{\rho} - \dot{\nu}y \\
&\quad = (1 + \nu)^2\left[(1 \pm \gamma_L)(1 + \rho) + x\right] - \frac{(1 - \mu)}{r_1^3}\left[(1 \pm \gamma_L)(1 + \rho) + x\right] \\
&\qquad \mp \frac{\mu}{r_2^3}\left[\gamma_L(1 + \rho) \pm x\right] - \frac{\mu}{(1 + \rho)^2} \\
&\ddot{y} + 2(1 + \nu)\left[(1 \pm \gamma_L)\dot{\rho} + \dot{x}\right] + \dot{\nu}\left[(1 \pm \gamma_L)(1 + \rho) + x\right] \\
&\quad = (1 + \nu)^2 y - \left[\frac{(1 - \mu)}{r_1^3} + \frac{\mu}{r_2^3}\right] y \\
&\ddot{z} = -\left[\frac{(1 - \mu)}{r_1^3} + \frac{\mu}{r_2^3}\right] z
\end{aligned} \tag{1-42}$$

Expanding Eq. (1-42) in a power series including third-order terms, a moderate amount of algebra leads to*

*The complete series converges in a region that is common to the interiors of two spheres. One sphere is centered at $1 - \mu$ and has a radius of $\sqrt{2}\,(1 \pm \gamma_L)(1 + \rho)$, while the other is centered at μ, and has a radius of $\sqrt{2}\,\gamma_L(1 + \rho)$.

$$\ddot{x} - 2(1 + \nu)\dot{y} = \left[(1 + \nu)^2 + 2(1 + \rho)^{-3}B_L\right]x + \dot{\nu}y$$

$$\mp \frac{3}{2} C_L(1 + \rho)^{-4}\left[2x^2 - (y^2 + z^2)\right]$$

$$+ 2D_L(1 + \rho)^{-5}\left[2x^2 - 3(y^2 + z^2)\right]x$$

$$- (1 \pm \gamma_L)\left\{\ddot{\rho} - (1 + \rho)^{-2}\left[(1 + \nu)^2(1 + \rho)^3 - 1\right]\right\} \quad (1\text{-}43a)$$

$$\ddot{y} + 2(1 + \nu)\dot{x} = -\dot{\nu}x + \left[(1 + \nu)^2 - (1 + \rho)^{-3}B_L\right]y$$

$$\pm 3C_L(1 + \rho)^{-4}xy - \frac{3}{2} D_L(1 + \rho)^{-5}\left[4x^2 - (y^2 + z^2)\right]y$$

$$- (1 \pm \gamma_L)\left[2(1 + \nu)\dot{\rho} + (1 + \rho)\dot{\nu}\right] \quad (1\text{-}43b)$$

$$\ddot{z} = -(1 + \rho)^{-3}B_L z \pm 3C_L(1 + \rho)^{-4}xz$$

$$- \frac{3}{2} D_L(1 + \rho)^{-5}\left[4x^2 - (y^2 + z^2)\right]z \quad (1\text{-}43c)$$

where

$$B_L \equiv \left[\frac{(1 - \mu)}{(1 \pm \gamma_L)^3} + \frac{\mu}{\gamma_L^3}\right] \quad (1\text{-}44)$$

$$C_L \equiv \left[\frac{\mu}{\gamma_L^4} \pm \frac{(1 - \mu)}{(1 \pm \gamma_L)^4}\right] \quad (1\text{-}45)$$

$$D_L \equiv \left[\frac{(1 - \mu)}{(1 \pm \gamma_L)^5} + \frac{\mu}{\gamma_L^5}\right] \quad (1\text{-}46)$$

In Ref. 23, it is shown that $B_L > 1$ for all values of μ. For $\mu \ll 1$, Eqs. (1-30) and (1-31) show that $\mu \cong 3\gamma_L^3$. In this instance, the coefficients defined in Eqs. (1-44) to (1-46) are $B_L \cong 4$, $C_L \cong 3/\gamma_L$, and $D_L \cong 3/\gamma_L^2$.

The accuracy of the derivation can be checked by verifying that the L_1 and L_2 points are equilibrium solutions in the elliptical case. For this to be true, the expressions for ρ and ν given in Eqs. (1-5) and (1-6) must vanish when they are substituted into the final terms of Eqs. (1-43a) and (1-43b). Restricting this verification to the linear terms, it is only necessary to have

$$\begin{aligned} 3\rho - \ddot{\rho} + 2\nu &= 0 \\ 2\dot{\rho} + \dot{\nu} &= 0 \end{aligned} \tag{1-47}$$

It can be seen by inspection that the linear eccentricity terms of Eqs. (1-5) and (1-6) satisfy Eq. (1-47).

A linearized version of Eq. (1-43) is sufficient for many applications. If the quantities ρ and ν are also neglected, Eq. (1-43) reduces to

$$\ddot{x} - 2\dot{y} - (2B_L + 1)x = 0 \tag{1-48a}$$

$$\ddot{y} + 2\dot{x} + (B_L - 1)y = 0 \tag{1-48b}$$

$$\ddot{z} + B_L z = 0 \tag{1-48c}$$

It is readily seen that the motion perpendicular to the xy-plane is simple-harmonic with frequency $\sqrt{B_L}$. The motion in the xy-plane is coupled and the characteristic equation is given by

$$s^4 - (B_L - 2)s^2 - (2B_L + 1)(B_L - 1) = 0 \tag{1-49}$$

This equation possesses two real roots, which are equal in magnitude, but opposite in sign. The two remaining roots are pure imaginaries. Since a positive real root exists, the collinear points are unstable.

2. Equilateral-Triangle Points

The geometry for satellite motion in the vicinity of the equilateral-triangle points is shown in Fig. 1-3. Equations (1-33), (1-34), (1-35), and (1-38) are still valid for this section, and the position and velocity vectors relative to the larger body are*

$$\vec{r} = \left[\frac{1}{2}(1+\rho) + x\right]\hat{i} + \left[\pm\frac{\sqrt{3}}{2}(1+\rho) + y\right]\hat{j} + z\hat{k} \qquad (1\text{-}50)$$

$$\dot{\vec{r}} = \left\{\frac{1}{2}\dot{\rho} + \dot{x} - (1+\nu)\left[\pm\frac{\sqrt{3}}{2}(1+\rho) + y\right]\right\}\hat{i}$$
$$+ \left\{\pm\frac{\sqrt{3}}{2}\dot{\rho} + \dot{y} + (1+\nu)\left[\frac{1}{2}(1+\rho) + x\right]\right\}\hat{j} + \dot{z}\hat{k} \qquad (1\text{-}51)$$

(The position vector relative to the libration point is $\vec{r}_L = x\hat{i} + y\hat{j} + z\hat{k}$.) The kinetic energy $T = \frac{1}{2}\dot{\vec{r}} \cdot \dot{\vec{r}}$ and effective potential energy

$$U = -\frac{(1-\mu)}{r_1} - \mu\left\{\frac{1}{r_2} - \frac{\left[\frac{1}{2}(1+\rho) + x\right]}{(1+\rho)^2}\right\} \qquad (1\text{-}52)$$

where

$$r_1^2 = \left[\frac{1}{2}(1+\rho) + x\right]^2 + \left[\pm\frac{\sqrt{3}}{2}(1+\rho) + y\right]^2 + z^2 \qquad (1\text{-}53)$$

$$r_2^2 = \left[-\frac{1}{2}(1+\rho) + x\right]^2 + \left[\pm\frac{\sqrt{3}}{2}(1+\rho) + y\right]^2 + z^2 \qquad (1\text{-}54)$$

are used to form the Lagrangian $L = T - U$, which leads to the equations of motion:

---

*Whenever double signs appear in this section, the upper sign will hold at L_4, and the lower sign at L_5.

$$\ddot{x} - 2(1 + \nu)\dot{y}$$

$$= -\frac{1}{2}\ddot{\rho} \pm \sqrt{3}(1 + \nu)\dot{\rho}$$

$$\pm \frac{\sqrt{3}}{2}(1 + \rho)\dot{\nu} + \frac{1}{2}(1 + \rho)(1 + \nu)^2 + (1 + \nu)^2 x + \dot{\nu} y$$

$$- \frac{(1 - \mu)}{r_1^3}\left[\frac{1}{2}(1 + \rho) + x\right] - \frac{\mu}{r_2^3}\left[-\frac{1}{2}(1 + \rho) + x\right] - \frac{\mu}{(1 + \rho)^2}$$

$$\ddot{y} + 2(1 + \nu)\dot{x}$$

$$= \mp \frac{\sqrt{3}}{2}\ddot{\rho} - (1 + \nu)\dot{\rho} - \frac{1}{2}(1 + \rho)\dot{\nu} \pm \frac{\sqrt{3}}{2}(1 + \rho)(1 + \nu)^2 - \dot{\nu} x + (1 + \nu)^2 y$$

$$- \left[\frac{(1 - \mu)}{r_1^3} + \frac{\mu}{r_2^3}\right]\left[\pm \frac{\sqrt{3}}{2}(1 + \rho) + y\right]$$

$$\ddot{z} = -\left[\frac{(1 - \mu)}{r_1^3} + \frac{\mu}{r_2^3}\right] z \qquad (1\text{-}55)$$

A power series expansion of Eq. (1-55) including terms up to third order is given by*

$$\ddot{x} - 2(1 + \nu)\dot{y}$$

$$= \left[(1 + \nu)^2 - \frac{1}{4}(1 + \rho)^{-3}\right] x + \left[\dot{\nu} \pm \frac{3\sqrt{3}}{4}(1 - 2\mu)(1 + \rho)^{-3}\right] y$$

$$+ (1 + \rho)^{-4}\left[\frac{21}{16}(1 - 2\mu)x^2 \mp \frac{3\sqrt{3}}{8} xy - \frac{33}{16}(1 - 2\mu)y^2 + \frac{3}{4}(1 - 2\mu)z^2\right]$$

$$- (1 + \rho)^{-5}\left[\frac{37}{32} x^3 \pm \frac{75}{32}\sqrt{3}(1 - 2\mu)x^2 y - \frac{123}{32} xy^2\right.$$

$$\left. \mp \frac{45}{32}\sqrt{3}(1 - 2\mu)y^3 + \frac{3}{8} xz^2 \pm \frac{15\sqrt{3}}{8} yz^2\right]$$

(Equation continued next page)

*The complete series converges in a region that is common to the interiors of two spheres of radii $\sqrt{2}(1 + \rho)$. These spheres are centered at $1 - \mu$ and μ.

$$- \frac{1}{2}\ddot{\rho} \pm \sqrt{3}(1+\nu)\dot{\rho} \pm \frac{\sqrt{3}}{2}(1+\rho)\dot{\nu}$$

$$- \frac{1}{2}(1+\rho)^{-2}\left[1 - (1+\rho)^3(1+\nu)^2\right] \qquad (1\text{-}56a)$$

$$\ddot{y} + 2(1+\nu)\dot{x}$$

$$= \left[\pm \frac{3\sqrt{3}}{4}(1-2\mu)(1+\rho)^{-3} - \dot{\nu}\right] x + \left[(1+\nu)^2 + \frac{5}{4}(1+\rho)^{-3}\right] y$$

$$- (1+\rho)^{-4}\left[\pm \frac{3}{16}\sqrt{3}x^2 + \frac{33}{8}(1-2\mu)xy \pm \frac{9}{16}\sqrt{3}y^2\right.$$

$$\left. \mp \frac{3\sqrt{3}}{4}z^2\right]$$

$$- (1+\rho)^{-5}\left[\pm \frac{25}{32}\sqrt{3}(1-2\mu)x^3 - \frac{123}{32}x^2y \mp \frac{135}{32}\sqrt{3}(1-2\mu)xy^2\right.$$

$$\left. - \frac{3}{32}y^3 \mp \frac{15}{8}\sqrt{3}(1-2\mu)xz^2 - \frac{33}{8}yz^2\right]$$

$$\mp \frac{\sqrt{3}}{2}\ddot{\rho} - (1+\nu)\dot{\rho} - \frac{1}{2}(1+\rho)\dot{\nu}$$

$$\mp \frac{\sqrt{3}}{2}(1+\rho)^{-2}\left[1 - (1+\rho)^3(1+\nu)^2\right] \qquad (1\text{-}56b)$$

$$\ddot{z} = - (1+\rho)^{-3}z + \frac{3}{2}(1+\rho)^{-4}\left[(1-2\mu)x \pm \sqrt{3}y\right]z$$

$$- (1+\rho)^{-5}\left[\frac{3}{8}x^2 \pm \frac{15}{4}\sqrt{3}(1-2\mu)xy + \frac{33}{8}y^2 - \frac{3}{2}z^2\right]z \qquad (1\text{-}56c)$$

Some confidence in the accuracy of this result is attained by noticing that the eccentricity check of the previous section again leads to the conditions given in Eq. (1-47).

If $\rho = \nu = 0$ and only linear terms are retained, Eq. (1-56) is reduced to

$$\ddot{x} - 2\dot{y} - \frac{3}{4}x \mp \frac{3\sqrt{3}}{4}(1-2\mu)y = 0 \qquad (1\text{-}57a)$$

$$\ddot{y} + 2\dot{x} \mp \frac{3\sqrt{3}}{4}(1 - 2\mu)x - \frac{9}{4}y = 0 \tag{1-57b}$$

$$\ddot{z} + z = 0 \tag{1-57c}$$

The coupling of x and y in Eqs. (1-57a) and (1-57b) can be eliminated by a coordinate rotation. This simplification will be useful when feedback controls are considered in a later chapter. The angle for this rotation is conveniently determined by expanding the modified potential function to second order (this is sufficient for linearized equations of motion), and then eliminating the xy term which causes the coupling. The modified potential function to second order is written as

$$W \equiv T_o - U = \frac{1}{2}\left[\left(\frac{1}{2} + x\right)^2 + \left(\pm\frac{\sqrt{3}}{2} + y\right)^2\right] - U$$

$$\cong \frac{1}{2}(3 - \mu) + \frac{3}{8}\left[x^2 \pm 2\sqrt{3}(1 - 2\mu)xy + 3y^2\right] - \frac{1}{2}z^2 \tag{1-58}$$

It is readily verified that the xy term of Eq. (1-58) can be removed by utilizing the coordinate transformation (see Fig. 1-3)*

$$\begin{aligned} x &= x' \cos\psi - y' \sin\psi \\ y &= x' \sin\psi + y' \cos\psi \\ z &= z' \end{aligned} \tag{1-59}$$

where

$$\tan 2\psi = \mp\sqrt{3}(1 - 2\mu) \tag{1-60}$$

With this transformation, Eqs. (1-58) and (1-57) become

$$2W = (3 - \mu) + \alpha x'^2 + \beta y'^2 - z'^2 \tag{1-61}$$

and

*The barycenter lies on the x'-axis.

$$\ddot{x}' - 2\dot{y}' - \alpha x' = 0 \qquad (1\text{-}62a)$$

$$\ddot{y}' + 2\dot{x}' - \beta y' = 0 \qquad (1\text{-}62b)$$

$$\ddot{z}' + z' = 0 \qquad (1\text{-}62c)$$

where

$$\alpha = \frac{3}{2}\left[1 + \sqrt{1 - 3\mu(1 - \mu)}\right] \qquad (1\text{-}63)$$

$$\beta = \frac{3}{2}\left[1 - \sqrt{1 - 3\mu(1 - \mu)}\right] \qquad (1\text{-}64)$$

It can be seen at once that Eq. (1-62c) is simple-harmonic with unit frequency. It is also worth noting that for $\mu \ll 1$, $\alpha \cong 3 - 9\mu/4$, and $\beta \cong 9\mu/4$.

The stability of the linearized equations of motion can be examined by writing the characteristic equation for the gyroscopically-coupled portion of Eq. (1-62)

$$s^4 + s^2 + \alpha\beta = 0 \qquad (1\text{-}65a)$$

or in terms of the mass parameter μ

$$s^4 + s^2 + \frac{27}{4}\mu(1 - \mu) = 0 \qquad (1\text{-}65b)$$

The roots of this equation are pure imaginaries if $\mu < 0.03852...$, and the system is neutrally stable. For $\mu > 0.03852...$, the roots are complex with one pair possessing positive real parts, and the system is unstable.

3. Isosceles-Triangle Points

If a satellite moving in the mutual gravitational field of two finite bodies is equipped with a continuous thrust device, it is possible to artificially generate new equilibrium positions. This generalized libration-point concept was introduced by Dusek,[4] who developed general conditions for the existence of these points, and also examined the

stability of a variable-thrust satellite in their vicinity. In this section, the equations of motion of a satellite at the generalized points which form an isosceles triangle with the two finite bodies are derived. This case was not explicitly treated by Dusek.

The geometry for a general isosceles-triangle point is given in Fig. 1-4. Proceeding in the same manner as in the two previous sections, the position and velocity vectors are

$$\vec{r} = \left[(1 + \rho)\cos\theta + x\right]\hat{i} + \left[(1 + \rho)\sin\theta + y\right]\hat{j} + z\hat{k} \tag{1-66}$$

$$\dot{\vec{r}} = \left\{\dot{\rho}\cos\theta + \dot{x} - (1 + \nu)\left[(1 + \rho)\sin\theta + y\right]\right\}\hat{i} + \left\{\dot{\rho}\sin\theta + \dot{y} + (1 + \nu)\left[(1 + \rho)\cos\theta + x\right]\right\}\hat{j} + \dot{z}\hat{k} \tag{1-67}$$

The potential energy is

$$U = -\frac{(1 - \mu)}{r_1} - \mu\left\{\frac{1}{r_2} - \frac{[(1 + \rho)\cos\theta + x]}{(1 + \rho)^2}\right\} \tag{1-68}$$

where

$$r_1^2 = \left[(1 + \rho)\cos\theta + x\right]^2 + \left[(1 + \rho)\sin\theta + y\right]^2 + z^2 \tag{1-69}$$

$$r_2^2 = \left[(1 + \rho)(\cos\theta - 1) + x\right]^2 + \left[(1 + \rho)\sin\theta + y\right]^2 + z^2 \tag{1-70}$$

This time, the equations of motion are augmented with a planar thrust acceleration (F_{cx}, F_{cy}), and are given by

$$\ddot{x} - 2(1 + \nu)\dot{y}$$

$$= -\ddot{\rho}\cos\theta + 2(1 + \nu)\dot{\rho}\sin\theta + (1 + \rho)\dot{\nu}\sin\theta + (1 + \rho)(1 + \nu)^2\cos\theta + (1 + \nu)^2 x + \dot{\nu} y - \frac{(1 - \mu)}{r_1^3}\left[(1 + \rho)\cos\theta + x\right] - \frac{\mu}{r_2^3}\left[(1 + \rho)(\cos\theta - 1) + x\right] - \frac{\mu}{(1 + \rho)^2} + F_{cx}$$

$$\ddot{y} + 2(1 + \nu)\dot{x}$$

$$= - \ddot{\rho} \sin \theta - 2(1 + \nu)\dot{\rho} \cos \theta - (1 + \rho)\dot{\nu} \cos \theta + (1 + \rho)(1 + \nu)^2 \sin \theta$$

$$- \dot{\nu}x + (1 + \nu)^2 y - \left[\frac{(1 - \mu)}{r_1^3} + \frac{\mu}{r_2^3}\right]\left[(1 + \rho)\sin \theta + y\right] + F_{cy}$$

$$\ddot{z} = - \left[\frac{(1 - \mu)}{r_1^3} + \frac{\mu}{r_2^3}\right] z \qquad (1\text{-}71)$$

with

$$\vec{F}_c \equiv F_{cx}\, \hat{i} + F_{cy}\, \hat{j} \qquad (1\text{-}72)$$

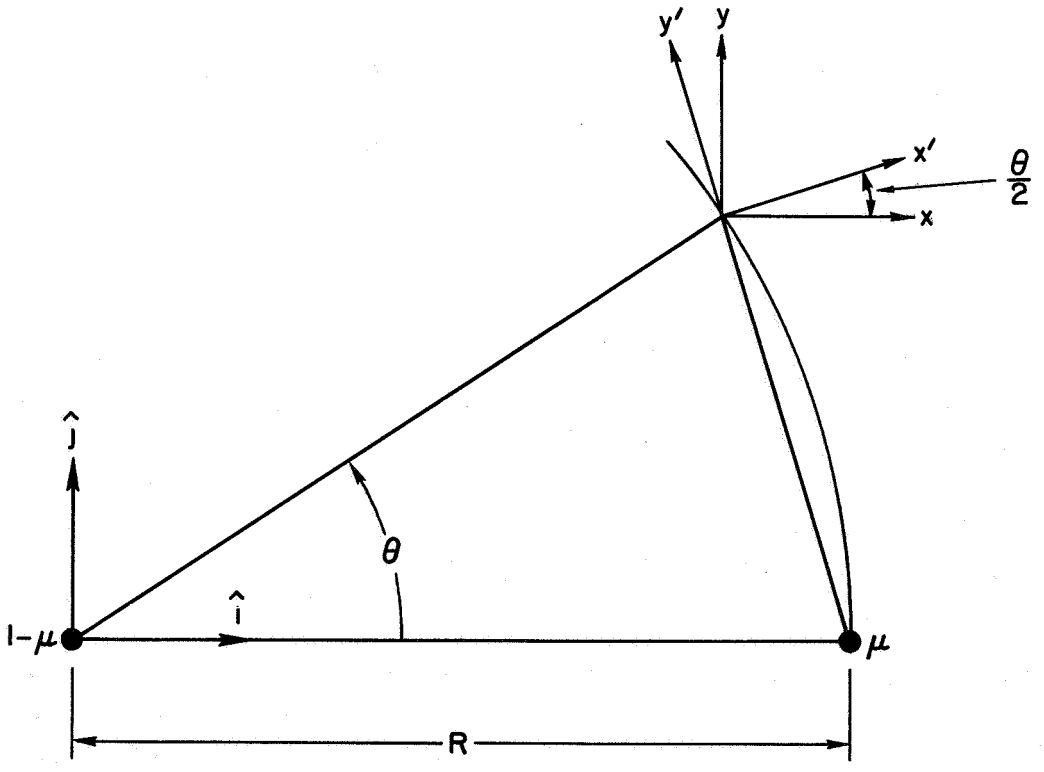

FIG. 1-4. ISOSCELES-TRIANGLE POINT.

From Eq. (1-71), it can be verified that the isosceles-triangle point is an equilibrium solution if*

$$\vec{F}_c = F_c \left[- \sin \frac{\theta}{2} \hat{i} + \cos \frac{\theta}{2} \hat{j} \right] \tag{1-73}$$

where

$$F_c = \frac{\mu}{2(1 + \rho)^2 (1 - \cos \theta)} \left\{ 1 - \left[2(1 - \cos \theta) \right]^{3/2} \right\} \tag{1-74}$$

In Fig. 1-4, it can be seen that this thrust vector is radial with respect to μ. Therefore, a simple coordinate rotation to the (x', y', z') system will uncouple the thrust acceleration terms in Eq. (1-71). Inspection of Fig. 1-4 shows that this coordinate rotation is

$$\begin{aligned} x &= x' \cos \frac{\theta}{2} - y' \sin \frac{\theta}{2} \\ y &= x' \sin \frac{\theta}{2} + y' \cos \frac{\theta}{2} \end{aligned} \tag{1-75}$$

Taking $\rho = \nu = 0$, and using Eqs. (1-72) to (1-75), Eq. (1-71) is expanded in a power series in the (x', y', z') coordinates.** Retaining only linear terms, Eq. (1-71) becomes

$$\ddot{x}' - 2\dot{y}' - h_1(\mu, \theta) x' - \frac{3}{2} \left[(1 - \mu) \sin \theta \right] y' = 0 \tag{1-76a}$$

---

*Equations (1-73) and (1-74) are true so long as ρ and ν are functions of the eccentricity only. In this case, $\ddot{\rho} - (1+\rho)^{-2}[(1+\nu)^2(1+\rho)^3 - 1] = 0$ and $2(1 + \nu)\dot{\rho} + (1 + \rho)\dot{\nu} = 0$. If ρ and ν also depend on gravitational perturbations from other bodies, these relations no longer hold, and Eqs. (1-73) and (1-74) will be more complicated.

**The region of convergence for this series is again a region which is common to the interiors of two spheres centered at $1 - \mu$ and μ. The sphere at $1 - \mu$ has a radius of $\sqrt{2}$, and the sphere at μ has a radius of $2\sqrt{1 - \cos \theta}$.

$$\ddot{y}' + 2\dot{x}' - \frac{3}{2}\left[(1 - \mu)\sin\theta\right]x' - h_2(\mu,\theta)y' = 0 \qquad (1\text{-}76b)$$

$$\ddot{z}' + h_3(\mu,\theta)z' = 0 \qquad (1\text{-}76c)$$

where

$$h_1(\mu,\theta) \equiv \frac{3}{2}(1 + \cos\theta) - \frac{\mu}{2}\left\{1 + 3\cos\theta + 2\left[2(1 - \cos\theta)\right]^{-3/2}\right\} \qquad (1\text{-}77)$$

$$h_2(\mu,\theta) \equiv \frac{3}{2}(1 - \cos\theta) - \frac{\mu}{2}\left\{1 - 3\cos\theta - 4\left[2(1 - \cos\theta)\right]^{-3/2}\right\} \qquad (1\text{-}78)$$

$$h_3(\mu,\theta) \equiv 1 + \mu\left\{\left[2(1 - \cos\theta)\right]^{-3/2} - 1\right\} \qquad (1\text{-}79)$$

The coefficients depending on μ and θ in Eq. (1-76) are shown as functions of θ in Figs. 1-5 and 1-6. Figure 1-5 is drawn for the Earth-Moon system ($\mu = 0.0121507$), and Fig. 1-6 gives the coefficients for the Sun-Earth system ($\mu = 3.0404 \times 10^{-6}$). The thrust accelerations in Earth gravity units ($g \equiv 9.81$ m/sec^2) for these two systems are given in Figs. 1-7 and 1-8.

Since the out-of-plane motion is once again simple-harmonic, the characteristic equation for the coupled portion of Eq. (1-76) is used to determine linear stability. This characteristic equation can be written in the form

$$s^4 + \left[4 - (h_1 + h_2)\right]s^2 + h_1h_2 - \frac{9}{4}(1 - \mu)^2\sin^2\theta = 0 \qquad (1\text{-}80)$$

For a fixed value of μ, all of the roots of Eq. (1-80) are pure imaginaries when $\theta > \theta_c$, and the system is neutrally stable. When $\theta < \theta_c$, the motion is unstable. The approximate values of θ_c for the Earth-Moon and Sun-Earth systems are 38.9° and 2.45°, respectively.

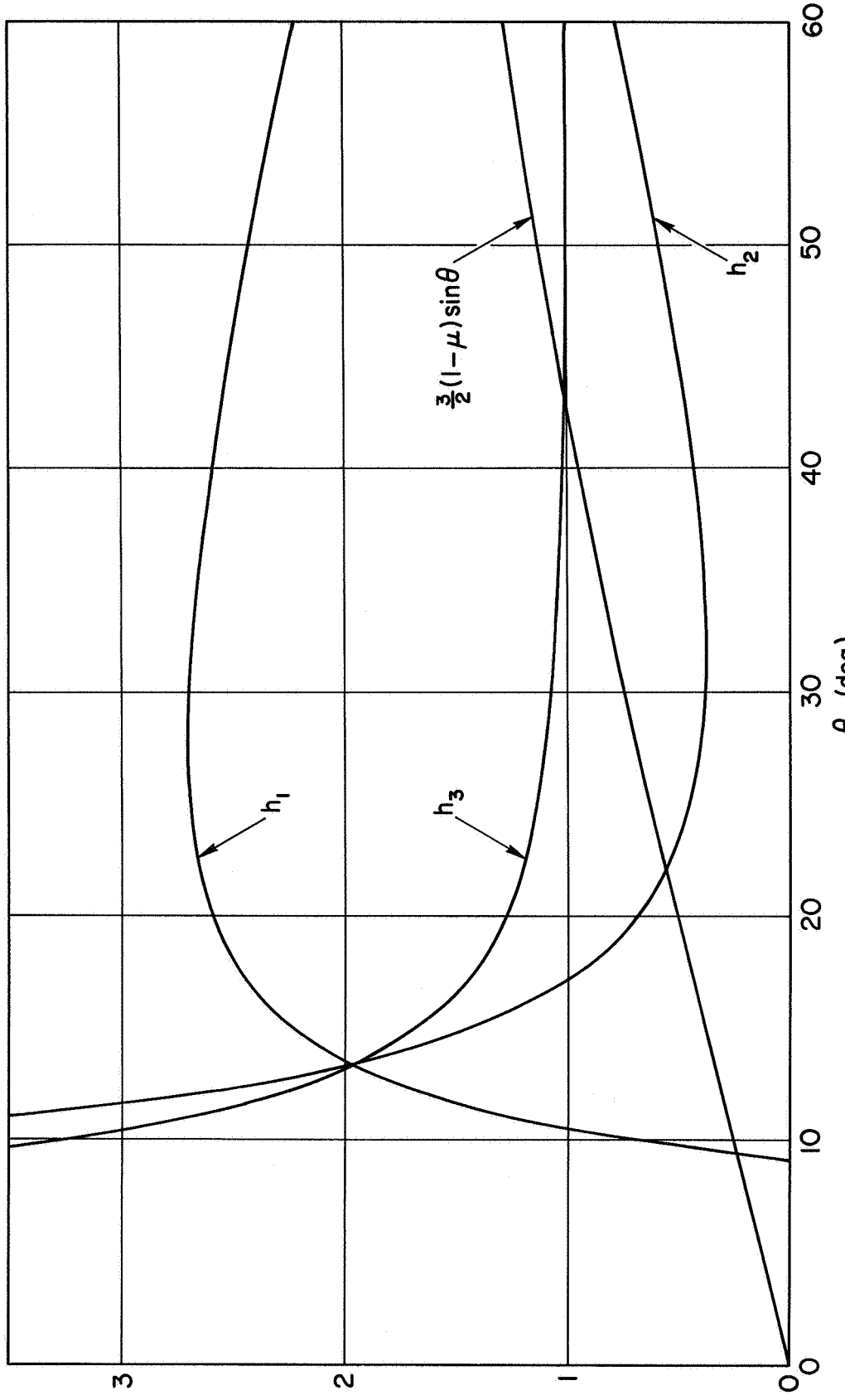

FIG. 1-5. COEFFICIENTS FOR AN ISOSCELES-TRIANGLE POINT IN THE EARTH-MOON SYSTEM.

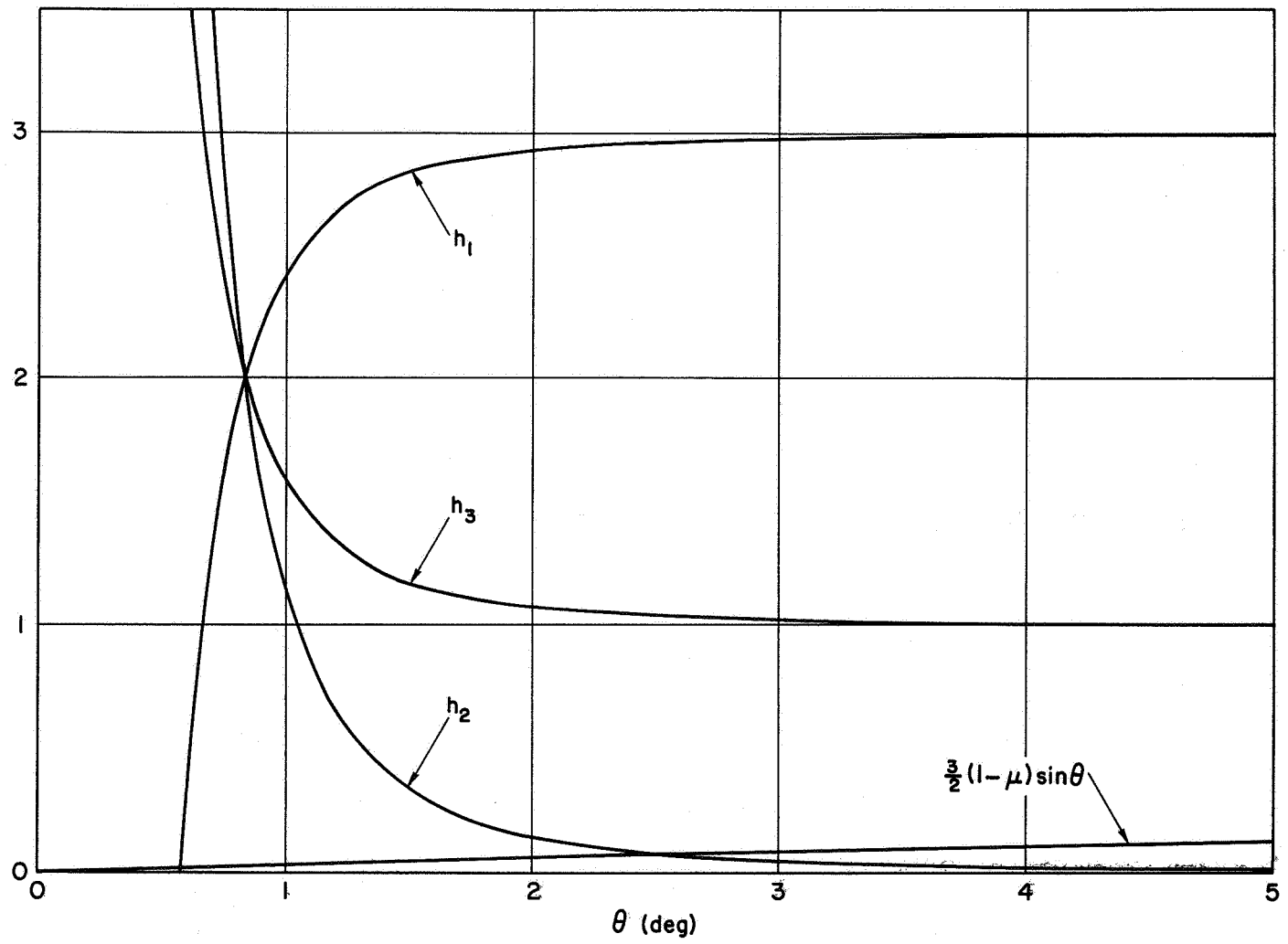

FIG. 1-6. COEFFICIENTS FOR AN ISOSCELES-TRIANGLE POINT IN THE SUN-EARTH SYSTEM.

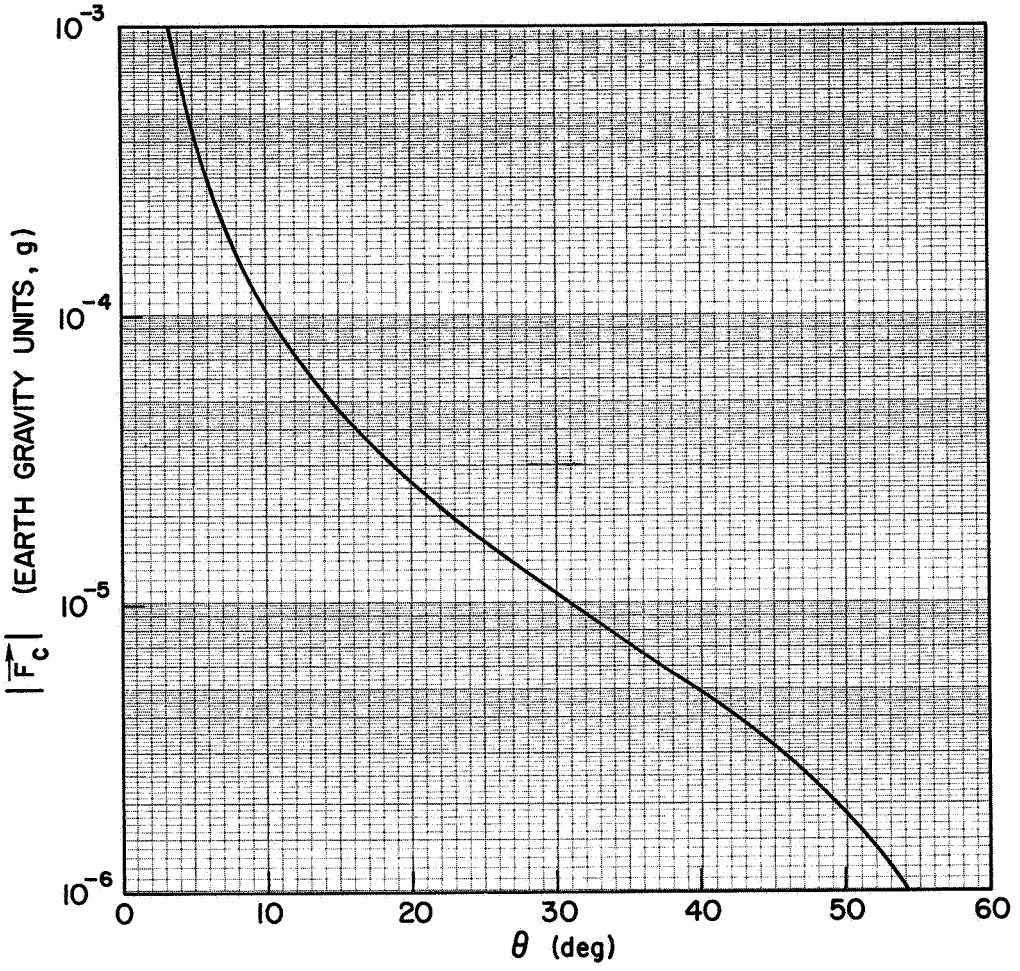

FIG. 1-7. THRUST ACCELERATION FOR AN ISOSCELES-TRIANGLE POINT IN THE EARTH-MOON SYSTEM.

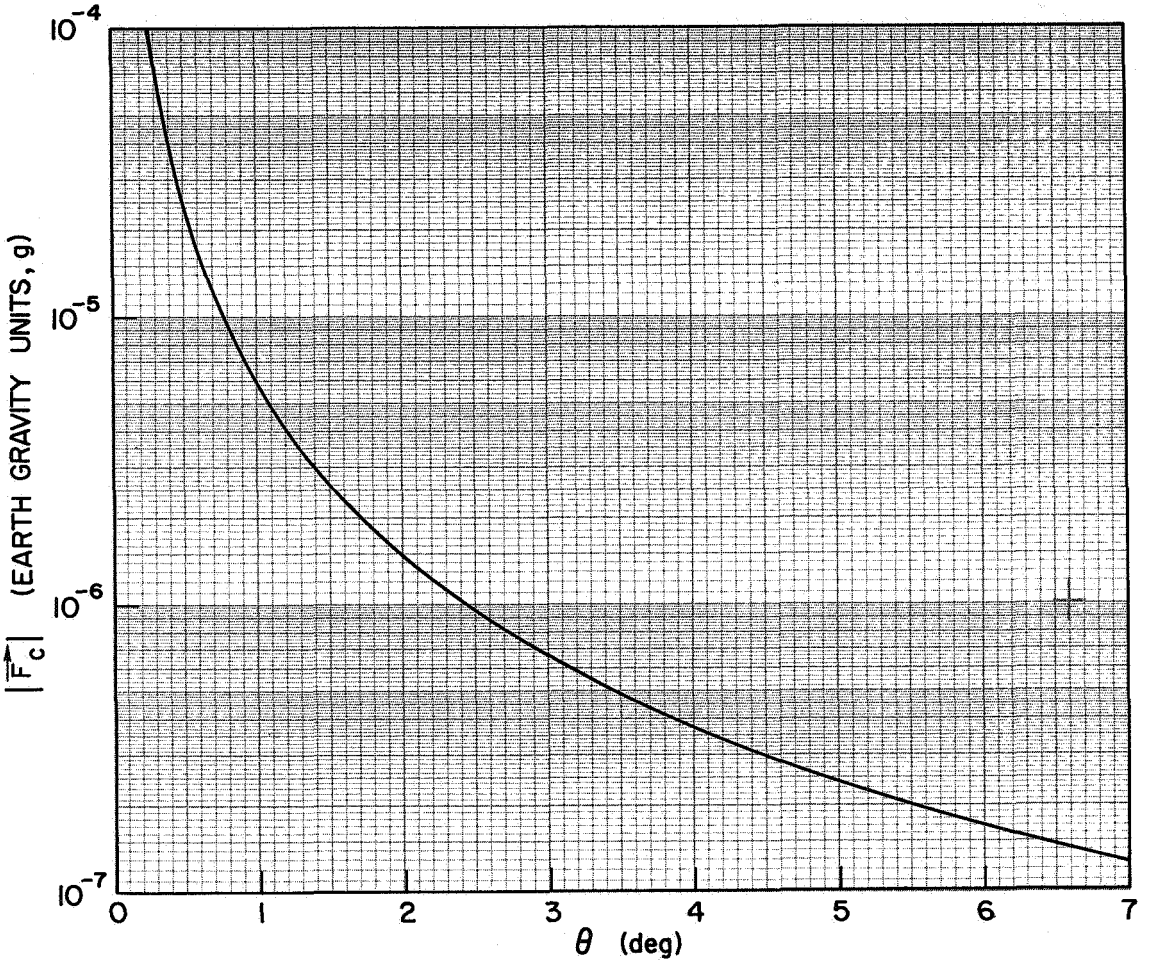

FIG. 1-8. THRUST ACCELERATION FOR AN ISOSCELES-TRIANGLE POINT IN THE SUN-EARTH SYSTEM.

4. Stability of the Linearized Equations of Motion in the Elliptic Case

In Sections 1-3 above, the linear stability investigation was limited to the special case, $\rho = \nu = 0$. For the more realistic situation, where the two finite bodies describe elliptic orbits, the linearized equations of motion possess periodic coefficients, and the stability test is more involved. A brief summary of some results for this problem is given below. The results of Bennett[24,25] are quoted here, since he investigated all five of the classical libration points. It should be noted that the stability results for the equilateral-triangle points were originally found by Colombo, et al.,[26] for the Earth-Moon system, and later by Danby[27] for the general case.

In his first paper,[24] Bennett used Floquet theory to examine the stability of the five classical libration points. For the collinear points, he found that the degree of instability increased with larger eccentricity. His results for the equilateral-triangle points are shown in Fig. 1-9.

Bennett's second paper[25] gives an analytical method for finding a characteristic root λ as a power series in the eccentricity; i.e., $\lambda = \lambda_o + \lambda_1 e + \lambda_2 e^2 + \ldots$, where λ_o is the root for the circular problem. This paper proves that $\lambda_1 = 0$, which shows that the first correction to a characteristic root is proportional to the square of the eccentricity. For most of the systems which are considered in the present research, the correction will be very small, and will usually be neglected.

C. Numerical Data for Some of the Collinear Points in the Solar System

In this section, numerical data for the L_1 and L_2 points of several Sun-planet and planet-satellite configurations are presented. This data will be needed to apply general results to certain Solar System points. It is important to note that although the derived parameters are given with several significant figures for consistency, their accuracy is really limited by the errors in the adopted constants.

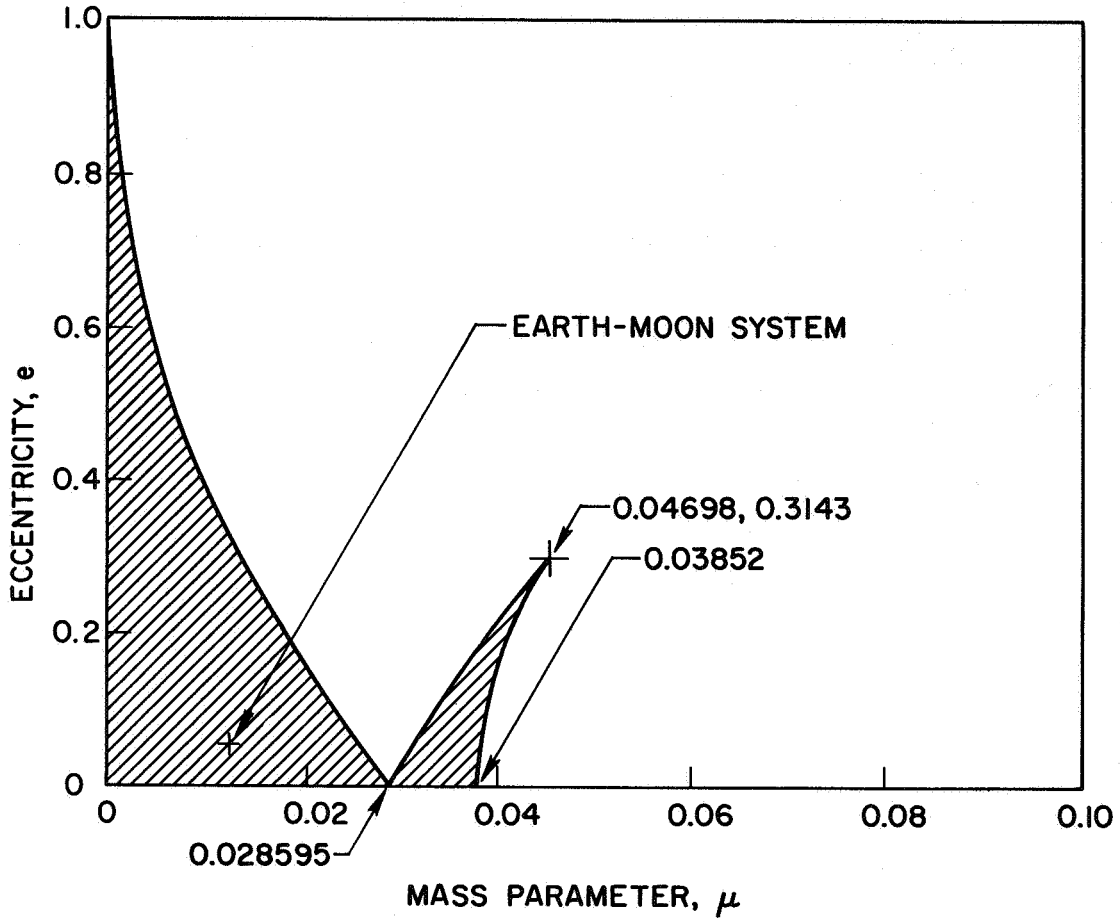

FIG. 1-9. STABILITY CHART FOR THE EQUILATERAL-TRIANGLE POINTS.[24] (Stable region is cross-hatched).

1. Mass-Ratio Dependent Quantities

The derived constants in Tables 1-1 to 1-3 depend on only one physical parameter: the mass ratio of the two finite bodies. The values for the mass ratios listed in column 1 of Table 1-1 were obtained from Ref. 28* with the exception of the following:

(1) Mercury: This constant is so poorly known that three values are used here to bracket its probable range. Recent estimates can be found in Refs. 29-31.

(2) Venus: Mariner-2 data.[32]

*Original sources are given in this reference.

(3) Earth: NASA Ad Hoc Standards Committee.[33]

(4) Earth + Moon: Derived from adopted values for $M_\odot/M_\oplus$ and $M_\oplus/M_\mathbb{D}$.

(5) Mars: Mariner-4 data.[34]

(6) Moon: Mariner-2 data.[32]

Columns 3 and 4 of Table 1-1 were obtained directly from Eqs. (1-27) and (1-28), respectively.

In Table 1-2, columns 1 and 2 were computed from Eq. (1-44), and columns 3 and 4 were found by using Eq. (1-45). The coefficient D_L defined in Eq. (1-46) was not included in this table, since B_L and C_L are sufficient for most applications. However, some representative values for D_L are

(1) Earth + Moon: $D_{L1} = 30,240 \quad D_{L2} = 29,243$

(2) Moon: $D_{L1} = 157.355 \quad D_{L2} = 91.7003$

The roots of the characteristic equation at L_1 and L_2, Eq. (1-49), are listed in Table 1-3. It should be recalled that there are two pairs of roots for each point which are equal in magnitude, but opposite in sign.

2. Conversion Factors for Normalized Units

Since virtually all general results will be presented in the normalized units which were introduced in Section A-1, a set of conversion factors will be needed to apply these results to specific systems. The conversion factors for length and angular rate are listed in columns 1 and 3 of Table 1-4. Manipulation of these two constants leads to the conversion factors for time, velocity, and acceleration given in Table 1-5. To convert a normalized quantity to ordinary units simply multiply by the appropriate factor. For example, if the normalized acceleration of an artificial satellite in the Earth-Moon system is given as $F = 1.186 \times 10^{-4}$, use of Table 1-5 gives

$$F = (1.186 \times 10^{-4}) \times (2.77611 \times 10^{-4} \text{ g}) = 3.292 \times 10^{-8} \text{ g}.$$

Multiplication of the distance ratios in Table 1-1 by the appropriate length factor furnishes the values in columns 1 and 2 of Table 1-6, which give the mean distances between the center of the smaller finite body and the collinear points. Comparison of columns 2 and 3 for the planet-satellite systems shows that the L_1 and L_2 points are sometimes located very close to the satellite's surface. The variation of the libration point distance due to the orbital eccentricity is given for a few systems in columns 1-4 of Table 1-7.

3. Comparison of L_2 Distance and Extent of Planetary Shadow

It is interesting to compare the distances of the apex of a planet's shadow cone and its L_2 point. The mean distance between a planet and the apex of its geometrical shadow cone is given by

$$d_s = \frac{a}{(R_\odot/R_p - 1)} \qquad (1\text{-}81)$$

where a is the semi-major axis of the planet's orbit, R_p is the planet's radius, and $R_\odot = 6.957 \times 10^5$ km (Ref. 28). Equation (1-81) was used to compute the planetary shadow distances given in column 4 of Table 1-8. The assumed values for the planetary radii are listed in column 1, and were obtained from Ref. 28 with the exception of the following:

(1) Mercury: Ref. 35
(2) Venus: Ref. 36
(3) Mars: Mariner-4 data.[37]

By comparing columns 3 and 4 of Table 1-8,* it can be seen that the L_2 point is located beyond the planetary shadow cone for Mercury, Venus, and Earth. To an observer placed at any of the L_2 points for these planets, the Sun would always be partially eclipsed. At the L_2 points of Mars, Jupiter, Saturn, Uranus, and Neptune, the Sun is totally

*A comparison of the mean distances is sufficient, since both distances fluctuate in the same manner for elliptical orbits.

eclipsed (neglecting atmospheric refraction). A "critical" planetary radius, which would make the length of the planetary shadow equal to the L_2 distance, is given in column 2.

Table 1-1 MASS PARAMETERS AND DISTANCE RATIOS

Planet	1	2	3	4
	Mass Ratio $(M_\odot/M_p)$	μ	γ_{L1}	γ_{L2}
Mercury - 1	5.5×10^{6}	1.8182×10^{-7}	3.9229×10^{-3}	3.9331×10^{-3}
Mercury- 2	6.0×10^{6}	1.6667×10^{-7}	3.8109×10^{-3}	3.8206×10^{-3}
Mercury - 3	6.5×10^{6}	1.5385×10^{-7}	3.7106×10^{-3}	3.7198×10^{-3}
Venus	4.0859×10^{5}	2.4474×10^{-6}	9.3148×10^{-3}	9.3730×10^{-3}
Earth	3.32951×10^{5}	3.0034×10^{-6}	9.9704×10^{-3}	1.0037×10^{-2}
Earth + Moon	3.28906×10^{5}	3.0404×10^{-6}	1.0011×10^{-2}	1.0078×10^{-2}
Mars	3.098×10^{6}	3.2279×10^{-7}	4.7487×10^{-3}	4.7640×10^{-3}
Jupiter	1.04736×10^{3}	9.5387×10^{-4}	6.6680×10^{-2}	6.9784×10^{-2}
Saturn	3.4997×10^{3}	2.8566×10^{-4}	4.4962×10^{-2}	4.6351×10^{-2}
Uranus	2.29×10^{4}	4.3666×10^{-5}	2.4216×10^{-2}	2.4613×10^{-2}
Neptune	1.889×10^{4}	5.2935×10^{-5}	2.5806×10^{-2}	2.6258×10^{-2}

(Sun-Planet Systems)

Satellite	1	2	3	4
	Mass Ratio (M_{sat}/M_p)	μ	γ_{L1}	γ_{L2}
Moon	81.30*	1.21507×10^{-2}	0.150935	0.167833
Io	3.81×10^{-5}	3.8099×10^{-5}	0.023148	0.023511
Europa	2.48×10^{-5}	2.4799×10^{-5}	0.020083	0.020355
Ganymede	8.17×10^{-5}	8.1693×10^{-5}	0.029781	0.030385
Callisto	5.09×10^{-5}	5.0897×10^{-5}	0.025474	0.025914
Mimas	6.68×10^{-8}	6.6800×10^{-8}	0.0028107	0.0028160
Enceladus	1.51×10^{-7}	1.5100×10^{-7}	0.0036877	0.0036967
Rhea	4×10^{-6}	4.0000×10^{-6}	0.010966	0.011047
Titan	2.48×10^{-4}	2.4794×10^{-4}	0.042920	0.044184
Triton	1.28×10^{-3}	1.2784×10^{-3}	0.073339	0.077111

*$M_\oplus/M_\mathbb{D}$

(Planet-Satellite Systems)

Table 1-2 CONSTANTS FOR EQUATIONS OF MOTION
[see Eq. (1-43)]

Planet	1	2	3	4
	B_{L1}	B_{L2}	C_{L1}	C_{L2}
Mercury - 1	4.0237	3.9766	766.74	760.75
Mercury - 2	4.0230	3.9772	789.23	783.22
Mercury - 3	4.0224	3.9778	810.48	804.48
Venus	4.0568	3.9446	324.07	318.07
Earth	4.0608	3.9408	302.89	296.89
Earth + Moon	4.0611	3.9405	301.67	295.67
Mars	4.0287	3.9716	633.75	627.75
Jupiter	4.4462	3.6228	46.933	40.984
Saturn	4.2905	3.7412	68.699	62.721
Uranus	4.1512	3.8580	125.88	119.89
Neptune	4.1616	3.8489	118.24	112.25

(Sun-Planet Systems)

Satellite	1	2	3	4
	B_{L1}	B_{L2}	C_{L1}	C_{L2}
Moon	5.14760	3.19042	21.5117	15.8451
Io	4.1443	3.8642	131.59	125.60
Europa	4.1246	3.8818	151.38	145.38
Ganymede	4.1877	3.8263	102.72	96.734
Callisto	4.1594	3.8508	119.76	113.77
Mimas	4.0169	3.9832	1069.4	1063.4
Enceladus	4.0223	3.9780	815.53	809.52
Rhea	4.0670	3.9349	275.57	269.57
Titan	4.2764	3.7525	71.876	65.896
Triton	4.4960	3.5873	42.835	36.898

(Planet-Satellite Systems)

Table 1-3 ROOTS OF CHARACTERISTIC EQUATION
[see Eq. (1-49)]

Planet	1	2	3	4
	Roots for L_1		Roots for L_2	
	Real	Imaginary	Real	Imaginary
Mercury - 1	2.5178	2.0774	2.4989	2.0659
Mercury - 2	2.5175	2.0772	2.4991	2.0660
Mercury - 3	2.5173	2.0771	2.4994	2.0662
Venus	2.5309	2.0854	2.4860	2.0580
Earth	2.5326	2.0864	2.4844	2.0571
Earth + Moon	2.5327	2.0865	2.4843	2.0570
Mars	2.5198	2.0786	2.4969	2.0647
Jupiter	2.6811	2.1777	2.3521	1.9772
Saturn	2.6222	2.1413	2.4022	2.0073
Uranus	2.5682	2.1082	2.4507	2.0366
Neptune	2.5723	2.1107	2.4469	2.0343

(Sun-Planet Systems)

Satellite	1	2	3	4
	Roots for L_1		Roots for L_2	
	Real	Imaginary	Real	Imaginary
Moon	2.93206	2.33439	2.15867	1.86265
Io	2.5655	2.1065	2.4532	2.0381
Europa	2.5577	2.1018	2.4604	2.0425
Ganymede	2.5824	2.1169	2.4376	2.0287
Callisto	2.5714	2.1102	2.4477	2.0348
Mimas	2.5151	2.0757	2.5015	2.0675
Enceladus	2.5172	2.0770	2.4994	2.0662
Rhea	2.5350	2.0879	2.4820	2.0556
Titan	2.6167	2.1380	2.4069	2.0102
Triton	2.6997	2.1892	2.3368	1.9681

(Planet-Satellite Systems)

Table 1-4 ORBITAL CONSTANTS

Planet	1a	1b	2	3
	Semi-Major Axis a		Eccentricity e	Mean Motion n (rad/sec)
	(A.U.)*	(km)		
Mercury	0.387099	5.7910×10^{7}	0.20563	8.2668×10^{-7}
Venus	0.723332	1.0821×10^{8}	0.00679	3.2364×10^{-7}
Earth + Moon	1.000000	1.4960×10^{8}	0.01673	1.9910×10^{-7}
Mars	1.523691	2.2794×10^{8}	0.09337	1.0586×10^{-7}
Jupiter	5.203705	7.7847×10^{8}	0.04863	1.6780×10^{-8}
Saturn	9.580337	1.4332×10^{9}	0.05099	6.7152×10^{-9}
Uranus	19.14103	2.8635×10^{9}	0.04579	2.3775×10^{-9}
Neptune	30.19825	4.5176×10^{9}	0.00456	1.1998×10^{-9}

*A.U. = 1.49599×10^{8} km: Mariner-2 data[32]

(Sun-Planet Systems)

Satellite	1	2	3
	Mean Distance from Planet a (km)	Eccentricity e	Mean Motion n (rad/sec)
Moon	3.84405×10^{5}	0.05490	2.66170×10^{-6}
Io	4.216×10^{5}	0.0000	4.1106×10^{-5}
Europa	6.708×10^{5}	0.0003	2.0478×10^{-5}
Ganymede	1.070×10^{6}	0.0015	1.0164×10^{-5}
Callisto	1.882×10^{6}	0.0075	4.3575×10^{-6}
Mimas	1.854×10^{5}	0.0201	7.7165×10^{-5}
Enceladus	2.379×10^{5}	0.00444	5.3073×10^{-5}
Rhea	5.267×10^{5}	0.00098	1.6098×10^{-5}
Titan	1.221×10^{6}	0.02890	4.5607×10^{-6}
Triton	3.534×10^{5}	0.000	1.2374×10^{-5}

(Planet-Satellite Systems)

Table 1-5 CONVERSION FACTORS FOR NORMALIZED UNITS

Planet	1	2	3	4
	Time (days)	Velocity (m/sec)	Acceleration	
			(m/sec^2)	(g)
Mercury	14.001	4.7872×10^{4}	3.9575×10^{-2}	4.0342×10^{-3}
Venus	35.762	3.5021×10^{4}	1.1334×10^{-2}	1.1554×10^{-3}
Earth + Moon	58.132	2.9785×10^{4}	5.9301×10^{-3}	6.0450×10^{-4}
Mars	109.34	2.4130×10^{4}	2.5543×10^{-3}	2.6038×10^{-4}
Jupiter	689.73	1.3063×10^{4}	2.1920×10^{-4}	2.2345×10^{-5}
Saturn	1723.6	9.6243×10^{3}	6.4629×10^{-5}	6.5881×10^{-6}
Uranus	4868.1	6.8081×10^{3}	1.6187×10^{-5}	1.6500×10^{-7}
Neptune	9646.7	5.4202×10^{3}	6.5031×10^{-6}	6.6291×10^{-8}

(Sun-Planet Systems)

Satellite	1	2	3	4
	Time (days)	Velocity (m/sec)	Acceleration	
			(m/sec^2)	(g)
Moon	4.34838	1.02317×10^{3}	2.72336×10^{-3}	2.77611×10^{-4}
Io	0.28157	1.7330×10^{4}	7.1237×10^{-1}	7.2617×10^{-2}
Europa	0.56519	1.3737×10^{4}	2.8131×10^{-1}	2.8675×10^{-2}
Ganymede	1.1387	1.0876×10^{4}	1.1055×10^{-1}	1.1269×10^{-2}
Callisto	2.6561	8.2008×10^{3}	3.5735×10^{-2}	3.6427×10^{-3}
Mimas	0.14999	1.4306×10^{4}	1.1040	1.1253×10^{-1}
Enceladus	0.21808	1.2626×10^{4}	6.7011×10^{-1}	6.8309×10^{-2}
Rhea	0.71898	8.4787×10^{3}	1.3649×10^{-1}	1.3913×10^{-2}
Titan	2.5378	5.5686×10^{3}	2.5396×10^{-2}	2.5888×10^{-3}
Triton	0.93533	4.3731×10^{3}	5.4114×10^{-2}	5.5162×10^{-3}

(Planet-Satellite Systems)

Table 1-6 DISTANCE BETWEEN THE SMALLER FINITE BODY AND A COLLINEAR POINT

Planet	1a	1b	2a	2b
	Mean Distance between Planet and L_1		Mean Distance between Planet and L_2	
	(A.U.)	(km)	(A.U.)	(km)
Mercury - 1	0.001519	2.2717×10^5	0.001523	2.2777×10^5
Mercury - 2	0.001475	2.2069×10^5	0.001479	2.2125×10^5
Mercury - 3	0.001436	2.1488×10^5	0.001440	2.1541×10^5
Venus	0.006738	1.0079×10^6	0.006780	1.0142×10^6
Earth	0.009970	1.4916×10^6	0.010037	1.5015×10^6
Earth + Moon	0.010011	1.4976×10^6	0.010078	1.5077×10^6
Mars	0.007236	1.0824×10^6	0.007259	1.0859×10^6
Jupiter	0.34699	5.1909×10^7	0.36314	5.4325×10^7
Saturn	0.43075	6.4439×10^7	0.44406	6.6431×10^7
Uranus	0.46352	6.9342×10^7	0.47112	7.0480×10^7
Neptune	0.77931	1.1658×10^8	0.79295	1.1863×10^8

(Sun-Planet Systems)

Satellite	1	2	3
	Mean Distance between Satellite and L_1 (km)	Mean Distance between Satellite and L_2 (km)	Radius of Satellite (km)
Moon	58,020	64,516	1,738
Io	9,759	9,912	1,620
Europa	13,471	13,654	1,415
Ganymede	31,866	32,511	2,450
Callisto	47,942	48,770	2,285
Mimas	521	522	350?
Enceladus	877	879	<470
Rhea	5,776	5,818	675
Titan	52,405	53,949	2,475
Triton	25,918	27,251	2,250

(Planet-Satellite Systems)

Table 1-7 DISTANCE VARIATION BETWEEN THE SMALLER FINITE BODY AND A COLLINEAR POINT

Body	1*	2*	3*	4*
	Min. Distance between Body and L_1 (km)	Max. Distance between Body and L_1 (km)	Min. Distance between Body and L_2 (km)	Max. Distance between Body and L_2 (km)
Moon	54,835	61,205	60,974	68,058
Mercury - 2	1.7531×10^5	2.6607×10^5	1.7576×10^5	2.6674×10^5
Earth + Moon	1.4726×10^6	1.5227×10^6	1.4825×10^6	1.5329×10^6
Mars	9.8137×10^5	1.1835×10^6	9.8449×10^5	1.1873×10^6
Jupiter	4.9384×10^7	5.4433×10^7	5.1683×10^7	5.6967×10^7

*$d_{min} = d(1 - e)$, $d_{max} = d(1 + e)$

Table 1-8 L_2 DISTANCE AND EXTENT OF PLANETARY SHADOW

Planet	1	2	3	4
	Mean Radius of Planet (km)	Critical Radius of Planet (km)	Mean Distance between Planet and L_2 (km)	Mean Distance between Planet and Apex of Shadow (km)
Mercury - 1	2,480	2,725.6	2.2777×10^5	2.0717×10^5
Mercury - 2	2,480	2,647.8	2.2125×10^5	2.0717×10^5
Mercury - 3	2,480	2,578.3	2.1541×10^5	2.0717×10^5
Venus	6,120*	6,460.2	1.0142×10^6	9.6036×10^5
Earth	6,371	6,913.4	1.5015×10^6	1.3826×10^6
Earth + Moon	6,371	6,941.4	1.5077×10^6	1.3826×10^6
Mars	3,390	3,298.5	1.0859×10^6	1.1162×10^6
Jupiter	69,750	45,382.0	5.4325×10^7	8.6745×10^7
Saturn	58,170	30,818.1	6.6431×10^7	1.3077×10^8
Uranus	23,750	16,712.2	7.0480×10^7	1.0121×10^8
Neptune	22,400	17,800.5	1.1863×10^8	1.5030×10^8

*Radius taken to top of cloud layer.

Chapter II

PERTURBATIONS AND NOMINAL PATH CONTROL

The restricted three-body model for the motion of a libration-point satellite is an idealization of the true physical situation. A more realistic model must account for the gravitational perturbations of other bodies and solar radiation pressure. In this chapter, the effect of these disturbances on a libration-point satellite is considered in some detail. Quantitative results are given for a few specific cases, and the concept of nominal path control is introduced.

A. Additional Accelerations Acting on a Libration-Point Satellite

1. Gravitational Perturbations

The analysis of the motion of a libration-point satellite is more intricate when gravitational perturbations of another finite body are introduced. The addition of this fourth body affects the motion of the other finite bodies, as well as the satellite, and great care must be taken to use a proper mathematical model. A recent discussion of certain models for a "restricted four-body problem" has been given by Mohn and Kevorkian.[38]

When Brown and Shook[39] calculated the perturbations of a Trojan asteroid* by Saturn, they found that the indirect effect produced by Saturn in altering Jupiter's motion was greater than its direct effect. This case is typical of perturbations of this type, and the examples given below show that direct and indirect effects are usually comparable.

2. Solar Radiation Pressure

The magnitude and direction of the acceleration caused by solar radiation pressure is somewhat random for a non-oriented satellite with an odd geometrical shape, and variable reflectivity, absorptivity, and transmissibility properties. However, for an attitude-controlled

*The Trojan asteroids are located in the vicinity of the equilateral-triangle points of the Sun-Jupiter system.

satellite with a simple configuration and uniform surface properties, the variation of this acceleration is largely predictable. Although this chapter views radiation pressure as an undesirable perturbation, it will be seen in Chapters IV and V that this effect could be used advantageously for satellite position control.

The magnitude of the acceleration acting on a plane surface, of mass m is given by*

$$K_p = C_p \left(\frac{A_s}{m}\right)\left(\frac{p_\oplus}{d_s^2}\right) \qquad (2\text{-}1)$$

where $p_\oplus$ is the solar pressure at 1 AU from the Sun (using the solar constant given in Ref. 12, $p_\oplus = 4.50 \times 10^{-6}$ newtons/m^2), d_s is the distance from the Sun in AU, A_s is the area of the plane surface, and C_p is a coefficient which depends on the surface properties. For a perfect absorber (black body), $C_p = 1$, while a value of $C_p = 2$ corresponds to a perfect reflector. The area-to-mass ratios range from about 0.001 m^2/kg for a very dense satellite to 0.1 m^2/kg for a satellite with very large solar panels. Assuming an average value of $(A_s/m) = 0.01$ m^2/kg, and taking $C_p = 2$, $d_s = 1$ AU, the acceleration due to radiation pressure is roughly $K_p = 9.17 \times 10^{-9}$ g.

3. Thrust Control

Satellite position control is usually achieved with low-thrust devices. These devices could be cold-gas jets, ion thrustors, resisto-jets, or some other suitable system. The thrust may be applied either continuously or discontinuously, depending on the control requirements. Detailed analyses of the controlled motion of a libration-point satellite are presented in the remaining chapters.

B. Control about Nominal Path

Although the concept introduced in this section is applicable to all of the libration points, the discussion here will be limited to the

*It is assumed that the incident solar radiation is perpendicular to the plane surface.

collinear points. The modification of this technique for the other points is straightforward.

1. Basic Strategy

The addition of perturbation and control terms to the linearized equations of motion at the collinear points, Eq. (1-48), gives

$$\ddot{x} - 2\dot{y} - (2B_L + 1)x = P_x(t) + F_{cx} \tag{2-2a}$$

$$\ddot{y} + 2\dot{x} + (B_L - 1)y = P_y(t) + F_{cy} \tag{2-2b}$$

$$\ddot{z} + B_L z = P_z(t) + F_{cz} \tag{2-2c}$$

where $\vec{P}(t)$ is a periodic perturbing acceleration, and $\vec{F}_c$ is a control acceleration. Due to the natural instability of a satellite in the vicinity of a collinear libration point, some thrust control for station-keeping will always be necessary. Additional thrust control could be used to cancel the perturbing acceleration. However, it is more economical to control about a suitable periodic perturbed-path. This "nominal path" is determined by simply solving for the forced response of Eq. (2-2) with $\vec{F}_c = 0$. The forced response to a sinusoidal input is well defined, except for exact resonance, even though the uncontrolled system, being unstable, has no steady-state response. Denoting the nominal path by (x_n, y_n, z_n), and using the coordinate transformation

$$\begin{aligned} \xi &= x - x_n \\ \eta &= y - y_n \\ \zeta &= z - z_n \end{aligned} \tag{2-3}$$

the equations of motion relative to the nominal path are

$$\ddot{\xi} - 2\dot{\eta} - (2B_L + 1)\xi = F_{cx}$$

$$\ddot{\eta} + 2\dot{\xi} + (B_L - 1)\eta = F_{cy} \qquad (2\text{-}4)$$

$$\ddot{\zeta} + B_L\zeta = F_{cz}$$

which is identical to Eq. (2-2) with $\vec{P}(t)$ absent. This result could have been stated earlier by simply using the principle of linear superposition.

The foregoing development is an approximation which is strictly valid only so long as the nominal path is very small. Equations of motion relative to a moderately large nominal path are derived below.

2. Periodic Orbits

It is well known that families of unstable periodic orbits can exist in the vicinity of the collinear libration points.[1] To satisfy certain mission constraints, it is sometimes necessary to insert a satellite into one of these orbits. For moderate-amplitude orbits located in the xy-plane, a good approximation can be obtained from Eqs. (2-2a) and (2-2b) with $\vec{P}(t) = \vec{F}_c = 0$. If certain initial conditions are satisfied, only the oscillatory mode is excited, and the satellite will follow a periodic orbit about the libration point, as shown in Fig. 2-1.

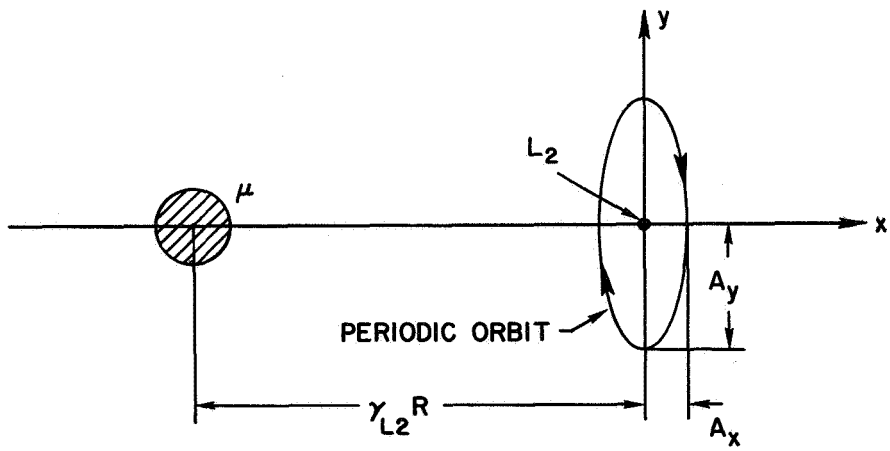

FIG. 2-1. PERIODIC ORBIT AROUND A COLLINEAR POINT.

The equations for this orbit are[1]

$$x_n = A_x \sin \omega_n t$$
$$y_n = A_y \cos \omega_n t \qquad (2\text{-}5)$$

where

$$A_x = \frac{2\omega_n}{\omega_n^2 + (2B_L + 1)} A_y \equiv kA_y \qquad (2\text{-}6)$$

and ω_n is the magnitude of an imaginary root of Eq. (1-49). It should be noted here that Eq. (2-5) is only a first approximation to the true orbit, and higher-order corrections are introduced when nonlinearities, eccentricity, and perturbations are taken into account. The corrected orbit is still bounded, but it is only quasi-periodic.

3. Higher-Order Corrections for a Periodic Orbit

The determination of the corrections to the orbit of Eq. (2-5) is a tedious and lengthy process. Fortunately, the computation of a few higher-order terms is usually sufficient, since the remaining small accelerations do not significantly add to the station-keeping cost. In this section, only second-order terms are considered. Although the corrections may be quite small, the station-keeping cost could be significantly increased if they are disregarded.

The method of successive approximations[40] can be used to determine the second-order correction to a periodic orbit around a collinear point. The equations of the corrected orbit to second order can be written in the form

$$x_n = x_{n1} + x_{n2}$$
$$y_n = y_{n1} + y_{n2} \qquad (2\text{-}7)$$

where x_{n1} and y_{n1} are given by Eq. (2-5). That is,

$$x_{n1} = A_{x1} \sin \omega_n t$$
$$y_{n1} = A_{y1} \cos \omega_n t \qquad (2\text{-}8)$$

with $A_{x1} = kA_{y1}$. Substitution of Eq. (2-7) into Eqs. (1-43a) and (1-43b) with $\vec{P}(t)$ included, and deletion of all terms higher than second order, yields two coupled linear differential equations for x_{n2} and y_{n2}. A_{y1}, ρ, ν, and $\vec{P}(t)$ are treated as first-order quantities, and coupling between the eccentricity and gravitational perturbations is neglected. With these restrictions, the second-order effects of nonlinearity, eccentricity, and perturbations can be treated separately. An analysis of this type is usually adequate for order of magnitude estimates of the different effects.

Frequency corrections are also present, and can be computed by expressing the frequency as

$$\omega_n = \omega_{n0} + \omega_{n1} + \omega_{n2} + \ldots \qquad (2\text{-}9)$$

Fortunately, $\omega_{n1} = 0$ for the cases considered below, and the frequency is well approximated by $\omega_n = \omega_{n0}$.

a. Response to a Periodic Input

It will be necessary to calculate the forced response to an input of the form $P(t) = K_x \cos(\omega t + \varphi)\,\hat{i} + K_y \sin(\omega t + \varphi)\,\hat{j}$. The linearized equations of motion near a collinear point with this input are

$$\ddot{x} - 2\dot{y} - (2B_L + 1)x = K_x \cos(\omega t + \varphi)$$
$$\ddot{y} + 2\dot{x} + (B_L - 1)y = K_y \sin(\omega t + \varphi) \qquad (2\text{-}10)$$

A particular solution of Eq. (2-10) can be written as

$$x_p = A_x \cos(\omega t + \varphi)$$
$$y_p = A_y \sin(\omega t + \varphi) \tag{2-11}$$

where

$$\begin{bmatrix} A_x \\ A_y \end{bmatrix} = \frac{\begin{bmatrix} \left[-\omega^2 + (B_L - 1)\right] & 2\omega \\ 2\omega & \left[-\omega^2 - (2B_L + 1)\right] \end{bmatrix} \begin{bmatrix} K_x \\ K_y \end{bmatrix}}{\left[\omega^4 + (B_L - 2)\omega^2 - (2B_L + 1)(B_L - 1)\right]} \tag{2-12}$$

This result will be used repeatedly below.

b. Nonlinear Correction

Employing the procedure outlined above, it can be deduced that the differential equations for the nonlinear correction are

$$\ddot{x}_{n2} - 2\dot{y}_{n2} - (2B_L + 1)x_{n2} = C_x + K_x \cos 2\omega_n t$$
$$\ddot{y}_{n2} + 2\dot{x}_{n2} + (B_L - 1)y_{n2} = K_y \sin 2\omega_n t \tag{2-13}$$

where

$$C_x = \pm \frac{3}{2} C_L \left(\frac{1}{2} - k^2\right) A_{y1}^2 \tag{2-14}$$

$$K_x = \pm \frac{3}{2} C_L \left(\frac{1}{2} + k^2\right) A_{y1}^2 \tag{2-15}$$

$$K_y = \pm \frac{3}{2} C_L k A_{y1}^2 \tag{2-16}$$

Therefore

$$x_{n2} = x_{c2} + A_{x2} \cos 2\omega_n t$$

$$y_{n2} = A_{y2} \sin 2\omega_n t \qquad (2\text{-}17)$$

where A_{x2} and A_{y2} are computed by making use of Eqs. (2-10) to (2-12), and $x_{c2} = -C_x/(2B_L + 1)$. As an example, consider the L_2 point of the Earth-Moon system. For this point, $B_{L2} = 3.19042$, $C_{L2} = 15.8451$, $\omega_n = 1.86265$, $k = 0.343336$, and

$$C_x = 9.0821\ A_{y1}^2 \qquad x_{c2} = -1.2305\ A_{y1}^2$$

$$K_x = 14.686\ A_{y1}^2 \qquad A_{x2} = -0.57443\ A_{y1}^2$$

$$K_y = 8.1603\ A_{y1}^2 \qquad A_{y2} = -0.33203\ A_{y1}^2$$

Choosing $A_{y1} = 0.02 = 7{,}688.1$ km, these relationships give

$$C_x = 1.0085 \times 10^{-6} g \qquad x_{c2} = -189.20 \text{ km}$$

$$K_x = 1.6307 \times 10^{-6} g \qquad A_{x2} = -88.33 \text{ km}$$

$$K_y = 9.0617 \times 10^{-7} g \qquad A_{y2} = -51.05 \text{ km}$$

and $A_{x1} = 0.343336\ A_{y1} = 2{,}639.6$ km.

It should be mentioned that Plummer[41,42] has calculated the nonlinear corrections to third order for all of the collinear points. Unfortunately, Plummer's solutions are limited to the case where $\mu = 1/11$.

c. Eccentricity Correction

For the eccentricity correction, the differential equations are

$$\ddot{x}_{n2} - 2\dot{y}_{n2} - (2B_L + 1)x_{n2} = 2\nu\dot{y}_{n1} + \dot{\nu}y_{n1} + (2\nu - 6B_L\rho)x_{n1}$$

$$\ddot{y}_{n2} + 2\dot{x}_{n2} + (B_L - 1)y_{n2} = -2\nu\dot{x}_{n1} - \dot{\nu}x_{n1} + (2\nu + 3B_L\rho)y_{n1} \tag{2-18}$$

where the expressions for ρ and ν are obtained from Eqs. (1-5) and (1-6). Taking $\varphi = 0$, and neglecting terms of $O(e^2)$, these quantities are given by

$$\rho = -e\cos t$$

$$\nu = 2e\cos t \tag{2-19}$$

Using Eqs. (2-6), (2-8), and (2-19), Eq. (2-18) becomes

$$\ddot{x}_{n2} - 2\dot{y}_{n2} - (2B_L + 1)x_{n2} = K_x \sin(\omega_n + 1)t + K_x' \sin(\omega_n - 1)t$$

$$\ddot{y}_{n2} + 2\dot{x}_{n2} + (B_L - 1)y_{n2} = K_y \cos(\omega_n + 1)t + K_y' \cos(\omega_n - 1)t \tag{2-20}$$

where

$$K_x = e\left[-2\omega_n - 1 + k(3B_L + 2)\right]A_{y1} \tag{2-21}$$

$$K_x' = -e\left[2\omega_n - 1 - k(3B_L + 2)\right]A_{y1} \tag{2-22}$$

$$K_y = -e\left[k(2\omega_n + 1) + \left(\frac{3}{2}B_L - 2\right)\right]A_{y1} \tag{2-23}$$

$$K_y' = -e\left[k(2\omega_n - 1) + \left(\frac{3}{2}B_L - 2\right)\right]A_{y1} \tag{2-24}$$

The solutions can be written in the form

$$x_{n2} = A_{x2}\sin(\omega_n + 1)t + A_{x2}'\sin(\omega_n - 1)t$$

$$y_{n2} = A_{y2}\cos(\omega_n + 1)t + A_{y2}'\cos(\omega_n - 1)t \tag{2-25}$$

and A_{x2} , A'_{x2} , A_{y2} , A'_{y2} are again determined by using Eqs. (2-10) to (2-12). Returning to the example at the L_2 point of the Earth-Moon system (e = 0.05490), elementary calculations give

$$K_x = -0.041311\ A_{y1} \qquad A_{x2} = 0.026893\ A_{y1}$$

$$K'_x = 0.068489\ A_{y1} \qquad A'_{x2} = -0.030659\ A_{y1}$$

$$K_y = -0.24200\ A_{y1} \qquad A_{y2} = 0.065947\ A_{y1}$$

$$K'_y = -0.20430\ A_{y1} \qquad A'_{y2} = -0.10469\ A_{y1}$$

and for $A_{y1} = 0.02 = 7{,}688.1$ km

$$K_x = -2.2937 \times 10^{-7} g \qquad A_{x2} = 206.76 \text{ km}$$

$$K'_x = 3.8027 \times 10^{-7} g \qquad A'_{x2} = -235.71 \text{ km}$$

$$K_y = -1.3436 \times 10^{-6} g \qquad A_{y2} = 507.01 \text{ km}$$

$$K'_y = -1.1343 \times 10^{-6} g \qquad A'_{y2} = -804.84 \text{ km}$$

A comparison shows that the amplitudes of the eccentricity corrections are much larger than the amplitudes of the nonlinear corrections. It is shown below that these eccentricity corrections also dominate corrections caused by the Sun's gravitational field and radiation pressure.

d. Effect of Gravitational Perturbations and Solar Radiation Pressure

Since the analysis of gravitational perturbations is somewhat different for every libration point, a generalized result for periodic orbit corrections cannot be given. However, specific cases are readily analyzed, and the effect of the Sun's perturbation on a periodic orbit around a collinear point of the Earth-Moon system is described in Section C-1d below.

A general result for solar radiation pressure is even less probable, since this effect is highly dependent on the spacecraft

configuration and orientation. Nevertheless, a highly restricted example is examined here for illustrative purposes. Consider a satellite near the L_2 point of the Earth-Moon system. The major contribution to the satellite's cross-sectional area is given by a high gain antenna which has a diameter of 3 meters ($A_s = 7.0686\ m^2$). If the antenna is always directed toward the Moon as shown in Fig. 2-2, then the angle ψ of the incident solar radiation will vary sinusoidally. Assuming that all of the incident radiation is reflected specularly, the instantaneous acceleration acting on the spacecraft is[43]

$$P_x = \pm K_p \cos^2\psi \tag{2-26}$$

where K_p is given by Eq. (2-1), with $C_p = 2$. For a satellite mass of $m = 200$ kg, the average acceleration is $\overline{|P_x|} = K_p/2 = 1.62 \times 10^{-8}$ g. Accelerations of this magnitude may simply be cancelled by thrust control.

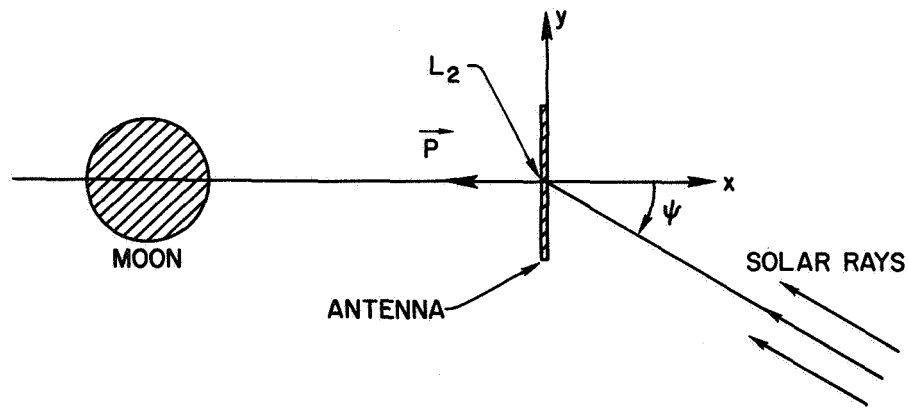

FIG. 2-2. GEOMETRY FOR RADIATION PRESSURE EXAMPLE.

4. Linearized Equations of Motion Relative to a Nominal Path

A nominal path can usually be represented as a series of successive approximations in the form

$$x_n = x_{n1} + x_{n2} + x_{n3} + \cdots$$

$$y_n = y_{n1} + y_{n2} + y_{n3} + \cdots \qquad (2\text{-}27)$$

$$z_n = z_{n1} + z_{n2} + z_{n3} + \cdots$$

where the second subscript denotes the order of the term. The equations of motion relative to the nominal path can be found by substituting Eq. (2-3) into Eq. (1-43). Only terms involving the coordinates (ξ, η, ζ) will be present, since Eq. (2-27) is a solution of Eq. (1-43) with $\vec{P}(t)$ included. Assuming that ρ and ν are negligible when compared to $3C_L x_{n1}$, etc., the linearized equations of motion are approximately*

$$\ddot{\xi} - 2\dot{\eta} - (2B_L + 1)\xi = \mp 3C_L\left[2x_{n1}\xi - y_{n1}\eta - z_{n1}\zeta\right] + F_{cx}$$

$$\ddot{\eta} + 2\dot{\xi} + (B_L - 1)\eta = \pm 3C_L\left[x_{n1}\eta + y_{n1}\xi\right] + F_{cy} \qquad (2\text{-}28)$$

$$\ddot{\zeta} + B_L\zeta = \pm 3C_L\left[x_{n1}\zeta + z_{n1}\xi\right] + F_{cz}$$

When the nominal path is very small, Eq. (2-28) reduces to Eq. (2-4).

For a quasi-periodic orbit, the first-order terms for the nominal path are given by Eq. (2-5). If the satellite is also performing an out-of-plane oscillation, it is obvious from Eq. (1-43c) that

$$z_{n1} = A_{z1} \cos(\omega_z t + \alpha_o) \qquad (2\text{-}29)$$

where $\omega_z = \sqrt{B_L}$, and α_o is a phase angle. Substitution of these first-order terms into Eq. (2-28) gives

*As in Chapter I, the upper sign holds at L_2, and the lower sign at L_1.

$$\ddot{\xi} - 2\dot{\eta} - (2B_L + 1)\xi = \mp 3C_L\left\{2\left[A_{x1} \sin \omega_n t\right]\xi\right.$$
$$\left. - \left[A_{y1} \cos \omega_n t\right]\eta - \left[A_{z1} \cos (\omega_z t + \alpha_o)\right]\zeta\right\} + F_{cx}$$
$$\ddot{\eta} + 2\dot{\xi} + (B_L - 1)\eta = \pm 3C_L\left\{\left[A_{x1} \sin \omega_n t\right]\eta\right. \qquad (2\text{-}30)$$
$$\left. + \left[A_{y1} \cos \omega_n t\right]\xi\right\} + F_{cy}$$
$$\ddot{\zeta} + B_L\zeta = \pm 3C_L\left\{\left[A_{x1} \sin \omega_n t\right]\zeta + \left[A_{z1} \cos (\omega_z t + \alpha_o)\right]\xi\right\} + F_{cz}$$

C. Examples of Gravitational Perturbations

1. Solar Perturbation near the Earth-Moon Collinear Points

The effect of the Sun's perturbation on a satellite at a collinear point of the Earth-Moon system was first investigated by Colombo.[3,44] He demonstrated that, to first order, the acceleration produced by the direct effect of the Sun is completely cancelled by the indirect effect of the Sun on the Moon. A more complete derivation of Colombo's solution has been given by Nicholson,[45] who also examined the forced motion caused by the higher-order terms.* It should be emphasized that Colombo's solution is valid only at the libration point, and cannot be applied to a satellite following a periodic orbit around the point.

To calculate the effect of the Sun's perturbation on a periodic orbit, a somewhat different approach is advisable. The method presented in this section uses the lunar theory of De Pontecoulant to account for the Sun's indirect effect. It is first shown that this method is in agreement with Colombo's result at the libration point, and then it is used to determine the correction to a periodic orbit around a collinear point. Since the mean inclination of the Moon's orbital plane to the

*The magnitude of the acceleration due to the higher-order terms is approximately 2×10^{-9}g. A nominal path calculation is unnecessary here, since the magnitude of this acceleration is comparable to random solar radiation pressure effects.

ecliptic is only about five degrees, and the eccentricities of the orbits of the Earth and the Moon are $e' = 0.01673$ and $e = 0.05490$, respectively, the analysis given below will be limited to zero-eccentricity, coplanar orbits.

a. De Pontecoulant's Expressions for the Motion of the Moon

A complete listing of De Pontecoulant's results for the motion of the Moon is given in Ref. 46, and an abbreviated version can be found in Ref. 47. Literally hundreds of terms are involved in these expressions, but if it is assumed that $e = e' = 0$, and three-dimensional effects are neglected, the formulas reduce to

$$\rho = -\frac{1}{6}m^2 + \frac{331}{288}m^4 - \left[m^2 + \frac{19}{6}m^3 + \frac{125}{18}m^4\right]\cos 2\omega_s t$$
$$- \frac{3}{8}m^4 \cos 4\omega_s t + \left[\frac{15}{16}m + \frac{81}{16}m^2\right]\frac{a}{a'}\cos \omega_s t$$
$$- \frac{25}{64}m^2 \frac{a}{a'}\cos 3\omega_s t + O(m^5) \qquad (2\text{-}31)$$

$$\nu = \left[\frac{11}{4}m^2 + \frac{85}{12}m^3 + \frac{539}{36}m^4\right]\cos 2\omega_s t$$
$$+ \frac{201}{64}m^4 \cos 4\omega_s t - \left[\frac{15}{8}m + \frac{39}{4}m^2\right]\frac{a}{a'}\cos \omega_s t$$
$$+ \frac{45}{32}m^2 \frac{a}{a'}\cos 3\omega_s t + O(m^5) \qquad (2\text{-}32)$$

where m is the ratio of the mean motions of the Earth and the Moon ($m = n'/n = 0.07480133$), a/a' is the ratio of the semi-major axes of the Earth and the Moon $\left[a/a' = 0.002559 \sim O(m^2)\right]$, $\omega_s = 1 - m = 0.92519867$, and $t = 0$ corresponds to new Moon. Differentiation of Eqs. (2-31) and (2-32) gives

$$\dot{\rho} = \left[2m^2 + \frac{13}{3} m^3 + \frac{68}{9} m^4\right] \sin 2\omega_s t$$

$$+ \frac{3}{2} m^4 \sin 4\omega_s t - \left[\frac{15}{16} m + \frac{33}{8} m^2\right] \frac{a}{a'} \sin \omega_s t$$

$$+ \frac{75}{64} m^2 \frac{a}{a'} \sin 3\omega_s t + O(m^5) \qquad (2\text{-}33)$$

$$\ddot{\rho} = \left[4m^2 + \frac{14}{3} m^3 + \frac{58}{9} m^4\right] \cos 2\omega_s t$$

$$+ 6m^4 \cos 4\omega_s t - \left[\frac{15}{16} m + \frac{51}{16} m^2\right] \frac{a}{a'} \cos \omega_s t$$

$$+ \frac{225}{64} m^2 \frac{a}{a'} \cos 3\omega_s t + O(m^5) \qquad (2\text{-}34)$$

$$\dot{\nu} = -\left[\frac{11}{2} m^2 + \frac{26}{3} m^3 + \frac{142}{9} m^4\right] \sin 2\omega_s t$$

$$- \frac{201}{16} m^4 \sin 4\omega_s t + \left[\frac{15}{8} m + \frac{63}{8} m^2\right] \frac{a}{a'} \sin \omega_s t$$

$$- \frac{135}{32} m^2 \frac{a}{a'} \sin 3\omega_s t + O(m^5) \qquad (2\text{-}35)$$

b. Derivation of Direct Solar Effect

The geometry for the direct solar perturbation in the vicinity of a collinear point is shown in Fig. 2-3. The contribution of this direct solar effect to the effective potential energy (for motion relative to the Earth) is

$$U_D = -M_\odot \left[\frac{1}{|\vec{r}_s - \vec{r}|} - \frac{\vec{r}_s \cdot \vec{r}}{r_s^3}\right] \qquad (2\text{-}36)$$

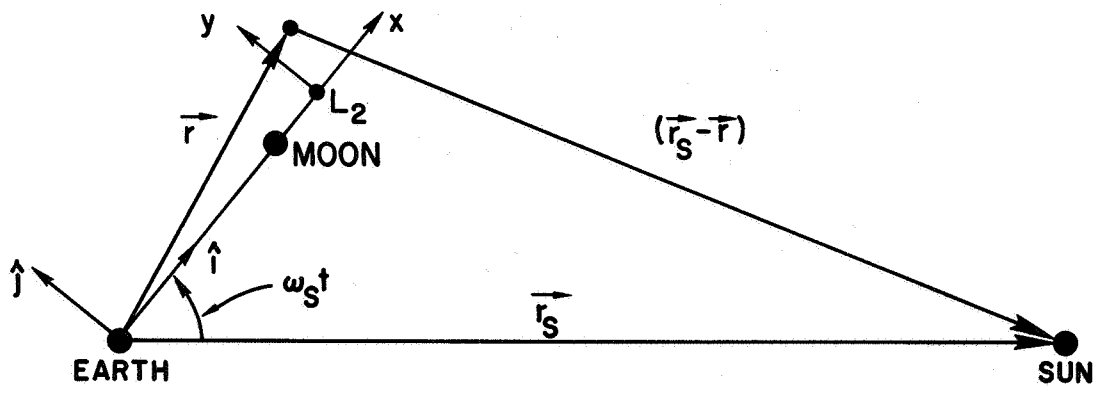

FIG. 2-3. GEOMETRY FOR DIRECT SOLAR PERTURBATION NEAR A COLLINEAR POINT OF THE EARTH-MOON SYSTEM.

where

$$\vec{r} = \left[(1 \pm \gamma_L)(1 + \rho) + x\right] \hat{i} + y\hat{j} \tag{2-37}$$

$$\vec{r}_s = r_s\left[\cos \omega_s t\, \hat{i} - \sin \omega_s t\, \hat{j}\right] \tag{2-38}$$

and $M_\odot$ is the mass of the Sun. Since $r_s \gg r$, Eq. (2-36) can be expanded in a power series

$$U_D = -\frac{M_\odot}{r_s}\left\{1 + \left[\frac{3}{2}\left(\frac{\vec{r}_s \cdot \vec{r}}{r_s^2}\right)^2 - \frac{1}{2}\left(\frac{r}{r_s}\right)^2\right] + \left[\frac{5}{2}\left(\frac{\vec{r}_s \cdot \vec{r}}{r_s^2}\right)^3 - \frac{3}{2}\left(\frac{\vec{r}_s \cdot \vec{r}}{r_s^2}\right)\left(\frac{r}{r_s}\right)^2\right] + \ldots\right\} \tag{2-39}$$

Therefore, the acceleration can be written

$$\vec{P}_D = -\nabla U_D = m^2 r\left\{\left[3(\hat{r} \cdot \hat{r}_s)\hat{r}_s - \hat{r}\right] + \left(\frac{r}{r_s}\right)\left[\frac{15}{2}(\hat{r} \cdot \hat{r}_s)^2 \hat{r}_s - 3(\hat{r} \cdot \hat{r}_s)\hat{r} - \frac{3}{2}\hat{r}_s\right] + \ldots\right\} \tag{2-40}$$

where $(M_\odot/r_s^3) = m^2$. The components of $\vec{P}_D$ are approximately

$$P_{xD} = \vec{P}_D \cdot \hat{i} \cong m^2 r \left\{ \frac{1}{2} (3 \cos 2\omega_s t + 1) - \frac{3}{2} \left(\frac{y}{r}\right) \sin 2\omega_s t \right.$$

$$+ \left(\frac{r}{r_s}\right) \left[\frac{3}{8} (3 \cos \omega_s t + 5 \cos 3\omega_s t) \right.$$

$$\left. \left. - \frac{3}{4} \left(\frac{y}{r}\right) (\sin \omega_s t + 5 \sin 3\omega_s t) \right] \right\} \qquad (2\text{-}41)$$

$$P_{yD} = \vec{P}_D \cdot \hat{j} \cong m^2 r \left\{ - \frac{3}{2} \sin 2\omega_s t + \frac{1}{2} \left(\frac{y}{r}\right) (1 - 3 \cos 2\omega_s t) \right.$$

$$- \left(\frac{r}{r_s}\right) \left[\frac{3}{8} (\sin \omega_s t + 5 \sin 3\omega_s t) \right.$$

$$\left. \left. - \frac{3}{4} \left(\frac{y}{r}\right) (\cos \omega_s t - 5 \cos 3\omega_s t) \right] \right\} \qquad (2\text{-}42)$$

c. Cancellation of First-Order Terms at Collinear Point

The indirect solar perturbation enters through ρ and ν. From Eqs. (1-43a) and (1-43b), it can be seen that the indirect acceleration at a collinear point is approximately

$$P_{xI} \cong - (1 \pm \gamma_L)(\ddot{\rho} - 2\nu - 3\rho) \qquad (2\text{-}43)$$

$$P_{yI} \cong - (1 \pm \gamma_L)(2\dot{\rho} + \nu) \qquad (2\text{-}44)$$

To be in harmony with Colombo's solution, it is only necessary to show that all acceleration terms to $O(m^3)$ vanish. The linear approximations in Eqs. (2-43) and (2-44) are sufficiently accurate for this purpose. To the same order of approximation, Eqs. (2-41) and (2-42) are

$$P_{xD} \cong \frac{1}{2} m^2 (1 \pm \gamma_L)(3 \cos 2\omega_s t + 1) \qquad (2\text{-}45)$$

$$P_{yD} \cong -\frac{3}{2} m^2 (1 \pm \gamma_L) \sin 2\omega_s t \qquad (2\text{-}46)$$

Substituting Eqs. (2-31) to (2-35) [keeping only terms to $O(m^3)$] into Eqs. (2-43) and (2-44), it is found that $P_{xI} + P_{xD} = 0$ and $P_{yI} + P_{yD} = 0$ to $O(m^3)$.*

d. Periodic Orbit Correction

Using Eqs. (1-43a), (1-43b), (2-41), (2-42), and neglecting terms of $O(m^4)$, the linearized equations of motion in the vicinity of a collinear point are

$$\ddot{x} - 2\dot{y} - (2B_L + 1)x = \left[2\nu - 6B_L\rho + \frac{m^2}{2}(1 + 3\cos 2\omega_s t)\right]x + \left[\dot{\nu} - \frac{3}{2} m^2 \sin 2\omega_s t\right]y + 2\nu\dot{y}$$

$$\ddot{y} + 2\dot{x} + (B_L - 1)y = -\left[\dot{\nu} + \frac{3}{2} m^2 \sin 2\omega_s t\right]x + \left[2\nu + 3B_L\rho + \frac{m^2}{2}(1 - 3\cos 2\omega_s t)\right]y - 2\nu\dot{x} \qquad (2\text{-}47)$$

As before, the first approximation to a periodic orbit around a collinear point is given by Eq. (2-8). A frequency correction to this periodic orbit can be obtained from Eq. (2-47). The constant coefficients of $O(m^2)$ in Eq. (2-47) lead to a modified characteristic equation [cf. Eq. (1-49)]

$$s^4 - \left[(B_L - 2) + \frac{m^2}{2}(B_L + 2)\right]s^2 - (2B_L + 1)(B_L - 1)(1 + \frac{m^2}{2}) = 0 \qquad (2\text{-}48)$$

*In an earlier paper,[7] the present author reached an erroneous conclusion regarding this cancellation due to inappropriate expressions for ρ and ν.

For the L_2 point, the modified characteristic equation yields a corrected frequency of $\omega_n = 1.86247$. However, since $\omega_{no} = 1.86265$, this correction is usually negligible.

The second-order correction to the periodic orbit is found by employing the methods of Section B-3. Although the expressions for ρ and ν in Eqs. (2-31) and (2-32) contain periodic terms with frequencies ω_s and $2\omega_s$ when quantities of $O(m^3)$ are retained, only terms of frequency $2\omega_s$ are considered in this section. This should be sufficient for an order of magnitude estimate of the correction. The differential equations for the solar perturbation correction are

$$\ddot{x}_{n2} - 2\dot{y}_{n2} - (2B_L + 1)x_{n2} = K_x \sin(2\omega_s + \omega_n)t + K_x' \sin(\omega_n - 2\omega_s)t$$

$$\ddot{y}_{n2} + 2\dot{x}_{n2} + (B_L - 1)y_{n2} = K_y \cos(2\omega_s + \omega_n)t + K_y' \cos(\omega_n - 2\omega_s)t \qquad (2\text{-}49)$$

where

$$K_x = \left\{k\left[\nu_3 - 3B_L\rho_3 + \frac{3}{4}m^2\right] - \nu_3\omega_n + \frac{1}{2}\left[\dot{\nu}_3 - \frac{3}{2}m^2\right]\right\}A_{y1} \qquad (2\text{-}50)$$

$$K_x' = \left\{k\left[\nu_3 - 3B_L\rho_3 + \frac{3}{4}m^2\right] - \nu_3\omega_n - \frac{1}{2}\left[\dot{\nu}_3 - \frac{3}{2}m^2\right]\right\}A_{y1} \qquad (2\text{-}51)$$

$$K_y = \left\{k\left[\frac{1}{2}(\dot{\nu}_3 + \frac{3}{2}m^2) - \nu_3\omega_n\right] + \left[\nu_3 + \frac{3}{2}B_L\rho_3 - \frac{3}{4}m^2\right]\right\}A_{y1} \qquad (2\text{-}52)$$

$$K_y' = \left\{-k\left[\frac{1}{2}(\dot{\nu}_3 + \frac{3}{2}m^2) + \nu_3\omega_n\right] + \left[\nu_3 + \frac{3}{2}B_L\rho_3 - \frac{3}{4}m^2\right]\right\}A_{y1} \qquad (2\text{-}53)$$

with $\rho_3 \equiv -(m^2 + \frac{19}{6}m^3)$, $\nu_3 \equiv (\frac{11}{4}m^2 + \frac{85}{12}m^3)$ and $\dot{\nu}_3 \equiv -(\frac{11}{2}m^2 + \frac{26}{3}m^3)$. Particular solutions for these differential

equations are

$$x_{n2} = A_{x2} \sin (2\omega_s + \omega_n)t + A'_{x2} \sin (\omega_n - 2\omega_s)t$$

$$y_{n2} = A_{y2} \cos (2\omega_s + \omega_n)t + A'_{y2} \cos (\omega_n - 2\omega_s)t \qquad (2\text{-}54)$$

Once again, consider the example of Section B-3. Using the values

$$\rho_3 = -0.00692059, \quad \nu_3 = 0.0183515,$$

$$\dot{\nu}_3 = -0.0344011, \quad \omega_s = 0.925199,$$

$$m = 0.07480133, \quad B_{L2} = 3.19042,$$

$$\omega_n = 1.86265, \quad \text{and} \quad k = 0.343336,$$

it is found that

$$K_x = -0.025096\ A_{y1} \qquad A_{x2} = 0.0029012\ A_{y1}$$

$$K'_x = 0.017698\ A_{y1} \qquad A'_{x2} = -0.0024375\ A_{y1}$$

$$K_y = -0.035165\ A_{y1} \qquad A_{y2} = 0.0048903\ A_{y1}$$

$$K'_y = -0.026236\ A_{y1} \qquad A'_{y2} = -0.011951\ A_{y1}$$

and for $A_{y1} = 0.02 = 7{,}688.1$ km

$$K_x = -1.3934 \times 10^{-7}\ g \qquad A_{x2} = 22.30 \text{ km}$$

$$K'_x = 9.8264 \times 10^{-8}\ g \qquad A'_{x2} = -18.74 \text{ km}$$

$$K_y = -1.9524 \times 10^{-7}\ g \qquad A_{y2} = 37.60 \text{ km}$$

$$K'_y = -1.4567 \times 10^{-7}\ g \qquad A'_{y2} = -91.88 \text{ km}$$

Although these corrections are small, the solar perturbation terms should be included in periodic orbit calculations, since accelerations of 10^{-7} g are not insignificant.

2. Effect of the Moon at the Sun-Earth Collinear Points

The geometry for the Sun-Earth-Moon system is depicted in Fig. 2-4. Consider a point 0 that is collinear with the Earth-Moon barycenter B and the Sun. The distance r_{B0} is determined by assuming that the total mass of the Earth and Moon are concentrated at B, and then taking r_{B0} as the libration point distance γ_L for $\mu = (m_1 + m_2)/(m_1 + m_2 + m_3)$. Does the point 0 lie closer to an equilibrium solution in the Sun-Earth-Moon system than the classical Sun-Earth collinear libration point? This question can be resolved by finding the perturbed path (dynamic equilibrium point or "nominal path") for a satellite in the vicinity of the point 0. If the maximum radius of the perturbed path relative to 0 is smaller than the distance from 0 to the classical collinear point, then it is more appropriate to consider 0 to be a collinear libration point of the Sun-Earth-Moon system.

The accelerations relative to an inertial reference system can be obtained with the aid of Fig. 2-4. Defining $\vec{r}_{ij} \equiv \vec{r}_j - \vec{r}_i$, these accelerations are

$$\ddot{\vec{r}}_0 = \frac{m_1\vec{r}_{01}}{r_{01}^3} + \frac{m_2\vec{r}_{02}}{r_{02}^3} + \frac{m_3\vec{r}_{03}}{r_{03}^3} \qquad (2\text{-}55)$$

$$\ddot{\vec{r}}_1 = \frac{m_2\vec{r}_{12}}{r_{12}^3} + \frac{m_3\vec{r}_{13}}{r_{13}^3} \qquad (2\text{-}56)$$

$$\ddot{\vec{r}}_2 = -\frac{m_1\vec{r}_{12}}{r_{12}^3} + \frac{m_3\vec{r}_{23}}{r_{23}^3} \qquad (2\text{-}57)$$

$$\ddot{\vec{r}}_3 = -\frac{m_1\vec{r}_{13}}{r_{13}^3} - \frac{m_2\vec{r}_{23}}{r_{23}^3} \qquad (2\text{-}58)$$

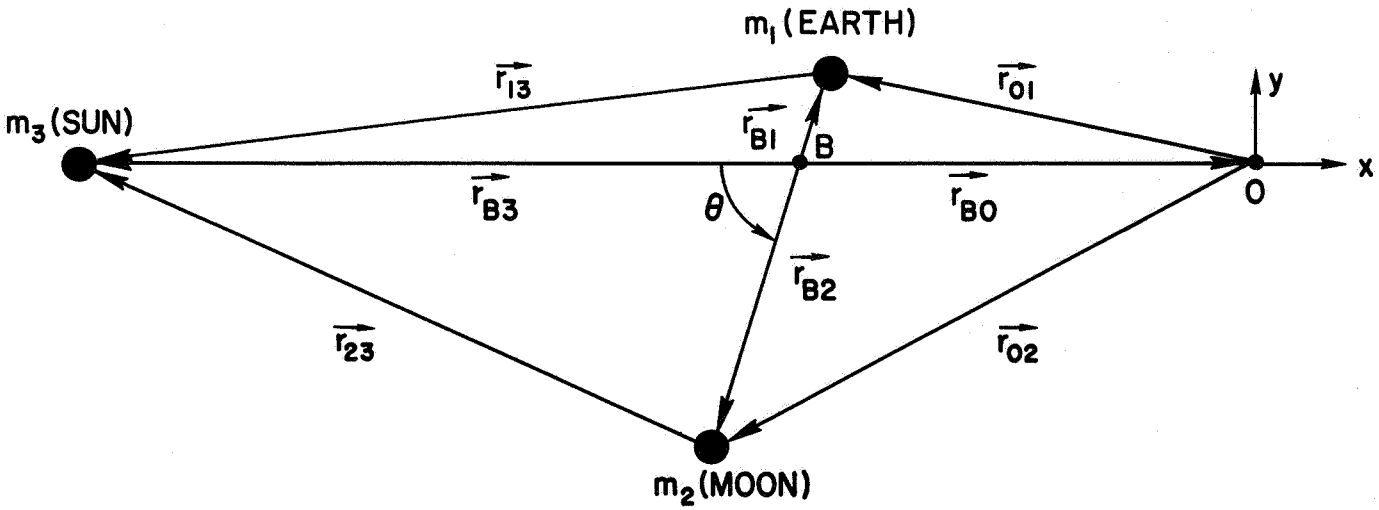

FIG. 2-4. GEOMETRY FOR A COLLINEAR POINT IN THE SUN-EARTH-MOON SYSTEM.

Using the definition of the barycenter $(m_1\vec{r}_{B1} + m_2\vec{r}_{B2} = 0)$, it is found that

$$\vec{r}_B = \vec{r}_2 - \vec{r}_{B2} = \vec{r}_2 - \frac{m_1}{m_1 + m_2}(\vec{r}_2 - \vec{r}_1)$$

$$= \frac{m_2}{m_1 + m_2}\vec{r}_2 + \frac{m_1}{m_1 + m_2}\vec{r}_1 \qquad (2\text{-}59)$$

Differentiating Eq. (2-59) and substituting Eqs. (2-56) and (2-57) gives

$$\ddot{\vec{r}}_B = m_3\left[\frac{m_1\vec{r}_{13}}{(m_1 + m_2)r_{13}^3} + \frac{m_2\vec{r}_{23}}{(m_1 + m_2)r_{23}^3}\right] \qquad (2\text{-}60)$$

This relation, along with Eq. (2-58), leads to*

$$\ddot{\vec{r}}_{B3} = \ddot{\vec{r}}_3 - \ddot{\vec{r}}_B = -\frac{m_1 + m_2 + m_3}{m_1 + m_2}\left[\frac{m_1\vec{r}_{13}}{r_{13}^3} + \frac{m_2\vec{r}_{23}}{r_{23}^3}\right]$$

$$\simeq -\frac{(m_1 + m_2 + m_3)}{r_{B3}^3}\vec{r}_{B3} \qquad (2\text{-}61)$$

Making use of Eqs. (2-55), (2-60), and (2-61), it is now possible to give the acceleration of a satellite at 0 relative to the Sun

$$\ddot{\vec{r}}_{30} = \ddot{\vec{r}}_{B0} - \ddot{\vec{r}}_{B3} = \ddot{\vec{r}}_0 - \ddot{\vec{r}}_B - \ddot{\vec{r}}_{B3}$$

$$= -\frac{m_3\vec{r}_{30}}{r_{30}^3} + \frac{(m_1 + m_2 + m_3)}{r_{B3}^3}\vec{r}_{B3} - \frac{1}{r_{01}^3}(m_2\vec{r}_{B2} + m_1\vec{r}_{B0}) + \frac{m_2}{r_{02}^3}(\vec{r}_{B2} - \vec{r}_{B0})$$

$$- \frac{m_3}{(m_1 + m_2)r_{13}^3}(m_1\vec{r}_{B3} + m_2\vec{r}_{B2}) - \frac{m_3m_2}{(m_1 + m_2)r_{23}^3}(\vec{r}_{B3} - \vec{r}_{B2}) \qquad (2\text{-}62)$$

*This result is obtained by keeping only the first term in an expansion where the ratio of the second term to the first term is about 8×10^{-8}.

Neglecting terms of $O(r_{B2}/r_{B0})^4$ ($r_{B2}/r_{B0} \cong 1/4$), a moderate amount of algebra reduces Eq. (2-62) to

$$\ddot{\vec{r}}_{30} \cong -\frac{m_3\vec{r}_{30}}{r_{30}^3} - (m_1 + m_2)\left[\frac{\vec{r}_{B0}}{r_{B0}^3} - \frac{\vec{r}_{B3}}{r_{B3}^3}\right] + \vec{P} \qquad (2\text{-}63)$$

where

$$\vec{P} = \frac{m_2}{r_{B0}^3}\left\{\left[3\frac{\vec{r}_{B2}\cdot\vec{r}_{B0}}{r_{B0}^2} - \frac{3}{2}\left(\frac{r_{B2}}{r_{B0}}\right)^2 + \frac{15}{2}\left(\frac{\vec{r}_{B2}\cdot\vec{r}_{B0}}{r_{B0}^2}\right)^2\right]\vec{r}_{B2}\right.$$

$$+\left[\frac{3}{2}\left(\frac{r_{B2}}{r_{B0}}\right)^2 - \frac{15}{2}\left(\frac{\vec{r}_{B2}\cdot\vec{r}_{B0}}{r_{B0}^2}\right)^2 + \frac{15}{2}\left(\frac{r_{B2}}{r_{B0}}\right)^2\left(\frac{\vec{r}_{B2}\cdot\vec{r}_{B0}}{r_{B0}^2}\right)\right.$$

$$\left.\left. - \frac{35}{2}\left(\frac{\vec{r}_{B2}\cdot\vec{r}_{B0}}{r_{B0}^2}\right)^3\right]\vec{r}_{B0}\right\} \qquad (2\text{-}64)$$

Since $r_{B0} = \gamma_L$, it is immediately obvious from Eq. (2-63) that $\ddot{\vec{r}}_{30} = \vec{P}$.

For the remainder of the analysis, the orbital eccentricities, and the inclination of the Earth-Moon orbit to the ecliptic are neglected. Essentially nothing is lost here, since this approximation is consistent with the deletion of terms of $O(r_{B2}/r_{B0})^4$. Using $\vec{r}_{B2}\cdot\vec{r}_{B0} = \mp r_{B2}r_{B0}\cos\theta$ (upper sign for L_2; lower sign for L_1), the linearized equations of motion relative to 0 become

$$\ddot{x} - 2\dot{y} - (2B_L + 1)x = P_x$$

$$\ddot{y} + 2\dot{x} + (B_L - 1)y = P_y \qquad (2\text{-}65)$$

where

$$P_x = \frac{m_2}{r_{B0}^2}\left(\frac{r_{B2}}{r_{B0}}\right)^2\left\{\mp\frac{3}{4}\left[1 + 3\cos 2\theta\right] + \frac{1}{2}\left[3\cos\theta + 5\cos 3\theta\right]\left(\frac{r_{B2}}{r_{B0}}\right)\right\} \tag{2-66}$$

$$P_y = \frac{3}{2}\frac{m_2}{r_{B0}^2}\left(\frac{r_{B2}}{r_{B0}}\right)^2\left\{\pm\sin 2\theta - \frac{1}{4}\left[\sin\theta + 5\sin 3\theta\right]\left(\frac{r_{B2}}{r_{B0}}\right)\right\} \tag{2-67}$$

and $\theta = nt$ ($n = 13.369$). A particular solution of Eq. (2-65) is the perturbed path

$$\begin{aligned} x_n &= x_c + A_x\cos\theta + A_x'\cos 2\theta + A_x''\cos 3\theta \\ y_n &= A_y\sin\theta + A_y'\sin 2\theta + A_x''\sin 3\theta \end{aligned} \tag{2-68}$$

For the perturbed path at the L_2 point:

$$m_2 = 3.7397 \times 10^{-8} \qquad B_{L2} = 3.9405$$

$$r_{B0} = 1.0078 \times 10^{-2} \qquad \left(\frac{r_{B2}}{r_{B0}}\right) = 0.25187$$

$$K \equiv \frac{m_2}{r_{B0}^2}\left(\frac{r_{B2}}{r_{B0}}\right)^2 = 2.5358 \times 10^{-5} = 1.4120 \times 10^{-8}\,g$$

$$x_c = 295.10 \text{ km}$$

$$A_x = -7.47 \text{ km} \qquad A_y = 3.01 \text{ km}$$

$$A_x' = 11.47 \text{ km} \qquad A_y' = -8.22 \text{ km}$$

$$A_x'' = -1.41 \text{ km} \qquad A_y'' = 1.10 \text{ km}$$

The constant term x_c represents a shift along the x-axis to a new point $0'$. Relative to $0'$, the maximum distance to the perturbed path is about 20 km. Therefore, the point $0'$ is never further than about 20 km from a dynamic "equilibrium" point of the restricted four-body problem (Sun, Earth, Moon, satellite)!

3. Some Other Interesting Examples

a. Jupiter's Effect at the Sun-Earth Isosceles-Triangle Points

A satellite moving in the Earth's orbit around the Sun will be perturbed by several bodies (e.g., Earth, Moon, Jupiter). The relative importance of the different effects may be quite variable, depending on the distance of the satellite from the Earth. In Chapter I, the Earth's effect was considered, and artificial libration points were created by cancelling this effect with a constant thrust acceleration. The principal objective of this section is to obtain an estimate of Jupiter's effect at these artificial libration points (isosceles-triangle points) when the satellite is relatively close to the Earth.

The geometry for Jupiter's perturbation at a Sun-Earth isosceles-triangle point is shown in Fig. 2-5. Neglecting some small indirect effects, Jupiter's perturbative acceleration is

$$\vec{P}_J = M_J \left[\frac{\vec{r}}{r^3} - \frac{\vec{r}_E}{r_E^3} \right] \tag{2-69}$$

Assuming that $\left(\frac{a}{r}\right)$ is small, Eq. (2-69) becomes

$$\vec{P}_J \cong \frac{M_J}{r^3} \left[-\vec{a} + 3 \frac{\vec{r} \cdot \vec{a}}{r^2} \vec{r} \right] \tag{2-70}$$

and the components are given by

$$P_{Jx} = \vec{P}_J \cdot \hat{i} = \frac{3}{2} \frac{M_J}{r^2} \left(\frac{a}{r}\right) \sin 2\alpha \tag{2-71}$$

$$P_{Jy} = \vec{P}_J \cdot \hat{j} = \frac{1}{2} \frac{M_J}{r^2} \left(\frac{a}{r}\right) \left[1 + 3 \cos 2\alpha \right] \tag{2-72}$$

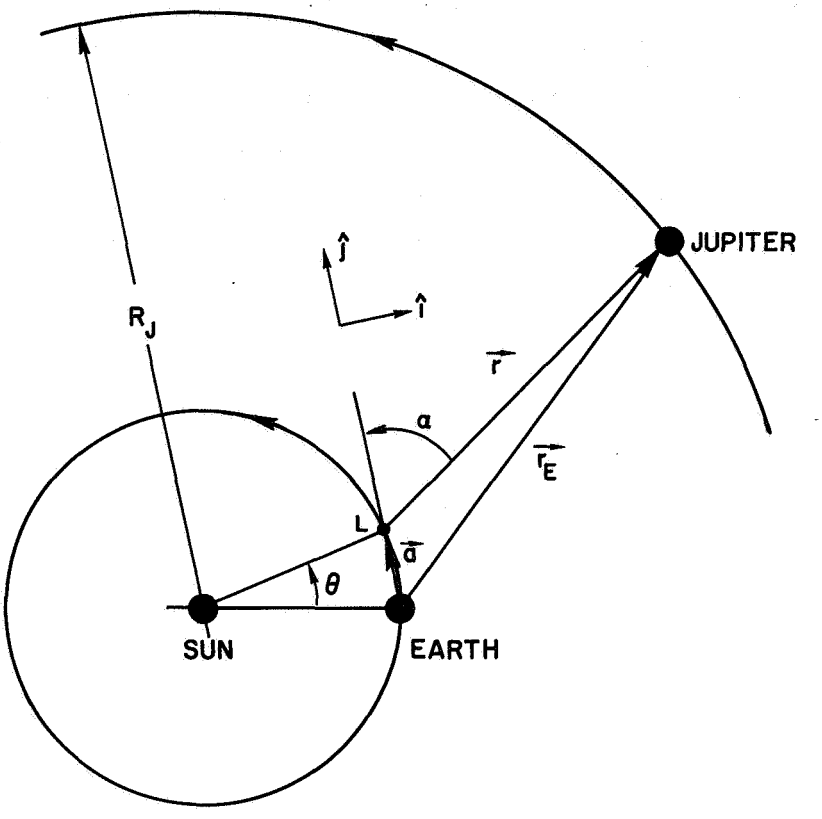

FIG. 2-5. GEOMETRY FOR JUPITER'S PERTURBATION AT A SUN-EARTH ISOSCELES-TRIANGLE POINT.

The magnitude of Jupiter's acceleration is

$$|\vec{P}_J| = \frac{1}{2}\frac{M_J}{r^2}\left(\frac{a}{r}\right)\left[10 + 6\cos 2\alpha\right]^{1/2} \qquad (2\text{-}73)$$

For $\theta = 10°$ and $\alpha = 90°$, rough calculations give $|\vec{P}_J| \cong 1.35 \times 10^{-9}$g (this value is relatively constant for $0° < \alpha < 180°$). Since the thrust acceleration at $\theta = 10°$ is $|\vec{F}_c| \cong 6.02 \times 10^{-8}$g, Jupiter's perturbation can be ignored when $\theta < 10°$.

b. Solar Effect at the Earth-Moon Equilateral-Triangle Points

The analysis of the uncontrolled motion of a satellite in the vicinity of the Sun-perturbed Earth-Moon equilateral-triangle points represents one of the most difficult problems in celestial mechanics. In

the past few years, several papers (e.g., see Refs. 48-55) have appeared on this subject. A recent analytical study by Schechter[54] is probably the most productive to date, and some of his conclusions have been verified by the numerical work of Kolenkiewicz and Carpenter.[55] However, the general problem remains unsolved, since the important effect of the lunar eccentricity was not considered in Schechter's study.

Chapter III

LINEAR FEEDBACK CONTROL

After a satellite has been injected into the vicinity of a libration point, a translation control system can be used to eliminate the initial errors. This control system can also be used for station-keeping. To implement this control, closed-loop guidance laws (feedback control logic) will be needed. In this chapter, simple linear feedback control laws are developed for the collinear and equilateral-triangle points. Although the control acceleration is treated as if it were continuous, this assumption is not overly restrictive, since a pulsed control will behave essentially like a continuous control if the frequency of the pulse control is much higher than any of the natural frequencies of the system.*

For motion in the immediate vicinity of a libration point, the linearized equations of motion are sufficiently accurate. These equations will contain periodic coefficients if eccentricity is present or if the satellite is following a nominal path. In many instances, these effects are small and can be neglected. However, to obtain some estimate of the importance of these periodic coefficients, Floquet stability investigations for some representative cases are included here.

A. Collinear Points

For small eccentricities, the linearized equations of motion at a collinear point (or relative to a small nominal path about the point) are approximately [from Eq. (2-4)]**

$$\ddot{x} - 2\dot{y} - (2B_L + 1)x = F_{cx} \tag{3-1a}$$

$$\ddot{y} + 2\dot{x} + (B_L - 1)y = F_{cy} \tag{3-1b}$$

$$\ddot{z} + B_L z = F_{cz} \tag{3-1c}$$

---

*The continuous approximation is probably adequate if the pulsing rate is greater than 10 times any of the natural frequencies of the system.

**For the equations relative to a nominal path, the variables (ξ, η, ζ) should be used $(\xi = x - x_n$, etc.). However, this distinction will be overlooked when the equations have the same form.

The z-axis motion is bounded and can be damped by simply taking $F_{cz} = - k_1' \dot{z}$, where the feedback gain $k_1' > 0$. The control synthesis for the unstable xy-motion is less obvious, but it can be accomplished with classical methods (Routh criterion[56] and root locus[57]).

1. Routh Stability Conditions

For a radial-axis (x-axis) control using only range and range-rate (x and $\dot{x}$) feedback, the control is

$$F_{cx} = - k_1 \dot{x} - k_2 x$$
$$F_{cy} = 0 \qquad (3\text{-}2)$$

This leads to the characteristic equation

$$s^4 + k_1 s^3 + [k_2 - (B_L - 2)]s^2 + k_1(B_L - 1)s + [k_2 - (2B_L + 1)](B_L - 1) = 0 \qquad (3\text{-}3)$$

From Routh's criterion, the necessary and sufficient conditions for asymptotic stability are

$$k_1 > 0$$
$$k_2 > (2B_L + 1) \qquad (3\text{-}4)$$

It is shown in the next section that, for certain values of k_1 and k_2, more damping can be obtained by adding some positive y-feedback. For this case

$$F_{cx} = - k_1 \dot{x} - k_2 x + k_4 y$$
$$F_{cy} = 0 \qquad (3\text{-}5)$$

and the characteristic equation is*

$$s^4 + k_1 s^3 + [k_2 - (B_L - 2)]s^2 + [k_1(B_L - 1) + 2k_4]s$$

$$+ [k_2 - (2B_L + 1)](B_L - 1) = 0 \qquad (3\text{-}6)$$

The Routh conditions are

$$k_1 > 0 \quad , \quad k_2 > (2B_L + 1)$$

$$k_1(B_L - 1) + 2k_4 > 0 \qquad (3\text{-}7)$$

$$2k_1^2(B_L - 1) - k_4\left\{k_1[3B_L - (k_2 + 4)] + 2k_4\right\} > 0$$

If cross-axis (y-axis) control is used, it is necessary to feed back all of the state variables for stability. This control can be written

$$F_{cx} = 0$$

$$F_{cy} = - k_5\dot{x} - k_6 x - k_7\dot{y} + k_8 y \qquad (3\text{-}8)$$

The characteristic equation is given by**

$$s^4 + k_7 s^3 + [2k_5 - k_8 - (B_L - 2)]s^2$$

$$+ [2k_6 - k_7(2B_L + 1)]s + [k_8 - (B_L - 1)](2B_L + 1) = 0 \qquad (3\text{-}9)$$

---

*The same characteristic equation is obtained with the dual-axis control, $F_{cx} = - k_1\dot{x} - k_2 x$, $F_{cy} = - k_6 x$, with k_6 replacing k_4.

**This characteristic equation can also be obtained with the dual-axis control, $F_{cx} = k_3\dot{y} + k_4 y$, $F_{cy} = - k_7\dot{y} + k_8 y$, with k_3 and k_4 replacing k_5 and k_6, respectively.

and the Routh conditions are

$$k_7 > 0, \quad 2k_5 > k_8 + (B_L - 2), \quad 2k_6 > k_7(2B_L + 1), \quad k_8 > (B_L - 1)$$
$$k_6\left\{k_7[2k_5 - k_8 + (3B_L + 4)] - 2k_6\right\} - k_7^2(k_5 + 2)(2B_L + 1) > 0 \tag{3-10}$$

2. Root Loci and Closed-Loop Response

The preceding section has shown that it is possible to obtain a stable radial-axis control that requires only range and range-rate measurements. However, it is still necessary to select the gains, k_1 and k_2, for a satisfactory response. A simple method for determining these gains is to use root-locus plots. Taking $k_1 = 0$, and writing Eq. (3-3) in the form

$$\frac{k_2[s^2 + (B_L - 1)]}{s^4 - (B_L - 2)s^2 - (2B_L + 1)(B_L - 1)} = -1 \tag{3-11}$$

leads to the root-locus plot of Fig. 3-1. It is seen that neutral stability is obtained when $k_2 > (2B_L + 1)$. When $k_1 \neq 0$, Eq. (3-3) can be written

$$\frac{k_1 s[s^2 + (B_L - 1)]}{s^4 + [k_2 - (B_L - 2)]s^2 + (B_L - 1)[k_2 - (2B_L + 1)]} = -1 \tag{3-12}$$

The root loci of Eq. (3-12), and some corresponding response diagrams* are depicted in Figs. 3-2 to 3-7 for three values of k_2. Inspection of these figures shows that, for $B_L = 4$, a well-damped response can be achieved by taking $k_1 = 4.0$ and $k_2 = 12.0$ (note that $k_1 = \frac{1}{3} k_2$).

*The response diagrams were obtained from a TR-48 analog computer simulation.

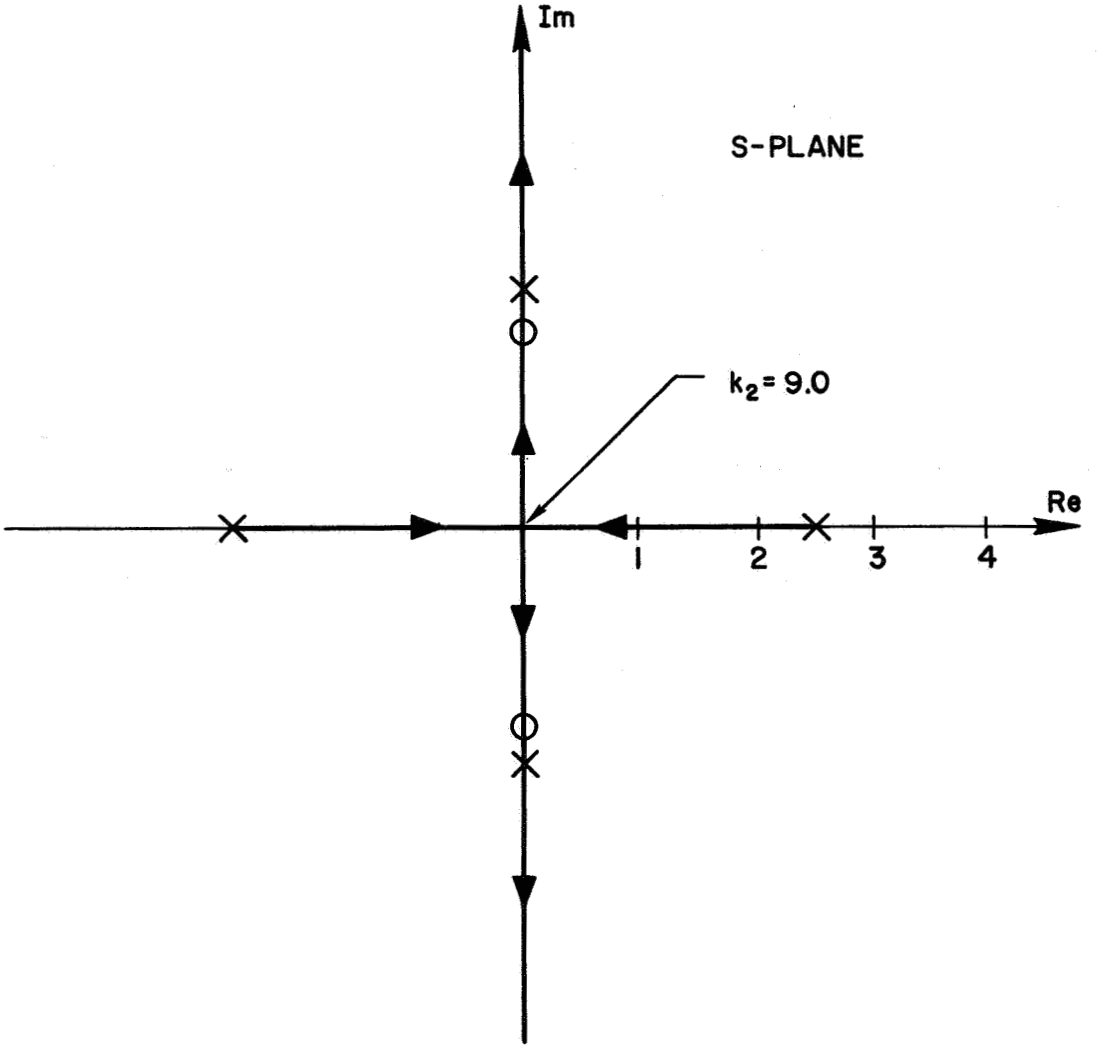

FIG. 3-1. ROOT-LOCUS PLOT FOR EQ. (3-11).
Gain is k_2 and $B_L = 4$.

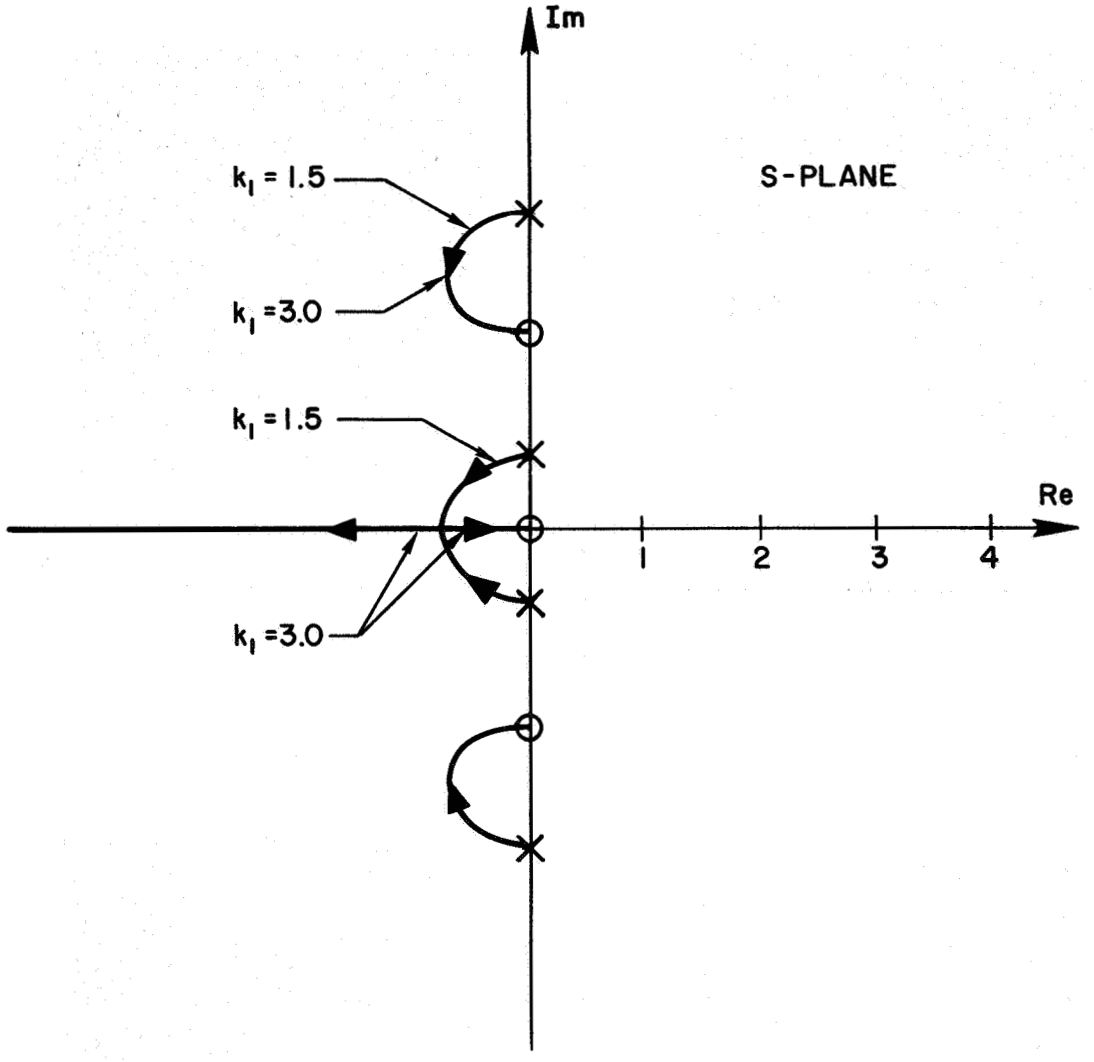

FIG. 3-2. ROOT-LOCUS PLOT FOR EQ. (3-12).
Gain is k_1 and $k_2 = 10$, $B_L = 4$.

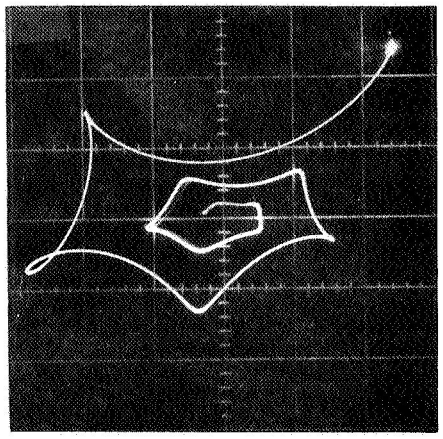

($k_1 = 0.5$)

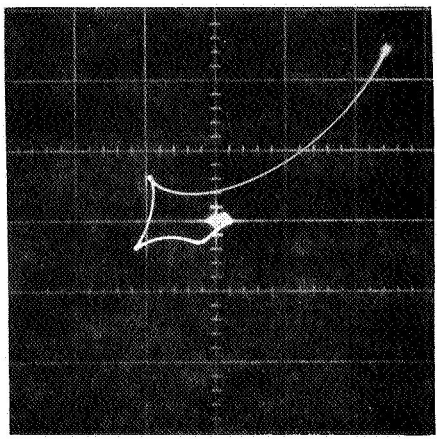

($k_1 = 1.5$)

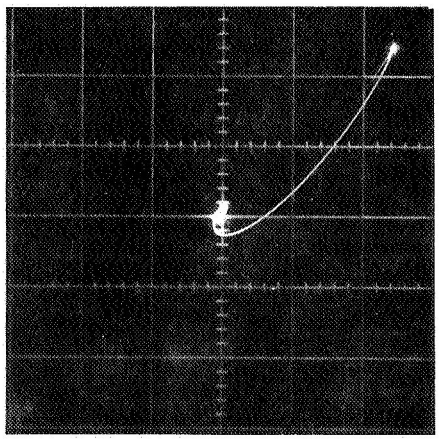

($k_1 = 3$)

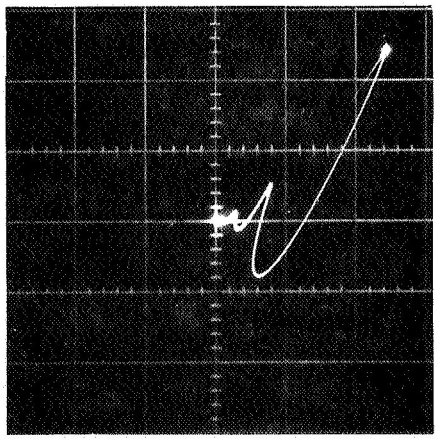

($k_1 = 5$)

FIG. 3-3. RESPONSE WITH RADIAL-AXIS CONTROL OF EQ. (3-2): y vs x. $k_2 = 10$, $B_L = 4$, and $\dot{x}(0) = \dot{y}(0) = 0$.

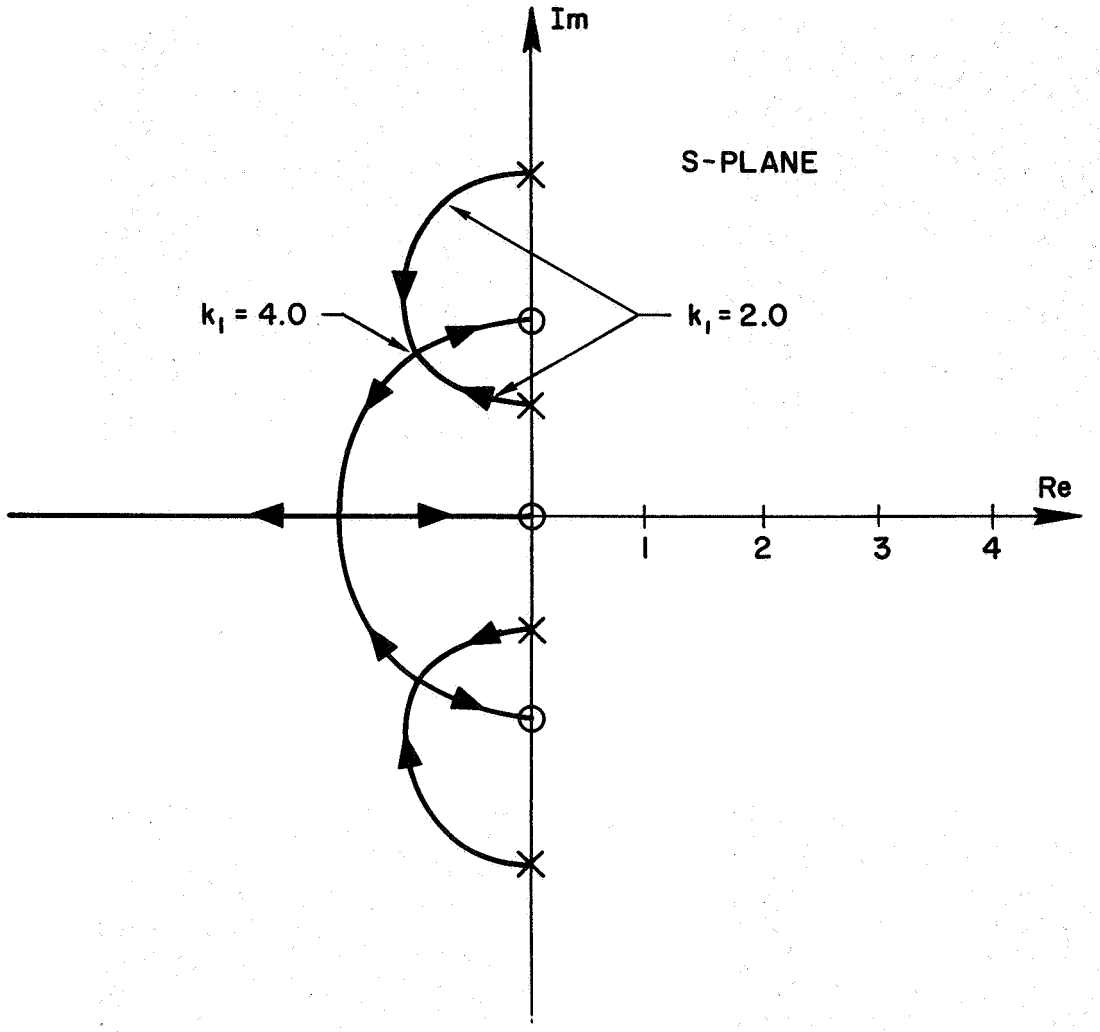

FIG. 3-4. ROOT-LOCUS PLOT FOR EQ. (3-12).
Gain is k_1 and $k_2 = 12$, $B_L = 4$.

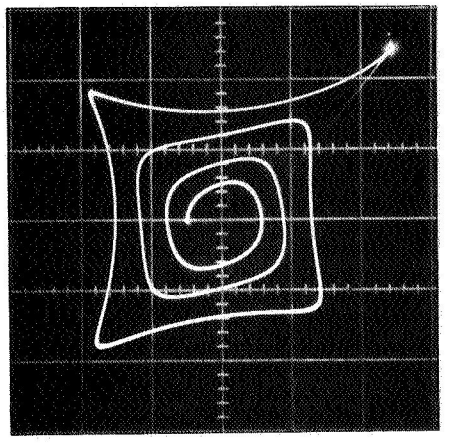

($k_1 = 0.5$)

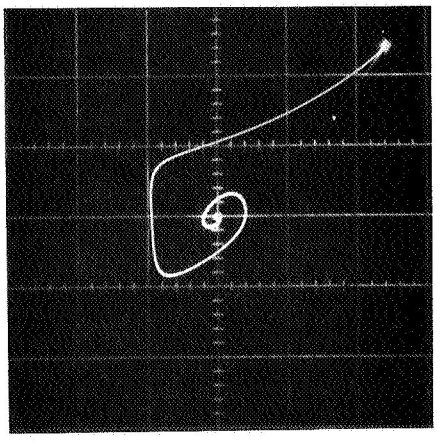

($k_1 = 2$)

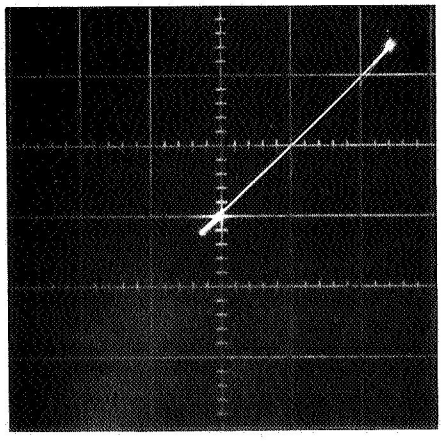

($k_1 = 4$)

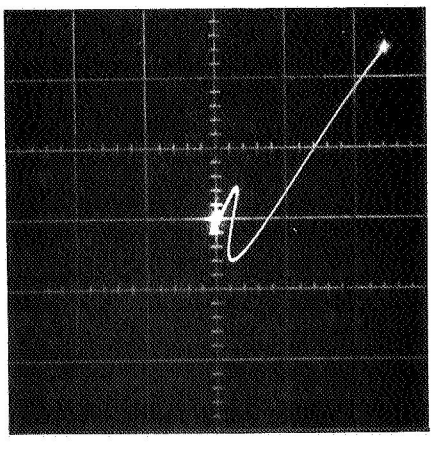

($k_1 = 6$)

FIG. 3-5. RESPONSE WITH RADIAL-AXIS CONTROL OF EQ. (3-2): y vs x. $k_2 = 12$, $B_L = 4$, and $\dot{x}(0) = \dot{y}(0) = 0$.

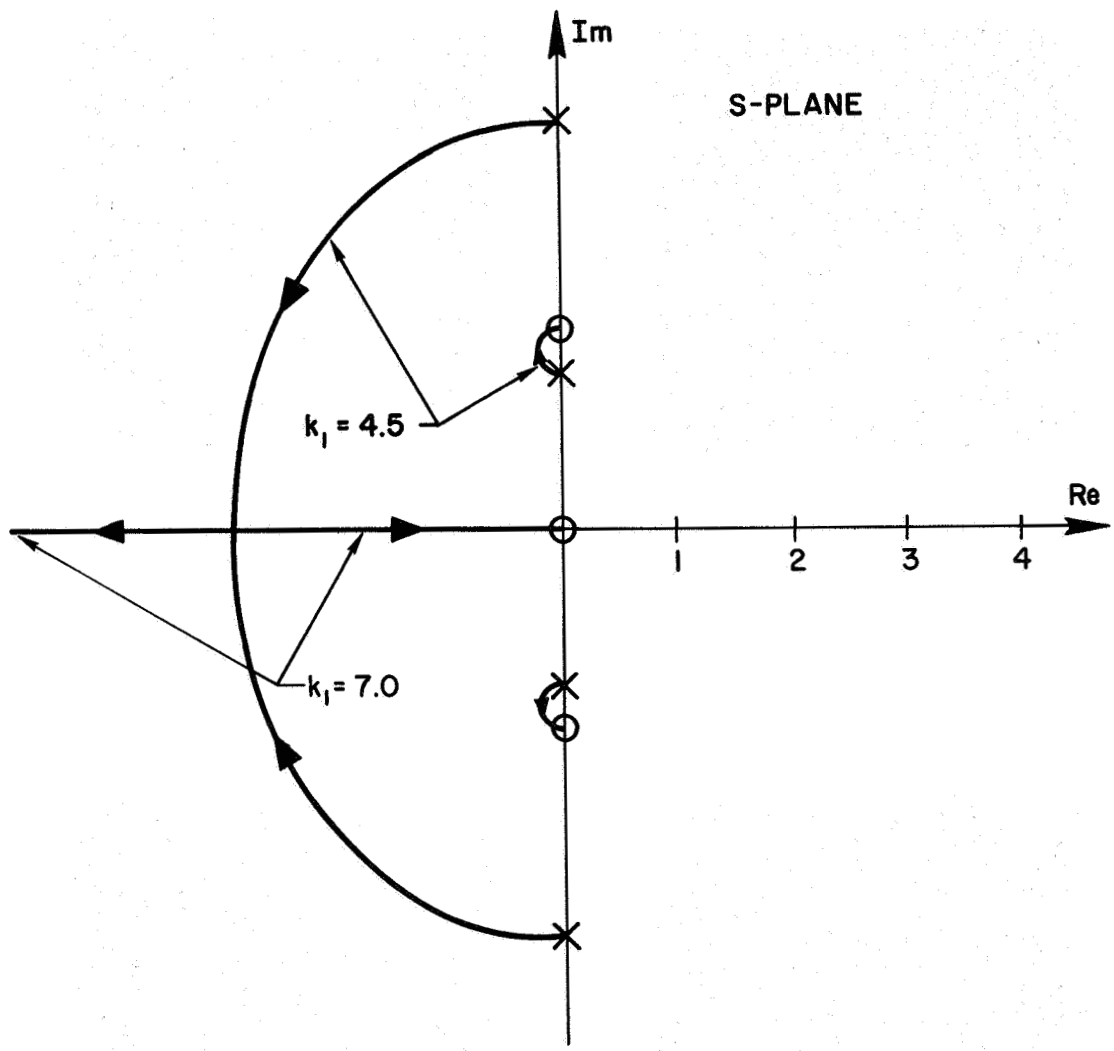

FIG. 3-6. ROOT-LOCUS PLOT FOR EQ. (3-12).
Gain is k_1 and $k_2 = 16$, $B_L = 4$.

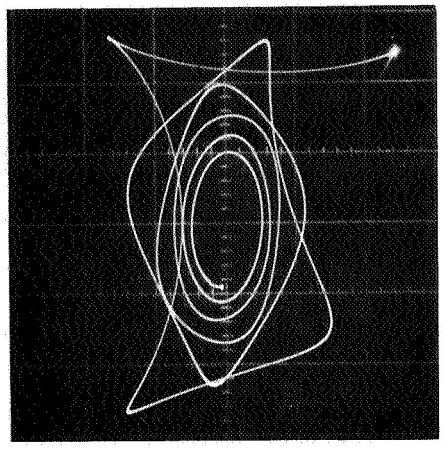

($k_1 = 0.5$)

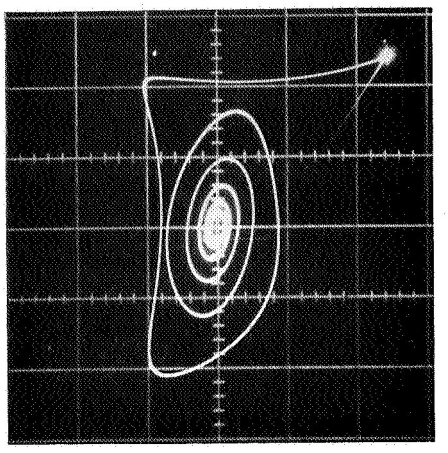

($k_1 = 1.5$)

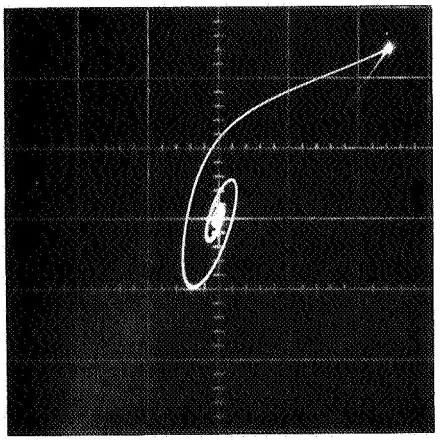

($k_1 = 4.5$)

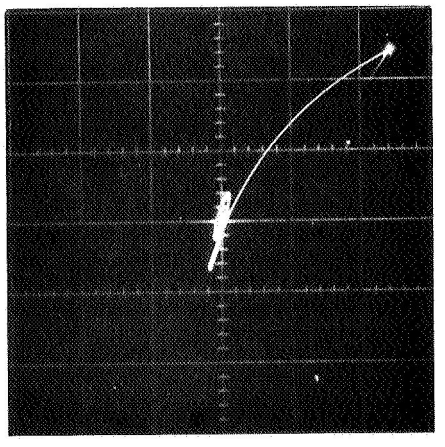

($k_1 = 7$)

FIG. 3-7. RESPONSE WITH RADIAL-AXIS CONTROL OF EQ. (3-2): y vs x. $k_2 = 16$, $B_L = 4$, and $\dot{x}(0) = \dot{y}(0) = 0$.

It is obvious that the response will be underdamped whenever k_2 is too large. However, when the radial-axis control is augmented with positive y-feedback, it is possible to obtain more damping. This can be seen at once by comparing Figs. 3-7 and 3-8 (note instability at $k_1 = 0.5$ in Fig. 3-8). An explanation for this behavior can be found by writing Eq. (3-9) as

$$\frac{2k_4 s}{s^4 + k_1 s^3 + [k_2 - (B_L - 2)]s^2 + k_1(B_L - 1)s + (B_L - 1)[k_2 - (2B_L + 1)]} = -1 \tag{3-13}$$

and examining the resulting root-locus plot given in Fig. 3-9. It can be seen that the damping will be increased for small values of k_4, but instability can occur if k_4 becomes too large.

3. Floquet Stability Investigations

In some instances, the magnitudes of the periodic coefficients in the linearized equations of motion are appreciable. Therefore, the effects of these coefficients on the stability of the closed-loop system should be examined. If the effects due to the eccentricity and to the amplitude of a nominal path are analyzed separately,* this examination can be performed in an efficient manner by making use of Floquet theory.[58]

The linearized equations of motion can be written in the matrix form

$$\dot{X}(t) = F(t)X(t) \tag{3-14}$$

For a two-dimensional analysis (fourth-order system), $X(t)$ is a 4×1 state vector and $F(t)$ is a 4×4 periodic matrix [i.e., $F(t) = F(t + T)$]. To implement Floquet's theory, it is first necessary to define a 4×4 matrix $H(t)$ by

$$\begin{aligned} \dot{H}(t) &= F(t)H(t) \\ H(0) &= I \quad \text{(unit matrix)} \end{aligned} \tag{3-15}$$

*In general, some coupling is present.

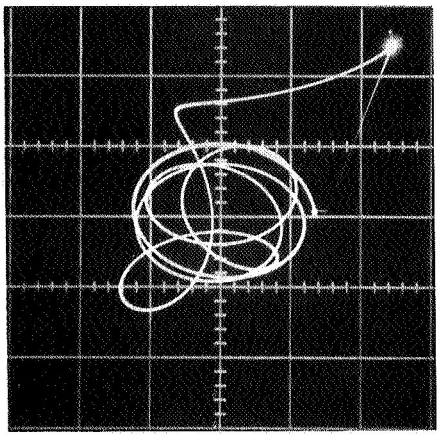

($k_1 = 0.5$)

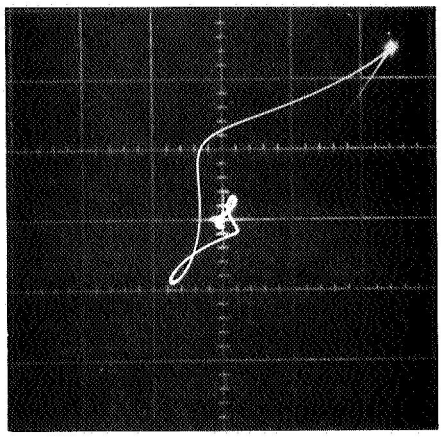

($k_1 = 1.5$)

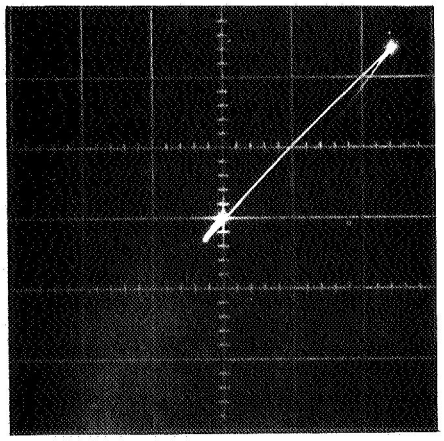

($k_1 = 4.5$)

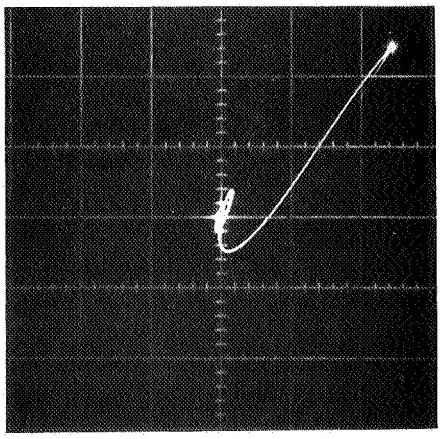

($k_1 = 7$)

FIG. 3-8. RESPONSE WITH RADIAL-AXIS CONTROL OF EQ. (3-5): y vs x. $k_2 = 16$, $k_4 = 3.5$, $B_L = 4$, and $\dot{x}(0) = \dot{y}(0) = 0$.

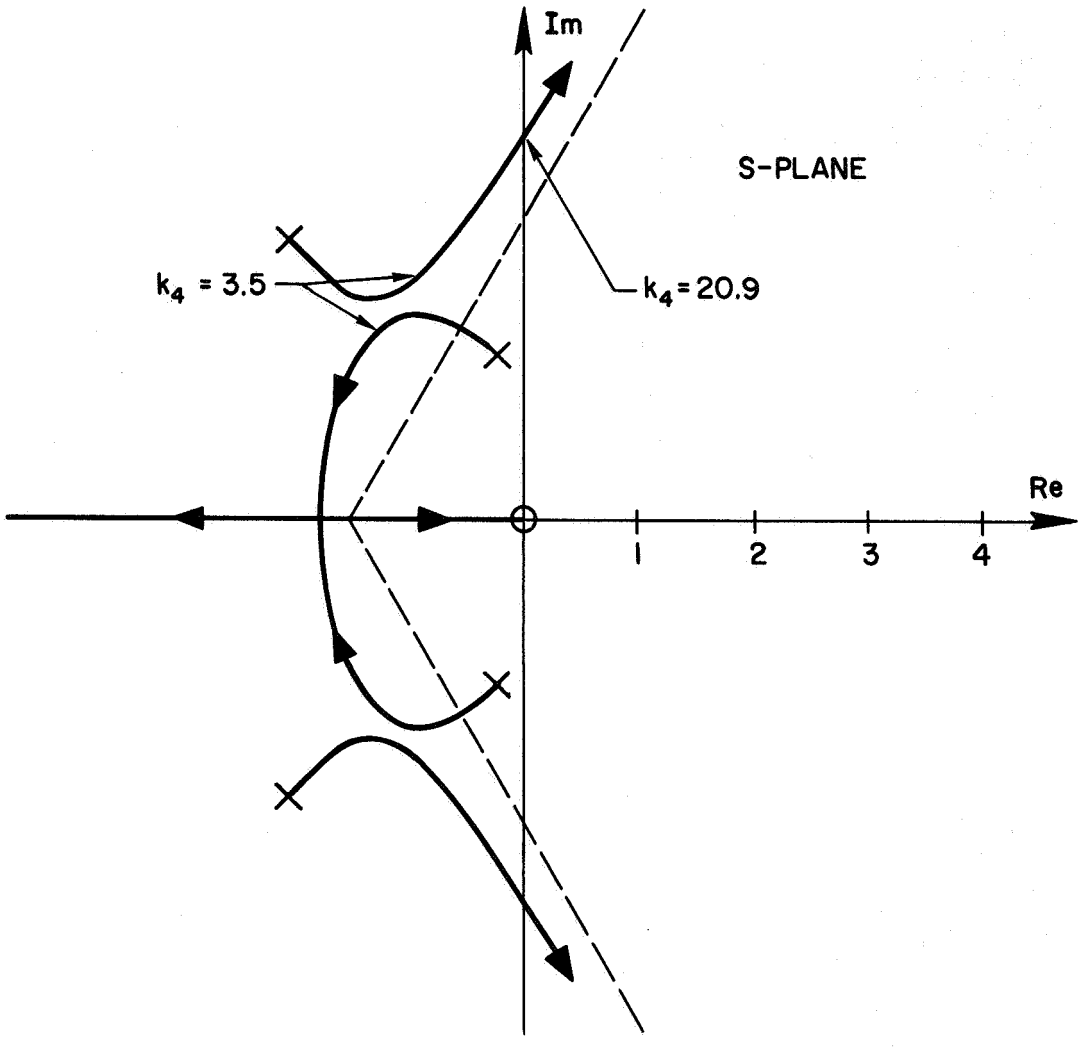

FIG. 3-9. ROOT-LOCUS PLOT FOR EQ. (3-13). Gain is k_4 and $k_1 = 4.5$, $k_2 = 16$, $B_L = 4$.

Equation (3-15) is integrated numerically to obtain $H(T)$, and the following characteristic equation is formed

$$\det[H(T) - \lambda I] = 0 \tag{3-16}$$

On the assumption that the roots λ_j $(j = 1, 2, 3, 4)$ of Eq. (3-16) are distinct, Floquet's theorem states that all solutions of Eq. (3-14) are bounded if and only if

$$|\lambda_j| \leq 1 \qquad (j = 1, 2, 3, 4) \tag{3-17}$$

a. Eccentricity Effect

From Eqs. (1-43) and (3-2), the linearized equations of motion at a collinear point with radial-axis control are

$$\begin{aligned} \ddot{x} - 2(1 + \nu)\dot{y} - (2B_L + 1)x &= (2\nu - 6B_L\rho)x + \dot{\nu}y - k_1\dot{x} - k_2x \\ \ddot{y} + 2(1 + \nu)\dot{x} + (B_L - 1)y &= -\dot{\nu}x + (2\nu + 3B_L\rho)y \end{aligned} \tag{3-18}$$

and neglecting terms of $O(e^2)$ [cf Eq. (2-19)]

$$\begin{aligned} \rho &= -e \cos t \\ \nu &= 2e \cos t \end{aligned} \tag{3-19}$$

Therefore, $T = 2\pi$, and

$$X(t) = \begin{bmatrix} x(t) \\ \dot{x}(t) \\ y(t) \\ \dot{y}(t) \end{bmatrix} \tag{3-20}$$

$$F(t) = \begin{bmatrix} 0 & 1 & 0 & 0 \\ F_{21} & -k_1 & F_{23} & F_{24} \\ 0 & 0 & 0 & 1 \\ F_{41} & F_{42} & F_{43} & 0 \end{bmatrix} \tag{3-21}$$

$$F_{21} = [(2B_L + 1) - k_2 + 2e(2 + 3B_L)\cos t] \tag{3-22}$$

$$F_{23} = - F_{41} = - 2e \sin t \tag{3-23}$$

$$F_{24} = - F_{42} = 2(1 + 2e \cos t) \tag{3-24}$$

$$F_{43} = - [(B_L - 1) + e(3B_L - 4)\cos t] \tag{3-25}$$

When Eqs. (3-20) to (3-25) are substituted into Eq. (3-14), and when the aforementioned procedure is carried out, the instability regions of the parameter space (k_1, k_2) are determined. Instability charts for the collinear points of the Earth-Moon system are given in Fig. 3-10.

Two interesting features of these charts should be pointed out. By analogy with the constant coefficient system, Eq. (3-22) suggests that the periodic coefficient system may be stable if

$$k_2 > (2B_L + 1) + 2e(2 + 3B_L) \tag{3-26}$$

For the Earth-Moon system, Eq. (3-26) gives $(k_2)_{L1} > 13.19$ and $(k_2)_{L2} > 8.65$. When these inequalities are satisfied, the larger instability regions of Fig. 3-10 are excluded. The remaining points of instability can be explained by resonance. The value of k_2 for closed-loop resonance of the constant coefficient system can be found from Eq. (3-3).

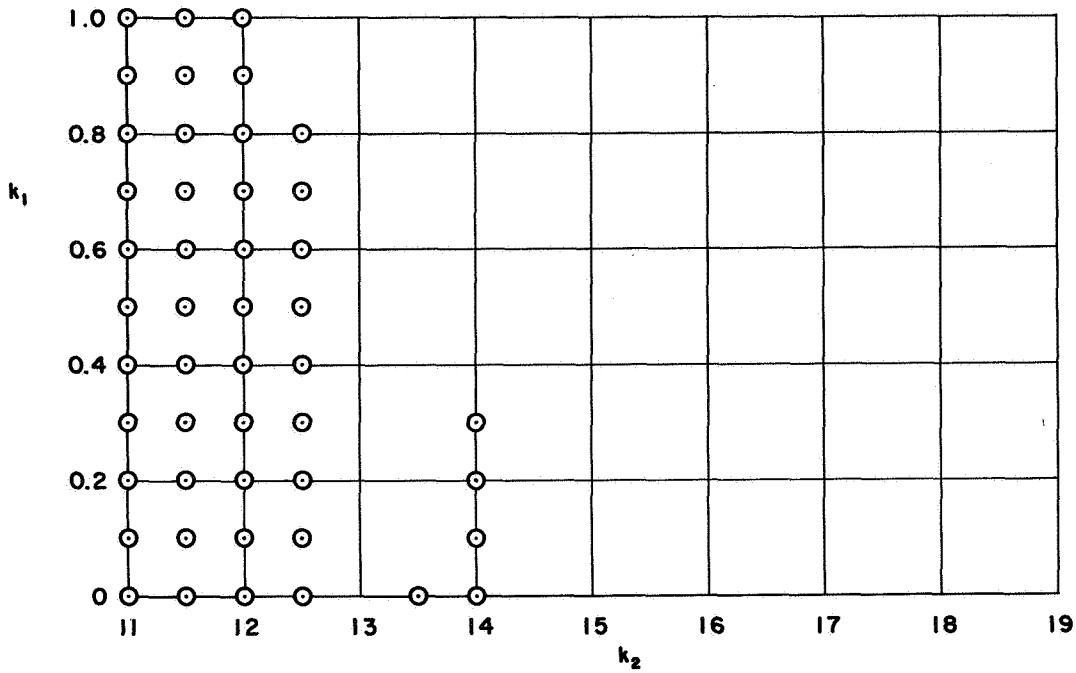

L_1 Point (B_{L1} = 5.14760)

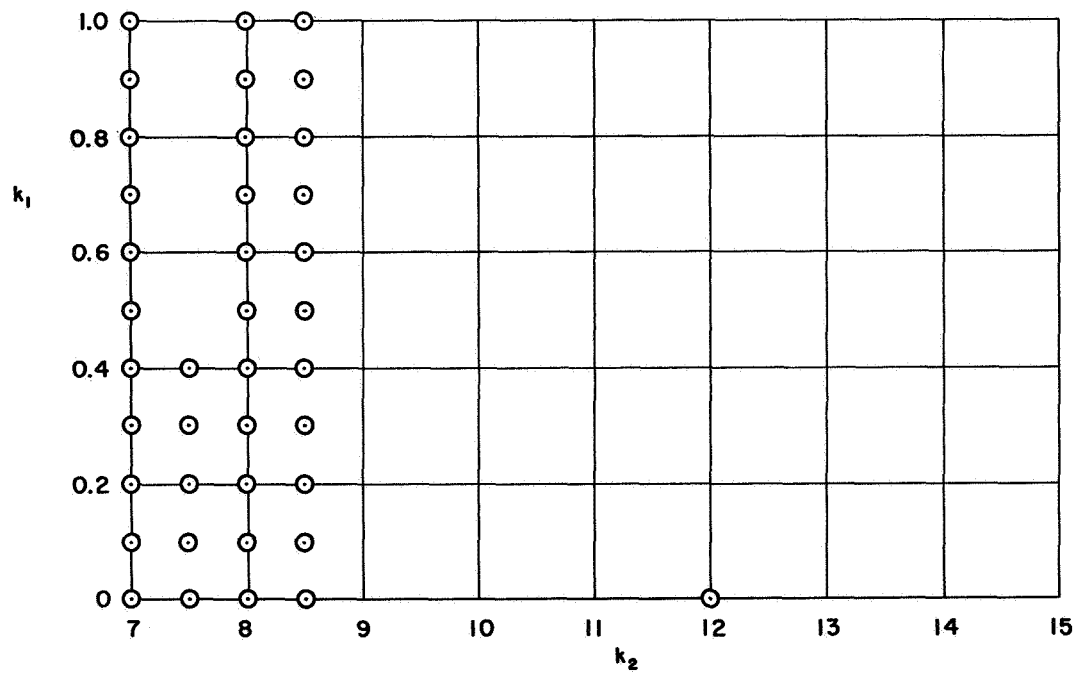

L_2 Point (B_{L2} = 3.19042)

FIG. 3-10. INSTABILITY CHARTS FOR CONTROLLED MOTION, WITH RADIAL-AXIS CONTROL OF EQ. (3-2), AT THE COLLINEAR POINTS OF THE EARTH-MOON SYSTEM. e = 0.05490; ⊙ - unstable.

For $k_1 = 0$, this value of k_2 is given by

$$k_2 = \frac{(2B_L + 1)(B_L - 1) - (B_L - 2)\omega^2 - \omega^4}{(B_L - 1) - \omega^2} \qquad (3\text{-}27)$$

When $\omega = 1$, the critical values of k_2 in the Earth-Moon system are $(k_2)_{L1} = 13.57$ and $(k_2)_{L2} = 11.74$. Figure 3-10 shows that points of instability are located in the vicinity of these critical values.

It is tempting to assume that Eqs. (3-26) and (3-27) can be used to find the principal instability regions for any system. At the L_2 point of the Sun-Mercury system, Eq. (3-26) gives $k_2 > 14.68$, and Eq. (3-27) yields $k_2 = 11.98$. A comparison of these values with the instability chart of Fig. 3-11 shows that a more sophisticated interpretation is needed for larger eccentricities.

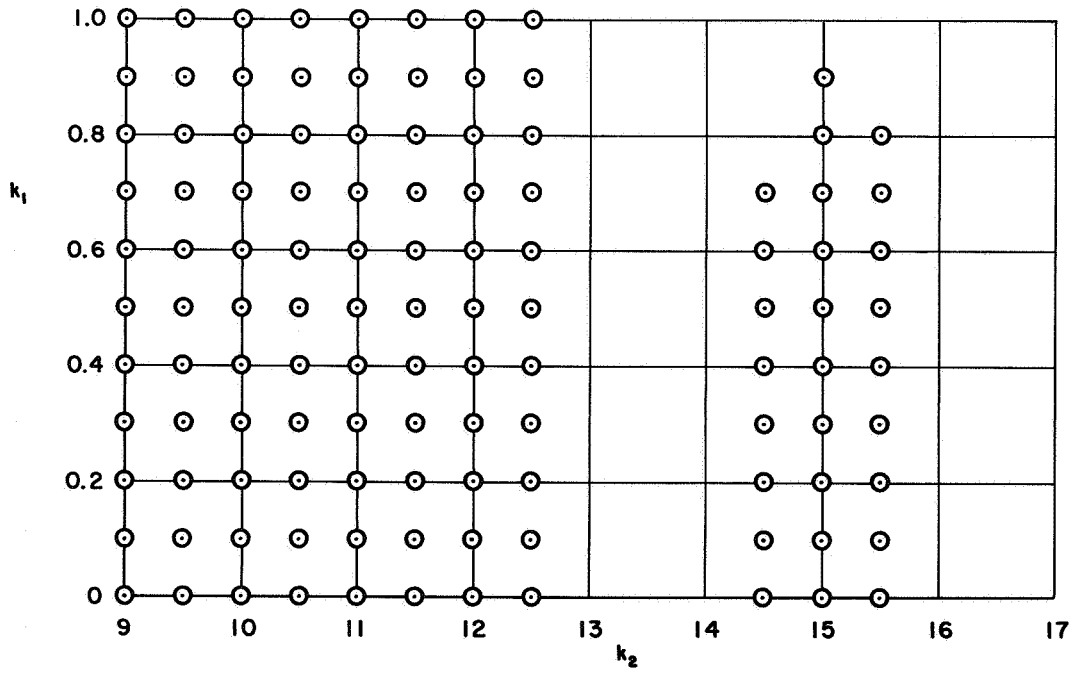

FIG. 3-11. INSTABILITY CHART FOR CONTROLLED MOTION, WITH RADIAL-AXIS CONTROL OF EQ. (3-2), AT THE L_2 POINT OF THE SUN-MERCURY SYSTEM. $B_{L2} = 3.9772$; $e = 0.20563$; ⊙ - unstable.

b. Motion Relative to a Periodic Orbit

If eccentricity terms are neglected, the linearized equations of motion relative to a periodic orbit around a collinear point with radial-axis control are [see Eqs. (2-30) and (3-2)]

$$\ddot{\xi} - 2\dot{\eta} - (2B_L + 1)\xi = \mp 3C_L A_{y1}[2k(\sin \omega_n t)\xi - (\cos \omega_n t)\eta] - k_1\dot{\xi} - k_2\xi$$

$$\ddot{\eta} + 2\dot{\xi} + (B_L - 1)\eta = \pm 3C_L A_{y1}[k(\sin \omega_n t)\eta + (\cos \omega_n t)\xi] \tag{3-28}$$

In this case, $T = 2\pi/\omega_n$, and

$$X(t) = \begin{bmatrix} \xi(t) \\ \dot{\xi}(t) \\ \eta(t) \\ \dot{\eta}(t) \end{bmatrix} \tag{3-29}$$

$$F(t) = \begin{bmatrix} 0 & 1 & 0 & 0 \\ F_{21} & -k_1 & F_{23} & 2 \\ 0 & 0 & 0 & 1 \\ F_{41} & -2 & F_{43} & 0 \end{bmatrix} \tag{3-30}$$

$$F_{21} = [(2B_L + 1) - k_2 \mp 6C_L k A_{y1} \sin \omega_n t] \tag{3-31}$$

$$F_{23} = F_{41} = \pm 3C_L A_{y1} \cos \omega_n t \tag{3-32}$$

$$F_{43} = -[(B_L - 1) \mp 3C_L k A_{y1} \sin \omega_n t] \tag{3-33}$$

The instability regions of the parameter space (A_{y1}, k_1, k_2) can be obtained by substituting Eqs. (3-29) to (3-33) into Eq. (3-14) and following the procedure given above. Instability charts for the L_2 point of the Earth-Moon system are given in Fig. 3-12 for six values of the gain k_1. For a lightly-damped system $(k_1 = 0.1)$, the region of instability is rather large. However, the size of this region shrinks quite rapidly as the damping is increased. At $k_1 = 2.5$, it has almost disappeared from the parameter space of Fig. 3-12. For $\omega = \omega_n/2 = 0.931325$, Eq. (3-27) gives $k_2 = 10.87$. Thus, the instability region of Fig. 3-12 is caused by a subharmonic resonance at $\omega = \omega_n/2$ as might be expected from the form of $F(t)$.

B. Equilateral-Triangle Points

If eccentricity is neglected, the linearized equations of motion at an equilateral-triangle point are [from Eq. (1-62)]

$$\ddot{x}' - 2\dot{y}' - \alpha x' = F_{cx'} \tag{3-34a}$$

$$\ddot{y}' + 2\dot{x}' - \beta y' = F_{cy'} \tag{3-34b}$$

$$\ddot{z}' + z' = F_{cz'} \tag{3-34c}$$

Once again, the z'-axis motion can be damped by using the control $F_{cz'} = -k_1'\dot{z}'$ with $k_1' > 0$. As shown in Chapter I, for $\mu < 0.03852...$, the coupled motion in the $x'y'$-plane is neutrally stable when $F_{cx'} = F_{cy'} = 0$. In this section, a simple single-axis feedback control is designed; this control will provide adequate damping for the oscillatory motion.*

*Fleming[5] has designed a dual-axis feedback control to perform the same task.

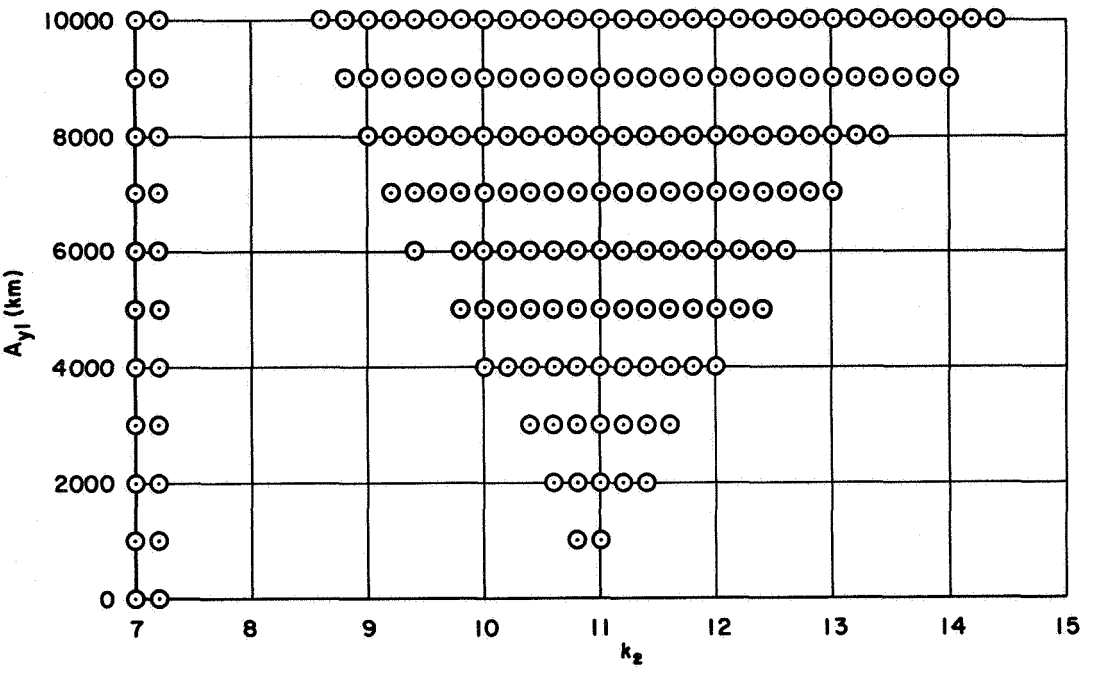

($k_1 = 0.1$)

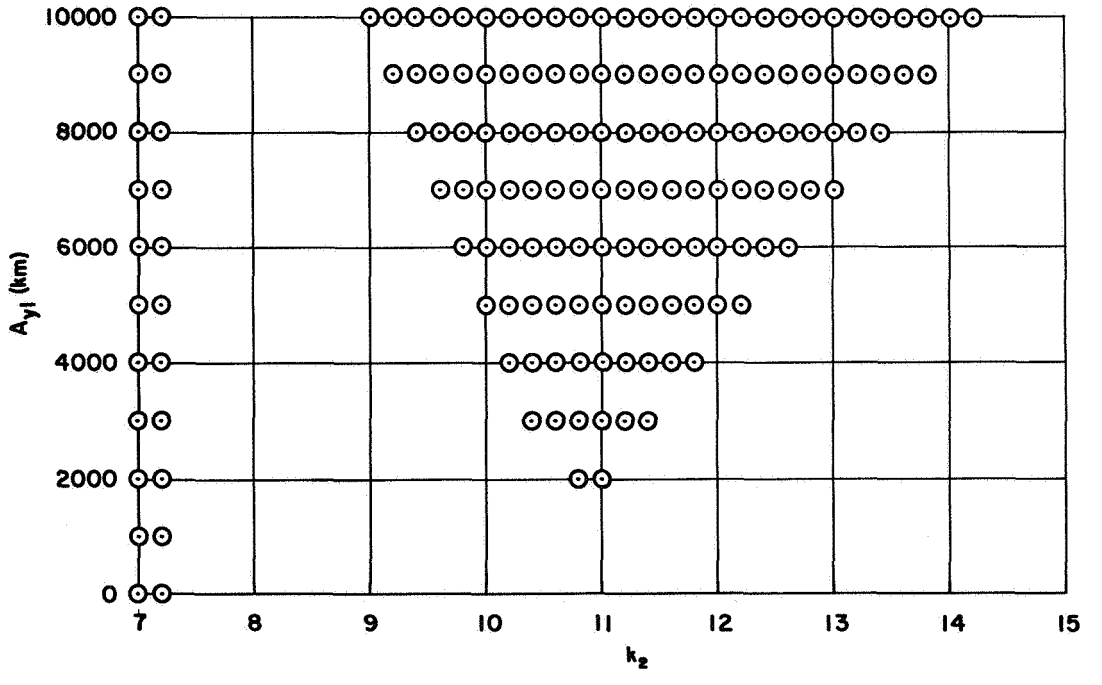

($k_1 = 0.5$)

FIG. 3-12. INSTABILITY CHARTS FOR CONTROLLED MOTION, WITH RADIAL-AXIS CONTROL OF EQ. (3-2), RELATIVE TO A PERIODIC ORBIT AROUND THE L_2 POINT OF THE EARTH-MOON SYSTEM.
⊙ - unstable.

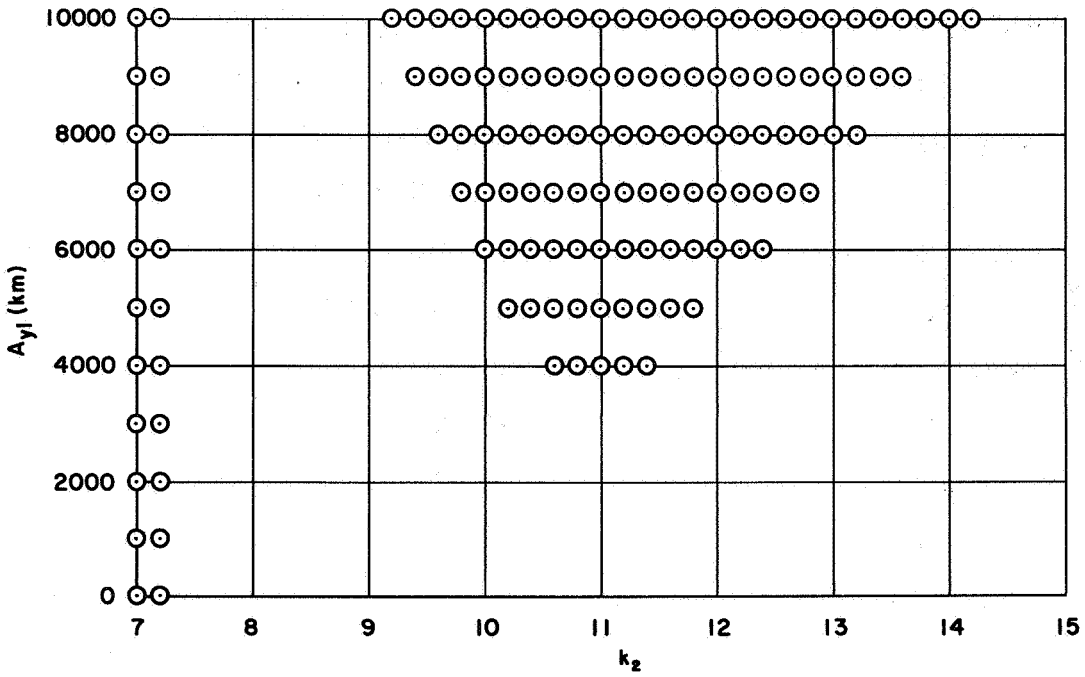

(k_1 = 1.0)

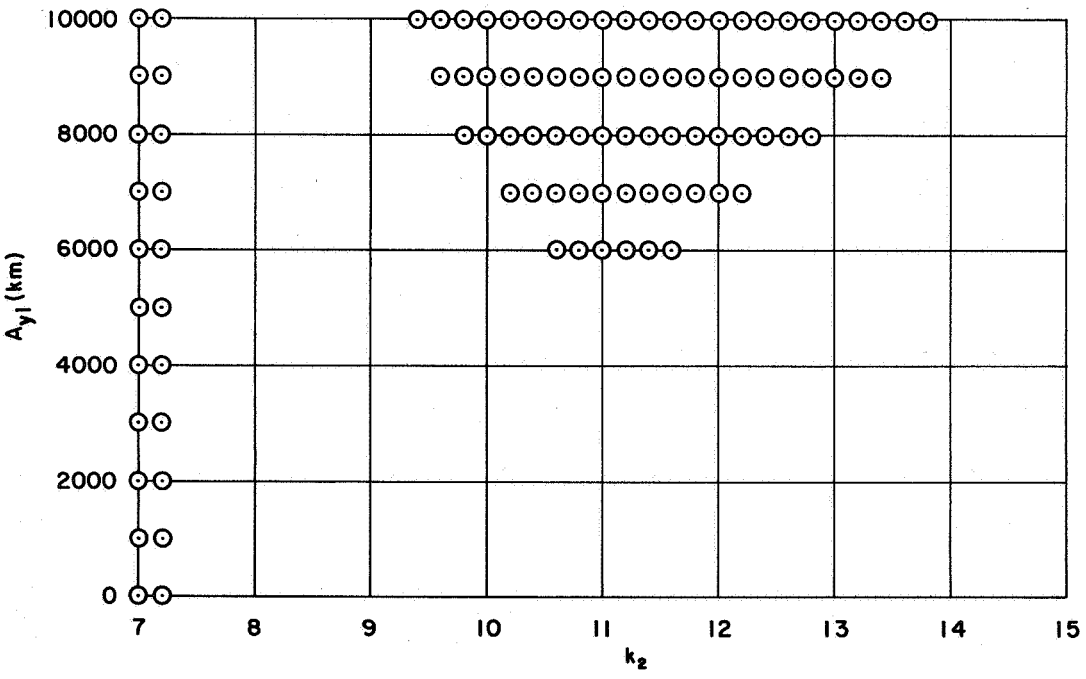

(k_1 = 1.5)

FIG. 3-12. (CONTINUED).

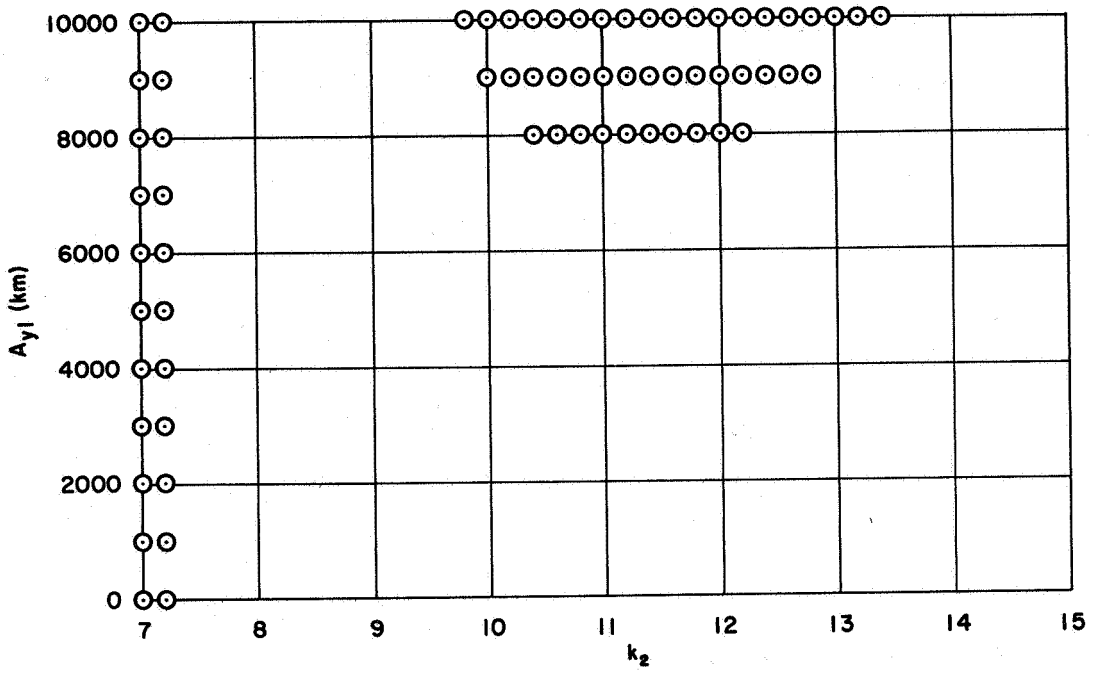

(k_1 = 2.0)

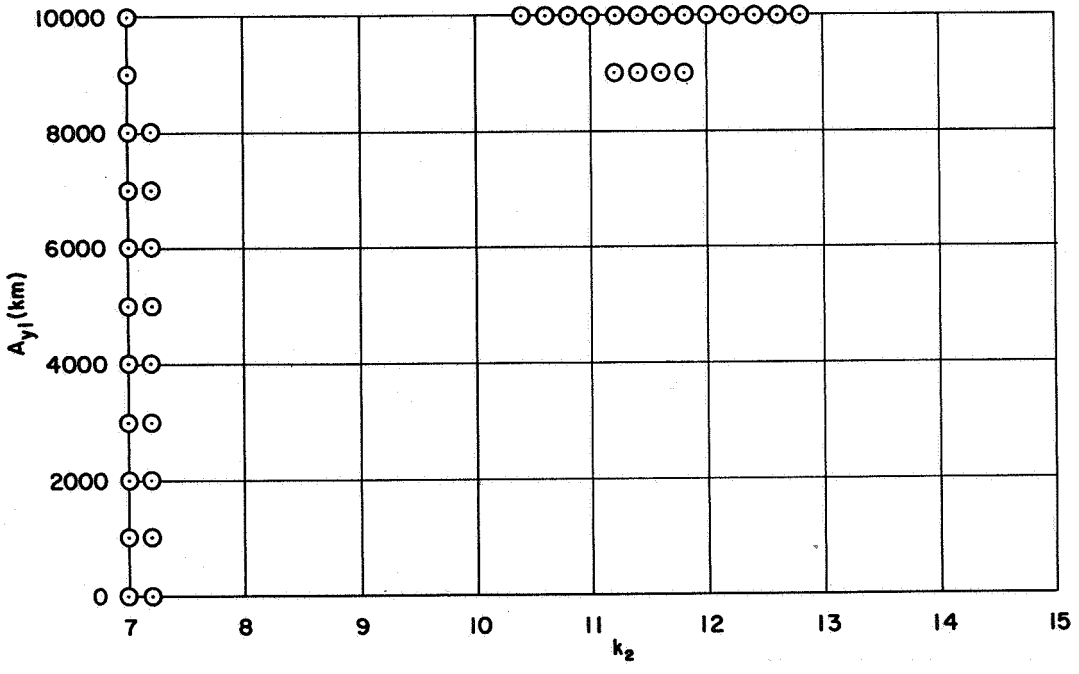

(k_1 = 2.5)

FIG. 3-12. (CONTINUED).

1. Routh Stability Conditions

Damping can be accomplished with the radial-axis (x′-axis) control

$$F_{cx'} = - k_1\dot{x}' + k_4 y'$$
$$F_{cy'} = 0 \qquad (3\text{-}35)$$

With this control, the characteristic equation becomes*

$$s^4 + k_1 s^3 + s^2 + (2k_4 - k_1\beta)s + \alpha\beta = 0 \qquad (3\text{-}36)$$

and the Routh conditions are

$$k_1 > 0, \quad 2k_4 > k_1\beta$$
$$k_1[k_4(1 + 2\beta) - 2k_1\beta] > 2k_4^2 \qquad (3\text{-}37)$$

The damping can also be obtained with the cross-axis (y′-axis) control

$$F_{cx'} = 0$$
$$F_{cy'} = - k_6 x' - k_7\dot{y}' \qquad (3\text{-}38)$$

For this case, the characteristic equation is**

$$s^4 + k_7 s^3 + s^2 + (2k_6 - k_7\alpha)s + \alpha\beta = 0 \qquad (3\text{-}39)$$

---

*The dual-axis control, $F_{cx'} = - k_1\dot{x}'$, $F_{cy'} = - k_6 x'$, yields the same characteristic equation, with k_6 replacing k_4.

**The dual-axis control, $F_{cx'} = k_4 y'$, $F_{cy'} = - k_7\dot{y}'$, yields the same characteristic equation, with k_4 replacing k_6.

and the Routh conditions are

$$k_7 > 0, \quad 2k_6 > k_7\alpha$$
$$k_7[k_6(1 + 2\alpha) - 2k_7\alpha] > 2k_6^2 \tag{3-40}$$

Notice that Eq. (3-40) has the same form as Eq. (3-37), with α replacing β.

2. Root Loci and Closed-Loop Response

Due to the similarity of Eqs. (3-36) and (3-39), the root-locus plots for the radial-axis and cross-axis controls are equivalent. Therefore, only the radial-axis control of Eq. (3-35) is considered here. To obtain quantitative results, the parameters α and β are computed for the Earth-Moon system [see Eqs. (1-63) and (1-64)]

$$\alpha = 2.97275, \quad \beta = 0.02725 \tag{3-41}$$

If $k_4 = 0$, Eq. (3-36) can be written as

$$\frac{k_1 s(s^2 - \beta)}{s^4 + s^2 + \alpha\beta} = -1 \tag{3-42}$$

and the root-locus plot of Fig. 3-13 is obtained. By choosing appropriate values for k_1 and k_4, the unstable roots are taken into the left-half plane. This can be seen graphically by writing Eq. (3-36) as

$$\frac{2k_4 s}{s^4 + k_1 s^3 + s^2 - k_1\beta s + \alpha\beta} = -1 \tag{3-43}$$

and inspecting a root-locus plot for a fixed value of k_1. For $k_1 = 2.0$, the root-locus plot of Eq. (3-43) is given in Fig. 3-14. The Routh conditions of Eq. (3-37) show that asymptotic stability is obtained when

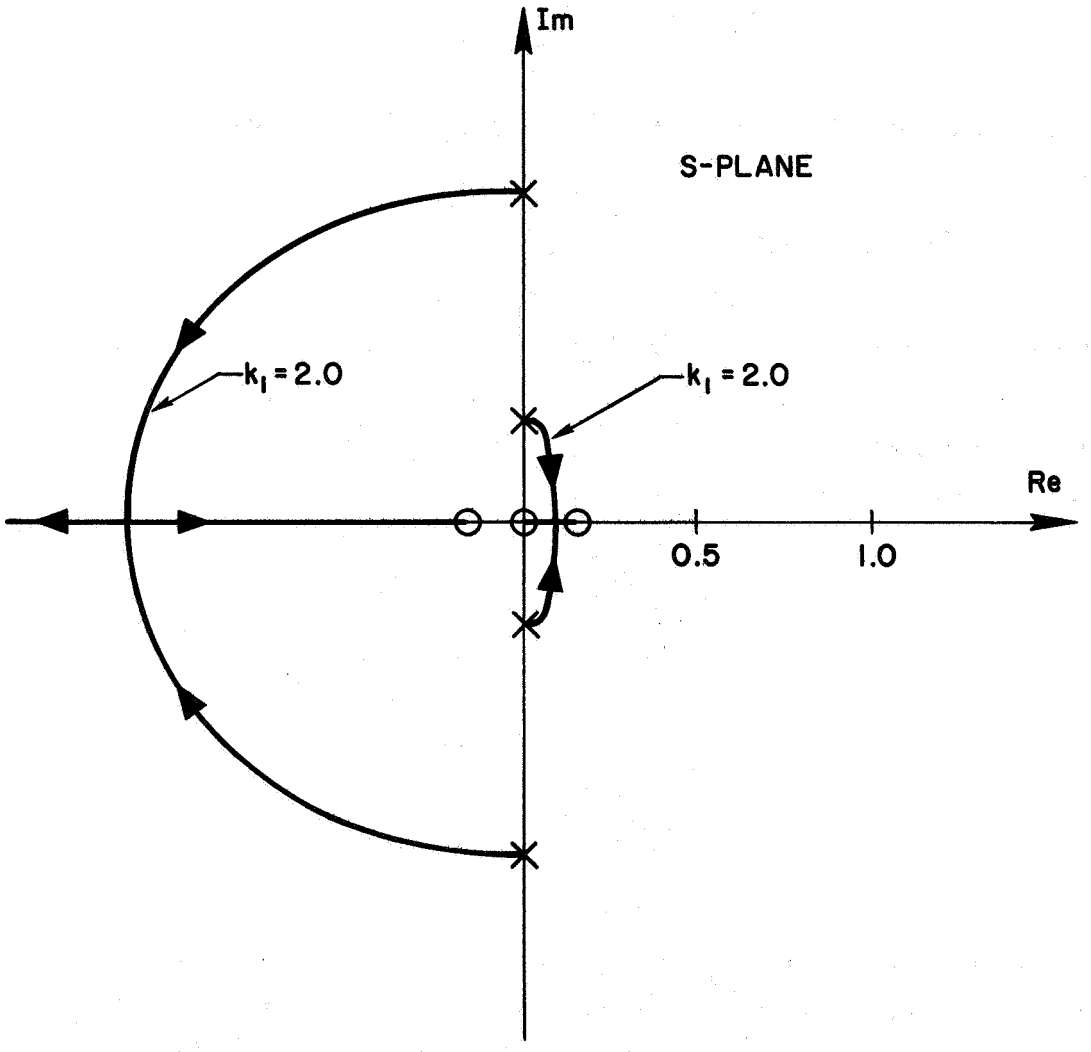

FIG. 3-13. ROOT-LOCUS PLOT FOR EQ. (3-42).
Gain is k_1 and $\alpha = 2.97275$, $\beta = 0.02725$.

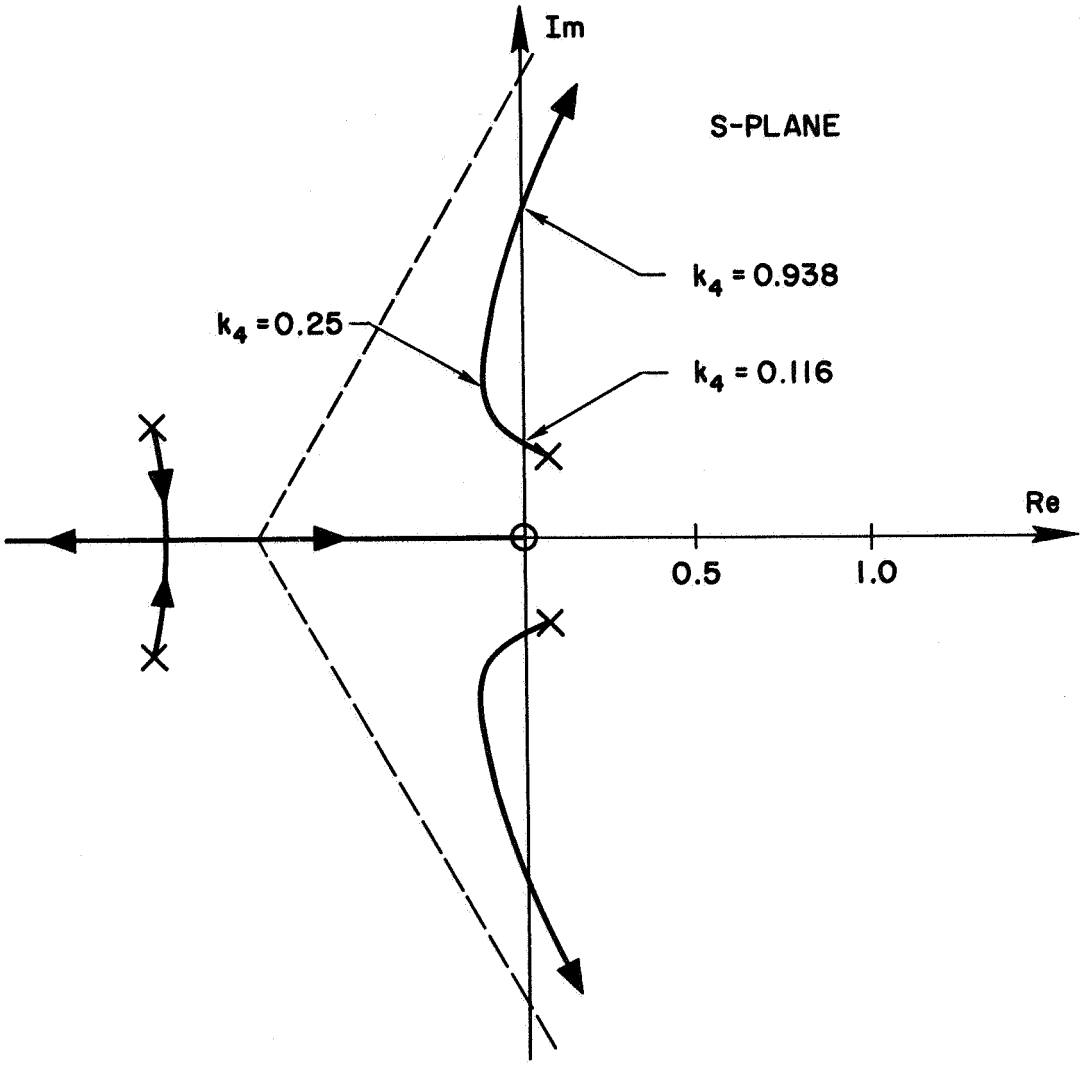

FIG. 3-14. ROOT-LOCUS PLOT FOR EQ. (3-43). Gain is k_4 and $k_1 = 2.0$, $\alpha = 2.97275$, $\beta = 0.02725$.

$$0.05808 < \frac{k_4}{k_1} < 0.4692 \qquad (3\text{-}44)$$

In Fig. 3-15, the closed-loop response for $k_1 = 2.0$ and $k_4 = 0.25$ is compared with the uncontrolled motion.

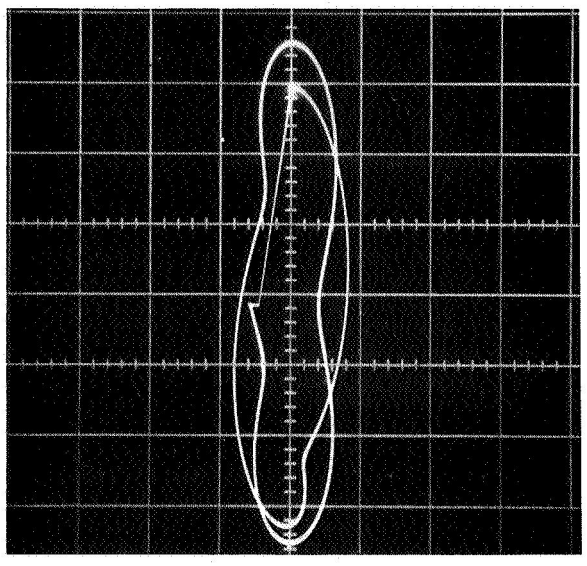

Without control.

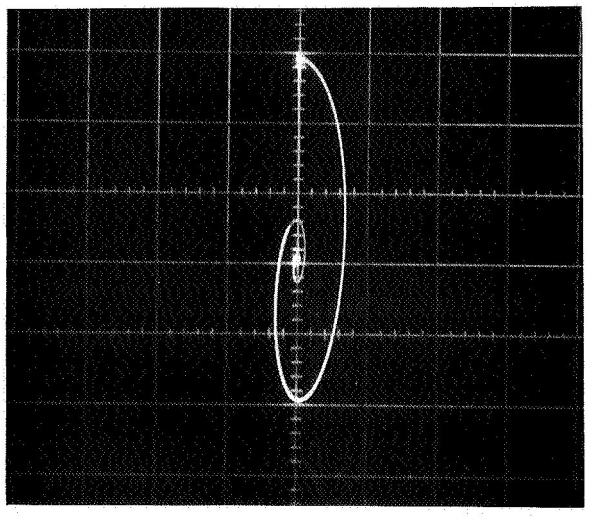

With radial-axis control of Eq. (3-35) $k_1 = 2.0$, $k_4 = 0.25$.

FIG. 3-15. RESPONSE AT THE EQUILATERAL-TRIANGLE POINTS: y' vs x'. $\alpha = 2.97275$, $\beta = 0.02725$, and $\dot{x}'(0) = x'(0) = \dot{y}'(0) = 0$.

Chapter IV

STATION-KEEPING

Several methods for satellite station-keeping in the vicinity of a collinear libration point are examined in Chapters IV-VI. An on-off control system is analyzed in Chapter V, and an unconventional method is investigated in Chapter VI. In the present chapter, the radial-axis control of Eq. (3-2) is treated. General analytical relationships for the control requirements are formulated, and a solar-sail control technique is also presented.

As noted earlier, station-keeping problems for libration-point satellites have not received very much attention. On the other hand, station-keeping techniques for synchronous satellites of the Earth (24-hour satellites) have been thoroughly analyzed,[59-63] and a large reservoir of practical experience has been acquired.[64-66] This knowledge could be very useful in the design of propulsion systems, sensors, attitude-control systems, etc., for libration-point satellites.

A. Average Control-Acceleration Requirements

Realistic estimates of station-keeping costs are needed for feasibility studies of libration-point satellite missions. In this section, some general expressions for these costs are derived. To establish a basis for comparison, note that the average control accelerations for synchronous satellites are about 1.5×10^{-7} g (1 fps/yr $\cong 1 \times 10^{-9}$ g) for north-south station-keeping, and about one-tenth of this value for east-west station-keeping.[63]

1. Cost Estimates for Noise Inputs

The station-keeping cost for a satellite that is following a nominal path around a collinear libration point is a function of measurement noise, engine fluctuations, and random accelerations (gas leakage, random solar radiation pressure effects, etc.). A block diagram of the radial-axis control system with noise inputs is shown in Fig. 4-1. The measurement noise is denoted by n_x, $n_{\dot{x}}$; the engine noise is n_{ex}; and the random accelerations are n_{px}, n_{py}. A simple lag-filter has been added to reduce the effect of the measurement noise. An optimum design

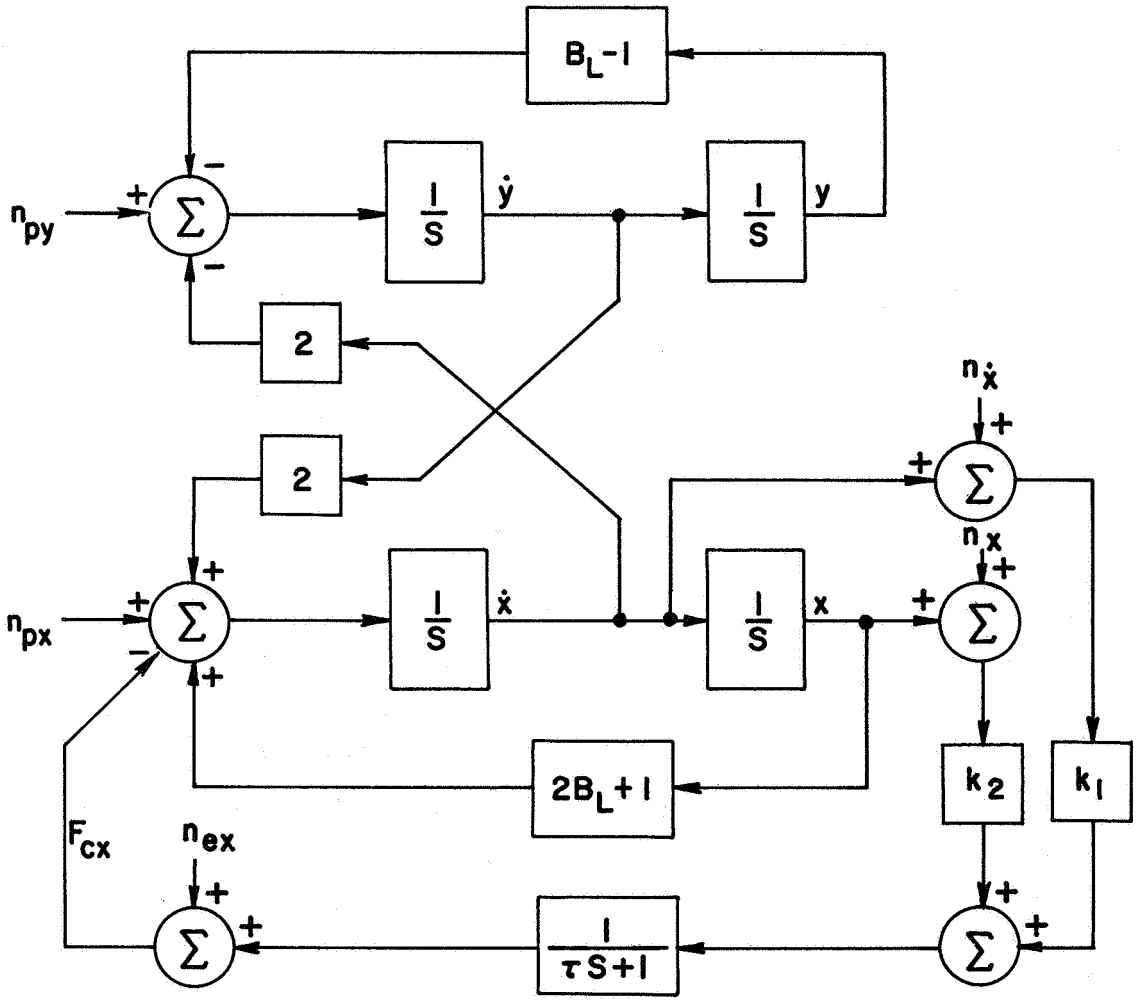

FIG. 4-1. RADIAL-AXIS CONTROL SYSTEM WITH NOISE INPUTS.

can be achieved by choosing the control parameters (k_1, k_2, τ) so as to minimize the mean-square value of the control acceleration F_{cx} (a description of this minimization procedure can be found in Ref. 67). Since the uncontrolled system is unstable, this minimization is meaningful even when $n_{px} = n_{py} = 0$.

a. Optimization

From Fig. 4-1, it can be seen that the control acceleration is

$$F_{cx}(s) = \frac{1}{\tau s + 1}\left[(k_1 s + k_2)x(s) + (k_1 n_{\dot{x}} + k_2 n_x)\right] + n_{ex} \qquad (4\text{-}1)$$

which can be written as

$$F_{cx}(s) = \frac{(k_1 n_{\dot{x}} + k_2 n_x)}{h(s)}\left[s^4 - (B_L - 2)s^2 - (2B_L + 1)(B_L - 1)\right]$$

$$+ \frac{(k_1 s + k_2)}{h(s)}\left\{\left[s^2 + (B_L - 1)\right](n_{px} - n_{ex}) + 2s n_{py}\right\} + n_{ex} \qquad (4\text{-}2)$$

where

$$h(s) = \tau s^5 + s^4 + \left[k_1 - \tau(B_L - 2)\right]s^3 + \left[k_2 - (B_L - 2)\right]s^2$$

$$+ \left[k_1 - \tau(2B_L + 1)\right](B_L - 1)s + \left[k_2 - (2B_L + 1)\right](B_L - 1) \qquad (4\text{-}3)$$

For the characteristic equation, $h(s) = 0$, the Routh stability conditions are

$$\tau \geq 0$$

$$k_2 > (2B_L + 1) \qquad (4\text{-}4)$$

$$\left(\frac{k_1}{k_2}\right) > \tau$$

Writing the characteristic equation in the form

$$\frac{k_1\left(s + \frac{k_2}{k_1}\right)\left[s^2 + (B_L - 1)\right]}{(\tau s + 1)\left[s^4 - (B_L - 2)s^2 - (2B_L + 1)(B_L - 1)\right]} = -1 \qquad (4\text{-}5)$$

the root-locus plot of Fig. 4-2 is obtained.

The engine noise and random accelerations can usually be neglected in a first approximation, and the control acceleration then becomes

$$F_{cx}(s) = \frac{(k_1 n_{\dot{x}} + k_2 n_x)}{h(s)}\left[s^4 - (B_L - 2)s^2 - (2B_L + 1)(B_L - 1)\right] \qquad (4\text{-}6)$$

Assuming that $n_{\dot{x}}$ and n_x are independent, white, Gaussian processes, the mean-square value of Eq. (4-6) is

$$\overline{(F_{cx})^2} = N_{\dot{x}}\left[k_1^2 + k_2^2 R_N\right]\frac{1}{2\pi j}\int_{-j\infty}^{+j\infty}\frac{g(s)}{h(s)h(-s)}\,ds \equiv N_{\dot{x}} P_5 \qquad (4\text{-}7)$$

where

$$g(s) = s^8 - 2(B_L - 2)s^6 + \left[(B_L - 2)^2 - 2(2B_L + 1)(B_L - 1)\right]s^4$$
$$+ 2(B_L - 2)(2B_L + 1)(B_L - 1)s^2 + (2B_L + 1)^2(B_L - 1)^2 \qquad (4\text{-}8)$$

$N_{\dot{x}}$ and N_x are the noise levels, and $R_N \equiv (N_x/N_{\dot{x}})$. The integral of Eq. (4-7) can be written as an algebraic function of the control parameters (k_1, k_2, τ) by using a special table of integrals.[67] Since the resulting expressions are rather cumbersome, a numerical search procedure[68] is used to find a minimum value of the cost parameter P_5, while the stability conditions of Eq. (4-4) are satisfied. It is found that the optimum values are

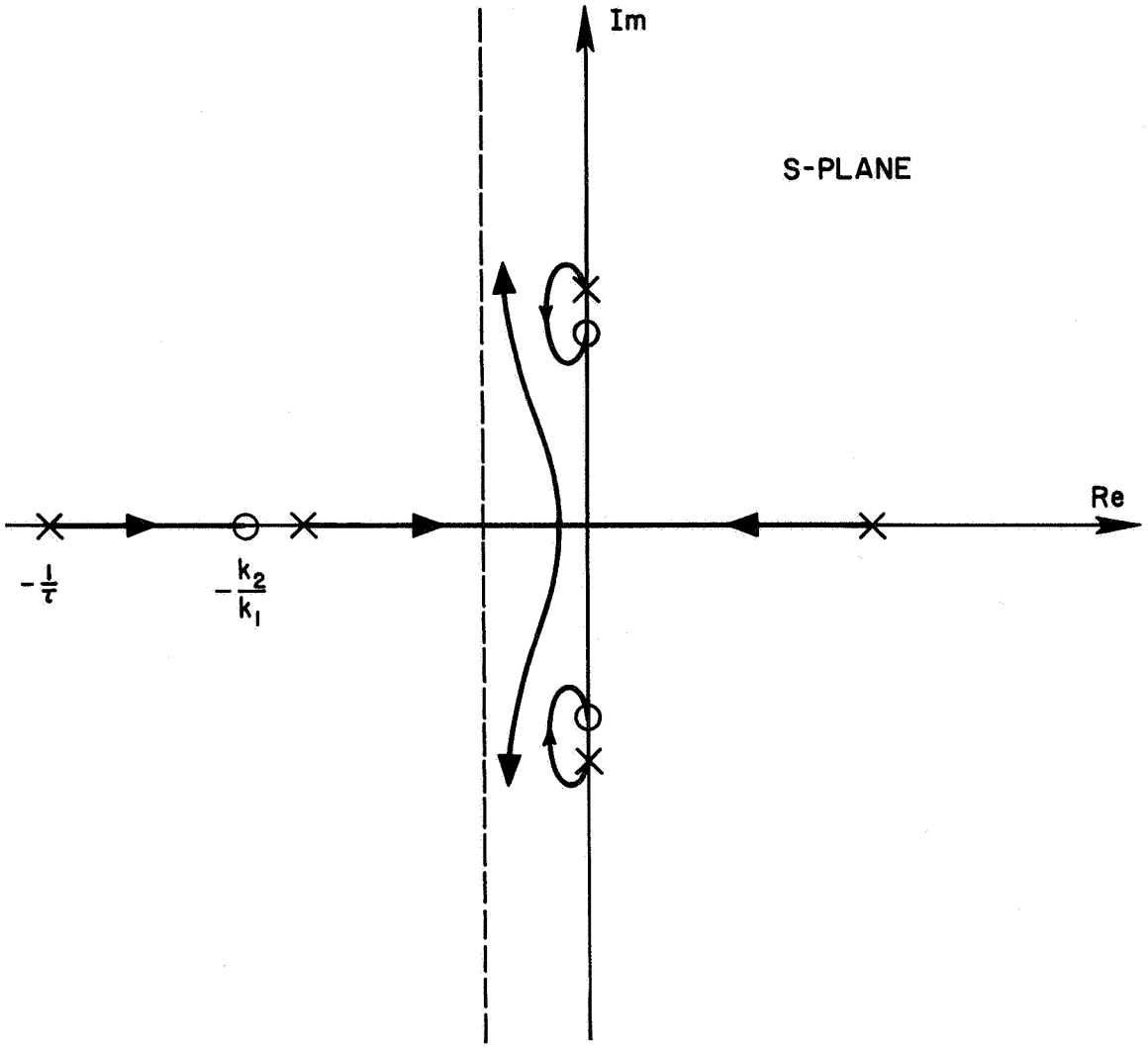

FIG. 4-2. ROOT-LOCUS PLOT FOR EQ. (4-5). Gain is k_1. (Not to scale).

$$P_5 = \frac{k_1}{k_2} Q \qquad k_2 = \frac{4}{3}\left(2B_L + 1\right)$$
$$\tau = \frac{1}{3}\left(\frac{k_1}{k_2}\right) \qquad \frac{k_1}{k_2} = \sqrt{R_N} \tag{4-9}$$

where Q is a function of B_L, and is plotted in Fig. 4-3. Therefore, the minimum average control acceleration is given by*

$$\overline{|F_{cx}|} \cong 0.8\sqrt{\frac{k_1}{k_2} Q N_{\dot{x}}} \tag{4-10}$$

The effects of periodic coefficients (see Chapter III) have not been considered in the foregoing optimization. This omission is probably not too serious as long as the unstable regions of the parameter space are avoided, but some method of assessing the influence of these coefficients would be useful. Equation (3-26) implies that an effective value of B_L,

$$B_L' \equiv B_L + e(2 + 3B_L) \tag{4-11}$$

may be more appropriate for the general case. Although this conjecture seems to be reasonable, verification is required.

b. Estimation of Noise Level

The noise level $N_{\dot{x}}$ can be estimated by using

$$N_{\dot{x}} = \left(\frac{\sigma_{\dot{x}}^2}{W_s T_1}\right) T_M \tag{4-12}$$

where $\sigma_{\dot{x}}^2$ is the range-rate variance, W_s is the sample rate, T_1 is the time interval for a single set of measurements, and T_M is the time

*For a Gaussian process, $\overline{|F_{cx}|} = \frac{2}{\sqrt{2\pi}} \left(F_{cx}\right)_{RMS} \cong 0.8\left(F_{cx}\right)_{RMS}$

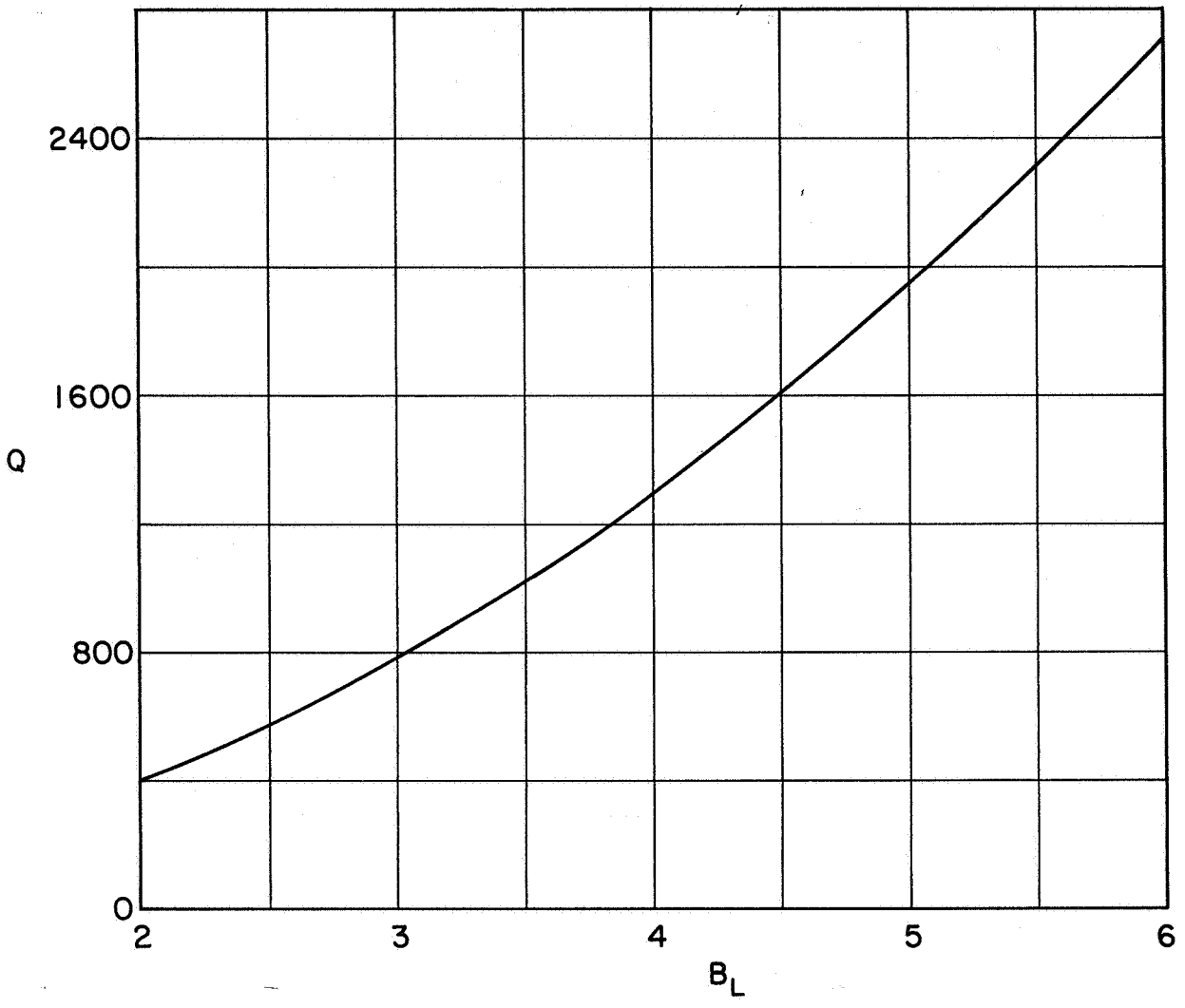

FIG. 4-3. COST PARAMETER Q VS B_L.

interval between sets of measurements. For deep space instrumentation facility (DSIF) measurements, $\sigma_{\dot{x}} \cong 0.02$ m/sec with $W_s = (\text{min})^{-1}$ (Ref. 69). Estimates of $\sigma_{\dot{x}}$ for on-board sensors can be found in Refs. 70-71.

c. Costs at the Earth-Moon Collinear Points

The general results of Eq. (4-9) can be used to find typical values for the station-keeping costs at the Earth-Moon collinear points. For the examples given here, periodic-coefficient stability results are taken into account while choosing the ratio k_1/k_2, but Eq. (4-11) is not employed.

With DSIF measurements,* and T_M = 1 day, T_1 = 5 min, Eq. (4-12) gives $N_x = 1.757 \times 10^{-11} = 6.912$ m^2/sec. The ratio k_1/k_2 is chosen to be 0.1, which means that $R_N = 0.01$. Taking $N_x = (\sigma_x^2/W_s T_1)T_M$, and solving for σ_x, yields $\sigma_x = 0.751$ km. (This accuracy is easily attained with DSIF measurements.) Equations (4-9) and (4-10), along with Fig. 4-3, give

L_1: $k_1 = 1.505$ $\quad k_2 = 15.05$

$\tau = 0.033$ $\quad P_5 \cong 204$

$\overline{|F_{cx}|} = 4.790 \times 10^{-5} = 1.330 \times 10^{-8}$ g

L_2: $k_1 = 0.9841$ $\quad k_2 = 9.841$

$\tau = 0.033$ $\quad P_5 \cong 86$

$\overline{|F_{cx}|} = 3.110 \times 10^{-5} = 8.858 \times 10^{-9}$ g

The values of $\overline{|F_{cx}|}$ for these examples are roughly equal to the average control accelerations that are needed for east-west station-keeping of synchronous satellites.

2. Cost for Sinusoidal Control Acceleration with Noise

In some instances (see Chapter VII), the station-keeping cost is given by $\overline{|F^*_{cx}|}$ where

$$F^*_{cx} = p(t) + F_{cx} \tag{4-13}$$

$$p(t) = K_c \cos \omega t \tag{4-14}$$

*It is assumed here that the satellite in the vicinity of L_2 is following a quasi-periodic orbit around the point, and is visible from the Earth tracking station.

and F_{cx} is a random variable with a Gaussian distribution. Therefore, F^*_{cx} has a Gaussian density function

$$\Phi_{F^*}(x,t) = \frac{1}{\sigma_F\sqrt{2\pi}} \exp\left\{-\frac{[x - p(t)]^2}{2\sigma_F^2}\right\} \tag{4-15}$$

with $\sigma_F \equiv \left(F_{cx}\right)_{RMS}$ (for the radial-axis control of Fig. 4-1, $\sigma_F = \sqrt{\dot{N}_x P_5}$). For this case, the average control acceleration is given by

$$\overline{|F^*_{cx}|} = E\left\{\frac{\omega}{2\pi}\int_0^{2\pi/\omega} |F^*_{cx}(t)|dt\right\} = \frac{\omega}{2\pi}\int_0^{2\pi/\omega} E\left\{|F^*_{cx}(t)|\right\}dt \tag{4-16}$$

where

$$E\left\{|F^*_{cx}(t)|\right\} = \int_{-\infty}^{+\infty} |x|\Phi_{F^*}(x,t)dx \tag{4-17}$$

and $E\{y\}$ is the "expected value" of a random variable y. After some rather lengthy manipulations (see Appendix A), Eq. (4-16) becomes

$$\overline{|F^*_{cx}|} = \frac{e^{-u}}{\sqrt{2\pi}}\left\{2\sigma_F I_o(u) + \frac{K_c^2}{\sigma_F}\left[I_o(u) + I_1(u)\right]\right\} \tag{4-18}$$

where $I_o(u)$ and $I_1(u)$ are modified Bessel functions, and $u \equiv K_c^2/4\sigma_F^2$. Using well-known series expansions[72] for $I_o(u)$ and $I_1(u)$, two limiting cases of Eq. (4-18) can be deduced:

(1) for small values of u

$$\overline{|F^*_{cx}|} \cong \frac{2\sigma_F}{\sqrt{2\pi}}\left[1 + \frac{K_c^2}{4\sigma_F^2}\right] \tag{4-19}$$

(2) for large values of u

$$\overline{|F^*_{cx}|} \cong \frac{2K_c}{\pi}\left[1 + \frac{\sigma_F^2}{2K_c^2}\right] \tag{4-20}$$

3. Cost for a Constant Displacement

A satellite is sometimes stationed at a constant distance δ from the libration point. This displacement may be intentional, or it may be the result of a bias-error in the measurements. In either case, the station-keeping cost will be increased. If terms of $O(\delta^4)$ are neglected, this cost can be obtained from Eq. (1-43). The special cases in which δ lies along a single coordinate axis are illustrative. If ρ and ν are neglected, these costs are approximately:

(1) δ_x only

$$\begin{aligned} F_{cx} &= -(2B_L + 1)\delta_x \pm 3C_L\delta_x^2 - 4D_L\delta_x^3 \\ F_{cy} &= F_{cz} = 0 \end{aligned} \tag{4-21}$$

(2) δ_y only

$$\begin{aligned} F_{cx} &= \mp \frac{3}{2} C_L\delta_y^2 \\ F_{cy} &= (B_L - 1)\delta_y - \frac{3}{2} D_L\delta_y^3 \\ F_{cz} &= 0 \end{aligned} \tag{4-22}$$

(3) δ_z only

$$F_{cx} = \mp \frac{3}{2} C_L \delta_z^2$$

$$F_{cy} = 0 \qquad (4\text{-}23)$$

$$F_{cz} = B_L \delta_z - \frac{3}{2} D_L \delta_z^3$$

The costs for a satellite in the vicinity of the L_2 point of the Earth-Moon system are given in Fig. 4-4. Notice that the contribution of the nonlinear portion of Eqs. (4-21) to (4-23) is extremely small for this range of δ.

B. Solar-Sail Control at the Earth-Moon Collinear Points

It has been shown that the magnitude of the control acceleration needed for station-keeping in the vicinity of a collinear point of the Earth-Moon system may be extremely small. Therefore, it may be feasible to obtain this acceleration with a small solar-sail. At first, the utilization of a solar-sail to perform this task appears to be straightforward, until it is realized that the control acceleration vector can never have a component directed toward the Sun. Furthermore, the direction of the incident solar radiation is varying continuously with respect to the xyz-coordinate system. Fortunately, these difficulties can be circumvented by using a method that was originally devised by Colombo.[3] Colombo demonstrated that the required accelerations could be obtained by forcing the libration-point satellite to follow a path that is synchronized with the Sun's motion.

An analysis of a particular solar-sail control technique is presented in this section. Colombo's strategy is employed, and explicit relations for the sail variations are derived. The analysis is limited to the xy-plane, and the effects of eccentricity and solar perturbations are neglected. Solar occultation periods are also neglected in this analysis. Although it is possible to use the solar-sail for both attitude and position stabilization, only position control is considered here.

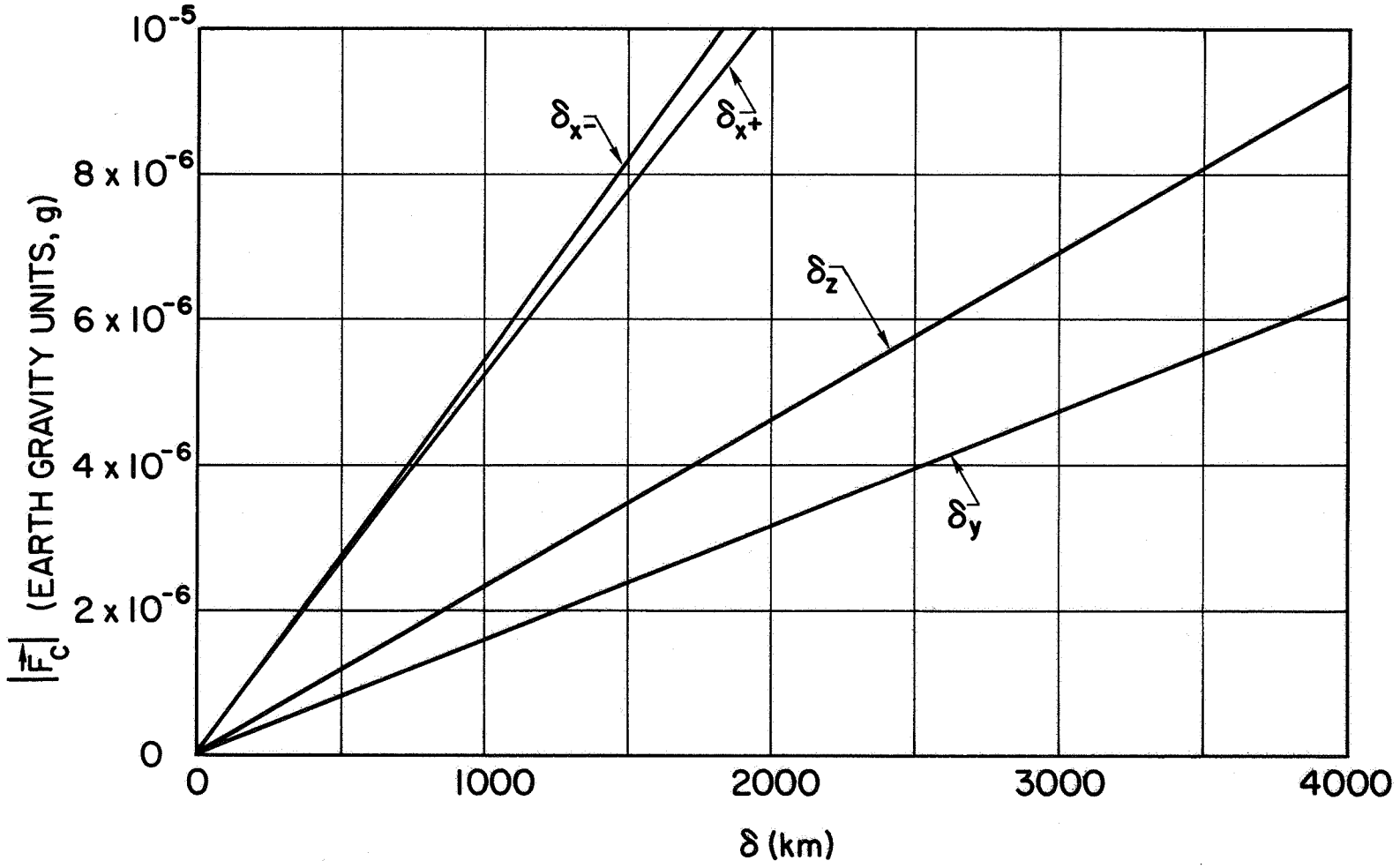

FIG. 4-4. STATION-KEEPING COST FOR A CONSTANT DISPLACEMENT FROM THE L_2 POINT OF THE EARTH-MOON SYSTEM.

1. Basic Concepts

The geometry for a plane solar-sail in the vicinity of a collinear libration point of the Earth-Moon system is depicted in Fig. 4-5. For

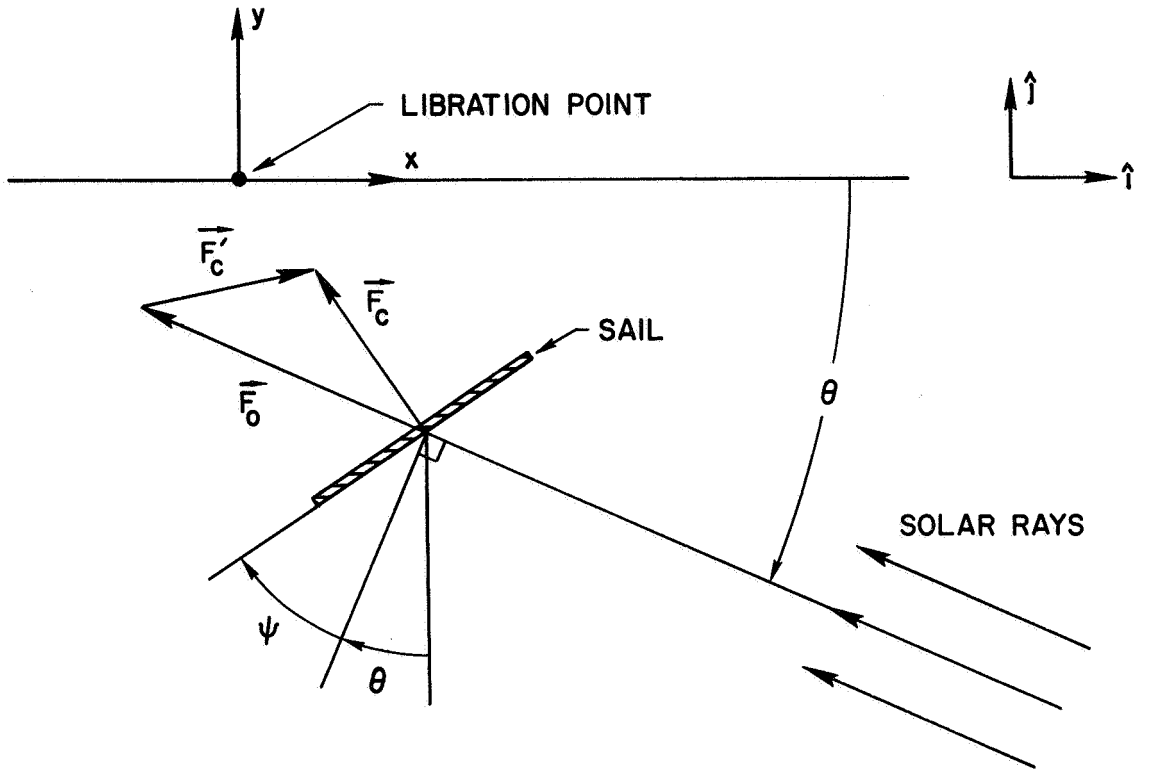

FIG. 4-5. PLANE SOLAR-SAIL IN THE VICINITY OF A COLLINEAR LIBRATION POINT OF THE EARTH-MOON SYSTEM.

specular reflection of the incident solar rays, the equations of motion are [cf Eq. (2-26)]

$$\ddot{x} - 2\dot{y} - (2B_L + 1)x = - K_p \cos^2\psi \cos(\theta + \psi) = F_{cx}$$
$$\ddot{y} + 2\dot{x} + (B_L - 1)y = K_p \cos^2\psi \sin(\theta + \psi) = F_{cy} \qquad (4\text{-}24)$$

where $\theta = \omega_s t$ ($\omega_s = 0.92519867$), K_p and ψ are bounded control variables ($K_p \geq 0$, $|\psi| \leq \pi/2$), and from Eq. (2-1)

$$K_p = 2p_{\oplus}\left(\frac{A_s}{m}\right) \tag{4-25}$$

Following Colombo's suggestion, the libration-point satellite is required to follow a path $[x_o(t), y_o(t)]$ which is determined by finding the forced response of

$$\begin{aligned} \ddot{x}_o - 2\dot{y}_o - (2B_L + 1)x_o &= -K_o \cos\theta \\ \ddot{y}_o + 2\dot{x}_o + (B_L - 1)y_o &= K_o \sin\theta \end{aligned} \tag{4-26}$$

The connection between the control accelerations is given by (see Fig. 4-5)

$$\vec{F}_c = \vec{F}_o + \vec{F}'_c \tag{4-27}$$

with

$$\vec{F}_c = F_{cx}\,\hat{i} + F_{cy}\,\hat{j} \tag{4-28}$$

$$\vec{F}_o = K_o[-\cos\theta\,\hat{i} + \sin\theta\,\hat{j}] \tag{4-29}$$

$$\vec{F}'_c = F'_{c\xi}\,\hat{i} + F'_{c\eta}\,\hat{j} \tag{4-30}$$

Using linear superposition, it is obvious that the equations of motion relative to the path $[x_o(t), y_o(t)]$ are

$$\begin{aligned} \ddot{\xi} - 2\dot{\eta} - (2B_L + 1)\xi &= F'_{c\xi} \\ \ddot{\eta} + 2\dot{\xi} + (B_L - 1)\eta &= F'_{c\eta} \end{aligned} \tag{4-31}$$

where $\xi = x - x_o$ and $\eta = y - y_o$.

A graphic exposition of the solar-sail control technique can be obtained by inspecting the acceleration diagram of Fig. 4-6. In this figure, the magnitudes of the control accelerations needed for station-keeping are represented by:

(1) K_b (measurement bias-errors)

(2) K_n (measurement noise)

(3) K_d (perturbations, etc., which are not eliminated by following a nominal path)

and

$$K_1 \equiv K_b + K_n + K_d \tag{4-32}$$

It is easily seen that the required acceleration can be provided by suitably adjusting the control variables, K_p and ψ. Figure 4-6 can also be used to determine $(K_p)_{max}$. From Eq. (4-25), it can be seen that this specification is equivalent to finding the maximum size of the solar-sail. The minimum required value of $(K_p)_{max}$ can be found by observing that, for this special case, the curve $|\vec{F}_c| = (K_p)_{max} \cos^2\psi$ has a common tangent with the circle of radius K_1. For $\psi_{max} \leq 30°$ ($\sin \psi_{max} = K_1/K_o$), the common tangent is at $\psi = 0°$, and it is obvious that

$$(K_p)_{max} = K_o + K_1 \tag{4-33}$$

When $\psi_{max} \geq 30°$, the analysis is more involved, but it can be shown that

$$(K_p)_{max} = \frac{3\sqrt{3}}{4} K_o \left[1 - \left(\frac{K_1}{K_o}\right)^2\right]^{-1/2} \tag{4-34}$$

and the common point of tangency can be determined from

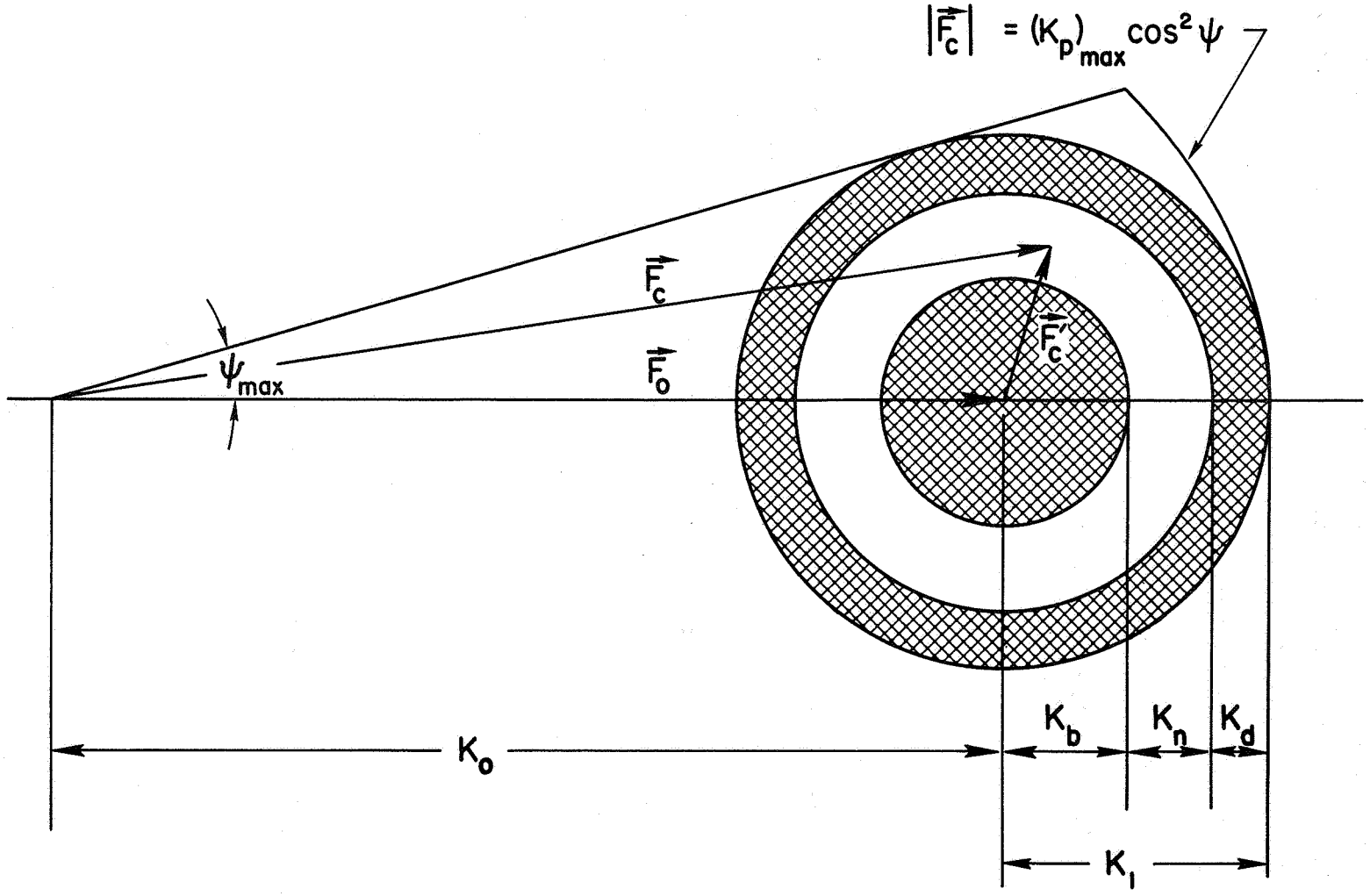

FIG. 4-6. SOLAR-SAIL ACCELERATION DIAGRAM.

$$\cos \psi = \frac{2}{\sqrt{3}}\left[1 - \left(\frac{K_1}{K_o}\right)^2\right]^{1/2} \tag{4-35}$$

2. Sail Variations with Radial-Axis Control

For a radial-axis control, $F'_{c\eta} = 0$, and Eqs. (4-24), (4-26), and (4-31) give

$$\begin{aligned} -K_p \cos^2\psi \cos(\theta + \psi) + K_o \cos\theta &= F'_{c\xi} \\ K_p \cos^2\psi \sin(\theta + \psi) - K_o \sin\theta &= 0 \end{aligned} \tag{4-36}$$

It is convenient to use the definition

$$K_p \equiv K_o + Q_p \tag{4-37}$$

where Q_p represents the variable portion of K_p. The sail variations, ψ and Q_p, can be expressed as functions of the variables, $F'_{c\xi}$ and θ. Equations (4-36) and (4-37) yield

$$\tan \psi = \frac{F'_{c\xi} \sin\theta}{K_o - F'_{c\xi}} \tag{4-38}$$

$$Q_p = K_o\left[\frac{(K_o - F'_{c\xi})/\cos^3\psi}{K_o - F'_{c\xi}(1 - \cos\theta)} - 1\right] \tag{4-39}$$

and if the radial-axis control of Eq. (3-2) is used

$$F'_{c\xi} = -k_1\dot{\xi} - k_2\xi \tag{4-40}$$

When $F'_{c\xi} \ll K_o$, Eqs. (4-38) and (4-39) lead to the approximate relations

$$\psi \cong \frac{F'_{c\xi}}{K_o} \sin\theta$$

$$Q_p \cong -F'_{c\xi} \cos\theta \tag{4-41}$$

3. Examples

The variation of the area of the solar-sail is minimized by choosing $K_o \gg K_1$. (The variation of ψ is also minimized.) It is quite possible that the mechanization of the solar-sail control system will be less complicated if only small sail variations are required. Therefore, a value of $K_o = 15\, K_1$ ($\psi_{max} = 3.82°$) is adopted for the examples given below.*

For both examples, it is assumed that $K_d \cong 0$, $\delta_\xi = 1$ km, and $m = 400$ kg. K_n is obtained from Section A-1c, and $p_\oplus = 4.50 \times 10^{-6}$ newtons/m^2. The forced response of Eq. (4-26) is written as

$$x_o = A_{xo} \cos\omega_s t$$

$$y_o = A_{yo} \sin\omega_s t \tag{4-42}$$

With the values mentioned above, some of the important parameters for satellites in the vicinity of the Earth-Moon collinear points are found to be:

*Although sail variations are minimized when $K_o \gg K_1$, the required sail area A_s is increased. This trade-off is not considered here.

L_1:

$$K_b = 2.938 \times 10^{-5} = 8.157 \times 10^{-9} g$$

$$K_n = 4.790 \times 10^{-5} = 1.330 \times 10^{-8} g$$

$$K_o = 1.159 \times 10^{-3} = 3.218 \times 10^{-7} g$$

$$A_{xo} = 14.8 \text{ km}, \quad A_{yo} = 143.7 \text{ km}$$

$$A_s = 149.7 \text{ m}^2, \quad (A_s/m) = 0.374 \text{ m}^2/\text{kg}$$

L_2:

$$K_b = 1.920 \times 10^{-5} = 5.330 \times 10^{-9} g$$

$$K_n = 3.110 \times 10^{-5} = 8.858 \times 10^{-9} g$$

$$K_o = 7.545 \times 10^{-4} = 2.128 \times 10^{-7} g$$

$$A_{xo} = -10.4 \text{ km}, \quad A_{yo} = 202.9 \text{ km}$$

$$A_s = 97.4 \text{ m}^2, \quad (A_s/m) = 0.244 \text{ m}^2/\text{kg}$$

Notice that the forced oscillation is counterclockwise for L_1 and clockwise for L_2. In both cases, $|A_{yo}| \gg |A_{xo}|$.

Chapter V

ON-OFF CONTROL SYSTEM

It is quite possible that the station-keeping of a libration-point satellite will be accomplished with an on-off control system. Accordingly, an analysis of the ensuing limit-cycle motion is in order. Two methods of analysis are presented in this chapter. The first is an exact method that makes use of Fourier expansions; the second is an approximate phase-plane technique.

Once again, a radial-axis control that requires only range and range-rate measurements is utilized. If eccentricity, perturbations, etc., are neglected, the equations of motion in the vicinity of a collinear libration point are

$$\begin{aligned} \ddot{x} - 2\dot{y} - (2B_L + 1)x &= -F(\xi) \\ \ddot{y} + 2\dot{x} + (B_L - 1)y &= 0 \end{aligned} \tag{5-1}$$

where

$$\xi = \dot{x} + \lambda x \tag{5-2}$$

and the assumed on-off control characteristic $F(\xi)$ has a deadzone ξ_d and a hysteresis loop of width 2δ (see Fig. 5-1). An asymmetric characteristic was chosen since only "one-sided" limit cycles are considered here.* The constant λ in Eq. (5-2) is just the slope of the "switching line" in the $\dot{x}$-x phase plane.

A. Limit Cycles: Exact Analysis

Conditions for the existence of limit cycles in Eq. (5-1) can be found by using harmonic methods. Approximate methods[73,74] which neglect all harmonics higher than the first are very popular, but their validity

*One-sided limit cycles are possible because the uncontrolled system is unstable.

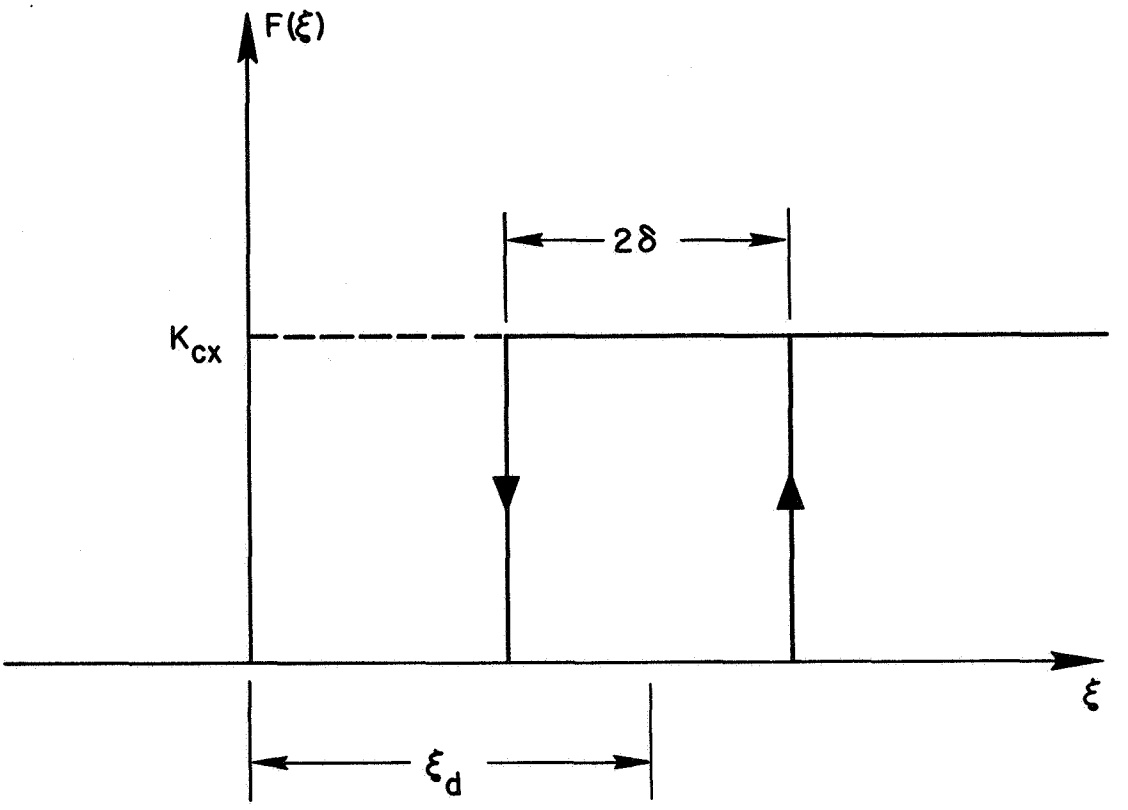

FIG. 5-1. ON-OFF CONTROL CHARACTERISTIC.

is sometimes questionable. Therefore, the higher harmonics are retained in the analysis employed in this section. Although differing in some details, the exact harmonic method used here is essentially the same as a method of Tsypkin.[75,76]

1. Application of Harmonic Method

A block diagram of the on-off control system is shown in Fig. 5-2, and it is clear that

$$\xi(s) = G(s)F(s) \tag{5-3}$$

From Eqs. (5-1) and (5-2), it is found that the transfer function is

$$G(s) = \frac{(s + \lambda)[s^2 + (B_L - 1)]}{(2B_L + 1)(B_L - 1) + (B_L - 2)s^2 - s^4} \tag{5-4}$$

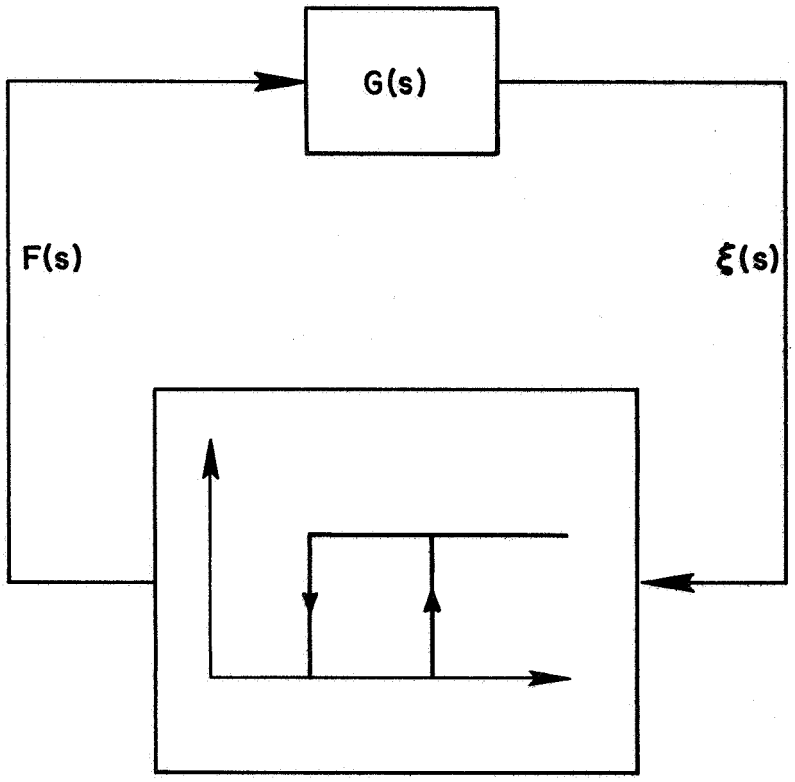

FIG. 5-2. BLOCK DIAGRAM OF THE ON-OFF CONTROL SYSTEM.

For convenience, $g(s) \equiv 1/G(s)$, and Eq. (5-3) becomes

$$g(s)\xi(s) = F(s) \tag{5-5}$$

Typical oscillation waveforms for a stable limit cycle are depicted in Fig. 5-3.* In this figure

$$\theta = \omega t \tag{5-6}$$

*Notice that there are discontinuities in $\dot{\xi}$ whenever the control is turned on or off. Tsypkin's graphical method as given in Refs. 75 and 76 is not applicable to this special case. However, a modified method, which can be applied to problems with discontinuities of this type, has been given by Korolev.[77]

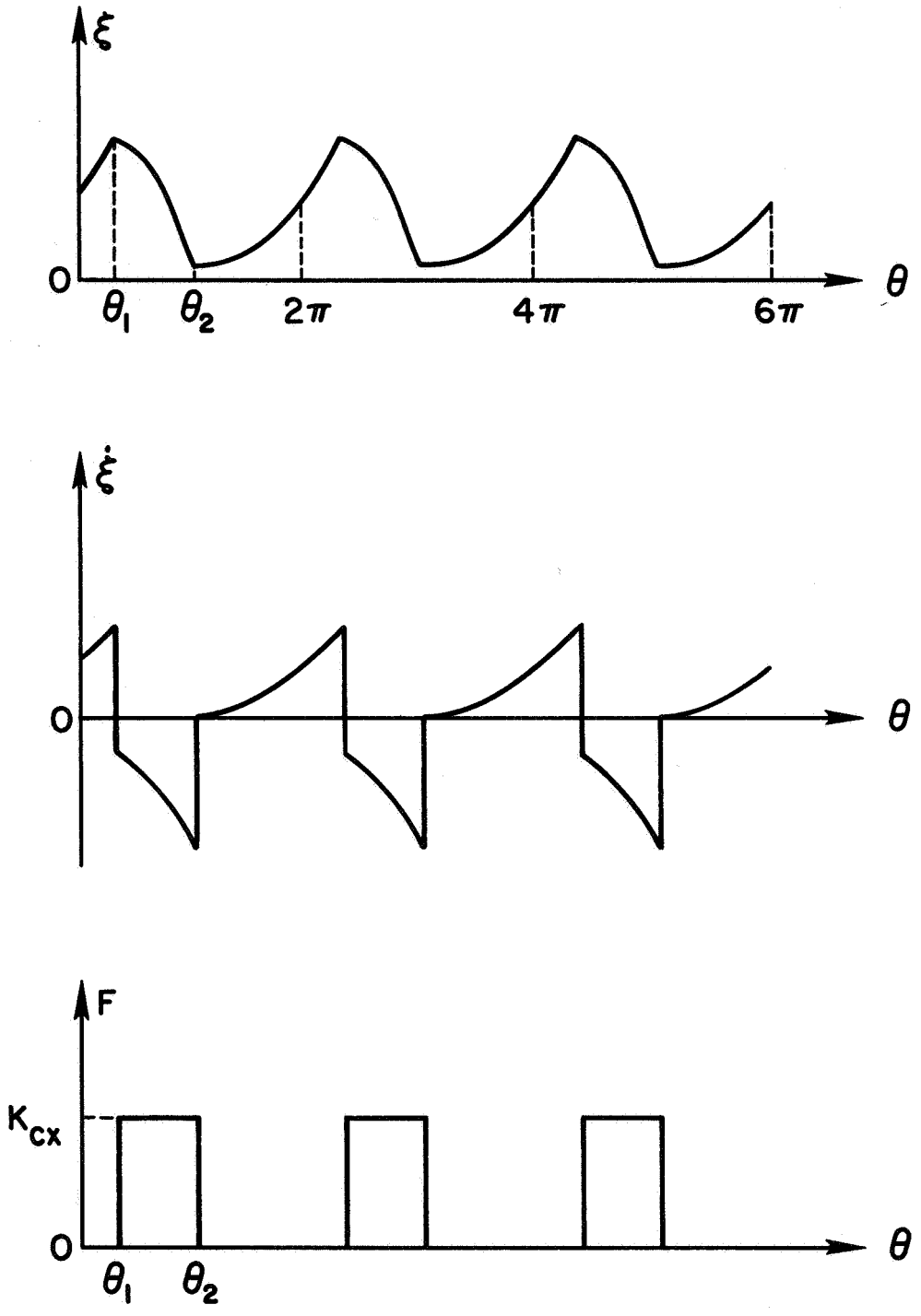

FIG. 5-3. OSCILLATION WAVEFORMS ($\theta = \omega t$).

where ω is the limit-cycle frequency. The Fourier representations of ξ and F can be written

$$\xi(\theta) = a_o + a_1 \sin \theta + \sum_{n=2}^{\infty} a_n \sin (n\theta + \psi_n) \tag{5-7}$$

$$F(\theta) = \frac{b_o}{2} + \sum_{n=1}^{\infty} (b_n \cos n\theta + c_n \sin n\theta) \tag{5-8}$$

Using the waveform for $F(\theta)$ in Fig. 5-3, the Fourier coefficients of Eq. (5-8) are found to be

$$b_o = \frac{1}{\pi}\int_0^{2\pi} F(\theta)d\theta = \frac{K_{cx}(\theta_2 - \theta_1)}{\pi} \tag{5-9}$$

$$b_n = \frac{1}{\pi}\int_0^{2\pi} F(\theta)\cos n\theta \, d\theta = \frac{K_{cx}}{n\pi}\left(\sin n\theta_2 - \sin n\theta_1\right) \tag{5-10}$$

$$c_n = \frac{1}{\pi}\int_0^{2\pi} F(\theta)\sin n\theta \, d\theta = \frac{K_{cx}}{n\pi}\left(\cos n\theta_1 - \cos n\theta_2\right) \tag{5-11}$$

Writing

$$g(s) = g(j\omega) = R(\omega)e^{j\varphi(\omega)} \tag{5-12}$$

and taking the inverse transform of Eq. (5-5) gives

$$g(0)a_o + R(\omega)a_1 \sin [\theta + \varphi(\omega)] + \sum_{n=2}^{\infty} R(n\omega)a_n \sin [n\theta + \psi_n + \varphi(n\omega)] = F(\theta) \tag{5-13}$$

Equation (5-13) leads to the relations

$$a_o = \frac{K_{cx}(\theta_2 - \theta_1)}{2\pi g(0)} \tag{5-14}$$

$$a_1 = \frac{2K_{cx}}{\pi R(\omega)} \sin \frac{\theta_2 - \theta_1}{2} \tag{5-15}$$

$$a_n = \frac{2K_{cx}}{n\pi R(n\omega)} \sin \frac{n(\theta_2 - \theta_1)}{2} \tag{5-16}$$

$$\varphi(\omega) = \frac{1}{2}\left[\pi - (\theta_1 + \theta_2)\right] \tag{5-17}$$

$$\psi_n = \frac{1}{2}\left[\pi - n(\theta_1 + \theta_2)\right] - \varphi(n\omega) \tag{5-18}$$

From Eqs. (5-4) and (5-12), it is found that

$$g(j\omega) = \frac{(2B_L + 1)(B_L - 1) - (B_L - 2)\omega^2 - \omega^4}{(\lambda + j\omega)[(B_L - 1) - \omega^2]} \tag{5-19}$$

$$R(\omega) = \frac{\omega^4 + (B_L - 2)\omega^2 - (2B_L + 1)(B_L - 1)}{[\omega^2 - (B_L - 1)]\sqrt{\lambda^2 + \omega^2}}$$

$$\equiv \frac{(\omega^2 - \alpha^2)(\omega^2 + \beta^2)}{(\omega^2 - \gamma^2)\sqrt{\lambda^2 + \omega^2}} \tag{5-20}$$

$$\tan \varphi(\omega) = -\frac{\omega}{\lambda} \tag{5-21}$$

The constants α and β can be obtained from Table 1-3. $\alpha > \gamma$, and it is apparent that $R(\omega) < 0$ for the frequency range $\gamma < \omega < \alpha$. This frequency range is not examined in this study, and it will always be assumed that $R(\omega) > 0$.* Equations (5-14), (5-17), and (5-18) can now be written in the form

$$a_o = \frac{K_{cx}(\theta_2 - \theta_1)\lambda}{2\pi(2B_L + 1)} \tag{5-22}$$

$$(\theta_1 + \theta_2) = \pi + 2\tan^{-1}(\omega/\lambda) \tag{5-23}$$

$$\psi_n = \frac{1}{2}\left[\pi - n(\theta_1 + \theta_2)\right] + \tan^{-1}(n\omega/\lambda) \tag{5-24}$$

From Figs. 5-1 and 5-3, it is clear that the deadzone and hysteresis constants for the on-off control characteristic are given by

$$\xi_d = \frac{1}{2}\left[\xi(\theta_1) + \xi(\theta_2)\right] \tag{5-25}$$

$$\delta = \frac{1}{2}\left[\xi(\theta_1) - \xi(\theta_2)\right] \tag{5-26}$$

Finally, with the aid of Eqs. (5-1) and (5-2), it can be shown that

$$x(\theta) = \frac{a_o}{\lambda} + \frac{a_1}{\sqrt{\lambda^2 + \omega^2}} \sin\left[\theta - \tan^{-1}(\omega/\lambda)\right]$$

$$+ \sum_{n=2}^{\infty} \frac{a_n}{\sqrt{\lambda^2 + (n\omega)^2}} \sin\left[n\theta + \psi_n - \tan^{-1}(n\omega/\lambda)\right] \tag{5-27}$$

*In the frequency range $\gamma < \omega < \alpha$, the control is turned on when ξ is decreasing and is turned off when ξ is increasing. Therefore, the presence of a stable limit cycle in this frequency range is highly improbable.

$$y(\theta) = \frac{2a_1\omega}{[\omega^2 - (B_L - 1)]\sqrt{\lambda^2 + \omega^2}} \cos\,[\theta - \tan^{-1}(\omega/\lambda)]$$

$$+ \sum_{n=2}^{\infty} \frac{2na_n\omega}{[(n\omega)^2 - (B_L - 1)]\sqrt{\lambda^2 + (n\omega)^2}} \cos\,[n\theta + \psi_n - \tan^{-1}(n\omega/\lambda)] \qquad (5\text{-}28)$$

Notice that K_{cx} is just a scale factor, and the "normalized" limit-cycle is completely determined by choosing the following parameters:

(1) $(\theta_2 - \theta_1)$: $(\theta_2 - \theta_1)/2\pi \equiv m$ is the fraction of the total time that the control is on.

(2) λ: Slope of the switching line in the $\dot{x}$-x phase plane.

(3) ω: Limit-cycle frequency.

2. Closed-Form Solution

Although the results of the previous section are exact, they are in the form of infinite series. With the results in this form, the synthesis of the control is sometimes inconvenient. Fortunately, some simplification is possible for the important special case where the control is on for half of the limit-cycle period and off during the other half. That is

$$\theta_2 - \theta_1 = \pi \qquad (5\text{-}29)$$

and with Eq. (5-16), Eq. (5-7) becomes

$$\xi(\theta) = a_o + a_1 \sin\,\theta + \frac{2K_{cx}}{\pi} \sum_{n=1}^{\infty} \frac{(-1)^n \sin\,[(2n+1)\theta + \psi_{2n+1}]}{(2n+1)R[(2n+1)\omega]} \qquad (5\text{-}30)$$

From Eq. (5-23)

$$\theta_1 = \tan^{-1}(\omega/\lambda)$$
$$\theta_2 = \pi + \tan^{-1}(\omega/\lambda) \tag{5-31}$$

and

$$\sin\theta_1 = \frac{\omega}{\sqrt{\lambda^2 + \omega^2}}$$
$$\sin\theta_2 = -\frac{\omega}{\sqrt{\lambda^2 + \omega^2}} \tag{5-32}$$

Similar expressions can be found for Eq. (5-24), and it can be deduced that

$$\xi(\theta_1) = \frac{K_{cx}\lambda}{2(2B_L + 1)} + \frac{2K_{cx}\omega}{\pi}\sum_{n=0}^{\infty}\frac{[(2n+1)^2\omega^2 - \gamma^2]}{[(2n+1)^2\omega^2 - \alpha^2][(2n+1)^2\omega^2 + \beta^2]}$$
$$\xi(\theta_2) = \frac{K_{cx}\lambda}{2(2B_L + 1)} - \frac{2K_{cx}\omega}{\pi}\sum_{n=0}^{\infty}\frac{[(2n+1)^2\omega^2 - \gamma^2]}{[(2n+1)^2\omega^2 - \alpha^2][(2n+1)^2\omega^2 + \beta^2]} \tag{5-33}$$

Substitution of Eq. (5-33) into Eqs. (5-25) and (5-26) yields

$$\xi_d = \frac{K_{cx}\lambda}{2(2B_L + 1)} \tag{5-34}$$

$$\delta = \frac{2K_{cx}\omega}{\pi}\left\{\frac{\alpha^2 - \gamma^2}{\alpha^2 + \beta^2}\sum_{n=0}^{\infty}\frac{1}{[(2n+1)^2 - (\alpha/\omega)^2]} + \frac{\beta^2 + \gamma^2}{\alpha^2 + \beta^2}\sum_{n=0}^{\infty}\frac{1}{[(2n+1)^2 + (\beta/\omega)^2]}\right\} \tag{5-35}$$

Closed-form expressions for the two infinite series are given in Ref. 78, and Eq. (5-35) becomes

$$\delta = \frac{K_{cx}}{2}\left[\frac{\alpha^2 - \gamma^2}{\alpha(\alpha^2 + \beta^2)} \tan\left(\frac{\pi\alpha}{2\omega}\right) + \frac{\beta^2 + \gamma^2}{\beta(\alpha^2 + \beta^2)} \tanh\left(\frac{\pi\beta}{2\omega}\right)\right] \qquad (5\text{-}36)$$

A graph of Eq. (5-36) for $B_L = 4$ ($\alpha^2 = 4.2915$, $\beta^2 = 6.2915$, $\gamma^2 = 3$) is given in Fig. 5-4.

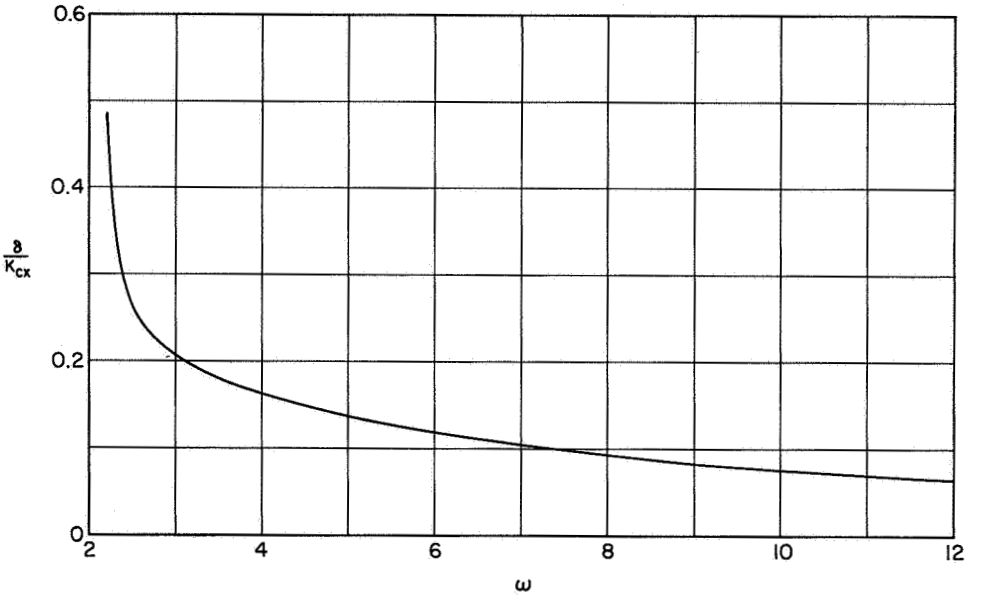

FIG. 5-4. HYSTERESIS VS LIMIT-CYCLE FREQUENCY ($B_L = 4$, $\theta_2 - \theta_1 = \pi$).

It can be shown that the maximum and minimum values of $x(\theta)$ occur at $\theta = \theta_1 + \frac{\pi}{2}$ and $\theta = \theta_2 + \frac{\pi}{2}$, respectively. Substituting these values into Eq. (5-27), it is found that

$$x_{max} = \frac{K_{cx}}{2(2B_L + 1)} + \Xi \qquad (5\text{-}37)$$

$$x_{min} = \frac{K_{cx}}{2(2B_L + 1)} - \Xi \tag{5-38}$$

where

$$\Xi = \frac{2K_{cx}}{\pi} \sum_{n=0}^{\infty} \frac{(-1)^n[(2n+1)^2\omega^2 - \gamma^2]}{(2n+1)[(2n+1)^2\omega^2 - \alpha^2][(2n+1)^2\omega^2 + \beta^2]} \tag{5-39}$$

The summation formulae of Ref. 78 can be used to write Eq. (5-39) as

$$\Xi = \frac{2K_{cx}}{\pi\omega^2}\left\{\frac{\alpha^2 - \gamma^2}{\alpha^2 + \beta^2} \sum_{n=0}^{\infty} \frac{(-1)^n}{(2n+1)[(2n+1)^2 - (\alpha/\omega)^2]}\right.$$

$$\left. + \frac{\beta^2 + \gamma^2}{\alpha^2 + \beta^2} \sum_{n=0}^{\infty} \frac{(-1)^n}{(2n+1)[(2n+1)^2 + (\beta/\omega)^2]}\right\}$$

$$= \frac{K_{cx}}{2}\left\{\frac{\alpha^2 - \gamma^2}{\alpha^2(\alpha^2 + \beta^2)}\left[\sec\left(\frac{\pi\alpha}{2\omega}\right) - 1\right]\right.$$

$$\left. + \frac{\beta^2 + \gamma^2}{\beta^2(\alpha^2 + \beta^2)}\left[1 - \operatorname{sech}\left(\frac{\pi\beta}{2\omega}\right)\right]\right\}$$

$$= \frac{K_{cx}}{2}\left[\left(\frac{\gamma}{\alpha\beta}\right)^2 + \frac{\alpha^2 - \gamma^2}{\alpha^2(\alpha^2 + \beta^2)} \sec\left(\frac{\pi\alpha}{2\omega}\right) - \frac{\beta^2 + \gamma^2}{\beta^2(\alpha^2 + \beta^2)} \operatorname{sech}\left(\frac{\pi\beta}{2\omega}\right)\right] \tag{5-40}$$

A graph of Eq. (5-40) for $B_L = 4$ is shown in Fig. 5-5.

Equation (5-38) shows that $x_{min} < 0$ when $\Xi > K_{cx}/2(2B_L + 1)$. Intuitive reasoning suggests that limit cycles with $x_{min} < 0$ are unstable. This conjecture will be substantiated by the stability analysis given below.

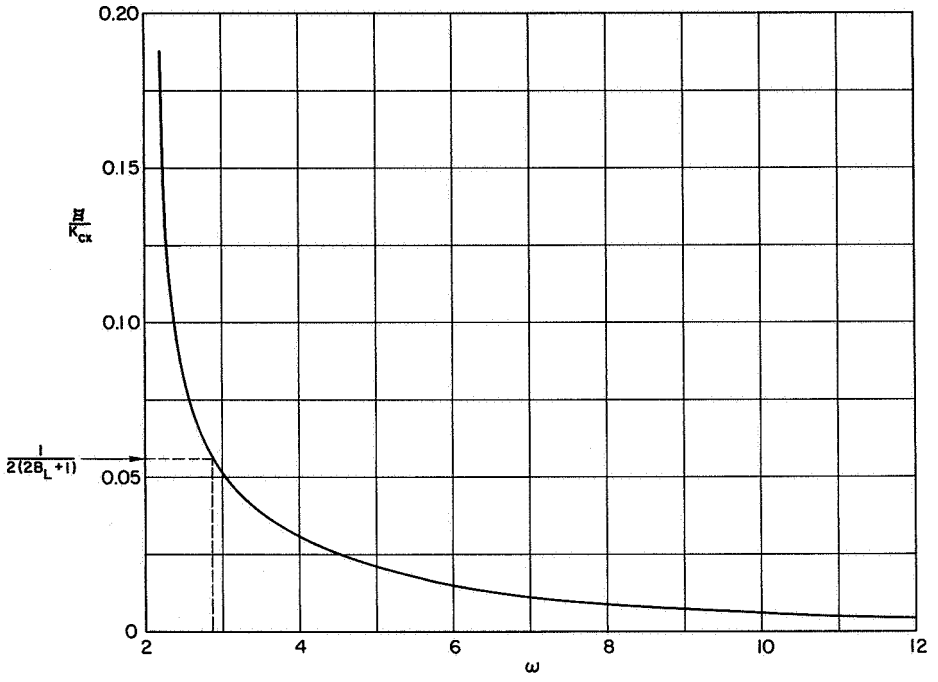

FIG. 5-5. Ξ VS LIMIT-CYCLE FREQUENCY ($B_L = 4$, $\theta_2 - \theta_1 = \pi$).

B. Stability of Limit Cycles

The results of the previous section cannot be used with confidence until the stability of the predicted limit cycle is verified. Tsypkin[75] has devised a method that reduces this stability investigation to that of an equivalent sampled-data system. A brief outline of this method is given below, and quantitative results are obtained for the special case where $\theta_2 - \theta_1 = \pi$.

1. Tsypkin's Method

Consider the perturbed limit-cycle motion of the system shown in Fig. 5-2. The input to the on-off characteristic is

$$\xi(t) = \xi_{LC}(t) + \xi_{\epsilon}(t) \tag{5-41}$$

where $\xi_{LC}(t)$ corresponds to the assumed limit cycle, and $\xi_{\epsilon}(t)$

represents a small deviation. Similarly,

$$F(t) = F_{LC}(t) + F_{\epsilon}(t) \tag{5-42}$$

The deviation in the output $F_{\epsilon}(t)$ is just a sequence of pulses, of height K_{cx} and width Δt_n, which occur at the beginning or end of the switching instants t_n. Assuming that $\xi_{\epsilon} \ll \xi_{LC}$, this deviation can be represented by the impulse train

$$F_{\epsilon}(t) \cong K_{cx} \sum_{n=0}^{\infty} \Delta t_n \delta(t - t_n) \tag{5-43}$$

where $\delta(t)$ is the Dirac delta function, and following Korolev,[77] Δt_n is expressed in terms of the conditions which immediately precede the switching instant

$$\Delta t_n \cong \frac{\xi_{\epsilon}(t_n^-)}{|\dot{\xi}_{LC}(t_n^-)|} \tag{5-44}$$

For the special case where the on and off periods are equal (i.e., $\theta_2 - \theta_1 = \pi$), the switching intervals are $T = T_{LC}/2 = \pi/\omega$, and the deviation is given by

$$F_{\epsilon}(t) = \frac{K_{cx}}{|\dot{\xi}_{LC}(\theta_1^-)|} \sum_{n=0}^{\infty} \xi_{\epsilon}(t_n^-)\delta(t - t_n) \tag{5-45}$$

Consequently, for small deviations, the stability of the limit-cycle motion where $\theta_2 - \theta_1 = \pi$ can be determined by checking the stability of the sampled-data system shown in Fig. 5-6.

2. Results for Special Case $(\theta_2 - \theta_1 = \pi)$

The characteristic equation for the sampled-data system of Fig. 5-6 can be written in terms of the z-transform $(z \equiv e^{TS})$ as

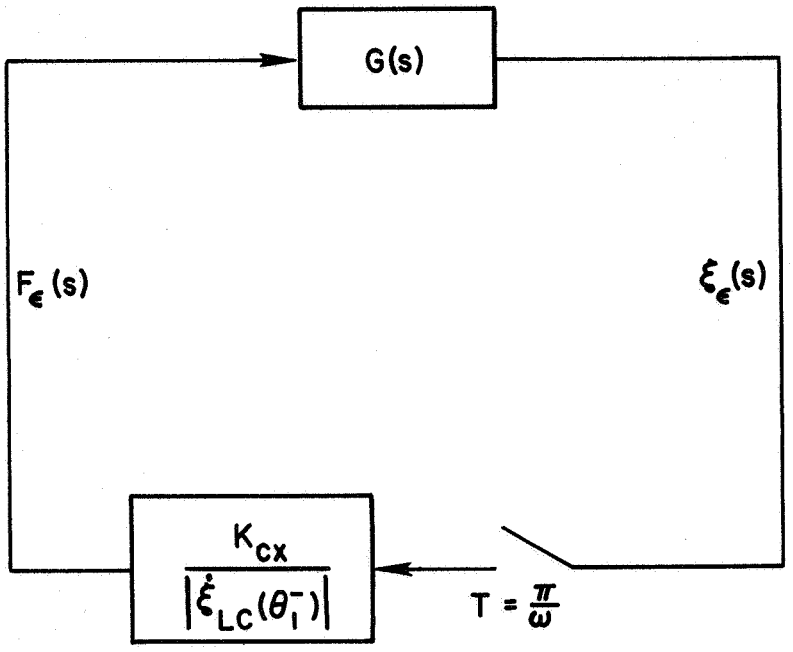

FIG. 5-6. SAMPLED-DATA SYSTEM FOR LIMIT-CYCLE STABILITY TEST $(\theta_2 - \theta_1 = \pi)$.

$$1 + kG_N(z) = 0 \tag{5-46}$$

where

$$k \equiv \frac{K_{cx}}{|\dot{\xi}_{LC}(\theta_1^-)|} \tag{5-47}$$

$$G_N(s) = - G(s) = \frac{P(s)}{Q(s)} \tag{5-48}$$

Denoting the poles of $G_N(s)$ by p_n, the z-transform of $G_N(s)$ is[79]

$$G_N(z) = \sum_{n=1}^{4} \frac{P(p_n)}{Q'(p_n)}\left[\frac{z}{z - e^{p_n T}}\right]$$

$$= \left(\frac{\alpha^2 - \gamma^2}{\alpha^2 + \beta^2}\right)\frac{z[z - \cos \alpha T + (\lambda/\alpha)\sin \alpha T]}{z^2 - 2z \cos \alpha T + 1}$$

$$+ \left(\frac{\beta^2 + \gamma^2}{\alpha^2 + \beta^2}\right)\frac{z[z - \cosh \beta T + (\lambda/\beta)\sinh \beta T]}{z^2 - 2z \cosh \beta T + 1} \qquad (5\text{-}49)$$

The denominator of Eq. (5-47) is found by the following process. First, Eq. (5-7) is differentiated with respect to time. This gives

$$\dot{\xi}_{LC}(\theta) = a_1 \omega \cos \theta + \sum_{n=2}^{\infty} a_n n\omega \cos (n\theta + \psi_n) \qquad (5\text{-}50)$$

and at $\theta = \theta_1$

$$\cos \theta_1 = \frac{\lambda}{\sqrt{\lambda^2 + \omega^2}} \qquad (5\text{-}51)$$

$$\dot{\xi}_{LC}(\theta_1) = \frac{2K_{cx}\omega\lambda}{\pi} \sum_{n=0}^{\infty} \frac{[(2n + 1)^2\omega^2 - \gamma^2]}{[(2n + 1)^2\omega^2 - \alpha^2][(2n + 1)^2\omega^2 + \beta^2]}$$

$$= \frac{K_{cx}\lambda}{2}\left[\frac{\alpha^2 - \gamma^2}{\alpha(\alpha^2 + \beta^2)} \tan\left(\frac{\pi\alpha}{2\omega}\right) + \frac{\beta^2 + \gamma^2}{\beta(\alpha^2 + \beta^2)} \tanh\left(\frac{\pi\beta}{2\omega}\right)\right] \qquad (5\text{-}52)$$

However, there is a discontinuity in $\dot{\xi}_{LC}(\theta)$ at $\theta = \theta_1$ (see Fig. 5-3), and the Fourier series converges to the average value

$$\dot{\xi}_{LC}(\theta_1) = \frac{\dot{\xi}_{LC}(\theta_1^+) + \dot{\xi}_{LC}(\theta_1^-)}{2} \qquad (5\text{-}53)$$

It is obvious that

$$\dot{\xi}_{LC}(\theta_1^-) - \dot{\xi}_{LC}(\theta_1^+) = K_{cx} \tag{5-54}$$

Therefore

$$\dot{\xi}_{LC}(\theta_1^-) = \dot{\xi}_{LC}(\theta_1) + \frac{K_{cx}}{2} \tag{5-55}$$

and this expression is used in Eq. (5-47). Notice that k is independent of K_{cx}.

Equation (5-46) is a fourth-degree polynomial in z. Since self-oscillations are examined here, one root of this characteristic equation is found at $z = -1$, and the stability of the assumed limit cycle depends on the locations of the three remaining roots. If these roots are located within the unit circle in the z-plane, the limit cycle is stable. Numerical calculations reveal that the limit cycles are stable for $\lambda > 0$ and $\omega > \omega_c$, where ω_c is a function of B_L only. For three important values of B_L, the critical frequencies are

$B_L = 3.19042$ (Earth-Moon L_2 point): $\omega_c = 3.102$

$B_L = 5.14760$ (Earth-Moon L_1 point): $\omega_c = 3.522$

$B_L = 4.00000$: $\omega_c = 3.287$

The variations of the roots for $B_L = 4$ are shown in Figs. 5-7 and 5-8.

3. Procedure for General Case $(\theta_2 - \theta_1 \neq \pi)$

The characteristic equation for the general case where $\theta_2 - \theta_1 \neq \pi$ is more complicated than Eq. (5-46). It is shown in Ref. 75 that this characteristic equation is

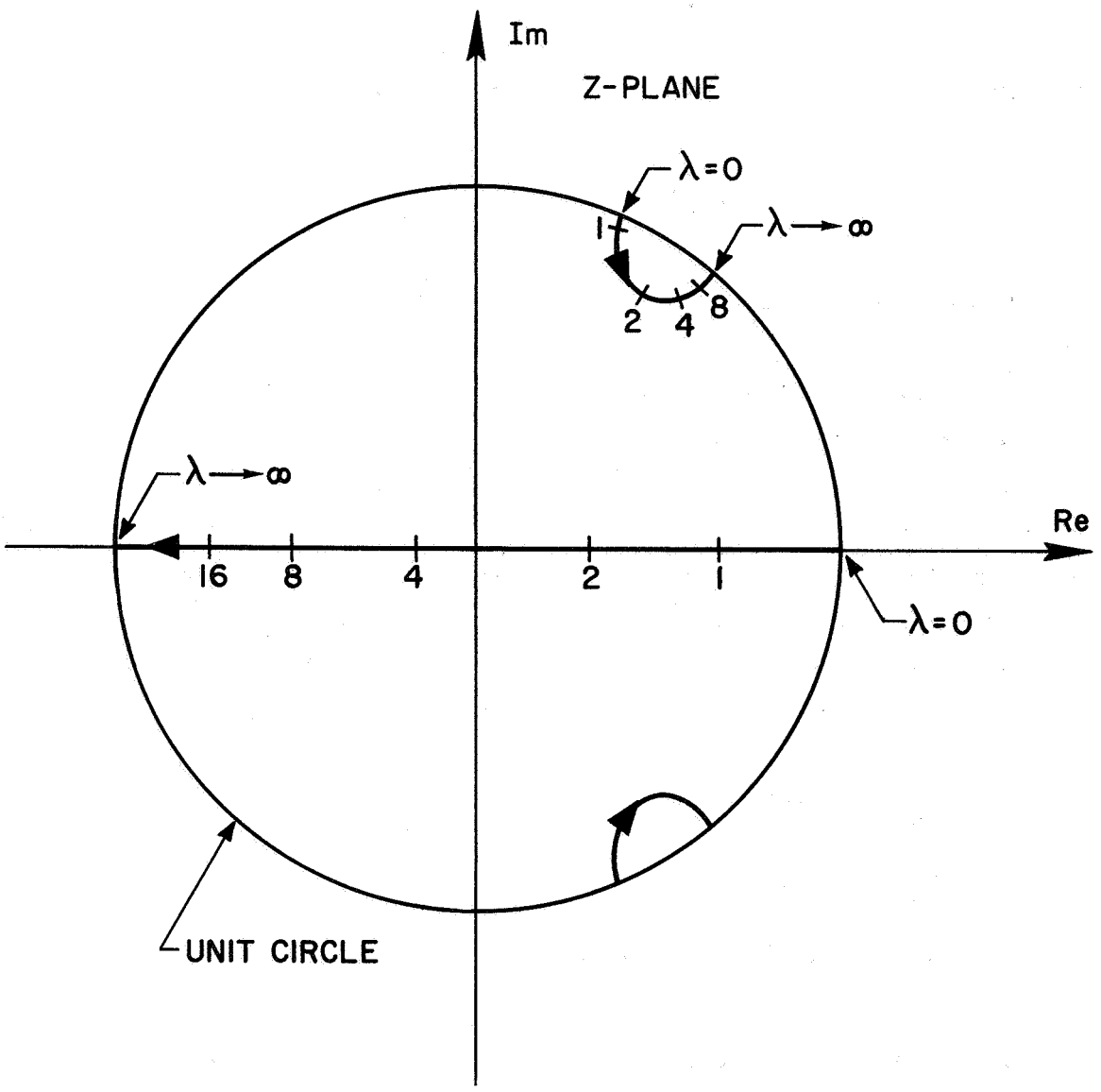

FIG. 5-7. ROOT VARIATIONS AS A FUNCTION OF λ ($\theta_2 - \theta_1 = \pi$, $B_L = 4$, $\omega = 4$).

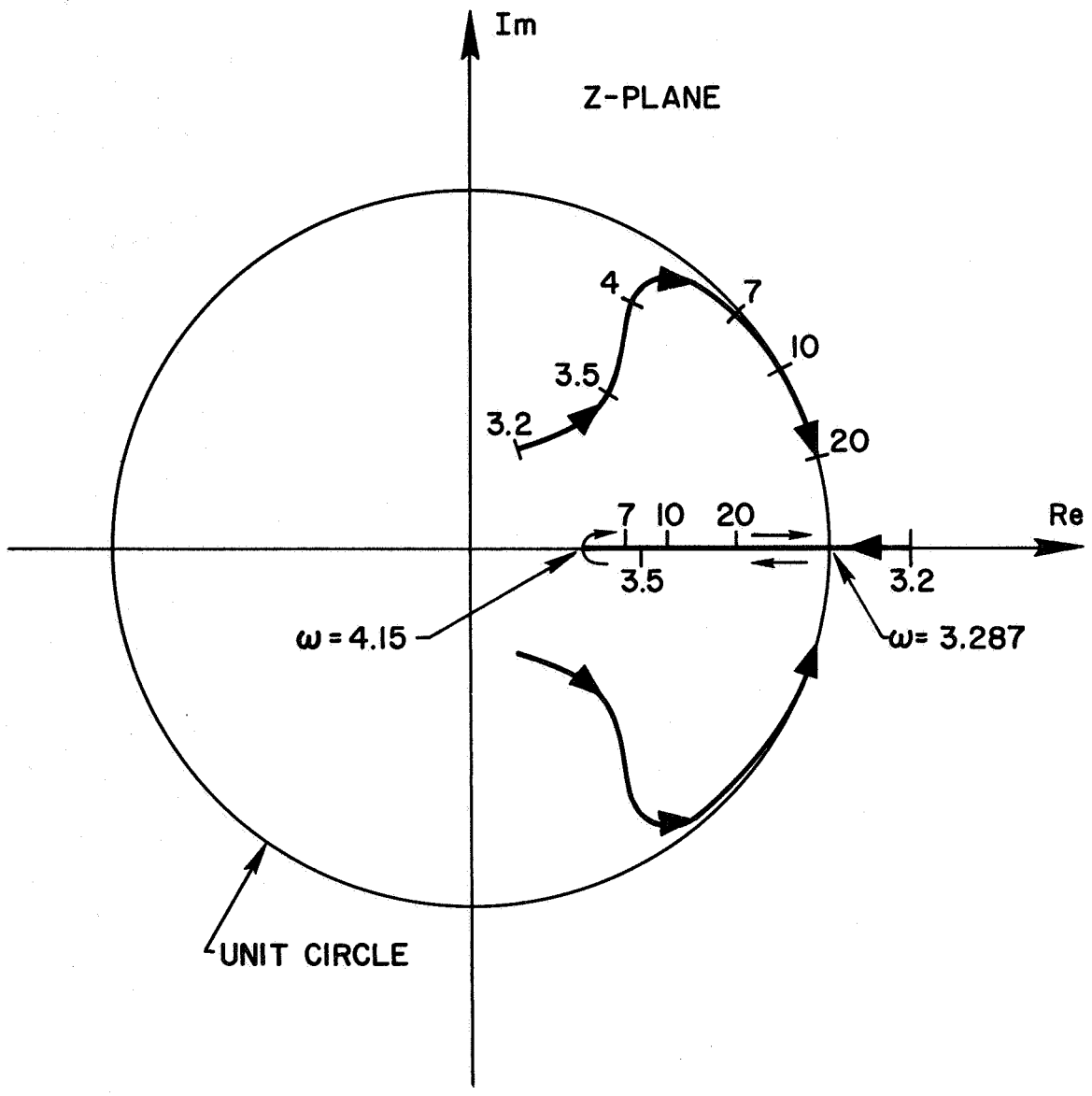

FIG. 5-8. ROOT VARIATIONS AS A FUNCTION OF ω ($\theta_2 - \theta_1 = \pi$, $B_L = 4$, $\lambda = 2$).

$$1 + \left[\frac{K_{cx}}{|\dot{\xi}_{LC}(\theta_1^-)|} + \frac{K_{cx}}{|\dot{\xi}_{LC}(\theta_2^-)|}\right] G_N(z)$$

$$+ \frac{K_{cx}^2}{|\dot{\xi}_{LC}(\theta_1^-)|\,|\dot{\xi}_{LC}(\theta_2^-)|}\left[G_N^2(z) - G_N(z,m)G_N(z,-m)\right] = 0 \qquad (5\text{-}56)$$

where $G_N(z)$ is given by Eq. (5-49) with $T = T_{LC} = 2\pi/\omega$, $m \equiv (\theta_2 - \theta_1)/2\pi$, and[79]

$$G_N(z,m) = \sum_{n=1}^{4} \frac{P(p_n)}{Q'(p_n)}\left[\frac{ze^{mp_nT}}{z - e^{p_nT}}\right] = z\left[\frac{N_1(z,m)}{D_1(z)} + \frac{N_2(z,m)}{D_2(z)}\right] \qquad (5\text{-}57)$$

$$G_N(z,-m) = \sum_{n=1}^{4} \frac{P(p_n)}{Q'(p_n)}\left[\frac{e^{(1-m)p_nT}}{z - e^{p_nT}}\right] = \left[\frac{N_1(z,1-m)}{D_1(z)} + \frac{N_2(z,1-m)}{D_2(z)}\right] \qquad (5\text{-}58)$$

$$N_1(z,m) = \left(\frac{\alpha^2 - \gamma^2}{\alpha^2 + \beta^2}\right)\Big\{z\cos\alpha mT - \cos(1-m)\alpha T + \frac{\lambda}{\alpha}\left[z\sin\alpha mT + \sin(1-m)\alpha T\right]\Big\} \qquad (5\text{-}59)$$

$$N_2(z,m) = \left(\frac{\beta^2 + \gamma^2}{\alpha^2 + \beta^2}\right)\Big\{z\cosh\beta mT - \cosh(1-m)\beta T + \frac{\lambda}{\beta}\left[z\sinh\beta mT + \sinh(1-m)\beta T\right]\Big\} \qquad (5\text{-}60)$$

$$D_1(z) = z^2 - 2z\cos\alpha T + 1 \qquad (5\text{-}61)$$

$$D_2(z) = z^2 - 2z\cosh\beta T + 1 \qquad (5\text{-}62)$$

It can also be deduced that

$$\dot{\xi}_{LC}(\theta_1^-) = \dot{\xi}_{LC}(\theta_1) + \frac{K_{cx}}{2} \tag{5-63}$$

$$\dot{\xi}_{LC}(\theta_2^-) = \dot{\xi}_{LC}(\theta_2) - \frac{K_{cx}}{2} \tag{5-64}$$

The roots of the characteristic equation can now be found. Although eight roots are obtained from Eq. (5-56), four of them are extraneous and should be disregarded. These extraneous roots are just solutions of the quadratic equations, $D_1(z) = 0$ and $D_2(z) = 0$. Another root is found at $z = -1$, and the stability of the limit cycle is determined by the three remaining roots.

C. Solar-Sail Control at the Sun-Earth L_1 Point

To illustrate the use of the preceding formulae, a solar-sail control system for a satellite in the vicinity of the Sun-Earth L_1 point is considered here. By merely changing the area of the sail in the prescribed manner, the on-off control system shown in Fig. 5-2 can be obtained. For the Sun-Earth L_1 point, the one-sided limit cycle is located between the Sun and the libration point.

Consider the case where $\theta_2 - \theta_1 = \pi$. To make use of graphical results, the constant B_{L1} is approximated by $B_{L1} \cong 4$. For $B_L = 4$, $\omega_c = 3.287$, and a good stability margin can be achieved by choosing a limit-cycle frequency of $\omega = 4$ ($T_{LC} = 2\pi/\omega = 91.31$ days). Figure 5-7 indicates that, for $\omega = 4$, small deviations from the nominal limit-cycle motion are adequately damped by choosing $\lambda = 2$. The choice of x_{min} (this specifies K_{cx}) is usually dictated by measurement accuracy limitations. For $x_{min} = 100$ km, the formulae of Section A-2 give:

$$K_{cx} = 1.613 \times 10^{-8} g \qquad x_{max} = 343.6 \text{ km}$$

$$\xi_d = 2.965 \times 10^{-6} \qquad \delta = 4.358 \times 10^{-6}$$

Equation (2-1) shows that, for a satellite mass of 10,000 kg and $C_p = 2$, the area of the solar-sail is only $A_s = 172.3\ m^2$.

By using a conical-shaped solar-sail, it may be possible to stabilize the satellite's attitude as well as its position. Analyses of the attitude motion for a configuration of this type can be found in Refs. 80 and 81.

D. Limit Cycles: Approximate Analysis

The results of Section A-1 are not easy to apply when x_{max} and x_{min} are specified and the limit-cycle frequency ω is arbitrary. Therefore, an approximate technique that uses x_{max} and x_{min} as inputs is presented here.

By neglecting the gyroscopic coupling in Eq. (5-1), a closed-form solution for all values of $\theta_2 - \theta_1$ can be obtained. Without this coupling, the y-axis motion is simple-harmonic. The remaining portion of Eq. (5-1) is just

$$\ddot{x} - (2B_L + 1)x = - F(\xi) \tag{5-65}$$

This equation is only second order and can be conveniently analyzed in the phase plane. However, before the phase plane analysis is presented, the accuracy of this single-axis approximation is checked for the special case where $\theta_2 - \theta_1 = \pi$.

1. Accuracy of Single-Axis Approximation

Proceeding in the same manner as in Section A, and denoting single-axis quantities with primes, it can be shown that

$$g'(s) = \frac{(2B_L + 1) - s^2}{s + \lambda} \tag{5-66}$$

$$R'(\omega) = \frac{\omega^2 + (2B_L + 1)}{\sqrt{\lambda^2 + \omega^2}} \equiv \frac{\omega^2 + \epsilon^2}{\sqrt{\lambda^2 + \omega^2}} \tag{5-67}$$

$$\tan \varphi'(\omega) = -\frac{\omega}{\lambda} \tag{5-68}$$

Equation (5-68) is identical to Eq. (5-21), and many of the equations of Section A are valid here. With these relations, it is easy to see that

$$\xi_d' = \frac{K_{cx}\lambda}{2(2B_L + 1)} \tag{5-69}$$

$$\delta' = \frac{2K_{cx}}{\pi\omega} \sum_{n=0}^{\infty} \frac{1}{[(2n + 1)^2 + (\epsilon/\omega)^2]} = \frac{K_{cx}}{2\epsilon} \tanh\left(\frac{\pi\epsilon}{2\omega}\right) \tag{5-70}$$

$$x'_{max} = \frac{K_{cx}}{2(2B_L + 1)} + \Xi' \tag{5-71}$$

$$x'_{min} = \frac{K_{cx}}{2(2B_L + 1)} - \Xi' \tag{5-72}$$

$$\Xi' = \frac{2K_{cx}}{\pi\omega^2} \sum_{n=0}^{\infty} \frac{(-1)^n}{(2n + 1)[(2n + 1)^2 + (\epsilon/\omega)^2]} = \frac{K_{cx}}{2\epsilon^2}\left[1 - \operatorname{sech}\left(\frac{\pi\epsilon}{2\omega}\right)\right] \tag{5-73}$$

With the exception of the quantities δ' and Ξ', the solutions for the single-axis and coupled systems are equivalent. Therefore, a measure of the accuracy of the single-axis approximation can be obtained by comparing these quantities. The percentage errors for the single-axis solutions are shown in Fig. 5-9 for $B_L = 4$ ($\epsilon^2 = 9$). Although the discrepancy is quite large at the lower frequencies, it is less than 10% in both cases when $\omega > 6$.

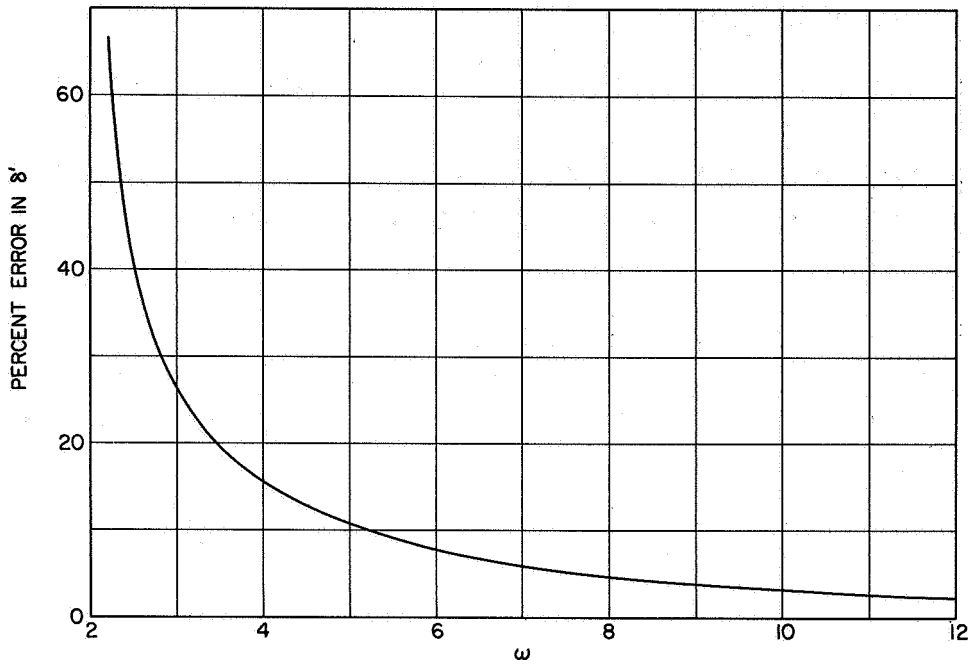

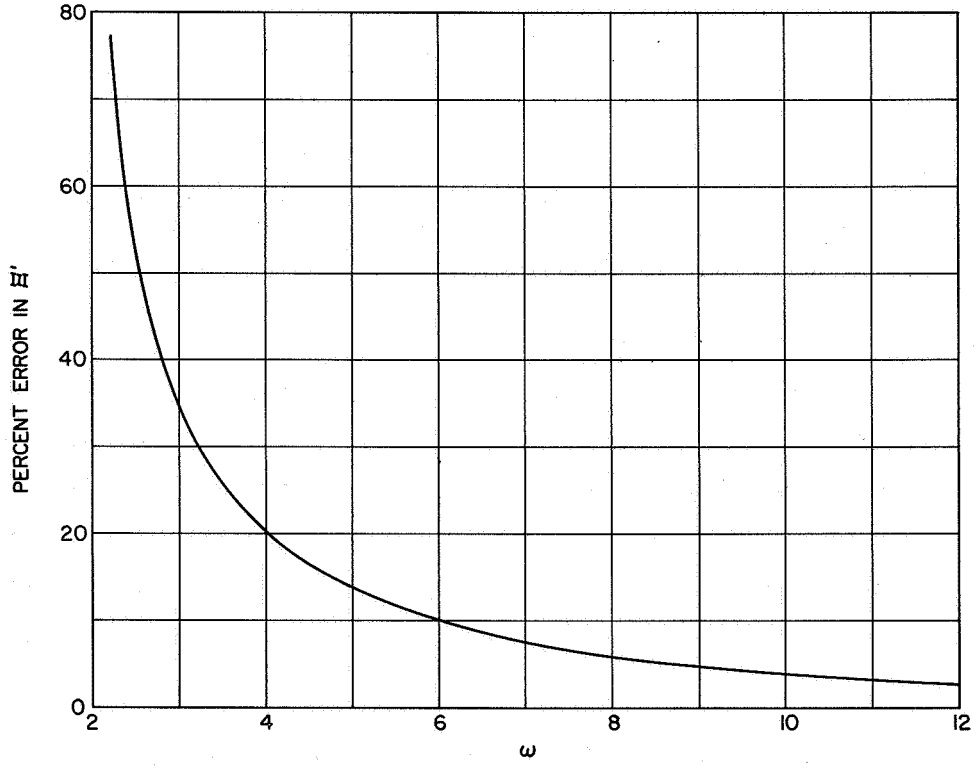

FIG. 5-9. ERRORS FOR SINGLE-AXIS APPROXIMATION VS LIMIT-CYCLE FREQUENCY ($B_L = 4$, $\theta_2 - \theta_1 = \pi$).

2. Phase-Plane Method

The basic equations for the single-axis approximation are

$$\ddot{x} - (2B_L + 1)x = - F(\xi) \tag{5-74}$$

$$\xi = \dot{x} + \lambda x \tag{5-75}$$

and $F(\xi)$ is shown in Fig. 5-1. The geometry for a typical limit cycle in the $\dot{x}$-x phase plane is illustrated in Fig. 5-10. From the figure, it is obvious that

$$\xi_d = \lambda x_2 \tag{5-76}$$

$$\delta = \dot{x}_2 \tag{5-77}$$

Between points 1 and 2, $F(\xi) = 0$, and integration of Eq. (5-74) gives

$$\dot{x}^2 = \epsilon^2(x^2 - x_1^2) \tag{5-78}$$

$$\dot{x}_2 = \epsilon x_1\sqrt{q^2 - 1} \tag{5-79}$$

$$t_{12} = \frac{1}{\epsilon} \log \left|q + \sqrt{q^2 - 1}\right| \tag{5-80}$$

where

$$\epsilon^2 \equiv (2B_L + 1) \tag{5-81}$$

$$q \equiv x_2/x_1 > 1 \tag{5-82}$$

Between points 2 and 3, $F(\xi) = K_{cx}$, and a single integration of Eq. (5-74) in this region gives

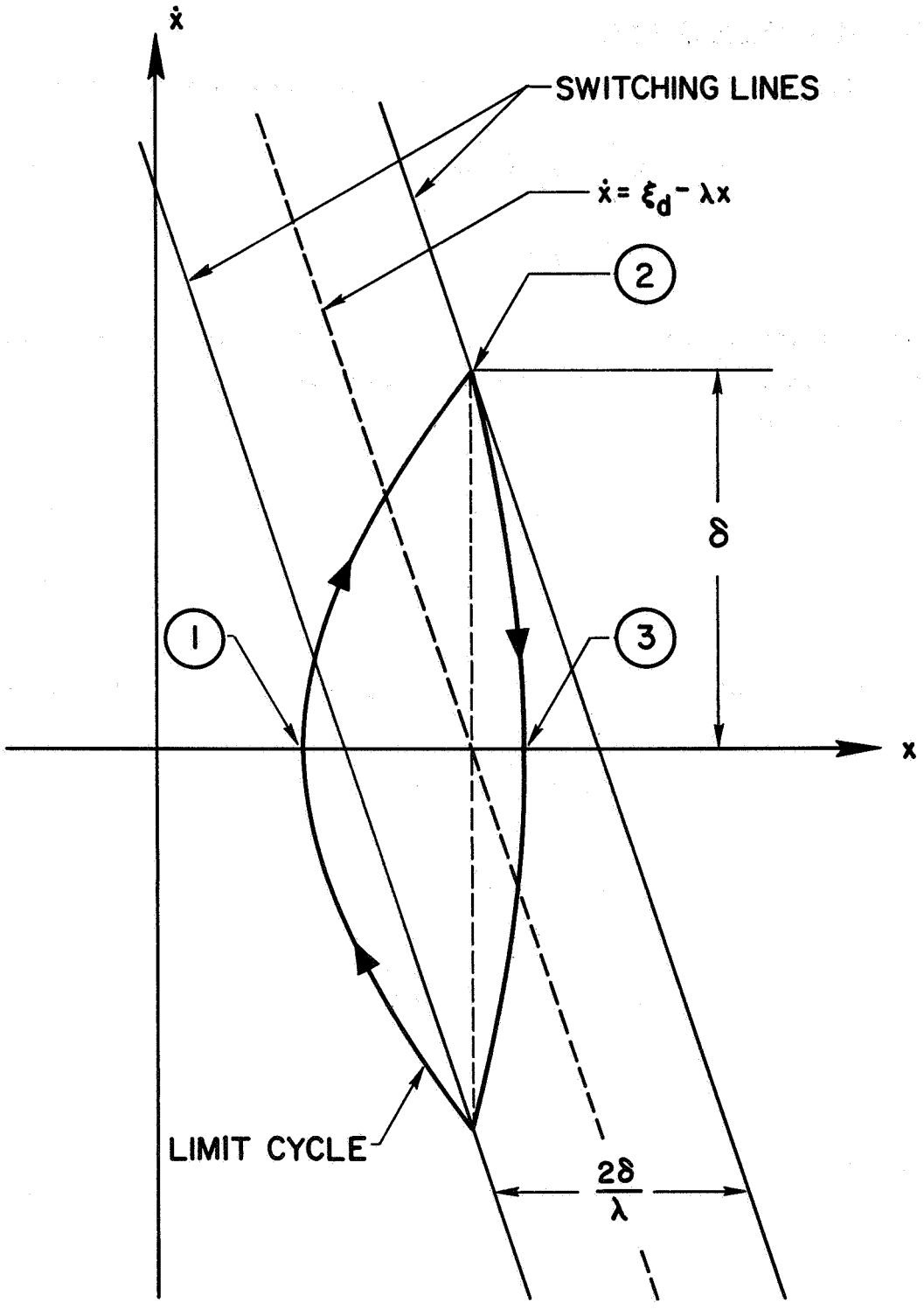

FIG. 5-10. ONE-SIDED LIMIT CYCLE IN THE $\dot{x}$-x PHASE PLANE.

$$\dot{x}^2 = \epsilon^2(x^2 - x_3^2) - 2K_{cx}(x - x_3) \tag{5-83}$$

$$\dot{x}_2^2 = \epsilon^2 q^2 x_1^2(1 - r^2) - 2K_{cx} q x_1(1 - r) \tag{5-84}$$

where

$$r \equiv x_3/x_2 > 1 \tag{5-85}$$

From Eqs. (5-79) and (5-84)

$$K_{cx} = \frac{\epsilon^2(q^2r^2 - 1)}{2q(r - 1)}\, x_1 \tag{5-86}$$

With Eq. (5-86), the necessary stability condition, $K_{cx} > \epsilon^2 x_3$, can be written in terms of q and r as

$$\frac{(q^2r^2 - 1)}{2q^2r(r - 1)} > 1 \tag{5-87}$$

Integration of Eq. (5-83) yields

$$t_{23} = \frac{1}{\epsilon} \log \left| \frac{q^2r(2 - r) - 1}{(q^2r^2 - 1) - 2q(r - 1)\left[q + \sqrt{q^2 - 1}\right]} \right| \tag{5-88}$$

Combining Eqs. (5-80) and (5-88) gives the limit-cycle period ($T_{LC} = 2\pi/\omega$)

$$T_{LC} = 2(t_{12} + t_{23}) = \frac{2}{\epsilon} \log \left| \frac{\left[q^2r(2 - r) - 1\right]\left[q + \sqrt{q^2 - 1}\right]}{(q^2r^2 - 1) - 2q(r - 1)\left[q + \sqrt{q^2 - 1}\right]} \right| \tag{5-89}$$

3. Sample Calculation at the Earth-Moon L_2 Point

As an example of the usefulness of the approximate formulae given above, consider the on-off control of a satellite in the vicinity of the Earth-Moon L_2 point ($B_{L2} = 3.1904$, $\epsilon = 2.7168$). By specifying the amplitude ratios, $x_2/x_1 = 2 = q$, and $x_3/x_1 = 2.5 = qr$ (therefore $r = 1.25$), Eq. (5-89) gives $T_{LC} = 1.407 = 6.12$ days. The fraction of the total time that the control is on can be determined from Eqs. (5-80) and (5-88)

$$m = \frac{t_{23}}{t_{12}} = 0.4512 \qquad (5\text{-}90)$$

This means that the control is turned on continuously for a period of 2.76 days. For thrust periods of this duration, an electrical propulsion device would probably be utilized. Measurement accuracy considerations influence the choice of x_1 (x_{min}). If $x_1 = 10$ km, then $x_2 = 20$ km, $x_3 = 25$ km, and Eq. (5-86) gives $K_{cx} = 2.798 \times 10^{-7}$ g. However, the average control acceleration is only $\overline{K_{cx}} = mK_{cx} = 1.262 \times 10^{-7}$ g. Finally, the slope of the switching line is taken as $\lambda = 3$, and simple calculations yield $\xi_d = 1.561 \times 10^{-4}$ and $\delta = 1.224 \times 10^{-4}$.

The values listed above for K_{cx}, λ, ξ_d, and δ were used in an analog computer simulation of the coupled system [Eq. (5-1)]. It was found that the error in T_{LC} was about 14.1% of the true value $(T_{LC})_{computer} = 1.233 = 5.36$ days. Additional results of this simulation are shown in Fig. 5-11. Notice that x_3/x_1 is very close to the value used in the single-axis approximation ($qr = 2.5$).

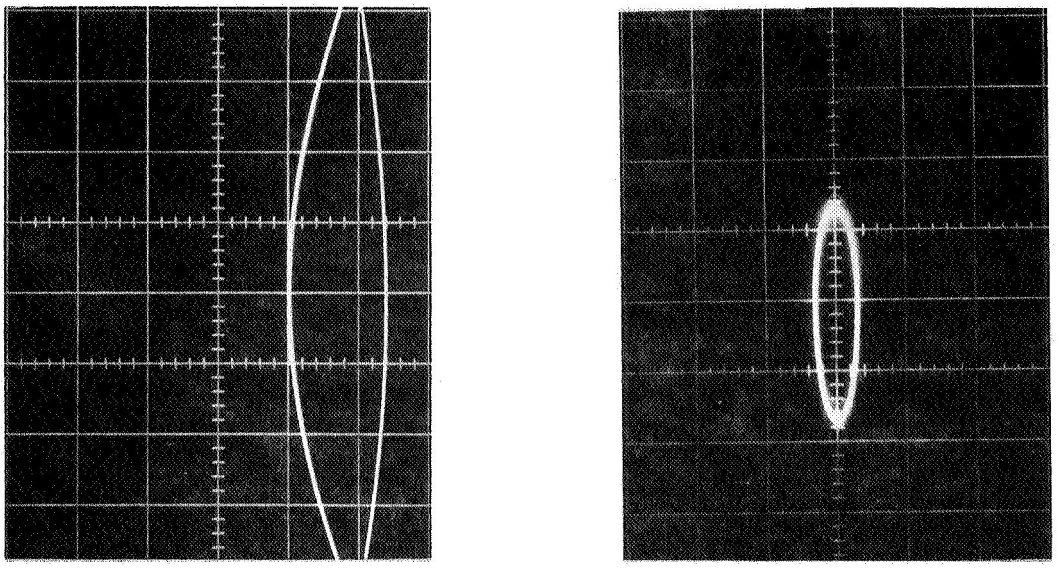

($\dot{x}$ vs x) ($\dot{y}$ vs y)

(Grid size is 0.027 m/sec × 10 km)

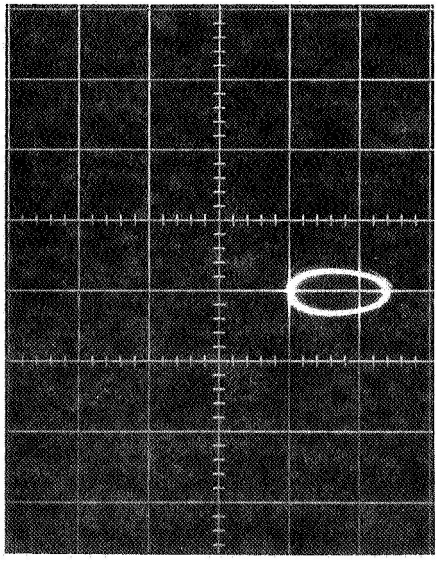

(y vs x)

(Grid size is 10 km × 10 km)

FIG. 5-11. ANALOG COMPUTER SIMULATION OF EQ. (5-1) FOR SAMPLE CALCULATION AT THE EARTH-MOON L_2 POINT. (All trajectories are clockwise).

Chapter VI

STABLE CABLE

Consider two satellites of equal mass that are connected by a light, adjustable-length cable. Is it possible to stabilize the position of the mass center of this configuration in the vicinity of a collinear libration point by simply changing the length of the cable with an internal mechanism? This intriguing possibility is examined below, and it is found that positional stability can be achieved by varying the length of the cable in a manner that takes advantage of the nonlinearities of the modified potential field in the vicinity of the libration point.

This problem was originally analyzed by Colombo,[3] who also concluded that appropriate variations in the length of the connecting cable would produce positional stability. However, Colombo's analysis considered only linear variations of the modified potential field in the vicinity of the libration point, and it can be shown that his conclusion was based on a fallacious argument. (The adjustable-length cable was treated as a workless constraint.)

A. Stabilization Procedure

In this section, the control logic for the cable variation is formulated, and the stability of the resulting system is examined. The geometry for the cable-connected satellite in the vicinity of a collinear libration point is shown in Fig. 6-1. If the mass of the cable is neglected, the equations of motion for the cable-connected satellite are approximately [terms higher than second order are neglected in Eq. (1-43), and it is assumed that $\rho = \nu = 0$].*

*As usual, the upper signs hold at L_2, and the lower signs at L_1.

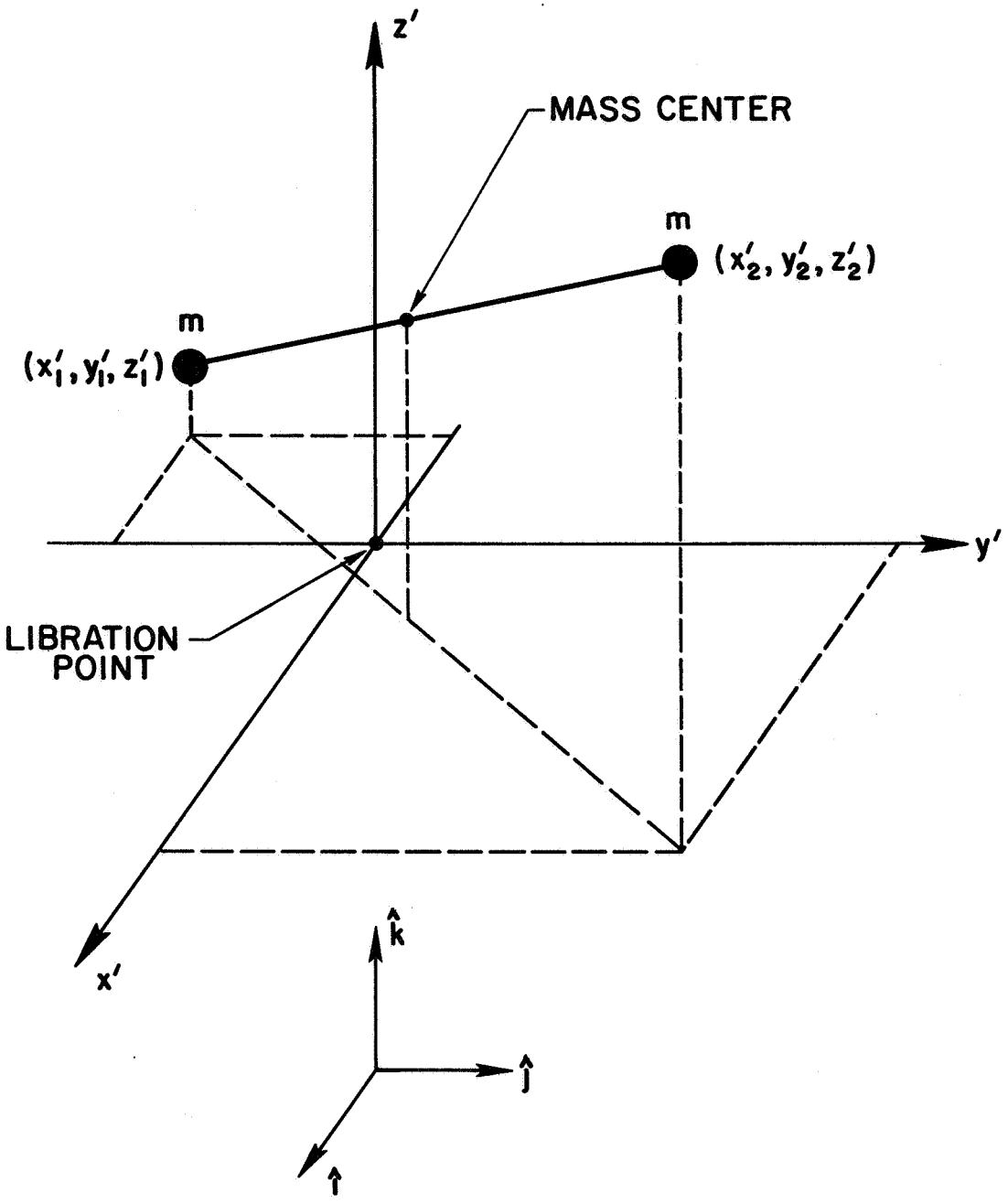

FIG. 6-1. CABLE-CONNECTED SATELLITE IN THE VICINITY OF A COLLINEAR LIBRATION POINT.

$$\ddot{x}_1' - 2\dot{y}_1' - (2B_L + 1)x_1' \pm \frac{3}{2} C_L\left[2x_1'^2 - \left(y_1'^2 + z_1'^2\right)\right] = F_x$$

$$\ddot{x}_2' - 2\dot{y}_2' - (2B_L + 1)x_2' \pm \frac{3}{2} C_L\left[2x_2'^2 - \left(y_2'^2 + z_2'^2\right)\right] = -F_x$$

$$\ddot{y}_1' + 2\dot{x}_1' + (B_L - 1)y_1' \mp 3C_L x_1' y_1' = F_y$$

$$\ddot{y}_2' + 2\dot{x}_2' + (B_L - 1)y_2' \mp 3C_L x_2' y_2' = -F_y \qquad (6\text{-}1)$$

$$\ddot{z}_1' + B_L z_1' \mp 3C_L x_1' z_1' = F_z$$

$$\ddot{z}_2' + B_L z_2' \mp 3C_L x_2' z_2' = -F_z$$

where

$$\vec{F} = F_x \hat{i} + F_y \hat{j} + F_z \hat{k} \qquad (6\text{-}2)$$

and the tension in the cable is

$$\vec{T} = m\vec{F} \qquad (6\text{-}3)$$

Although fluctuations of the tension will occur whenever the cable is extended or retracted, it is assumed here that some tension will always be present (i.e., the cable does not become slack).

1. One-Dimensional Analysis

To gain some physical feeling for the stabilization procedure, an approximate, one-dimensional analysis is presented before considering the more-complicated, three-dimensional system.

a. Shifting Equilibrium Point

Neglecting all coupling terms, and assuming that the motion is limited to the x′-axis, Eq. (6-1) is reduced to

$$\ddot{x}_1' - (2B_L + 1)x_1' \pm 3C_L x_1'^2 = F_x$$
$$\ddot{x}_2' - (2B_L + 1)x_2' \pm 3C_L x_2'^2 = -F_x \tag{6-4}$$

Elimination of F_x gives

$$\ddot{x}_1' + \ddot{x}_2' - (2B_L + 1)(x_1' + x_2') \pm 3C_L\left(x_1'^2 + x_2'^2\right) = 0 \tag{6-5}$$

Assume for the moment that the mass center of the satellite is at $x_{cm}' = \pm \alpha$, and that the cable length ℓ is a constant ($\ell = a$). In this case

$$x_1' = -\frac{a}{2} \pm \alpha$$
$$x_2' = \frac{a}{2} \pm \alpha \tag{6-6}$$

For equilibrium $\ddot{x}_1' = \ddot{x}_2' = 0$, and using Eqs. (6-5) and (6-6), it is found that

$$\alpha = \frac{(2B_L + 1)}{6C_L} - \frac{1}{2}\left[\frac{(2B_L + 1)^2}{9C_L^2} - a^2\right]^{1/2}$$
$$\cong \frac{3C_L}{4(2B_L + 1)}\, a^2 \tag{6-7}$$

Therefore, because of the nonlinear effect, the equilibrium point for the cable-connected satellite is dependent on the length of the cable.

To see how stabilization of the mass center might be attained by taking advantage of this consequence, consider a satellite near an L_2 point with an initial cable length of $\ell(0) = a_i$, and a corresponding equilibrium point at $x_{eq}'(0) = \alpha_i$. Because of the natural instability of the instantaneous equilibrium point x_{eq}', the mass center will always experience a repelling acceleration relative to this

point. Now suppose that the mass center is initially located at $x'_{cm}(0) = \alpha_i + \epsilon(0)$, and assume that $\dot{x}'_{cm}(0) = \dot{\epsilon}(0) = 0$. If $\epsilon(0) > 0$, the initial acceleration is $\ddot{x}'_{cm}(0) > 0$, and x'_{cm} will increase. However, by extending the cable, x'_{eq} can be increased, and it may be possible to shift the equilibrium point to the other side of the mass center [i.e., at some time t_f, $x'_{eq}(t_f) > \alpha_i + \epsilon(t_f)$]. This shift would decelerate the mass center, and if $\epsilon(0)$ is not too large, the motion of the mass center could be reversed. If $\epsilon(0) < 0$, the initial acceleration is $\ddot{x}'_{cm}(0) < 0$, and x'_{cm} will decrease. With this initial condition, the appropriate shift of the equilibrium point would be achieved by retracting the cable [notice that the equilibrium point cannot be shifted to the other side of the mass center when $\epsilon(0) < -\alpha_i$].

Naturally, the magnitudes of the initial errors $[\epsilon(0), \dot{\epsilon}(0)]$ that can be tolerated with this stabilization method are bounded. This limitation will be discussed in Section B-1.

b. Cable Control

For convenience, the coordinate translation

$$x' = x \pm \alpha \tag{6-8}$$

is introduced. With this translation, Eq. (6-5) becomes

$$\ddot{x}_1 + \ddot{x}_2 - (2B_L + 1)(x_1 + x_2 \pm 2\alpha) \pm 3C_L\left[x_1^2 + x_2^2 \pm 2\alpha(x_1 + x_2) + 2\alpha^2\right] = 0 \tag{6-9}$$

and the equilibrium solution is

$$x_1 = -\frac{a}{2}$$
$$x_2 = \frac{a}{2} \tag{6-10}$$

This equilibrium solution is unstable if the cable length is constant, but the situation is quite different when the cable length is varied according to the control law

$$\ell \equiv x_2 - x_1 = [a \pm b(x_1 + x_2) \pm c(\dot{x}_1 + \dot{x}_2)] \tag{6-11}$$

The form of this control law has been influenced by the qualitative arguments of the previous section.

Stability conditions for the constants a, b, and c can be determined by investigating small motions about the equilibrium solution of Eq. (6-10). Substitution of

$$\begin{aligned} x_1 &= -\frac{a}{2} + \xi_1 \\ x_2 &= \frac{a}{2} + \xi_2 \end{aligned} \tag{6-12}$$

into Eqs. (6-9) and (6-11) gives [neglecting terms of $0(\xi^2)$]

$$\ddot{\xi}_1 + \ddot{\xi}_2 - (2B_L + 1)(\xi_1 + \xi_2) \pm 3C_L\left[a(\xi_2 - \xi_1) \pm 2\alpha(\xi_1 + \xi_2)\right] = 0 \tag{6-13}$$

and

$$(\xi_2 - \xi_1) = \pm b(\xi_1 + \xi_2) \pm c(\dot{\xi}_1 + \dot{\xi}_2) \tag{6-14}$$

The coordinate for the mass center is

$$x_{cm} = \frac{x_1 + x_2}{2} = \frac{\xi_1 + \xi_2}{2} \tag{6-15}$$

From Eqs. (6-13), (6-14), and (6-15), it is clear that

$$\ddot{x}_{cm} + 3C_L ac\dot{x}_{cm} + \left[3C_L(ab + 2\alpha) - (2B_L + 1)\right]x_{cm} = 0 \tag{6-16}$$

Therefore, the mass center is asymptotically stable if

$$ac > 0 \tag{6-17}$$

$$(ab + 2\alpha) > \frac{2B_L + 1}{3C_L} \tag{6-18}$$

The constant α can usually be neglected in Eq. (6-18), and this stability condition can be approximated by

$$ab > \frac{2B_L + 1}{3C_L} \tag{6-19}$$

For the Earth-Moon L_2 point ($B_{L2} = 3.1904$, $C_{L2} = 15.845$), Eq. (6-19) gives $ab > 0.155$.

2. Three-Dimensional Analysis

Using the coordinate transformation [cf Eq. (6-8)]

$$x' = x \pm \alpha, \quad y' = y, \quad z' = z \tag{6-20}$$

in Eq. (6-1) gives

$$\begin{aligned}
&\ddot{x}_1 - 2\dot{y}_1 - (2B_L + 1)(x_1 \pm \alpha) \pm \frac{3}{2} C_L\left[2x_1^2 \pm 4\alpha x_1 + 2\alpha^2 - \left(y_1^2 + z_1^2\right)\right] = F_x \\
&\ddot{x}_2 - 2\dot{y}_2 - (2B_L + 1)(x_2 \pm \alpha) \pm \frac{3}{2} C_L\left[2x_2^2 \pm 4\alpha x_2 + 2\alpha^2 - \left(y_2^2 + z_2^2\right)\right] = -F_x \\
&\ddot{y}_1 + 2\dot{x}_1 + (B_L - 1)y_1 \mp 3C_L(x_1 \pm \alpha)y_1 = F_y \\
&\ddot{y}_2 + 2\dot{x}_2 + (B_L - 1)y_2 \mp 3C_L(x_2 \pm \alpha)y_2 = -F_y \\
&\ddot{z}_1 + B_L z_1 \mp 3C_L(x_1 \pm \alpha)z_1 = F_z \\
&\ddot{z}_2 + B_L z_2 \mp 3C_L(x_2 \pm \alpha)z_2 = -F_z
\end{aligned} \tag{6-21}$$

where α is given by Eq. (6-7). For a cable length $\ell = a$, it is readily verified that an equilibrium solution of Eq. (6-21) is

$$x_1 = -\frac{a}{2}, \quad x_2 = \frac{a}{2}$$

$$y_1 = y_2 = z_1 = z_2 = 0 \tag{6-22}$$

This equilibrium situation is depicted in Fig. 6-2. Notice that stabilization about this equilibrium solution must control the relative orientation of the cable-connected satellite as well as the position of its mass center.

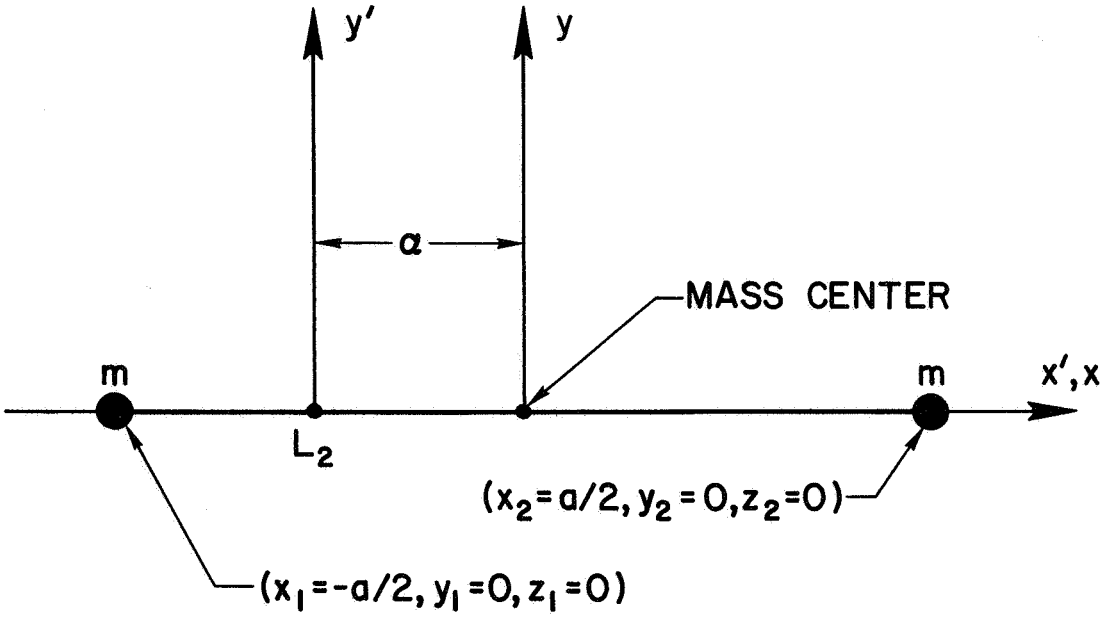

FIG. 6-2. EQUILIBRIUM SITUATION FOR THE CABLE-CONNECTED SATELLITE NEAR AN L_2 POINT.

The cable control law for the three-dimensional case is not obvious, but after a few trials, a satisfactory control law was devised. This control law is given by

$$\ell^2 = (x_2 - x_1)^2 + (y_2 - y_1)^2 + (z_2 - z_1)^2$$

$$= [a \pm b(x_1 + x_2) \pm c(\dot{x}_1 + \dot{x}_2) + \beta(y_1 - y_2)]^2 \tag{6-23}$$

where a, b, c, and β are constants. It is hoped that the reasoning behind this particular formulation will be made clear by the stability investigation presented below.

Before proceeding to the stability analysis, some useful equations are obtained. Using Fig. 6-1, it can be verified that [check Eqs. (6-2) and (6-20)]

$$\frac{F_x}{F_y} = \frac{x_2 - x_1}{y_2 - y_1} \tag{6-24}$$

$$\frac{F_x}{F_z} = \frac{x_2 - x_1}{z_2 - z_1} \tag{6-25}$$

$$\frac{F_y}{F_z} = \frac{y_2 - y_1}{z_2 - z_1} \tag{6-26}$$

Rearrangements of Eq. (6-21) give

$$\ddot{x}_1 + \ddot{x}_2 - 2(\dot{y}_1 + \dot{y}_2) - (2B_L + 1)(x_1 + x_2 \pm 2\alpha)$$
$$\pm \frac{3}{2} C_L \left[2\left(x_1^2 + x_2^2\right) \pm 4\alpha(x_1 + x_2) + 4\alpha^2 \right.$$
$$\left. - \left(y_1^2 + y_2^2 + z_1^2 + z_2^2\right) \right] = 0 \tag{6-27}$$

$$\ddot{y}_1 + \ddot{y}_2 + 2(\dot{x}_1 + \dot{x}_2) + (B_L - 1)(y_1 + y_2)$$
$$\mp 3C_L \left[(x_1 \pm \alpha) y_1 + (x_2 \pm \alpha) y_2 \right] = 0 \tag{6-28}$$

$$\ddot{z}_1 + \ddot{z}_2 + B_L(z_1 + z_2) \mp 3C_L \left[(x_1 \pm \alpha) z_1 + (x_2 \pm \alpha) z_2 \right] = 0 \tag{6-29}$$

$$2F_x = \ddot{x}_1 - \ddot{x}_2 - 2(\dot{y}_1 - \dot{y}_2) - (2B_L + 1)(x_1 - x_2)$$

$$\pm \frac{3}{2} C_L \left\{2\left(x_1^2 - x_2^2\right) \pm 4\alpha(x_1 - x_2) - \left[\left(y_1^2 - y_2^2\right) + \left(z_1^2 - z_2^2\right)\right]\right\} \qquad (6\text{-}30)$$

$$2F_y = \ddot{y}_1 - \ddot{y}_2 + 2(\dot{x}_1 - \dot{x}_2) + (B_L - 1)(y_1 - y_2)$$

$$\mp 3C_L\left[(x_1 \pm \alpha)y_1 - (x_2 \pm \alpha)y_2\right] \qquad (6\text{-}31)$$

$$2F_z = \ddot{z}_1 - \ddot{z}_2 + B_L(z_1 - z_2) \mp 3C_L\left[(x_1 \pm \alpha)z_1 - (x_2 \pm \alpha)z_2\right] \qquad (6\text{-}32)$$

For small motions about the equilibrium solution of Eq. (6-22)

$$x_1 = -\frac{a}{2} + \xi_1, \quad x_2 = \frac{a}{2} + \xi_2$$

$$y_1 = \eta_1, \quad y_2 = \eta_2, \quad z_1 = \zeta_1, \quad z_2 = \zeta_2 \qquad (6\text{-}33)$$

Substituting Eq. (6-33) into Eqs. (6-23), (6-27), (6-28), and (6-29), and retaining only linear terms in (ξ, η, ζ) gives

$$(\xi_1 - \xi_2) \pm b(\xi_1 + \xi_2) \pm c(\dot{\xi}_1 + \dot{\xi}_2) + \beta(\eta_1 - \eta_2) = 0 \qquad (6\text{-}34)$$

$$\ddot{\xi}_1 + \ddot{\xi}_2 - 2(\dot{\eta}_1 + \dot{\eta}_2) - (2B_L + 1)(\xi_1 + \xi_2 \pm 2\alpha)$$

$$\pm \frac{3}{2} C_L\left[a^2 + 2a(\xi_2 - \xi_1) \pm 4\alpha(\xi_1 + \xi_2) + 4\alpha^2\right] = 0 \qquad (6\text{-}35)$$

$$\ddot{\eta}_1 + \ddot{\eta}_2 + 2(\dot{\xi}_1 + \dot{\xi}_2) + (B_L - 1)(\eta_1 + \eta_2)$$

$$\mp 3C_L\left[\left(-\frac{a}{2} \pm \alpha\right)\eta_1 + \left(\frac{a}{2} \pm \alpha\right)\eta_2\right] = 0 \qquad (6\text{-}36)$$

$$\ddot{\zeta}_1 + \ddot{\zeta}_2 + B_L(\zeta_1 + \zeta_2) \mp 3C_L\left[\left(-\frac{a}{2} \pm \alpha\right)\zeta_1 + \left(\frac{a}{2} \pm \alpha\right)\zeta_2\right] = 0 \qquad (6\text{-}37)$$

Two more equations are obtained by eliminating F_x, F_y, and F_z in Eqs. (6-24), (6-25), (6-30), (6-31), and (6-32). Again keeping only linear terms in (ξ, η, ζ) this yields

$$\ddot{\eta}_2 - \ddot{\eta}_1 + 2(\dot{\xi}_2 - \dot{\xi}_1) \mp \frac{3}{2} C_L a(\eta_1 + \eta_2) + 3(B_L - 3C_L\alpha)(\eta_2 - \eta_1) = 0 \tag{6-38}$$

$$\ddot{\zeta}_2 - \ddot{\zeta}_1 \mp \frac{3}{2} C_L a(\zeta_1 + \zeta_2) + [3(B_L - 3C_L\alpha) + 1](\zeta_2 - \zeta_1) = 0 \tag{6-39}$$

Equations (6-34) to (6-39) constitute six independent equations for the six unknowns $(\xi_1, \xi_2, \eta_1, \eta_2, \zeta_1, \zeta_2)$. These equations will be used to test the stability of the controlled motion of the cable-connected satellite about the equilibrium solution of Eq. (6-22).

The linearized motion out of the xy-plane is uncoupled, and the characteristic equation for this motion can be determined from Eqs. (6-37) and (6-39). A simple calculation gives

$$s^4 + a_1 s^2 + a_2 = 0 \tag{6-40}$$

where

$$a_1 = (4B_L + 1) - 12C_L\alpha \tag{6-41}$$

$$a_2 = \frac{1}{2}\left\{\left[B_L - \frac{3}{2} C_L(2\alpha \mp a)\right]\left[(3B_L + 1) - \frac{3}{2} C_L(6\alpha \pm a)\right] + \left[B_L - \frac{3}{2} C_L(2\alpha \pm a)\right]\left[(3B_L + 1) - \frac{3}{2} C_L(6\alpha \mp a)\right]\right\} \tag{6-42}$$

Terms involving α and a^2 can usually be neglected, and the roots of Eq. (6-40) are approximately $\pm j\sqrt{B_L}$, $\pm j\sqrt{3B_L + 1}$ $(j \equiv \sqrt{-1})$. Therefore, according to the linearized analysis, the out-of-plane motion of the cable-connected satellite is bounded. However, small oscillations, which could be caused by initial-condition errors, cannot be damped by the cable control.

The characteristic equation for the coupled motion in the xy-plane is obtained from Eqs. (6-34), (6-35), (6-36), and (6-38). After

some tiresome manipulations, it is found that

$$s^6 + b_1 s^5 + b_2 s^4 + b_3 s^3 + b_4 s^2 + b_5 s + b_6 = 0 \tag{6-43}$$

where

$$b_1 = 3C_L ac - 2\beta \tag{6-44}$$

$$b_2 = (k_2 + k_3 + 4 - k_1) + 3C_L ab \tag{6-45}$$

$$b_3 = 3C_L(k_2 + k_3 + 2)ac + 2[k_1 - (k_2 + 4)]\beta \tag{6-46}$$

$$b_4 = k_3(k_2 + 4) - k_1(k_2 + k_3) - \frac{9}{4} C_L^2 a^2 + 3C_L(k_2 + k_3 + 2)ab \tag{6-47}$$

$$b_5 = 3C_L\left(k_2 k_3 - \frac{9}{4} C_L^2 a^2\right)ac + 2\left(k_1 k_2 + \frac{9}{2} C_L^2 a^2\right)\beta \tag{6-48}$$

$$b_6 = \left(k_2 k_3 - \frac{9}{4} C_L^2 a^2\right)(3C_L ab - k_1) \tag{6-49}$$

and

$$k_1 \equiv (2B_L + 1) - 6C_L\alpha \tag{6-50}$$

$$k_2 \equiv (B_L - 1) - 3C_L\alpha \tag{6-51}$$

$$k_3 \equiv 3B_L - 9C_L\alpha \tag{6-52}$$

The determination of suitable values for the control parameters b, c, and β can be accomplished in an efficient manner by employing the root-locus technique. Taking $c = \beta = 0$, Eq. (6-43) is written in the form

$$\frac{3C_L ab\left[s^4 + c_1 s^2 + c_2\right]}{s^6 + d_1 s^4 + d_2 s^2 + d_3} = -1 \tag{6-53}$$

where

$$c_1 = k_2 + k_3 + 2 \tag{6-54}$$

$$c_2 = k_2 k_3 - \frac{9}{4} C_L^2 a^2 \tag{6-55}$$

$$d_1 = k_2 + k_3 + 4 - k_1 \tag{6-56}$$

$$d_2 = - \left[k_1 (k_2 + k_3) - k_3 (k_2 + 4) - \frac{9}{4} C_L^2 a^2 \right] \tag{6-57}$$

$$d_3 = - k_1 \left(k_2 k_3 - \frac{9}{4} C_L^2 a^2 \right) \tag{6-58}$$

A root-locus plot of Eq. (6-53) for the Earth-Moon L_2 point is given in Fig. 6-3.* The root-locus plot shows that the system is neutrally stable when $ab > (ab)_3 = 0.600$. Notice that $(ab)_2$ corresponds to the critical gain for the one-dimensional case, i.e., $(ab)_2 \cong (2B_L + 1)/3C_L$ [cf Eq. (6-19)]. The critical gains, $(ab)_2$ and $(ab)_3$, are listed in Table 6-1 for several libration points. In every case, $(ab)_3/(ab)_2 < 4$, and it can be concluded that neutral stability is insured at any libration point when

$$ab > \frac{4(2B_L + 1)}{3C_L} \tag{6-59}$$

Damping is introduced by choosing appropriate values for the control parameters c and β. For this case, Eq. (6-43) is written as

$$\frac{3C_L ac \left[b_1' s^4 + b_3' s^2 + b_5' \right] s}{s^6 + b_2 s^4 + b_4 s^2 + b_6} = - 1 \tag{6-60}$$

*It was found that the contributions of terms involving a^2 and α were negligible for the values of a that are used in the present study. With $a = 0$ in Eqs. (6-54) to (6-58), the critical gains are $(ab)_1 = 0.084$, $(ab)_2 = 0.155$, and $(ab)_3 = 0.600$. For $a = 10^{-2}$ in Eqs. (6-54) to (6-58), the critical gains are $(ab)_1 = 0.085$, $(ab)_2 = 0.155$, and $(ab)_3 = 0.599$.

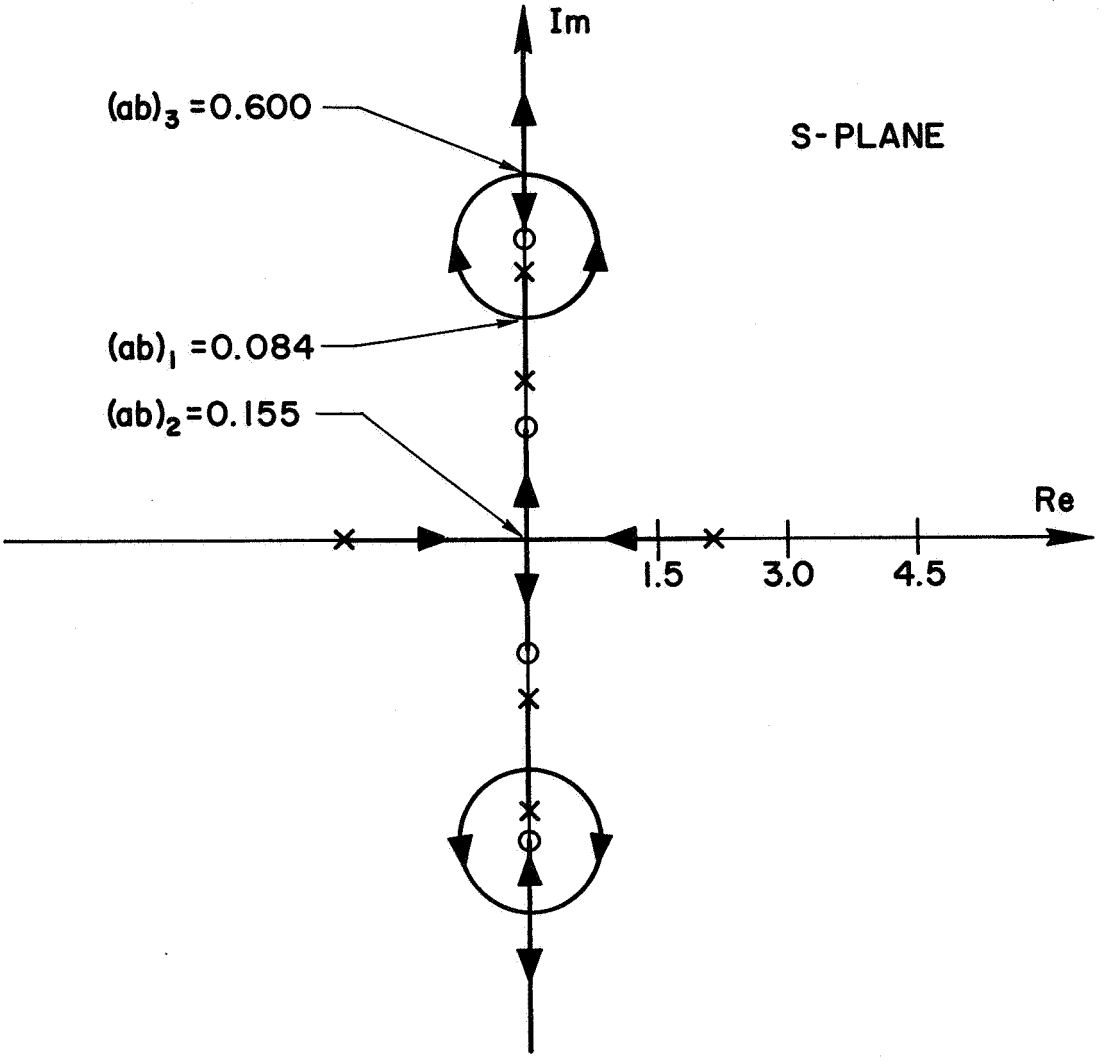

Fig. 6-3. ROOT-LOCUS PLOT FOR EQ. (6-53) AT THE EARTH-MOON L_2 POINT (B_{L2} = 3.1904, C_{L2} = 15.845). Gain is ab.

Table 6-1

CRITICAL GAINS FOR CABLE-CONNECTED SATELLITE

Libration Point	$(ab)_3$	$(ab)_2$	$\frac{(ab)_3}{(ab)_2}$
Earth-Moon L_1	0.651	0.175	3.72
Earth-Moon L_2	0.600	0.155	3.87
Sun-Mercury L_2	0.0144	0.00378	3.81
Sun-Venus L_2	0.0355	0.00932	3.81
Sun-Earth L_2	0.0380	0.00999	3.80
Sun-Mars L_2	0.0181	0.00475	3.81
Jupiter-Io L_2	0.0882	0.0232	3.80
Jupiter-Ganymede L_2	0.114	0.0298	3.83
Jupiter-Enceladus L_2	0.0140	0.00369	3.79

where

$$b_1' = 1 - 2\beta' \tag{6-61}$$

$$b_3' = (k_2 + k_3 + 2) + 2[k_1 - (k_2 + 4)]\beta' \tag{6-62}$$

$$b_5' = \left(k_2 k_3 - \frac{9}{4} C_L^2 a^2\right) + 2\left(k_1 k_2 + \frac{9}{2} C_L^2 a^2\right)\beta' \tag{6-63}$$

and

$$\beta' \equiv \frac{\beta}{3C_L ac} \tag{6-64}$$

It should be emphasized that <u>both</u> c and β are needed in Eq. (6-43) to obtain a damped system. The parameter β' (which determines β)

must be chosen so that the zeros in Eq. (6-60) are located between the poles on the imaginary axis. (This pole-zero configuration is not possible when $\beta' = 0$.) If this is not done, a segment of the root locus of Eq. (6-60) will be in the right half of the s-plane.

By fixing the values of ab and β', a root-locus plot of Eq. (6-60) for the gain ac can be constructed. The plot for the Earth-Moon L_2 point with $ab = 0.750$ and $\beta' = 0.200$ is shown in Fig. 6-4. Although more damping would be desirable, the system is asymptotically stable for all values of the gain ac. When $ac = 0.100$, the roots are located at $-0.0475 \pm j\,1.2249$, $-0.7595 \pm j\,3.8841$, and $-0.4764 \pm j\,4.9958$, and from Eq. (6-64), $\beta = 0.951$.

B. Other Considerations

Although the stability of small motions about the equilibrium solution of Eq. (6-22) has been established, several questions concerning the theoretical feasibility of the cable control system are still unanswered. Some of these questions are considered in this section.

1. Cable Extension Limitation

The extension of the cable is made possible by the gravitational gradient in the vicinity of the libration point. Therefore, the acceleration of the cable's length $\ddot{\ell}$ is bounded $[\ddot{\ell}_{max} \cong (2B_L + 1)\ell]$.* This restriction has the effect of placing upper bounds on the initial errors that can be tolerated with the cable stabilization technique. In this section, approximate analytical estimates of these error bounds are obtained by using the one-dimensional model of Section A-1.

Denoting initial values with a subscript i, the coordinate translation of Eq. (6-8) is specialized to**

$$x' = x + \alpha_i \tag{6-65}$$

---

*When the cable is retracted, $\ddot{\ell}_{max}$ is determined by the tensile strength of the cable.

**For clarity, double signs are deleted, and the analysis is limited to an L_2 point.

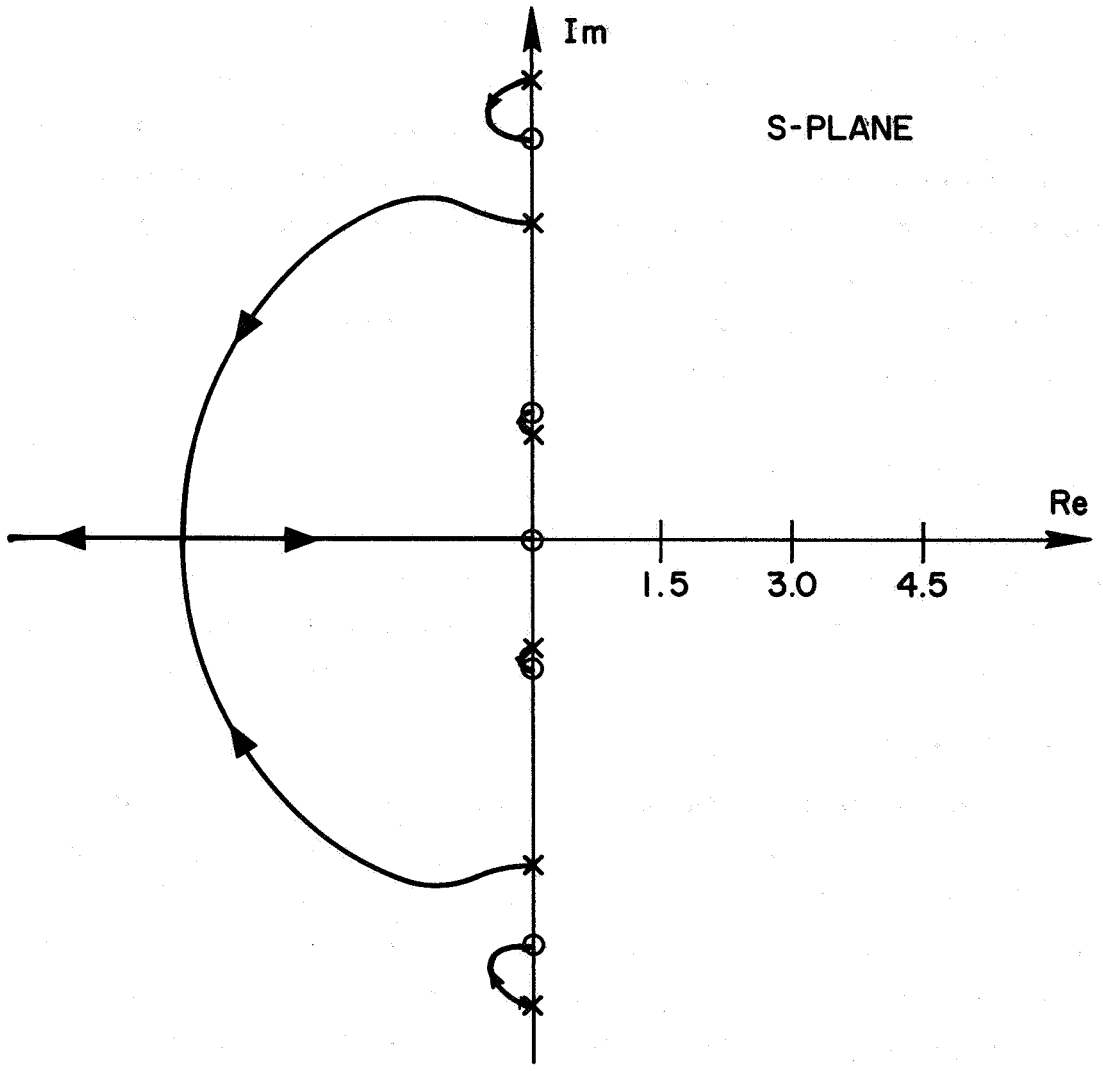

FIG. 6-4. ROOT-LOCUS PLOT FOR EQ. (6-60) AT THE EARTH-MOON L_2 POINT (B_{L2} = 3.1904, C_{L2} = 15.845). Gain is ac and ab = 0.750, β' = 0.200.

The coordinates of the two masses are

$$x_1 = - q + \epsilon$$
$$x_2 = q + \epsilon \tag{6-66}$$

Initially, it is assumed that $q(0) = a_i/2$, $\dot{q}(0) = 0$, and $\epsilon(0) \sim O(a_i^2)$. Substitution of Eq. (6-66) into Eq. (6-4) [using Eq. (6-65)] gives

$$- \ddot{q} + \ddot{\epsilon} - (2B_{L2} + 1)(\epsilon - q + \alpha_i)$$
$$+ 3C_{L2}\left[q^2 - 2q\epsilon + \epsilon^2 + 2\alpha_i(\epsilon - q) + \alpha_i^2\right] = F_x \tag{6-67}$$

$$\ddot{q} + \ddot{\epsilon} - (2B_{L2} + 1)(q + \epsilon + \alpha_i)$$
$$+ 3C_{L2}\left[q^2 + 2q\epsilon + \epsilon^2 + 2\alpha_i(q + \epsilon) + \alpha_i^2\right] = - F_x \tag{6-68}$$

If terms of $O(a_i^2)$ are neglected, Eq. (6-67) or Eq. (6-68) yields

$$\ddot{q} - (2B_{L2} + 1)q = - F_x \tag{6-69}$$

During the cable extension period $(0 \leq t \leq t_1)$ it is assumed that

$$F_x = (1 - \gamma)(2B_{L2} + 1)q = 0 \tag{6-70}$$

where $0 < \gamma < 1$. Equation (6-69) can now be written as

$$\ddot{q} - \gamma(2B_{L2} + 1)q = 0 \tag{6-71}$$

and with the initial conditions given above, the solution is

$$q(t) = \frac{a_i}{2} \cosh kt \tag{6-72}$$

$$\dot{q}(t) = \frac{ka_i}{2} \sinh kt \tag{6-73}$$

where $k^2 \equiv \gamma(2B_{L2} + 1)$. When the cable is fully extended, $q(t_1) = a_m/2$, and the extension time t_1 can be obtained from

$$\cosh kt_1 = \frac{1}{\delta} \tag{6-74}$$

where $\delta \equiv a_i/a_m$ $(0 < \delta < 1)$.

To find the motion of the mass center, add Eqs. (6-67) and (6-68), and neglect terms of $O(a_i^3)$. This yields [using Eq. (6-7)]

$$\ddot{\epsilon} - (2B_{L2} + 1)\epsilon + 3C_{L2}\left[q^2 - \frac{a_i^2}{4}\right] = 0 \tag{6-75}$$

For the cable extension period $(0 \leq t \leq t_1)$, Eq. (6-75) is

$$\ddot{\epsilon} - (2B_{L2} + 1)\epsilon + \frac{3}{8} C_{L2}\delta^2 a_m^2(\cosh 2kt - 1) = 0 \tag{6-76}$$

The solution of Eq. (6-76) is given by

$$\epsilon(t) = [\epsilon(0) + (A + B)]\cosh k't + \frac{\dot{\epsilon}(0)}{k'} \sinh k't - (A + B \cosh 2kt) \tag{6-77}$$

where $k'^2 \equiv (2B_{L2} + 1)$, $A = \dfrac{3C_{L2}\delta^2 a_m^2}{8(2B_{L2} + 1)}$, and $B = \dfrac{3C_{L2}\delta^2 a_m^2}{8(2B_{L2} + 1)(4\gamma - 1)}$.

After the cable has been fully extended $(t \geq t_1)$, Eq. (6-75) becomes

$$\ddot{\epsilon} - (2B_{L2} + 1)\epsilon + \frac{3}{4} C_{L2}a_m^2(1 - \delta^2) = 0 \tag{6-78}$$

The solution of Eq. (6-78) is

$$\epsilon(t) = [\epsilon(t_1) - A']\cosh k'(t - t_1) + \frac{\dot{\epsilon}(t_1)}{k'} \sinh k'(t - t_1) + A' \tag{6-79}$$

where $A' = \dfrac{3C_{L2}a_m^2(1 - \delta^2)}{4(2B_{L2} + 1)}$.

The maximum allowable initial conditions $[\epsilon(0), \dot{\epsilon}(0)]$ are determined by assuming that, at some time t_2

$$\dot{\epsilon}(t_2) = 0$$

$$\epsilon(t_2) = \alpha_m - \alpha_i \cong \frac{3C_{L2}a_m^2(1 - \delta^2)}{4(2B_{L2} + 1)} = A' \tag{6-80}$$

Using Eq. (6-80) in Eq. (6-79), it is readily deduced that

$$\tanh k'(t_2 - t_1) = \frac{\dot{\epsilon}(t_1)}{k'[A' - \epsilon(t_1)]} = 1 \tag{6-81}$$

Finally, with the aid of Eqs. (6-74), (6-77), and (6-81), it is found that

$$\epsilon(0) + \frac{\dot{\epsilon}(0)}{\sqrt{2B_{L2} + 1}} = \frac{3C_{L2}a_m^2}{8(2B_{L2} + 1)}\, G(\gamma, \delta) \tag{6-82}$$

where

$$G(\gamma,\delta) = e^{-k't_1}\left[(2 - \delta^2) + \frac{\delta^2}{(4\gamma - 1)}\,(\cosh 2kt_1 + 2\sqrt{\gamma}\sinh 2kt_1)\right] - \frac{4\gamma\delta^2}{(4\gamma - 1)} \tag{6-83}$$

When $\dot{\epsilon}(0) = 0$, the ratio $\epsilon(0)/\epsilon(t_2)$ may also be of some interest. From Eqs. (6-80) and (6-82), this can be written as

$$\frac{\epsilon(0)}{\epsilon(t_2)} = \frac{G(\gamma,\delta)}{2(1 - \delta^2)} \tag{6-84}$$

Graphs of $G(\gamma,\delta)$ and $\epsilon(0)/\epsilon(t_2)$ are given in Figs. 6-5 and 6-6, respectively.

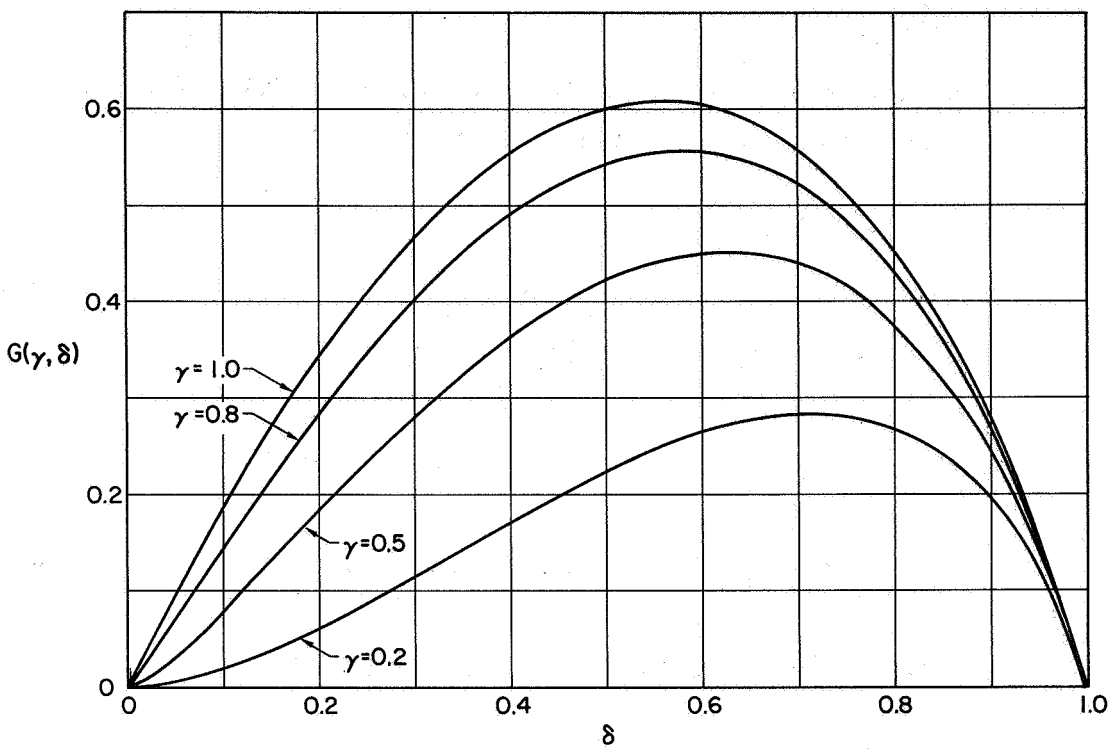

FIG. 6-5. THE FUNCTION $G(\gamma,\delta)$.

From Eq. (6-82) and Fig. 6-5, it can be seen that the allowable initial conditions are maximized by choosing $\gamma = 1$, $\delta \cong 0.55$, and letting a_m become very large. However, other factors call for small values of a_m and γ and larger values of δ.* These trade-offs are not investigated here.

As an example, consider a cable-connected satellite at the Earth-Moon L_2 point. For $\gamma = 0.50$, $\delta = 0.8$, and $a_m = 10^{-2} = 3{,}844.05$ km, it is found that $G(\gamma,\delta) \cong 0.375$, and

$$a_i = 3{,}075.24 \text{ km}, \qquad \alpha_i = 39.61 \text{ km}$$

*One of these factors is the impulsive deceleration that takes place when the cable reaches its maximum length at $t = t_1$. From Eqs. (6-73) and (6-74), this impulsive deceleration is given by $\Delta\dot{x}_2(t_1) = \frac{1}{2} a_m[\gamma(2B_{L2} + 1)(1 - \delta^2)]^{1/2}$. In actual practice, the deceleration will be distributed over a finite time interval which is determined by the maximum tensile strength of the cable. This deceleration period is neglected in the analysis presented in this section.

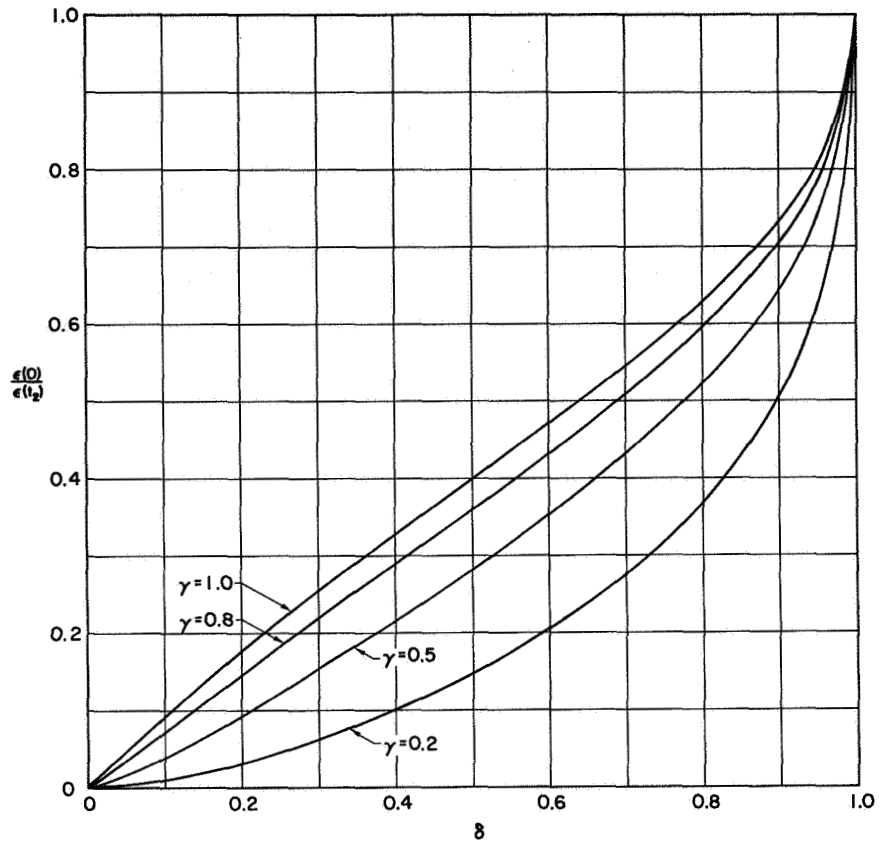

FIG. 6-6. MASS CENTER DISPLACEMENT RATIO $\epsilon(0)/\epsilon(t_2)$ $[\dot{\epsilon}(0) = \dot{\epsilon}(t_2) = 0]$.

If $\dot{\epsilon}(0) = 0$: $\epsilon(0) = 11.60$ km, $\epsilon(t_2) = 22.28$ km

If $\epsilon(0) = 0$: $\dot{\epsilon}(0) = 0.0839$ m/sec

Although this cable is rather long, significant reductions of the cable's length will require high measurement accuracy [e.g., $\epsilon(0) = 0.725$ km for $a_m = 961.01$ km].

2. Structural Comments

The structural aspects of extremely long, cable-connected satellites have received some attention in the literature.[82,83] In Ref. 83, the mechanical design of a device that would vary the length of the cable has also been considered. These studies have indicated that similar design problems for the cable-connected satellite proposed in this chapter would not be insurmountable.

To provide some idea of the magnitudes of the structural parameters for a cable-connected satellite at the Earth-Moon L_2 point, a few representative calculations are presented here. For the purposes of this calculation, it is assumed that

(1) $m = 10{,}000$ kg.

(2) The cable is an aluminum wire (modulus of elasticity $\equiv E_{A\ell} = 1.03 \times 10^7$ psi, density $\equiv \rho_{A\ell} = 2.70$ g/cm^3, and ultimate tensile strength $\equiv \sigma_{A\ell} = 30{,}000$ psi).

(3) The nominal length of the cable is $\ell = 3{,}844.05$ km.

(4) The cable tension is never greater than ten times its nominal value.

With these assumptions, a few elementary calculations give*

$$T_{nom} \cong m(2B_{L2} + 1)\frac{\ell}{2} = 1.005 \times 10^5 \text{ dynes} \quad \text{(nominal cable tension)}$$

$$\sigma_{des} = \frac{\sigma_{A\ell}}{10} = 3{,}000 \text{ psi} \quad \text{(design stress)}$$

$$d_c = 6.22 \times 10^{-3} \text{ cm} \quad \text{(cable diameter)}$$

$$m_c = 504.15 \text{ kg} \quad \text{(mass of cable)}$$

*It has been suggested to the author that the time delay, due to the finite propagation speed of a longitudinal wave in the cable, could be troublesome. However, the propagation speed is just $\sqrt{E_{A\ell}/\rho_{A\ell}} = 5.12$ km/sec, which corresponds to a time delay of $t_d = 12.5$ min for a cable length of $\ell = 3{,}844.05$ km. This time delay is clearly negligible.

Chapter VII

APPLICATIONS

In this chapter, a number of possible applications for libration-point satellites are presented. Some of these proposals are original, while others are derived from previous suggestions. It is not the author's intention to present an all-inclusive list, but rather to give some indication of the usefulness of libration-point satellites.

A. Supporting Role for Lunar and Planetary Missions

1. Utilization of the Earth-Moon Collinear Points in Future Lunar Operations

a. Lunar Communications

In the post-Apollo period, with the advent of semipermanent lunar bases and far-ranging surface vehicles, a capability for real-time communications between widely separated lunar terminals will be needed. For bases located on the far side of the Moon, an uninterrupted communications link with the Earth would also be desirable. In this section, it will be shown how these communications requirements can be satisfied by stationing relay satellites in the vicinity of the collinear libration points of the Earth-Moon system.

The possible use of libration-point satellites for communication between points on the lunar surface was first mentioned by Arthur C. Clarke[9] as early as 1947. However, it has been only recently that methods for using a single libration-point satellite to establish a communications link between the Earth and the far side of the Moon have been devised. Two of these methods, the "Lissajou-orbit" and "halo-orbit" concepts, were originally proposed by the present author in Ref. 7. Another technique, the "hummingbird" concept, has been presented by Vonbun.[18] A comparison of these methods is given below.

(i) Lissajou-Orbit Concept

(α) Occultation Geometry. Consider a satellite that is following a quasi-periodic orbit about the Earth-Moon L_2 point.

Neglecting higher-order corrections, the equations of the orbit are (see Chapter II)

$$x_n \cong A_{x1} \sin \omega_n t$$
$$y_n \cong A_{y1} \cos \omega_n t \qquad (7\text{-}1)$$

where $A_{x1} = kA_{y1}$, $k = 0.343336$, and $\omega_n = 1.86265$. The geometry for this orbit is given in Fig. 7-1. If the satellite is simultaneously executing an out-of-plane oscillation; then [cf Eq. (2-29)]

$$z_n = A_{z1} \cos (\omega_z t + \alpha_o) \qquad (7\text{-}2)$$

where $\omega_z = 1.78618$, and α_o is the initial phase angle. The trajectory of the satellite as seen from the Earth is just a Lissajou curve, and is depicted in Fig. 7-2. Since the frequency difference between the periodic orbit and the z-axis oscillation is very small, the trajectory in Fig. 7-2 can be viewed as a slowly changing elliptical path.

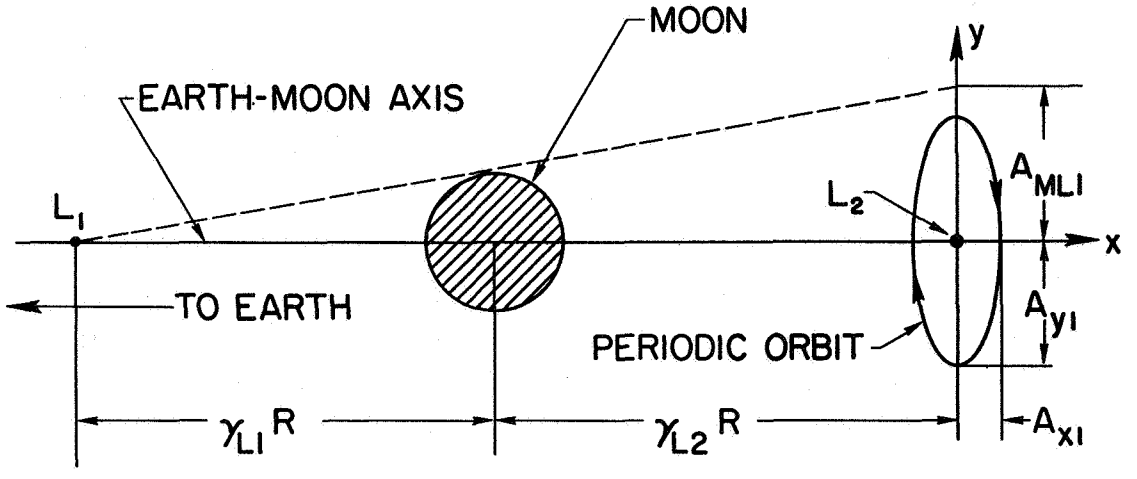

FIG. 7-1. GEOMETRY IN THE MOON'S ORBITAL PLANE. (Not to scale).

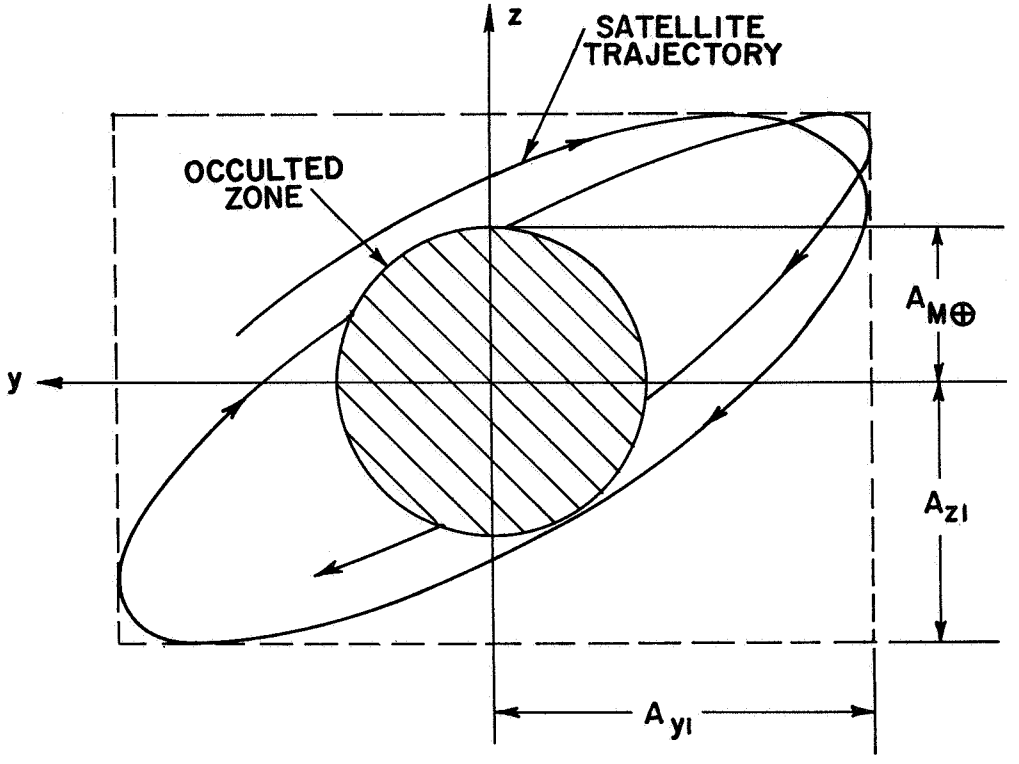

FIG. 7-2. SATELLITE TRAJECTORY ABOUT THE L_2 POINT AS SEEN FROM THE EARTH. (Not to scale).

To set up an efficient communications link between the Earth and the far side of the Moon, the satellite should perform oscillations that are large enough to be visible from any point on the Earth facing the Moon (see Fig. 7-3). Neglecting the small correction for A_{xl}, the radius of the occulted zone for Earth visibility is

$$A_{M\oplus} \cong \gamma_{L2}(R_\oplus + R_\leftmoon) + R_\leftmoon = 3{,}099 \text{ km} \qquad (7\text{-}3)$$

where $R_\oplus = 6{,}371$ km and $R_\leftmoon = 1{,}738$ km (Ref. 28). Slightly larger oscillations by the satellite near the L_2 point will enable it to obtain line-of-sight contact with the L_1 point as well as the Earth. By augmenting the oscillating satellite with a second satellite stationed at the L_1 point, a surface-to-surface communications link between the

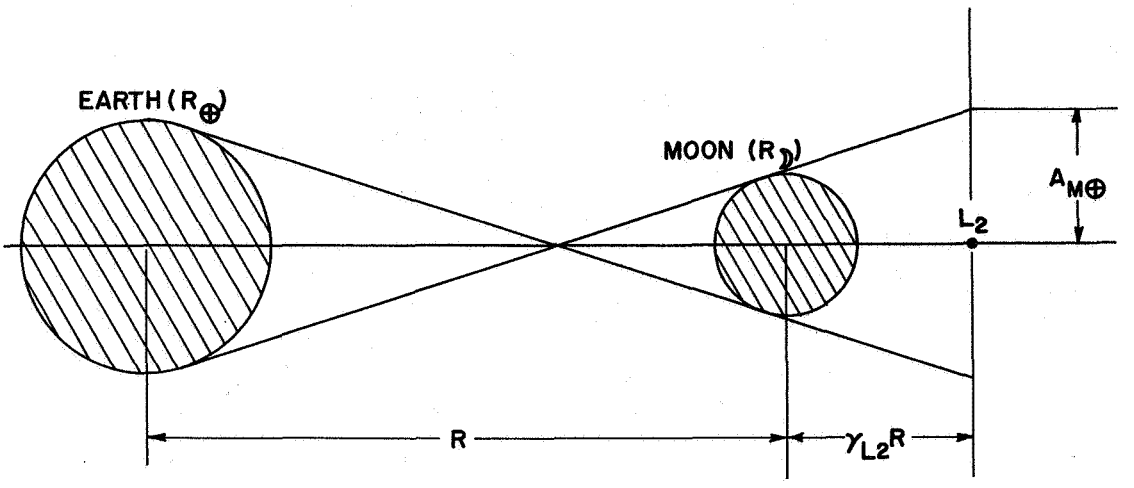

FIG. 7-3. GEOMETRY FOR EARTH VISIBILITY.
(Not to scale).

near and far sides of the Moon could be established. (This possibility was originally discussed by the present author in Ref. 16.) Using Fig. 7-1, it is easy to see that the radius of the occulted zone for this case is

$$A_{ML1} \cong \frac{\gamma_{L1} + \gamma_{L2}}{\gamma_{L1}} R_\mathbb{D} = 3{,}671 \text{ km} \qquad (7\text{-}4)$$

Unfortunately, the oscillating satellite will still enter the occulted zone at periodic intervals. The fraction of the total time that the satellite will be hidden is approximately [using Eqs. (7-1), (7-2), and Fig. 7-2]

$$\tau_{yz} = \frac{4}{\pi^2} \sin^{-1}(A_M/A_{y1}) \sin^{-1}(A_M/A_{z1}) \qquad (7\text{-}5)$$

For $A_{M\oplus} = 3{,}099$ km and $A_{y1} = A_{z1} = 0.02 = 7{,}688$ km, this fraction is only $\tau_{yz} \cong 0.070$ (i.e., 7% of total time). However, occultation periods as long as $t_y = (2/\omega_n)\sin^{-1}(A_{M\oplus}/A_{y1}) \cong 1.94$ days will occur periodically. Since this time is rather long, some means for completely eliminating this occultation would be useful.

The satellite's motion relative to the quasi-periodic orbit can be controlled by any of the methods discussed in Chapters III to V. If the radial-axis control of Fig. 4-1 is employed, the station-keeping cost could be as low as $\overline{|F_{cx}|} = 8.86 \times 10^{-9}$ g (see Section A-1 of Chapter IV). Of course, this low cost can only be realized when higher-order corrections are included in the nominal path calculation (see Chapter II).

(β) Phase-Jump Control. To prevent occultation of the satellite oscillating about L_2, an impulsive z-axis control can be used. Whenever the satellite is about to enter the occulted zone, a control pulse is applied to alter the phase angle, but not the amplitude, of the z-axis oscillation such that the portion of the trajectory that passes through the occulted zone is bypassed. This change in phase angle is accomplished by impulsively reversing the direction of $\dot{z}$ without changing its magnitude (see Fig. 7-4). From Eqs. (7-1) and (7-2), the parametric equations for the trajectory shown in Fig. 7-2 can be written as

$$\begin{aligned} y_n &= A_{y1} \cos \omega_n t \\ z_n &= A_{z1} \cos (\omega_n t + \alpha) \end{aligned} \tag{7-6}$$

where $\alpha \equiv \alpha_o - \epsilon t$, and $\epsilon \equiv \omega_n - \omega_z = 0.07647$. Since ϵ is small, the phase angle α will be approximated by an average value through one cycle. If α_c is the phase angle for the cycle that just misses the occulted zone, the magnitude of the control impulse is (see Fig. 7-4)

$$|\Delta \dot{z}_n| = 2\omega_n A_{z1} \sin \alpha_c \tag{7-7}$$

and since pulses must be imparted at intervals of

$$\Delta t = \frac{\pi - 2\alpha_c}{\epsilon} \tag{7-8}$$

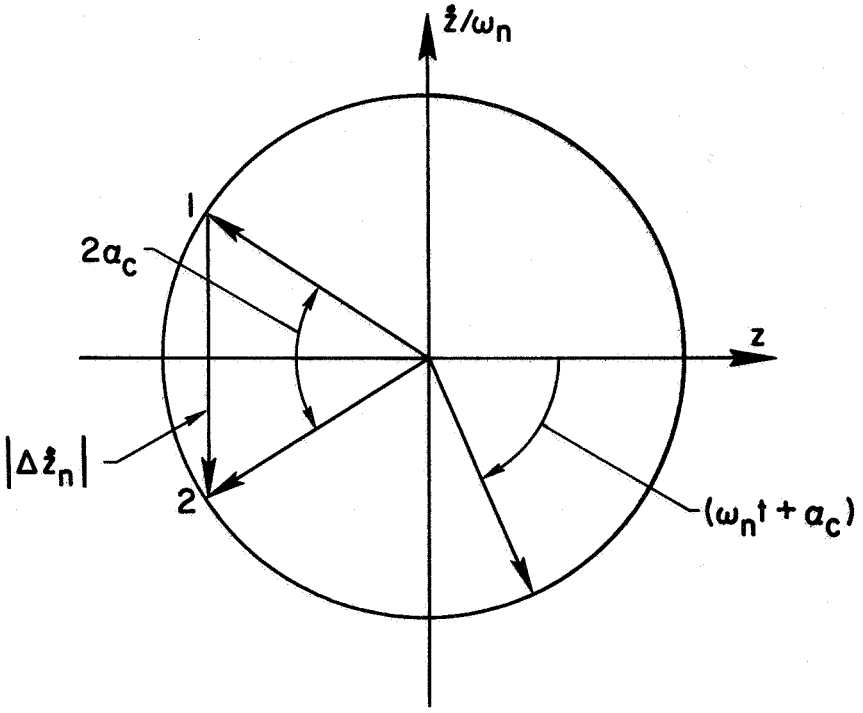

FIG. 7-4. PHASE PLANE REPRESENTATION OF THE CONTROL IMPULSE.

the average control acceleration is given by

$$\overline{|F_{cz}|} = \frac{2\epsilon\omega_n A_{z1} \sin \alpha_c}{\pi - 2\alpha_c} \tag{7-9}$$

It follows from Eq. (7-6) and the geometry of Fig. 7-2 that

$$2r^2 = (A_{y1}^2 + A_{z1}^2) + (A_{y1}^2 + A_{z1}^2 \cos 2\alpha)\cos 2\omega_n t - (A_{z1}^2 \sin 2\alpha)\sin 2\omega_n t \tag{7-10}$$

where r is the radial distance from the origin to the satellite. For a trajectory that just touches the occulted zone

$$2A_M^2 = (A_{y1}^2 + A_{z1}^2) - \left[(A_{y1}^2 + A_{z1}^2 \cos 2\alpha_c)^2 + (A_{z1}^2 \sin 2\alpha_c)^2\right]^{1/2} \tag{7-11}$$

$$\frac{A_{z1}}{A_M} = \left[\frac{\lambda^2 - 1}{\lambda^2 \sin^2 \alpha_c - 1}\right]^{1/2} \tag{7-12}$$

where $\lambda \equiv (A_{y1}/A_M)$. Substitution of Eq. (7-12) into Eq. (7-9) yields

$$\overline{|F_{cz}|} = 2\epsilon\omega_n A_M f(\lambda, \alpha_c) \tag{7-13}$$

where

$$f(\lambda, \alpha_c) \equiv \frac{(\lambda^2 - 1)^{1/2} \sin \alpha_c}{(\pi - 2\alpha_c)(\lambda^2 \sin^2 \alpha_c - 1)^{1/2}} \tag{7-14}$$

For a fixed value of λ, there exists a unique value of α_c, which minimizes the average control acceleration. An elementary analysis shows that this optimum value must satisfy the transcendental equation

$$2(\lambda^2 \sin^2 \alpha_c - 1)\tan \alpha_c = \pi - 2\alpha_c \tag{7-15}$$

The phase angle satisfying Eq. (7-15) is given in Fig. 7-5 as a function of λ.

Up to now, the higher-order corrections to the trajectory of Eq. (7-6) have been neglected. When these corrections are superimposed on the approximate trajectory, the occultation geometry will become more complicated. A simple way (possibly not the most efficient) to account for this complication is to define a new value of A_M (denoted by A_M') in such a way that the true trajectory will not enter the original occulted zone so long as the approximate trajectory does not enter an occulted zone of radius A_M'.

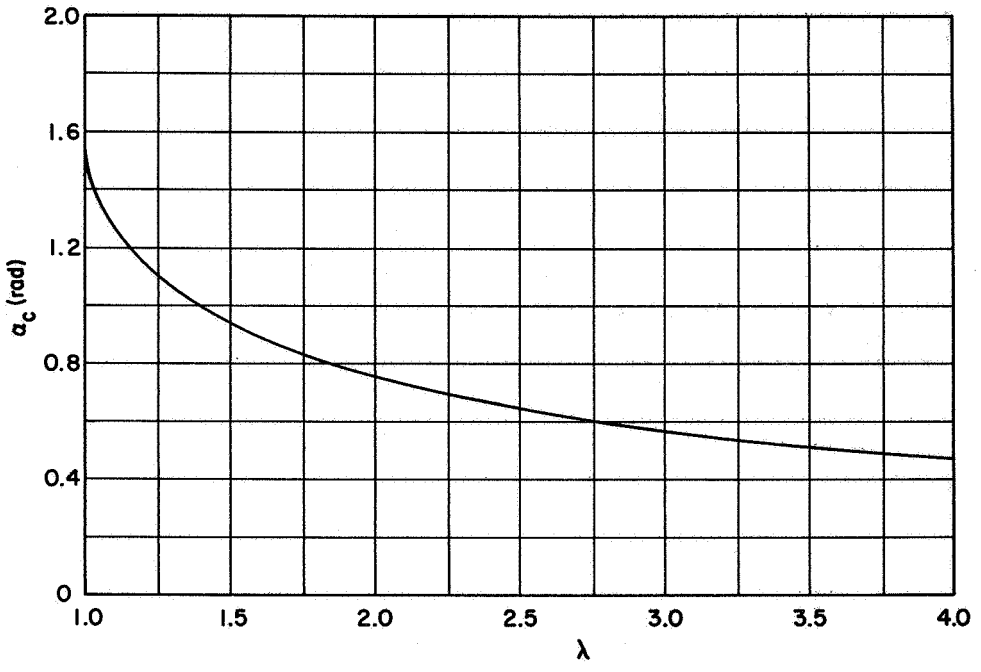

FIG. 7-5. OPTIMUM PHASE ANGLE.

In Chapter II, it was found that the amplitude corrections caused by the lunar eccentricity were much larger than those due to other effects. Therefore, amplitude corrections due to effects other than the lunar eccentricity will be neglected here. Using the results of Chapter II, A_M' is taken as*

$$A_M' = A_M + \beta A_{y1} = \frac{A_M}{1 - \beta\lambda'} \qquad (7\text{-}16)$$

where $\lambda' \equiv (A_{y1}/A_M')$, and $\beta \cong 0.17$. Replacing A_M in Eq. (7-13) by A_M' from Eq. (7-16) gives

*The eccentricity correction for the z-axis oscillation is given in Appendix B. For this case, $A_M' = A_M + \beta A_{z1}$, where $\beta \cong 0.16$.

$$\overline{|F_{cz}|} = 2\epsilon\omega_n A_M \frac{f(\lambda', \alpha_c)}{1 - \beta\lambda'}$$

$$\equiv 2\epsilon\omega_n A_M g(\lambda', \alpha_c, \beta) \qquad (7\text{-}17)$$

The function $g(\lambda', \alpha_c, \beta)$ for optimum values of α_c is plotted in Fig. 7-6 as a function of λ'. For $\beta = 0.17$, a near-optimum value of $g(\lambda', \alpha_c, \beta)$ is obtained by taking $\lambda' = 2$. With $A_{M\oplus} = 3{,}099$ km, it is found that

$A'_{M\oplus} = 4{,}695$ km $\qquad \alpha_c = 43.17°$

$A_{y1} = 9{,}391$ km $\qquad A_{z1} = 8{,}708$ km

$\Delta t = 93.04$ days $\qquad |\Delta\dot{z}_n| = 59.08$ m/sec

$\overline{|F_{cz}|} = 7.50 \times 10^{-7}$ g

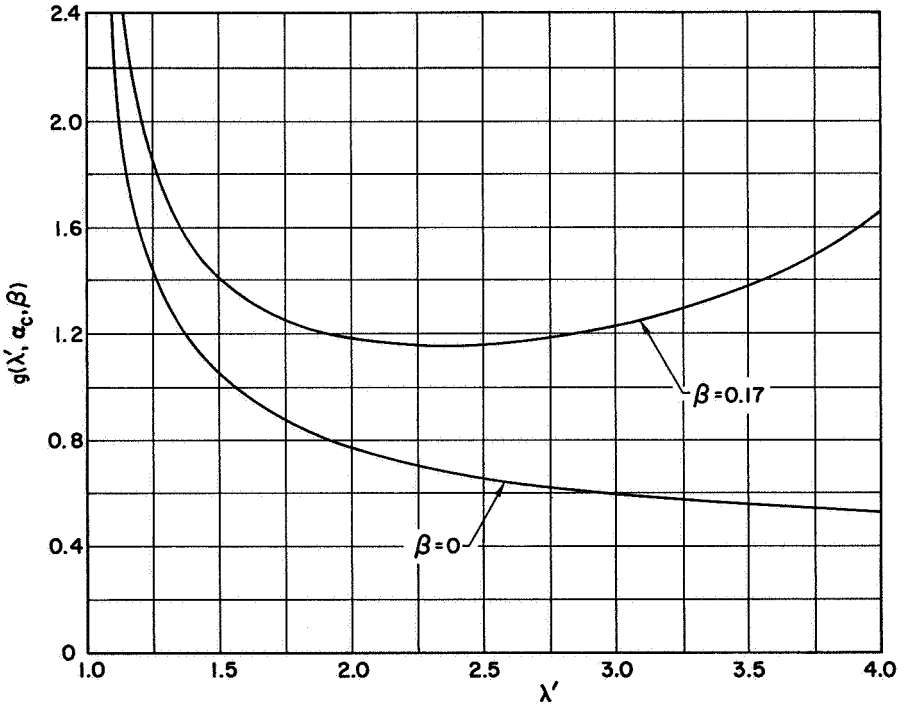

FIG. 7-6. THE FUNCTION $g(\lambda', \alpha_c, \beta)$ FOR OPTIMUM VALUES OF α_c.

(ii) Halo-Orbit Concept

Occultation of the satellite oscillating about L_2 can also be averted by using a frequency control technique. In this scheme, a single-axis control is used to synchronize the fundamental y-axis and z-axis oscillations. In other words, if higher-order trajectory corrections are neglected, the control will produce a closed elliptical path in the yz-plane that always avoids the occulted zone. Although frequency control can be applied in any axis, the cost will be different for each case. Minimum costs for three important cases are given below. As in the previous section, the effect of the eccentricity correction is included by using A_M' for the radius of the occulted zone.

The frequency control method is most easily understood by examining the case where z-axis control is employed. In this case, it is assumed that the approximate satellite orbit in the xy-plane is given by Eq. (7-1) with $A_{y1} \geq A_M'$. The z-axis control is used to force the satellite to follow the path

$$z_n = A_M' \cos \omega_n t \tag{7-18}$$

(i.e., a feedback control is used to zero the coordinate ζ, where $\zeta = z - z_n$). The cost for the frequency change is given by $\overline{|F_{cz}|}$, where $F_{cz} = K_{cz} \cos \omega_n t$.* Since

$$\ddot{z}_n + B_{L2} z_n = F_{cz} = K_{cz} \cos \omega_n t \tag{7-19}$$

it is easy to show that

$$K_{cz} = (\omega_n^2 - B_{L2}) A_M'$$

$$= \left(\omega_n^2 - B_{L2}\right) \frac{A_M}{1 - \beta} \tag{7-20}$$

*It is assumed here that noise inputs are negligible (see Section A-2 of Chapter IV).

($\beta \cong 0.16$ for z-axis). Therefore, the average control acceleration is

$$\overline{|F_{cz}|} = \left(\frac{2}{\pi}\right) K_{cz} = 0.2115\ A_M \tag{7-21}$$

Similarly, for a y-axis control, $F_{cy} = K_{cy} \cos \omega_z t$, and it is found that [using Eqs. (2-10) to (2-12)]

$$\overline{|F_{cy}|} = 0.1589\ A_M \tag{7-22}$$

With y-axis frequency control, $|A_{x1}/A_{y1}| = 0.3379$ ($|A_{x1}/A_{y1}| = 0.3433$ for the natural oscillatory mode).

For an x-axis control, $F_{cx} = K_{cx} \cos \omega_z t$, and a simple calculation gives

$$\overline{|F_{cx}|} = 0.4703\ A_M \tag{7-23}$$

with $|A_{x1}/A_{y1}| = 0.2799$.

Taking $A_{M\oplus} = 3{,}099$ km, Eqs. (7-21) to (7-23) yield

$$\overline{|F_{cz}|} = 4.73 \times 10^{-7} g$$

$$\overline{|F_{cy}|} = 3.56 \times 10^{-7} g$$

$$\overline{|F_{cx}|} = 1.05 \times 10^{-6} g$$

(iii) Hummingbird Concept

In both of the concepts presented above, an "orbiting" satellite was used to set up a communications link between the Earth and the far side of the Moon. However, this communications link can also be obtained by using a satellite that is permanently displaced to one side of the Earth-Moon L_2 point. In this case, a continuous thrust control is needed to station the communications satellite at the non-equilibrium position. The control acceleration can be minimized by

displacing the satellite along the y-axis, and is approximately [see Eq. (4-22) and Fig. 4-4]

$$|\vec{F}_c| \cong |F_{cy}| \cong (B_{L2} - 1)\delta_y = 2.1904\ \delta_y \qquad (7\text{-}24)$$

When $\delta_y = A_{M\oplus} = 3{,}099$ km, Eq. (7-24) gives $|\vec{F}_c| = 4.90 \times 10^{-6}$ g.

Although the displaced satellite would be stationary with respect to the libration point, its distance to the Moon would vary periodically due to the lunar eccentricity. Of course, a constant distance between the satellite and the Moon could be maintained by simply cancelling the eccentricity effect with additional thrust control. A rough calculation shows that the average control acceleration for this task would be about $\overline{|\vec{F}_c|} \cong 1.20 \times 10^{-5}$ g.

(iv) Comparison of Different Techniques

It is clear that, of the three procedures considered above, the halo-orbit concept with y-axis control is the most economical method for maintaining a continuous Earth to lunar far-side communications link. However, the cost for the halo-orbit concept with z-axis control is only slightly higher, and other factors may influence the choice between the y-axis and z-axis controls. The cost for the halo-orbit concept, with either y-axis or z-axis control, is lower than the cost for the hummingbird concept by an order of magnitude.

If occasional occultation periods can be tolerated, the Lissajou-orbit concept should be considered. Uninterrupted communications would still be possible for intervals of about three months, and the station-keeping cost could be reduced by an order of magnitude. (This is two orders of magnitude below the cost for the hummingbird concept.) For emergency situations, when longer continuous communication intervals are required, the phase-jump control technique could be employed.

(v) Concluding Remarks

Methods for using a single libration-point satellite to obtain continuous communications between the Earth and the far side

of the Moon have been presented. The possibility of using two libration-point satellites (one oscillating about the L_2 point while the other is stationed at L_1) to establish a point-to-point communications link covering most of the lunar surface has also been mentioned. The libration-point communications system would be useful during the early lunar exploration period, but its full potential will probably not be realized until more advanced lunar surface operations are carried out. For these more advanced missions, the libration-point network could also function as a navigation and control center for manned and unmanned surface vehicles.

Other proposals[84-86] for obtaining Earth to lunar far-side and long-range lunar surface-to-surface communications have recommended the use of relay satellites in lunar orbit. However, orbiting relay satellites have several obvious disadvantages. Some of these disadvantages are

(1) Many satellites are needed for adequate coverage.

(2) Tracking and acquisition problems are difficult. (These problems are considerably easier with libration-point satellites, since these satellites are almost stationary with respect to the lunar surface.)

(3) The contact time for any given satellite is relatively short, and frequent switchovers are necessary.

(4) The diverse antenna pointing requirements (satellite to Earth, satellite to lunar surface, and satellite to satellite) would complicate the attitude control problem.

Although orbiting satellites possess some advantages over libration-point satellites (e.g., communication distances are shorter and station-keeping is usually not required), they do not appear to outweigh the disadvantages listed above. A recent investigation by Schmid[87] has also expressed a preference for the libration-point satellite technique. In Schmid's study, a quantitative comparison of lunar far-side communication requirements (power, beamwidth, antenna gain, bit-rate, etc.) for a libration-point satellite and a 1000-km altitude satellite in a circular lunar orbit is presented.

b. Rendezvous Technique

Present plans for the Apollo lunar landing mission call for the insertion of the combined spacecraft [command module (CM) and

lunar landing vehicle (LLV)] into a low lunar orbit. After this is accomplished, the LLV will descend to the lunar surface, stay there for about 1-2 days, ascend to the lunar parking orbit, and rendezvous with the CM. The CM will then return to the Earth.

An alternate method uses the Earth-Moon L_1 point for rendezvous instead of a lunar parking orbit. Although this rendezvous scheme has been examined by a number of people since 1960, the first published work was presented by Raithel[12] in 1966. Since the libration-point rendezvous method has several attractive advantages over the lunar orbit rendezvous concept, a few comments are in order.

In Fig. 7-7, two transfer trajectories between an Earth parking orbit and the L_1 point are illustrated. A direct transfer (trajectory #1) uses two impulses, while an indirect transfer (trajectory #2) employs a third impulse at the closest approach to the Moon. In both cases, the velocity increment (ΔV) at the Earth parking orbit is approximately equal to the ΔV that is required for escape velocity. A digital computer simulation is needed to obtain the remaining ΔV's since a patched-conic approximation is not very accurate for these calculations. Some computer results of Nicholson[88] are quoted here. For the direct transfer, $\Delta V_{L1} \cong 2{,}350$ ft/sec for a 4-day transit. For the indirect transfer, $\Sigma\Delta V \cong 1{,}900$ ft/sec (the ΔV near the Moon is about 1000 ft/sec and $\Delta V_{L1} \cong 900$ ft/sec), but the trip time is 6 days. The same ΔV's are required for the reverse trajectories.

A transfer between the L_1 point and the Moon is also shown in Fig. 7-7 (trajectory #3). In this transfer, $\Delta V_{L1} \cong 1{,}700$ ft/sec, and the impact velocity at the Moon is about 7,790 ft/sec for a 24-hour transit.

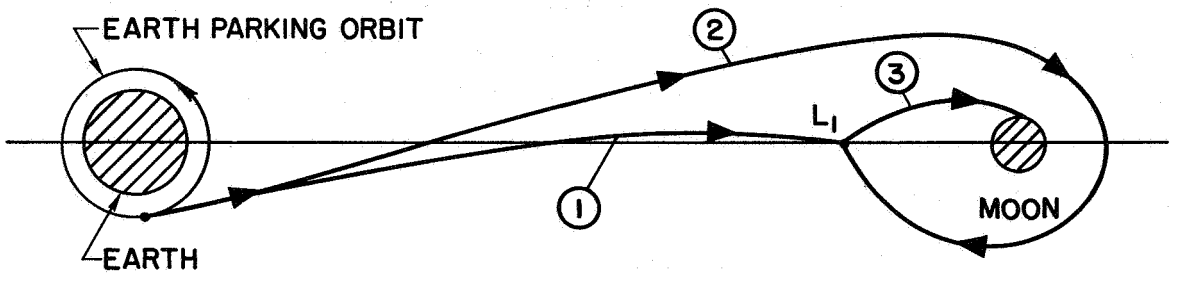

FIG. 7-7. TRANSFER PATHS TO AND FROM THE L_1 POINT IN THE MOON'S ORBITAL PLANE. (Not to scale).

For landing sites near the lunar equator or for surface stay times of a few days, the total ΔV requirements for lunar orbit rendezvous are slightly lower than the ΔV requirements for libration-point rendezvous. However, for landings at higher lunar latitudes or longer stay times, rather large plane changes are often necessary, and the ΔV cost for these plane changes is significantly higher if lunar orbit rendezvous is employed.[89] In some instances, this increased ΔV penalty is severe, and large portions of the lunar surface are not accessible with the present Apollo spacecraft. (An even greater restriction on lunar surface accessibility is imposed by requiring a continuous abort capability for the LLV.) On the other hand, the ΔV's for the libration-point rendezvous technique are virtually identical for any lunar landing site or stay time since the necessary plane changes can be accomplished quite cheaply at the L_1 point. This low-ΔV plane-change capability might very well favor a rendezvous at L_1 for long-duration or high-latitude lunar surface missions.

Since the L_1 point is stationary with respect to the lunar surface, the libration-point rendezvous technique also has an important operational advantage -- namely, an infinite "launch window" for the LLV to and from the lunar surface. This timing advantage, along with the low-ΔV plane-change capability, makes the L_1 point an ideal location for a lunar logistics staging depot (or a lunar-surface rescue facility). Supplies could be transported to and from the L_1 point with reusable shuttle vehicles. A low-thrust vehicle could be used between the Earth parking orbit and the L_1 point, but a high-thrust vehicle would be needed for the transfer between the L_1 point and the lunar surface.

From the preceding discussion, it is clear that a comprehensive investigation of the libration-point rendezvous concept is warranted. This investigation should consider several different transfer modes as well as various staging possibilities. The usefulness of the L_2 point for rendezvous should also be examined.

2. An Interplanetary Transportation System with Terminals at the Sun-Planet Collinear Points

A modified version of the libration-point rendezvous technique described above may be useful for planetary missions. Although a large variety of mission profiles with libration-point rendezvous could be contrived, only one possibility is presented here.

Consider a reusable shuttle vehicle that operates between the L_1 point of the Sun-Earth system and the L_2 point of a Sun-planet system. The outbound transfer path for the shuttle vehicle is shown in Fig. 7-8; the inbound transfer path is just the mirror image of the outbound transfer path. Either a high or low-thrust rocket could be used to perform the transfer, but it is quite possible that a hybrid system (high and low-thrust) would be more efficient. The transfer of the interplanetary shuttle vehicle (ISV) is initiated by applying a small impulse at the Sun-Earth L_1 point and then starting the low-thrust engine. As the ISV passes close to the Earth (point A in Fig. 7-8), a much larger impulse is administered. During the heliocentric portion of the transfer, only low-thrust is employed. At the closest approach to the planet (point B in Fig. 7-8), another large impulse is applied, and a planetary landing vehicle (PLV) is separated from the ISV and lands on the planet.* The ISV then proceeds to the Sun-planet L_2 point where capture is effected by another small impulse. A reverse procedure is used for the inbound transfer.

Additional shuttle vehicles can be used for the transfer of crew members, fuel, and other supplies between the Sun-Earth L_1 point and the Earth. This phase of the mission is similar to the elliptical orbit pickup procedure discussed in Ref. 90.

From the ΔV standpoint, the libration-point rendezvous technique probably does not have any significant advantage over the elliptical-orbit rendezvous method. However, the increased flexibility

*It may be more desirable to separate the PLV earlier or later, depend- on the descent mode (atmospheric or propulsive braking), guidance requirements, staging ratios, safety factors, etc.

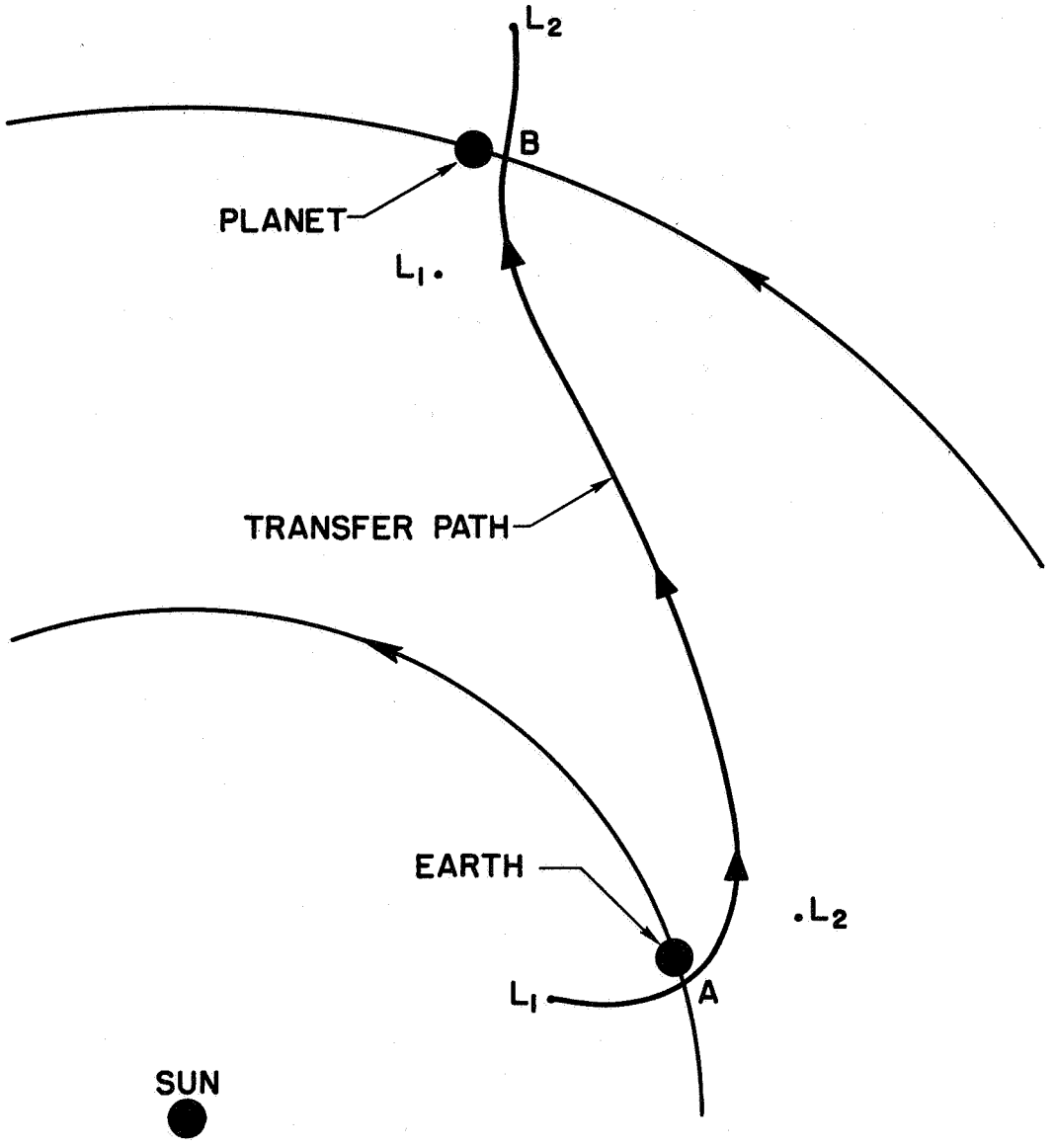

FIG. 7-8. TRANSFER PATH BETWEEN THE SUN-EARTH L_1 POINT AND A SUN-PLANET L_2 POINT. (Not to scale).

in the timing of various operations* (e.g., rendezvous, abort, and landing) may justify a quantitative investigation of the libration-point rendezvous concept.

*The timing problems associated with orbiting or landing missions to the satellites of Jupiter are particularly involved.[91]

3. Deep-Space Communications using a Relay Satellite at an Earth-Moon Equilateral-Triangle Point

Future deep-space missions will require much higher rates of data transmission than have been attained to date. Laser communications systems show considerable promise for furnishing these high data rates.[92] However, to avoid occultations caused by cloud cover and Earth rotation, a relay satellite between the deep-space vehicle (DSV) and the Earth-based station will usually be required.* A microwave link is used between the Earth and the relay satellite, while an optical link (laser beam) is used between the relay satellite and the DSV.

The selection of the orbit for the relay satellite is very important, and the trade-offs involved in this choice are discussed in Ref. 93. Although a preference for a synchronous orbit (24-hour orbit) was expressed in Ref. 93, the possibility of stationing the relay satellite at an Earth-Moon equilateral-triangle libration point was not considered. It is hoped that the equilateral-triangle points will be considered in future trade-off studies, since these locations seem to possess certain advantages over a synchronous orbit. Some of these advantages are

(1) Less Earth occultation (almost none) of the optical communications link between the relay satellite and the DSV.

(2) The Earth can usually be excluded from the field of view of the communications receiver on the DSV. (The Earth is a strong noise source.)

(3) The maximum relative velocity normal to the line-of-sight between the relay satellite and the DSV is smaller. Therefore, the pointing requirements for the laser beam are less stringent.

(4) The ΔV cost for the initial placement of the relay satellite is reduced by about 0.5 km/sec (Ref. 15).

Of course, the equilateral-triangle points also have some disadvantages when compared with a synchronous orbit (e.g., the path loss for the

*Occultation could also be avoided by using a large number of Earth stations, but frequent switchovers would be necessary. Since the acquisition of a narrow laser beam is rather difficult, these switchovers would probably result in the loss of some data.

microwave link is greater), and a complete systems evaluation is needed before a final choice can be made.

The libration-point communications system could also be used for another purpose. With two relay satellites, one at L_4 and the other at L_5, it would be possible to take advantage of the large separation distance (about 6.66×10^5 km) to establish a long-baseline interferometric tracking and navigation system.[94] However, since the baseline is rotating with respect to the DSV, it may be advisable to generate two more baselines by placing a third relay satellite at the Earth-Moon L_3 point. (The three baselines would form a triangle.)

B. Scientific Usefulness

1. A Multiple-Satellite System for Monitoring Solar-Induced Phenomena In and Beyond the Earth's Magnetosphere

Since 1957, scientific satellites have collected a large amount of data concerning particles and fields in the Earth's magnetosphere and in the interplanetary medium surrounding it.[95-97] These measurements have led to many impressive discoveries of previously unknown phenomena, but future progress will be largely dependent on the ability to perform simultaneous observations at different locations. Only in this way will it be possible to separate temporal from spatial variations.

Good coverage of cislunar space has already been achieved by using several satellites in highly eccentric Earth orbits. However, beyond the Moon's orbit, the data are usually discrete. To improve this situation, Robinson[14] has suggested that a satellite should be placed in the Earth's orbit about 6×10^6 mi in front of the Earth (this corresponds to a Sun-Earth isosceles-triangle point at about $\theta \cong 4°$) where it would continuously monitor the interplanetary medium that will be occupied by the Earth four days later. Another possibility has been advanced by Meissinger and Greenstadt,[17] who have examined the feasibility of obtaining long-term measurements in the Earth's geomagnetic tail by stationing a satellite in the vicinity of the Sun-Earth L_2 point. These stationary satellites would provide some of the data that are needed to discern the time-variation of solar-induced phenomena in the Earth's neighborhood, but more spatial coverage would be desirable.

Symmetrical spatial coverage could be obtained with a network of four satellites, as shown in Fig. 7-9. These satellites are stationed at the isosceles-triangle points, I_1 and I_2 ($\theta = \pm 2°$),* and the collinear points, L_1 and L_2.** When data collected at these points are compared with measurements taken in cislunar space, some interesting correlations may be apparent. It may also be possible to find some correlation with Earth weather data.

Notice that the satellite at the L_1 point could also function as an early-warning station for solar flares. Although the warning time would only be about 8-25 minutes (average velocities of solar flares are between 1000 and 3000 km/sec), this may be sufficient for some purposes (e.g., a high-flying supersonic transport could descend to a safer altitude on short notice).

The station-keeping costs for the satellites at the isosceles-triangle points can be obtained from Fig. 1-8. For $\theta = \pm 2°$, the cost is $|\vec{F}_c| \cong 1.50 \times 10^{-6}$ g. At the collinear points, the costs are negligibly small if DSIF tracking is utilized (see Chapter IV).

2. Low-Frequency Radio Astronomy from the Earth-Moon L_2 Point

The low-frequency cutoff for Earth-based radio telescopes is about 10 MHz. This limit could be extended with an Earth-orbiting radio telescope, but it would be extremely difficult to observe frequencies below 1 MHz since the ionosphere of the Earth is a source of low-frequency radio noise. However, a radio telescope located at the Earth-Moon L_2

---

*The value of θ that is given here was chosen somewhat arbitrarily. The optimum choice can only be determined after considering various trade-offs (station-keeping cost, communications requirements, scientific value, etc.).

**The placement of a second satellite at L_2 distance, but along the nominal direction of the geomagnetic tail, might also be profitable. By analyzing radio signals between this satellite and the satellite at L_2, it may be possible to monitor the electron density in a cross section of the geomagnetic tail. The station-keeping cost for the displaced satellite would be about $\overline{|F_{cy}|} \cong (B_{L2} - 1)\delta_y = 1.25 \times 10^{-6}$ g, with $\delta_y = 1.05 \times 10^5$ km.

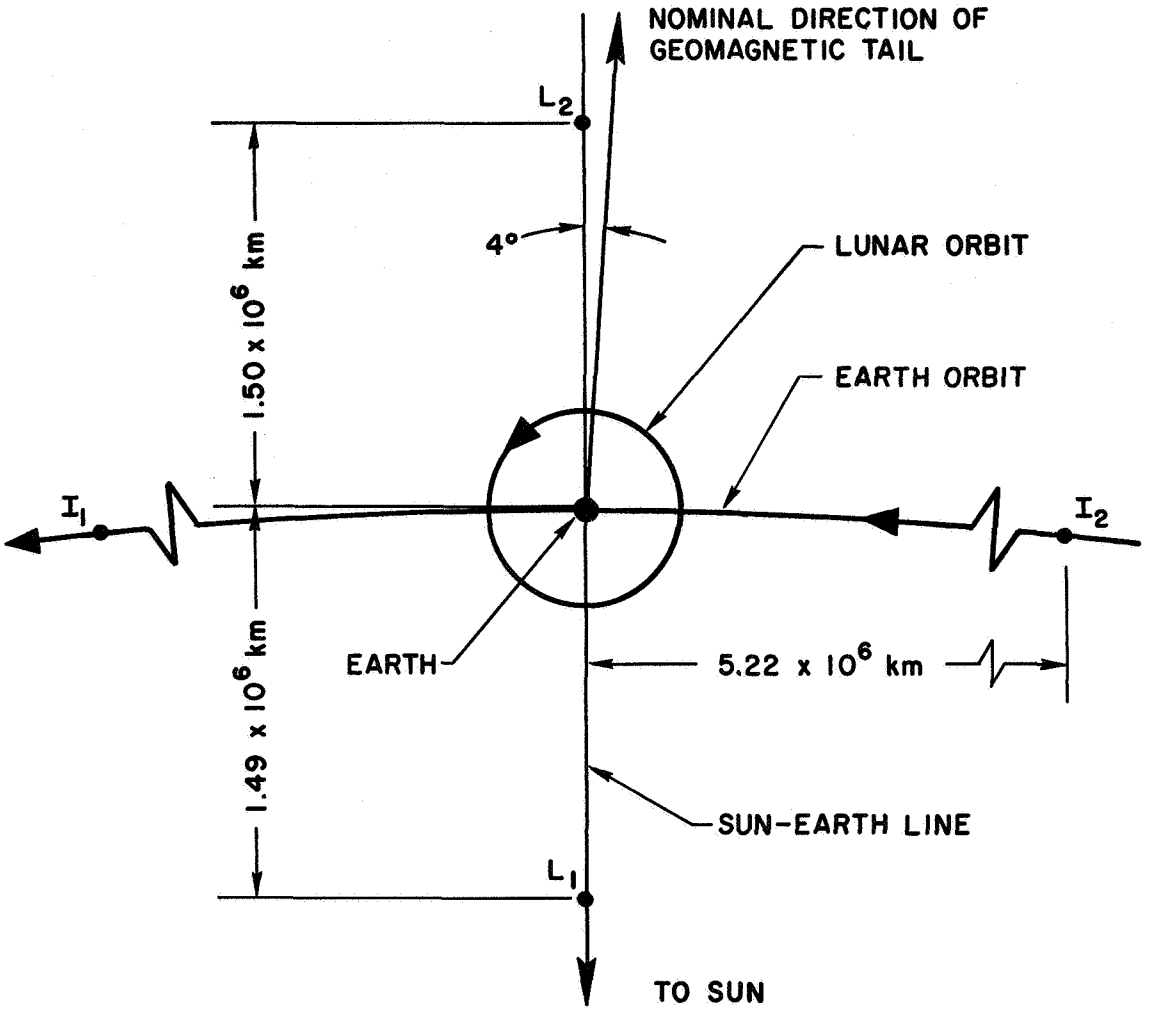

FIG. 7-9. MULTIPLE-SATELLITE NETWORK. (Satellites anchored at L_1, L_2, I_1, and I_2).

point would always be shielded from the Earth's ionosphere by the Moon.* Therefore, the Earth-Moon L_2 point may be an ideal location for low-frequency radio astronomy experiments. Of course, possible interference from the geomagnetic tail would not be completely eliminated, but the Earth-Moon L_2 point would remain outside of the tail region for periods of almost 3 weeks.

*The use of the Earth-Moon L_2 point as a site for radio astronomy was originally suggested by Hornby and Allen.[15]

CONCLUSIONS AND RECOMMENDATIONS

The translation control of a satellite in the vicinity of a libration point can be accomplished in a rather simple manner. For instance, at an unstable collinear point, a single-axis control using only range and range-rate measurements is sufficient. Moreover, the station-keeping costs are very low (comparable to costs for synchronous satellite station-keeping), and are well within the capability of present satellite translation-control systems.

The control system can be mechanized in many ways, and a few possibilities were presented in this study. (The author realizes that the engineering difficulties associated with the cable control technique are rather formidable, but the method is intriguing.) The author urges that specific designs of control systems for libration-point satellites be the focal point of future work; these studies should include detailed investigations of propulsion systems and measurement techniques.

The potential usefulness of a libration-point satellite is apparent (see Chapter VII). Therefore, the early construction and flight testing of a libration-point satellite is strongly recommended. A costly development program may not be necessary, since a satisfactory test vehicle could probably be obtained by modifying an Applications Technology Satellite. The Earth-Moon L_1 point might be a convenient location for station-keeping tests, but a lunar far-side communications capability could also be achieved if the tests were conducted in a quasi-periodic orbit around the Earth-Moon L_2 point.

Appendix A

DERIVATION OF EQ. (4-18)

Given the Gaussian density function

$$\Phi_{F^*}(x,t) = \frac{1}{\sigma_F\sqrt{2\pi}} \exp\left\{ - \frac{[x - p(t)]^2}{2\sigma_F^2} \right\} \tag{A-1}$$

with

$$p(t) = K_c \cos \omega t \tag{A-2}$$

it is required to find the average control acceleration

$$\overline{|F^*_{cx}|} = \frac{\omega}{2\pi}\int_0^{2\pi/\omega} E\left\{|F^*_{cx}(t)|\right\} dt \tag{A-3}$$

where

$$E\left\{|F^*_{cx}(t)|\right\} = \int_{-\infty}^{+\infty} |x| \Phi_{F^*}(x,t)dx$$

$$= -\int_{-\infty}^{0} x\Phi_{F^*}(x,t)dx + \int_0^{+\infty} x\Phi_{F^*}(x,t)dx \tag{A-4}$$

With the change of variables

$$y \equiv \frac{x - p(t)}{\sigma_F} \tag{A-5}$$

Eq. (A-4) becomes

$$E\left\{\left|F^*_{cx}(t)\right|\right\} = -\frac{1}{\sqrt{2\pi}}\int_{-\infty}^{-p/\sigma_F}\left[p + \sigma_F y\right]e^{-y^2/2}dy + \frac{1}{\sqrt{2\pi}}\int_{-p/\sigma_F}^{+\infty}\left[p + \sigma_F y\right]e^{-y^2/2}dy$$

$$= \frac{p}{\sqrt{2\pi}}\left[\int_{-\infty}^{p/\sigma_F} e^{-y^2/2}dy - \int_{-\infty}^{-p/\sigma_F} e^{-y^2/2}dy\right]$$

$$+ \frac{\sigma_F}{\sqrt{2\pi}}\left[\int_{-p/\sigma_F}^{+\infty} ye^{-y^2/2}dy - \int_{-\infty}^{-p/\sigma_F} ye^{-y^2/2}dy\right] \qquad \text{(A-6)}$$

$$\equiv G_1(t) + G_2(t)$$

In $G_2(t)$, let $v \equiv -y^2/2$; then

$$G_2(t) = \frac{2\sigma_F}{\sqrt{2\pi}}\int_{-\infty}^{-p^2/2\sigma_F^2} e^v dv = \frac{2\sigma_F}{\sqrt{2\pi}}\, e^{-p^2/2\sigma_F^2} \qquad \text{(A-7)}$$

The time average of Eq. (A-7) is

$$H_2 \equiv \frac{\omega}{2\pi}\int_0^{2\pi/\omega} G_2(t)dt = \frac{1}{2\pi}\int_0^{2\pi} G_2\left(\frac{\tau}{\omega}\right)d\tau = \frac{2\sigma_F}{(2\pi)^{3/2}}\int_0^{2\pi}\exp\left[-\frac{K_c^2\cos^2\tau}{2\sigma_F^2}\right]d\tau$$

$$= \frac{2\sigma_F}{(2\pi)^{3/2}}\exp\left[-\frac{K_c^2}{4\sigma_F^2}\right]\int_0^{2\pi}\exp\left[-\frac{K_c^2}{4\sigma_F^2}\cos 2\tau\right]d\tau$$

$$= \frac{4\sigma_F}{(2\pi)^{3/2}}\exp\left[-\frac{K_c^2}{4\sigma_F^2}\right]\int_0^{\pi}\exp\left[-\frac{K_c^2}{4\sigma_F^2}\cos\tau\right]d\tau = \frac{2\sigma_F}{\sqrt{2\pi}}\, e^{-u}I_o(u) \qquad \text{(A-8)}$$

where $I_o(u)$ is a modified Bessel function, and $u \equiv K_c^2/4\sigma_F^2$. The time average of $G_1(t)$ can be written

$$H_1 \equiv \frac{\omega}{2\pi}\int_0^{2\pi/\omega} G_1(t)dt = \frac{1}{2\pi}\int_0^{2\pi} G_1\left(\frac{\tau}{\omega}\right)d\tau$$

$$= \frac{K_c}{(2\pi)^{3/2}}\int_0^{2\pi}\left[\int_{-\infty}^{p/\sigma_F} e^{-y^2/2}dy - \int_{-\infty}^{-p/\sigma_F} e^{-y^2/2}dy\right]\cos\,\tau\,d\tau$$

$$\equiv \frac{K_c}{(2\pi)^{3/2}}\int_0^{2\pi}\left[\,\Phi\left(\frac{p}{\sigma_F}\right) - \Phi\left(-\frac{p}{\sigma_F}\right)\right]\cos\,\tau\,d\tau \qquad \text{(A-9)}$$

Integrating by parts, Eq. (A-9) becomes

$$H_1 = \frac{K_c}{(2\pi)^{3/2}}\left\{\left[\left(\Phi\left(\frac{p}{\sigma_F}\right) - \Phi\left(-\frac{p}{\sigma_F}\right)\right)\sin\,\tau\right]_0^{2\pi}\right.$$

$$\left. -\int_0^{2\pi}\left[\,\dot{\Phi}\left(\frac{p}{\sigma_F}\right) - \dot{\Phi}\left(-\frac{p}{\sigma_F}\right)\right]\sin\,\tau\,d\tau\right\} \qquad \text{(A-10)}$$

The first portion of Eq. (A-10) vanishes. Making use of the relation

$$\dot{\Phi}\left(\pm\frac{p}{\sigma_F}\right) = \Phi'\left(\pm\frac{p}{\sigma_F}\right)\frac{d\left(\pm\frac{p}{\sigma_F}\right)}{d\tau}$$

$$= \mp\frac{K_c}{\sigma_F}\sin\,\tau\,\exp\left[-\frac{p^2}{2\sigma_F^2}\right] \qquad \text{(A-11)}$$

the remaining portion of Eq. (A-10) is converted to

$$H_1 = \frac{2K_c^2}{(2\pi)^{3/2}\sigma_F} \int_0^{2\pi} \sin^2\tau \exp\left[-\frac{K_c^2 \cos^2\tau}{2\sigma_F^2}\right] d\tau$$

$$= \frac{2K_c^2}{(2\pi)^{3/2}\sigma_F} e^{-u}\left[\int_0^{\pi} e^{-u\cos\tau} d\tau - \int_0^{\pi} \cos\tau\, e^{-u\cos\tau} d\tau\right]$$

$$= \frac{K_c^2}{\sqrt{2\pi}\,\sigma_F} e^{-u}\left[I_o(u) + I_1(u)\right] \qquad \text{(A-12)}$$

Therefore, the average control acceleration is given by

$$\overline{|F^*_{cx}|} = H_1 + H_2$$

$$= \frac{e^{-u}}{\sqrt{2\pi}}\left\{2\sigma_F I_o(u) + \frac{K_c^2}{\sigma_F}\left[I_o(u) + I_1(u)\right]\right\} \qquad \text{(A-13)}$$

Appendix B

ECCENTRICITY CORRECTION FOR THE Z-AXIS OSCILLATION AT THE EARTH-MOON L_2 POINT

Following the procedures used in Chapter II, it is readily deduced that the differential equation for the eccentricity correction of the z-axis oscillation at a collinear libration point is [see Eq. (1-43c)]

$$\ddot{z}_{n2} + B_L z_{n2} = 3\rho B_L z_{n1} \tag{B-1}$$

where

$$\rho = - e \cos t \tag{B-2}$$

$$z_{n1} = A_{z1} \cos \omega_z t \tag{B-3}$$

The solution of Eq. (B-1) can be written in the form

$$z_{n2} = A_{z2} \cos (\omega_z + 1)t + A'_{z2} \cos (\omega_z - 1)t \tag{B-4}$$

At the Earth-Moon L_2 point, $B_{L2} = 3.19042$, $e = 0.05490$, and $\omega_z = 1.78618$. With these constants, it is found that

$$\begin{aligned} A_{z2} &= 0.057460\ A_{z1} \\ A'_{z2} &= - 0.10416\ A_{z1} \end{aligned} \tag{B-5}$$

REFERENCES

1. V. Szebehely, Theory of Orbits: The Restricted Problem of Three Bodies, Academic Press, New York, 1967.

2. L. Steg and J. P. De Vries, "Earth-Moon Libration Points: Theory, Existence and Applications," Space Science Reviews, Vol. 5, No. 2, Mar 1966, pp. 210-233.

3. G. Colombo, "The Stabilization of an Artificial Satellite at the Inferior Conjunction Point of the Earth-Moon System," Smithsonian Astrophysical Observatory Special Report, No. 80, Nov 1961.

4. H. M. Dusek, "Motion in the Vicinity of Libration Points of a Generalized Restricted Three-Body Model," AIAA Progress in Astronautics and Aeronautics: Methods in Astrodynamics and Celestial Mechanics, edited by R. L. Duncombe and V. G. Szebehely (Academic Press, New York, 1966), Vol. 17, pp. 37-54.

5. A. W. Fleming, "Use of the Properties of Frequency Symmetry and Complex Symmetry in the Control of Linear Dynamical Systems," Stanford University, Dept. of Aeronautics and Astronautics, SUDAAR-266, May 1966, pp. 36-44.

6. E. W. Paul and G. Shapiro, "Stabilization of the Lagrangian Solutions of the Three-Body Problem," Astronautica Acta, Vol. 11, No. 6, Nov-Dec 1965, pp. 410-417.

7. R. W. Farquhar, "Station-Keeping in the Vicinity of Collinear Libration Points with an Application to a Lunar Communications Problem," AAS Science and Technology Series: Space Flight Mechanics Specialist Symposium, edited by M. L. Anthony (AAS Publications, Tarzana, Calif., 1967), Vol. 11, pp. 519-535. (Presented at AAS Space Flight Mechanics Specialist Conference, Jul 1966.)

8. A. F. Kononenko, "Libration Points Approach," Presented at XVIIIth International Astronautical Congress, International Astronautical Federation, Sep 1967.

9. A. C. Clarke, "Stationary Orbits," Journal of the British Astronomical Association, Vol. 57, No. 6, Dec 1947, pp. 232-237.

10. C. A. Cross, "Orbits for an Extra-Terrestrial Observatory," Journal of the British Interplanetary Society, Vol. 13, No. 4, Jul 1954, pp. 204-207.

11. W. H. Michael Jr., "Considerations of the Motion of a Small Body in the Vicinity of the Vicinity of the Stable Libration Points of the Earth-Moon System," NASA, TR R-160, 1963.

12. W. Raithel, "The Role of the Cis-Lunar Libration Point in Lunar Operations" Proceedings of 3rd Space Congress, Canaveral Council of Technical Societies, Mar 1966.

13. D. Jamison "Uses of the Trojan Libration Points of the Earth-Sun System," Journal of Spacecraft and Rockets, Vol. 3, No. 4, Apr 1966, pp. 595-596.

14. A. I. Robinson, "An Heliocentric Earth Orbit Precursor Planetoid," RAND Corporation, P-3343, Apr 1966.

15. H. Hornby and W. H. Allen, "Mission to the Libration Centers," Astronautics and Aeronautics, Vol. 4, No. 7, Jul 1966, pp. 78-82.

16. R. W. Farquhar, "Lunar Communications with Libration-Point Satellites," Journal of Spacecraft and Rockets, Vol. 4, No. 10, Oct 1967, pp. 1383-1384.

17. H. F. Meissinger and E. W. Greenstadt, "Use of Electric Propulsion for Exploring the Distant Regions of the Geomagnetic Tail," AIAA Paper, 68-120, Jan 1968.

18. F. O. Vonbun, "A Hummingbird for the L_2 Lunar Libration Point," NASA, TN D-4468, Apr 1968.

19. F. R. Moulton, An Introduction to Celestial Mechanics, MacMillan, New York, 1914, p. 171.

20. M. W. Ovenden and A. E. Roy, "On the Use of the Jacobi Integral of the Restricted Three-Body Problem," Monthly Notices of the Royal Astronomical Society, Vol. 123, No. 1, 1961, pp. 1-14.

21. Z. Kopal and R. A. Lyttleton, "On the Elliptic Case of the Restricted Problem of Three Bodies and the Remote History of the Earth-Moon System," Icarus, Vol. 1, 1963, pp. 455-458.

22. V. Szebehely and G. E. O. Giacaglia, "On the Elliptic Restricted Problem of Three Bodies," Astronomical Journal, Vol. 69, No. 3, Apr 1964, pp. 230-235.

23. A. De Prit, " A Note Concerning the Collinear Libration Centers," Icarus, Vol. 4, 1965, pp. 273-278.

24. A. Bennett, "Characteristic Exponents of the Five Equilibrium Solutions in the Elliptically Restricted Problem," Icarus, Vol 4, 1965, pp. 177-187.

25. A. Bennett, "Analytical Determination of Characteristic Exponents," AIAA Progress in Astronautics and Aeronautics: Methods in Astrodynamics and Celestial Mechanics, edited by R. L. Duncombe and V. G. Szebehely (Academic Press, New York, 1966), Vol. 17, pp. 101-113.

26. G. Colombo, D. Lautman, and C. Munford, "On the Libration Orbits of a Particle Near the Triangular Point in the Semirestricted Three-Body Problem," Astronomical Journal, Vol, 68, No. 3, Apr 1963, pp. 159-162.

27. J. M. A. Danby, "Stability of the Triangular Points in the Elliptic Restricted Problem of Three Bodies," Astronomical Journal, Vol. 69. No. 2, Mar 1964, pp. 165-172.

28. V. M. Blanco and S. W. McCuskey, Basic Physics of the Solar System, Addison-Wesley, Reading, Mass., 1961.

29. S. G. Makover and N. A. Bokhan, "The Motion of Comet Encke-Backlund During 1898-1911 and a New Determination of the Mass of Mercury," Soviet Physics-Doklady, Vol. 5, No. 5, 1961, pp. 923-925.

30. E. Rabe, "Corrected Derivation of Astronomical Constants from the Observations of Eros 1926-1945," Astronomical Journal, Vol. 72, No. 7, Sep 1967, pp. 852-855.

31. E. Rabe, "The Earth + Moon Mass and other Astronomical Constants from the Eros Motion 1926-1965," Astronomical Journal, Vol. 72, No. 7, Sep 1967, pp. 856-864.

32. J. D. Anderson and M. R. Warner, "Determination of the Masses of the Moon and Venus, and the Astronomical Unit from the Radio Tracking of Mariner II," Trajectories of Artificial Celestial Bodies, edited by J. Kovalevsky (Springer-Verlag, Berlin, 1966), pp. 216-246.

33. V. C. Clarke, Jr., "Constants and Related Data for Use in Trajectory Calculations as Adopted by the Ad Hoc NASA Standards Committee," Jet Propulsion Laboratory, TR 32-604, Mar 6, 1964.

34. C. M. Michaux, "Handbook of the Physical Properties of the Planet Mars," NASA, SP-3030, 1967, p. 12.

35. H. Camichel, M. Hugon and J. Rösch, "Mesure du Diamètre de Mercure par la Méthode de Hertzsprung le 7 Novembre 1960," Icarus, Vol. 3, 1964, pp. 410-422.

36. G. De Vaucouleurs, "Geometric and Photometric Parameters of the Terrestrial Planets," Icarus, Vol. 3, 1964, pp. 187-235.

37. K. E. Bullen, "Implications of the Revised Mars Radius," Nature, Vol. 211, Jul 23, 1966, p. 396.

38. L. Mohn and J. Kevorkian, "Some Limiting Cases of the Restricted Four-Body Problem," Astronomical Journal, Vol. 72, No. 8, Oct 1967, pp. 959-963.

39. E. W. Brown and C. A. Shook, Planetary Theory, Dover Publications, New York, 1964, Chapter 9.

40. L. Cesari, Asymptotic Behavior and Stability Problems in Ordinary Differential Equations, 2nd Ed., Springer-Verlag, Berlin, 1963.

41. H. C. Plummer, "On Oscillating Satellites-1," Monthly Notices of the Royal Astronomical Society, Vol. 63, No. 8, 1903, pp. 436-443.

42. H. C. Plummer, "On Oscillating Satellites-2," Monthly Notices of the Royal Astronomical Society, Vol. 64, No. 2, 1903, pp. 98-105.

43. J. D. Acord and J. C. Nicklas, "Theoretical and Practical Aspects of Solar Pressure Attitude Control for Interplanetary Spacecraft," AIAA Progress in Astronautics and Aeronautics: Guidance and Control-II, edited by R. C. Langford and C. J. Mundo (Academic Press, New York, 1964), Vol. 13, pp. 73-101.

44. G. Colombo, "Sui Satelliti del Sistema Terra-luna," Rendiconti Accademia Nazionale Dei Lincei, Ser. 8, Vol. 28, 1960, pp. 169-172.

45. F. T. Nicholson, "Effect of Solar Perturbation on Motion near the Collinear Earth-Moon Libration Points," AIAA Journal, Vol. 5, No. 12, Dec 1967, pp. 2237-2241.

46. G. De Pontecoulant, Theorie Analytique du Systeme du Monde, Vol. 4, Bachelier, Paris, 1846.

47. E. W. Brown, An Introductory Treatise on the Lunar Theory, Dover Publications, New York, 1960.

48. J. P. De Vries, "The Sun's Perturbing Effect on Motion Near a Triangular Lagrange Point," Proceedings of XIIIth International Astronautical Congress (1962) (Springer-Verlag, New York, 1964), pp. 432-450.

49. B. D. Tapley and J. M. Lewallen, "Solar Influence on Satellite Motion Near the Stable Earth-Moon Libration Points," AIAA Journal, Vol. 2, No. 4, Apr 1964, pp. 728-732.

50. H. B. Schechter and W. C. Hollis, "Stability of the Trojan Points in the Four-Body Problem," RAND Corporation, RM-3992-PR, Sep 1964.

51. J. V. Breakwell and R. Pringle Jr., "Resonances Affecting Motion Near the Earth-Moon Equilateral Libration Points," AIAA Progress in Astronautics and Aeronautics: Methods in Astrodynamics and Celestial Mechanics, edited by R. L. Duncombe and V. G. Szebehely (Academic Press, New York, 1966), Vol. 17, pp. 55-74.

52. L. E. Wolaver, "Effect of Initial Configurations on Libration Point Motion," AIAA Progress in Astronautics and Aeronautics: Methods in Astrodynamics and Celestial Mechanics, edited by R. L. Duncombe and V. G. Szebehely (Academic Press, New York, 1966), Vol. 17, pp. 75-99.

53. B. D. Tapley and B. E. Schutz, "Further Results on Solar Influenced Libration Point Motion," AIAA Journal, Vol. 3, No. 10, Oct 1965, pp. 1954-1956.

54. H. B. Schechter, "Three-Dimensional Nonlinear Stability Analysis of the Sun-Perturbed Earth-Moon Equilateral Points," AIAA Paper 67-566, Aug 1967.

55. R. Kolenkiewicz and L. Carpenter, "Stable Periodic Orbits About the Sun-Perturbed Earth-Moon Triangular Points," NASA Goddard Space Flight Center, X-643-67-484, Oct 1967.

56. W. Kaplan, Operational Methods for Linear Systems, Addison-Wesley, Reading, Mass., 1962, Chapter 7.

57. O. I. Elgerd, Control Systems Theory, McGraw-Hill, New York, 1967.

58. J. K. Hale, Oscillations in Nonlinear Systems, McGraw-Hill, New York, 1963.

59. R. A. Boucher, "Electrical Propulsion for Control of Stationary Satellites," Journal of Spacecraft and Rockets, Vol. 1, No. 2, Mar-Apr 1964, pp. 164-169.

60. J. H. Molitor, "Ion Propulsion System for Stationary-Satellite Control," Journal of Spacecraft and Rockets, Vol. 1, No. 2, Mar-Apr 1964, pp. 170-175.

61. R. S. H. Toms and B. E. Kalensher, "Control of a Synchronous Satellite by Continuous Radial Thrust," AIAA Journal, Vol. 2, No. 7, Jul 1964, pp. 1179-1188.

62. M. J. Neufeld, "Orbit Correction," Space/Aeronautics, Vol. 43, No. 2, Feb 1965, pp. 48-55.

63. M. J. Neufeld and B. M. Anzel, "Synchronous Satellite Station-Keeping," AIAA Progress in Astronautics and Aeronautics: Communication Satellite Systems Technology, edited by R. B. Marsten (Academic Press, New York, 1966), Vol. 19, pp. 323-346.

64. R. H. Greene, "Early Bird Placement in a Stationary Orbit: Launch and Control System Maneuvers," AIAA Progress in Astronautics and Aeronautics: Communication Satellite Systems Technology, edited by R. B. Marsten (Academic Press, New York, 1966), Vol. 19, pp. 9-42.

65. R. E. Balsam and S. E. Dunin, "Orbit Determination for Stationary Satellites," AAS Science and Technology Series: Space Flight Mechanics Specialist Symposium, edited by M. L. Anthony (AAS Publications, Tarzana, Calif., 1967), Vol. 11, pp. 123-136.

66. R. E. Balsam and B. M. Anzel, "Determination of the Pacific Equilibrium Point for a Stationary Orbit," Journal of Spacecraft and Rockets, Vol. 4, No. 10, Oct 1967, pp. 1289-1294.

67. G. C. Newton, Jr., L. A. Gould, and J. F. Kaiser, Analytical Design of Linear Feedback Controls, J. Wiley & Sons, New York, 1957.

68. H. H. Rosenbrock, "An Automatic Method for Finding the Greatest or Least Value of a Function," Computer Journal, Vol 3, 1960, pp. 175-184.

69. W. J. Sjogren, D. W. Trask, C. J. Vegos, and W. R. Wollenhaupt, "Physical Constants as Determined from Radio Tracking of the Ranger Lunar Probes," AAS Science and Technology Series: Space Flight Mechanics Specialist Symposium, edited by M. L. Anthony (AAS Publications, Tarzana, Calif., 1967), Vol. 11, pp. 137-154.

70. E. J. Bowers, R. L. Taylor, E. H. Thompson, and J. W. Knight, "Study of Basic Requirements for a Navigation, Guidance, and Control System for an Unmanned Lunar Landing Vehicle," NASA, CR-61118, Dec 1965.

71. J. H. Lowry, "Electromagnetic Guidance Study," NASA, CR-865, Sep 1967.

72. M. Abramowitz and I. A. Stegun, eds., Handbook of Mathematical Functions, U. S. Govt. Printing Office, Washington, D. C., 1964.

73. J. Peschon and H. B. Smets, "Nonlinear Control Systems: Selected Topics," Disciplines and Techniques of Systems Control, edited by J. Peschon (Blaisdell, New York, 1965), pp. 187-266.

74. D. D. Siljak, "Analysis of Asymmetrical Nonlinear Oscillations in the Parameter Plane," IEEE Transactions on Automatic Control, Vol. AC-11, No. 2, Apr 1966, pp. 239-247.

75. Ja. S. Zypkin (Ya. Z. Tsypkin), Theorie der Relaissysteme der Automatischen Regelung, R. Oldenbourg-Verlag, Munich, 1958.

76. J. C. Gille, M. J. Pelegrin, and P. Decaulne, Feedback Control Systems, McGraw-Hill, New York, 1959, Chapter 26.

77. N. A. Korolev, "Periodic Modes in Relay Systems Containing Internal Feedback," Automation and Remote Control, Vol. 17, Nov 1956, pp. 1083-1094.

78. V. Mangulis, Handbook of Series for Scientists and Engineers, Academic Press, New York. 1965, p. 80.

79. B. C. Kuo, Analysis and Synthesis of Sampled-Data Control Systems, Prentice-Hall, Englewood Cliffs, N. J., 1963.

80. W. E. Frye and E. V. B. Stearns, "Stabilization and Attitude Control of Satellite Vehicles," ARS Journal, Vol. 29, No. 12, Dec 1959, pp. 927-931.

81. O. V. Gurko and L. I. Slabkii, "The Use of Forces Derived from the Solar Gravitational and Radiation Fields for the Orientation of Cosmic Devices," Artificial Satellites, Vol. 16, Mar 1964, pp. 30-41.

82. G. W. Sutton and F. W. Diederich, "Synchronous Rotation of a Satellite at Less than Synchronous Altitude," AIAA Journal, Vol. 5, No. 4, Apr 1967, pp. 813-815.

83. G. E. Taylor and J. R. Hunter, "Structural Design and Operation of a Large Radio Astronomy Antenna," AIAA Paper, 68-348, Apr 1968.

84. R. C. Nigam and B. V. Kit, "Some Astrodynamical Aspects of Lunar Communications Using Satellites," Proceedings of XVIth International Astronautical Congress: Astrodynamics (1965)(Gauthier-Villars, Paris, 1966), pp. 95-117.

85. G. E. Neuner, "Lunar Communication Satellites," AIAA Progress in Astronautics and Aeronautics: Communication Satellite Systems Technology, Edited by R. B. Marsten (Academic Press, New York, 1966), Vol. 19, pp. 887-908.

86. R. E. Marinaccio and R. R. Cavey, "Techniques for Lunar Surface Communications," Microwave Journal, Vol. 10, No. 11, Oct 1967, pp. 51-57.

87. P. E. Schmid, "Lunar Far-Side Communication Satellites," NASA, TN D-4509, Jun 1968.

88. F. T. Nicholson, "Vehicle Motion near the L_1 Earth-Moon Libration Point," General Electric Missile and Space Division, PIR-4T43-006, Jun 1966.

89. P. A. Penzo and R. W. Johnson, "The Extended Stay Lunar Exploration Mission," Advances in the Astronautical Sciences: Post Apollo Space Exploration, edited by F. Narin (AAS Publications, Tarzana, Calif., 1966), Vol. 20, part 2, pp. 1027-1060.

90. R. W. Luidens, R. R. Burley, J. D. Eisenberg, J. M. Kappraff, B. A. Miller, M. D. Shovlin, and E. A. Willis Jr., "Manned Mars Landing Mission by Means of High-Thrust Rockets," NASA, TN D-3181, Jan 1966.

91. R. W. Luidens and J. Edgar, "Round-Trip Trajectories to Moons of Jupiter," NASA, TN D-4167, Oct 1967.

92. F. Kalil, "Optical and Microwave Communications -- A Comparison," NASA, TN D-3984 (corrected copy), May 1968.

93. S. Gubin, R. B. Marsten, and D. Silverman, "Lasers vs Microwaves in Space Communications," Journal of Spacecraft and Rockets, Vol. 3, No. 6, Jun 1966, pp. 818-827.

94. A. D. Wheelon, "Midcourse and Terminal Guidance," Space Technology, Edited by H. S. Seifert (J. Wiley & Sons, New York, 1959), Chapter 26, pp. 18-20.

95. Anon., "Significant Achievements in Particles and Fields 1958-1964," compiled by W. Hess, G. Mead, and M. P. Nakada, NASA, SP-97, 1966.

96. A. W. Schardt and A. G. Opp, "Significant Achievements in Space Science 1965 - Particles and Fields," NASA, SP-136, 1967, pp. 31-88.

97. A. W. Schardt and A. G. Opp, "Significant Achievements in Space Science 1966 - Particles and Fields," NASA, SP-155, 1967, pp. 204-287.